Protein kinase D3 signaling
in the regulation of liver metabolism

♦♦♦♦

Proteinkinase D3 Signalwirkung
in der Regulation des Leberstoffwechsels

Doctoral thesis for a doctoral degree

at the Graduate School of Life Sciences,

Julius-Maximilians-Universität Würzburg,

Section Biomedicine

Submitted by

Alexander E. Mayer

from Ulm

Würzburg, November 2019

Submitted on: _____

Members of the *Promotionskomitee*:

Chairperson: Prof. Dr. Georg Gasteiger

Primary Supervisor: Dr. Grzegorz Sumara

Supervisor (Second):   Prof. Dr. Almut Schulze

Supervisor (Third):   Prof. Dr. Annette Schürmann

Date of Public Defense: _____

Date of Receipt of Certificates: _____

Table of Contents

Table of Contents

Table of Contents

Table of Contents

Summary

The liver plays a pivotal role in maintaining energy homeostasis. Hepatic carbohydrate and lipid metabolism are tightly regulated in order to adapt quickly to changes in nutrient availability. Postprandially, the liver lowers the blood glucose levels and stores nutrients in form of glycogen and *triglycerides* (TG). In contrast, upon fasting, the liver provides glucose, TG, and ketone bodies. However, obesity resulting from a discrepancy in food intake and energy expenditure leads to abnormal fat accumulation in the liver, which is associated with the development of hepatic insulin resistance, non-alcoholic fatty liver disease, and diabetes. In this context, hepatic insulin resistance is directly linked to the accumulation of *diacylglycerol* (DAG) in the liver. Besides being an intermediate product of TG synthesis, DAG serves as second messenger in response to G-protein coupled receptor signaling. *Protein kinase D* (PKD) family members are DAG effectors that integrate multiple metabolic inputs. However, the impact of PKD signaling on liver physiology has not been studied so far. In this thesis, PKD3 was identified as the predominantly expressed isoform in liver. Stimulation of primary hepatocytes with DAG as well as *high-fat diet* (HFD) feeding of mice led to an activation of PKD3, indicating its relevance during obesity. HFD-fed mice lacking PKD3 specifically in hepatocytes displayed significantly improved glucose tolerance and insulin sensitivity. However, at the same time, hepatic deletion of PKD3 in mice resulted in elevated liver weight as a consequence of increased hepatic lipid accumulation. Lack of PKD3 in hepatocytes promoted *sterol regulatory element-binding protein* (SREBP)-mediated de novo lipogenesis in vitro and in vivo, and thus increased hepatic triglyceride and cholesterol content. Furthermore, PKD3 suppressed the activation of SREBP by impairing the activity of the insulin effectors *protein kinase B* (AKT) and *mechanistic target of rapamycin complexes* (mTORC) 1 and 2. In contrast, liver-specific overexpression of constitutive active PKD3 promoted glucose intolerance and insulin resistance. Taken together, lack of PKD3 improves hepatic insulin sensitivity but promotes hepatic lipid accumulation. For this reason, manipulating PKD3 signaling might be a valid strategy to improve hepatic lipid content or insulin sensitivity. However, the exact molecular mechanism by which PKD3 regulates hepatocytes metabolism remains unclear.

Unbiased proteomic approaches were performed in order to identify PKD3 phosphorylation targets. In this process, numerous potential targets of PKD3 were

detected, which are implicated in different aspects of cellular metabolism. Among other hits, *phenylalanine hydroxylase* (PAH) was identified as a target of PKD3 in hepatocytes. PAH is the enzyme that is responsible for the conversion of phenylalanine to tyrosine. In fact, manipulation of PKD3 activity using genetic tools confirmed that PKD3 promotes PAH-dependent conversion of phenylalanine to tyrosine. Therefore, the data in this thesis suggests that PKD3 coordinates lipid and amino acid metabolism in the liver and contributes to the development of hepatic dysfunction.

Zusammenfassung

Die Leber spielt eine zentrale Rolle bei der Aufrechterhaltung der Energiehomöostase. Der hepatische Kohlenhydrat- und Fettstoffwechsel ist stark reguliert, um sich schnell an Veränderungen in der Nährstoffverfügbarkeit anzupassen. Die Leber senkt postprandial den Blutzuckerspiegel und speichert Nährstoffe in Form von Glykogen und *Triglyzeriden* (TG). Im Gegensatz dazu stellt die Leber beim Fasten Glukose, TG und Ketonkörper bereit. Fettleibigkeit, welche aus einer Diskrepanz zwischen Nahrungsaufnahme und Energieaufwand resultiert, führt allerdings zu einer abnormalen Fettansammlung in der Leber, die mit der Entwicklung von Leberinsulinresistenz, nicht-alkoholischen Fettlebererkrankungen und Diabetes einhergeht. Hepatische Insulinresistenz steht dabei in direktem Zusammenhang mit der Akkumulation von *Diacylglycerol* (DAG) in der Leber. DAG ist nicht nur ein Zwischenprodukt der TG-Synthese, sondern dient auch als sekundärer Messenger im G-Protein-gekoppelten Rezeptor-Signalweg. Die Mitglieder der *Proteinkinase D* (PKD)-Familie sind DAG-Effektoren, die vielfache metabolische Inputs integrieren. Jedoch wurden die Auswirkungen der PKD-Signalwirkung auf die Leberphysiologie bisher nicht untersucht. Im Rahmen dieser Thesis wurde PKD3 als die in der Leber überwiegend exprimierte Isoform identifiziert. Die Stimulation von primären Hepatozyten mit DAG sowie die Fütterung von Mäusen mit *fettreicher Nahrung* (HFD) führte zu einer Aktivierung von PKD3, was auf eine Relevanz von PKD3 bei Fettleibigkeit hinweist. Mäusen, welchen PKD3 spezifisch in Hepatozyten fehlte und mit HFD gefüttert wurden, zeigten eine deutlich verbesserte Glukosetoleranz und Insulinsensitivität. Gleichzeitig führte jedoch die hepatische Deletion von PKD3 bei Mäusen zu einem erhöhten Lebergewicht in Folge einer erhöhten Lipidakkumulation in der Leber. Das Fehlen von PKD3 in Hepatozyten förderte die *Sterol Regulatory Element-Binding Protein* (SREBP)-vermittelte de novo Lipogenese in vitro und in vivo und erhöhte damit den Gehalt an Triglyceriden und Cholesterol in der Leber. Darüber hinaus supprimierte PKD3 die Aktivierung von SREBP, indem es die Aktivität der Insulin-Effektoren *Proteinkinase B* (AKT) und *mechanistisches Ziel von Rapamycin-Komplexen* (mTORC) 1 und 2 verminderte. Im Gegensatz dazu förderte die leberspezifische Überexpression von konstitutiv aktiver PKD3 die Glukoseintoleranz und Insulinresistenz. Zusammenfassend verbessert der Mangel an PKD3 die hepatische Insulinempfindlichkeit, aber fördert gleichzeitig die Akkumulation von

Zusammenfassung

Lipiden in der Leber. Aus diesem Grund könnte das Eingreifen in den PKD3-Signalweg eine gute Strategie zur Verbesserung des hepatischen Lipidgehalts oder der Insulinempfindlichkeit sein. Allerdings bleibt der genaue molekulare Mechanismus, mit dem PKD3 den Stoffwechsel von Hepatozyten reguliert, unklar.

Es wurden unvoreingenommene proteomische Ansätze durchgeführt, um PKD3-Phosphorylierungsziele zu identifizieren. In diesem Prozess wurden zahlreiche potenzielle Ziele von PKD3 entdeckt, welche in den verschiedensten Aspekten des Zellstoffwechsels involviert sind. Unter anderem wurde *Phenylalaninhydroxylase* (PAH) als Ziel von PKD3 in Hepatozyten identifiziert. PAH ist das Enzym, welches für die Umwandlung von Phenylalanin in Tyrosin verantwortlich ist. Tatsächlich bestätigte die Manipulation der PKD3-Aktivität mit Hilfe von genetischen Werkzeugen, dass PKD3 die PAH-abhängige Umwandlung von Phenylalanin in Tyrosin fördert. Deswegen legen die Daten in dieser Arbeit nahe, dass PKD3 den Lipid- und Aminosäurestoffwechsel in der Leber koordiniert und zur Entwicklung von Leber-Dysfunktion beiträgt.

1 Introduction

1.1 The liver

1.1.1 Liver morphology and functions

The liver is the largest visceral organ in mammals even though it constitutes only 2.5% of body weight, and about 30% of the hepatic volume is blood[1]. The portal vein provides 75% of the blood and the other 25% are from the hepatic artery which makes the liver a unique organ[2]. Moreover, the liver is divided into lobes and further into the functional units lobules (portal vein, hepatic artery, bile duct) and acinus. Parenchymal cells and nonparenchymal cells are the main cell types that form the liver[3]. Parenchymal hepatocytes act in two different directions, the vascular poles serve in an ingestive sense, while the biliary poles have secretory functions[4]. Hepatic microvascularization comprises of sinusoids, arterial and portal vessels, and the terminal hepatic venule[4]. Sinusoids are formed between plates of hepatocytes from sinusoidal endothelial cells and phagocytic Kupffer cells, whereas hepatic stellate cells are found between sinusoids and hepatocytes in the perisinusoidal space[4].
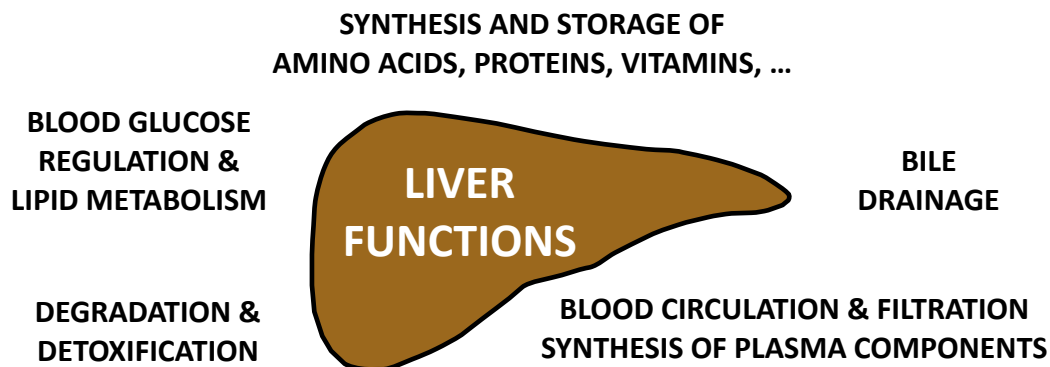
Figure 1: Liver functions. Main liver functions include blood glucose regulation, lipid metabolism, degradation and detoxification of substances, blood filtration and circulation, synthesis and storage of amino acids, proteins, and vitamins, and production of bile.

The unique location of the liver being connected to portal veins, hepatic arteries, and bile ducts makes it the ideal organ for metabolite uptake, metabolism, storage, synthesis, and release. The liver metabolically connects multiple tissues including skeletal muscle, adipose tissue, and the *gastrointestinal* (GI) tract[5]. In addition, it plays a major role in carbohydrate, lipid, protein, and amino acid anabolism and catabolism (Figure 1). About 25% of the whole body's protein are synthesized in the liver and the liver is the primary organ that can consume and produce large amounts of glucose[6]

and has a major function in lipid metabolism[7]. In addition, the liver synthesizes and releases amino acids, and proteins including carrier proteins [albumin, the most abundant protein in serum], coagulation factors [I (fibrinogen); II (prothrombin); V; VII; VIII; IX; X; XI; XII; XIII; protein C and S; and antithrombin], complement proteins, apolipoproteins, and (pro-) hormones [thrombopoietin; *insulin-like growth factor* (IGF) 1; angiotensinogen]. Furthermore, glucose (in form of glycogen), lipids (in lipid droplets), vitamins (A; B_{12}; D; E; K), and minerals (iron and copper) are stored in the liver. Another important function is the degradation and detoxification of hormones (insulin), bilirubin, ammonia (breakdown to urea), and drugs/xenobiotics. These products can then be used as substrates for other pathways (e.g. amino acids), secreted into the blood (e.g. urea), or excreted with the bile (e.g. conjugated molecules) which is also produced in the liver[8,9]. Moreover, hepatic Kupffer cells are an essential part of the innate immune system with a major function to capture fungi and bacteria from the blood[10].

1.1.2 Hepatic glucose and lipid metabolism
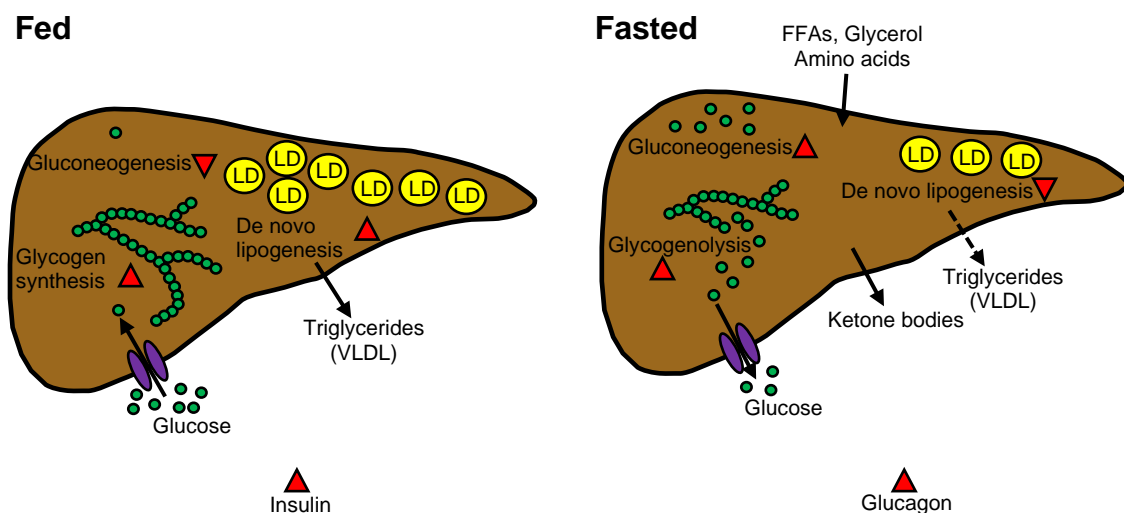
Figure 2: Liver as a main energy store of the organism.

The liver has a pivotal role in regulating metabolic homeostasis[11]. Postprandially, glucose enters hepatocytes via the *glucose transporter* (GLUT) 2 and is stored as glycogen or metabolized through glycolysis (breakdown of glucose) to pyruvate and subsequently to acetyl-CoA by *oxidative phosphorylation* (OXPHOS). The resulting acetyl-CoA can be used as energy source in the *tricarboxylic acid* (TCA) cycle or used for synthesizing fatty acids through de novo lipogenesis depending on nutrient

availability. De novo synthesized long-chain *free fatty acids* (FFA) or FFAs originating from diet (via chylomicrons) and extrahepatic tissues (adipose tissues) can be used either as energy source, used to form other lipids [*phospholipids* (PL)], or esterified and incorporated into TG and *cholesteryl esters* (CE), which in turn can be stored in *lipid droplets* (LD) or packed and secreted as *very low density lipoprotein* (VLDL) (Figure 2)[11,12].

In the fasted state, glucose is released from glycogen (glycogenolysis) and de novo synthesized by gluconeogenesis, which is the primary source for glucose during prolonged fasting[5]. Additionally, adipose tissue releases FFAs into circulation upon fasting through the process of lipolysis (breakdown of TG). Subsequently, liver takes up the FFAs and converts them into ketone bodies (ketogenesis) that serve as an energy source for peripheral tissues[5]. These processes are highly regulated by neuronal and hormonal circuits, most prominently by the pancreatic hormones insulin and glucagon. Postprandially, insulin promotes glycolysis and lipogenesis but suppresses gluconeogenesis. Its counterpart glucagon promotes glycogenolysis, gluconeogenesis and suppresses lipogenesis upon fasting[13]. However, there are multiple other factors other than insulin and glucagon regulating these processes. For instance, the availability of substrates, expression and activity of key enzymes, the metabolic state, circadian clock, the ER, cytokines, GI and *growth hormones* (GH), multiple transcription factors and coregulators control the metabolic state (reviewed in [5]). Particularly, the transcription factors *cAMP-response element-binding protein* (CREB), *forkhead box protein O* (FOXO) 1, *CCAAT/enhancer-binding proteins* (C/EBP) α/β, and *PPARγ coactivator* (PGC)-1α regulate expression of *glucose-6-phosphatase catalytic-subunit* (G6pc) and cytosolic *phosphoenolpyruvate carboxykinase* (Pepck), and thus gluconeogenesis (reviewed in [5,11]). In contrast, expression of lipogenic genes is controlled by the transcription factors *upstream-stimulatory factor* (USF), *sterol regulatory element-binding protein 1c* (SREBP1c), *carbohydrate-responsive element-binding protein* (ChREBP), and *liver X receptor* (LXR) (reviewed in [5,14]).

The three SREBP isoforms (SREBP1a, SREBP1c, and SREBP2) are master regulators of lipid metabolism[15]. SREBP1a and SREBP1c proteins are encoded by the same gene and generated by using alternative transcription start sites[15]. SREBP1c and SREBP2 are the predominantly found isoforms in the liver[15]. Functionally, SREBP1c enhances expression of genes for fatty acid synthesis[16], whereas SREBP2

3

promotes expression of genes for cholesterol synthesis[17]; however, the expression of most target genes is regulated by both transcription factors[18]. Newly synthesized SREBPs reside as inactive precursors in the *endoplasmic reticulum* (ER) membrane and bind to the *SREBP cleavage-activating protein* (SCAP)[16]. SCAP is a cholesterol sensor that mediates ER-Golgi transport of SREBPs in COPII vesicles[19]. Golgi-localized *Site-1 protease* (S1P) and *Site-2 protease* (S2P) proteolytically cleave and release the N-terminus of SREBPs, which can translocate to the nucleus to promote *Srebp* and its target gene expression[16]. Beside low cholesterol levels, ER stress[20] and low phosphatidylcholine pools[21] promote the activation of SREBPs, whereas lipin 1 negatively regulates SREBP action[22]. Moreover, SREBP activity is controlled through an inhibitory phosphorylation of SREBP on Ser372 by *AMP-activated protein kinase* (AMPK)[23] and through deacetylation of SREBP1c by SIRT1[24].

1.1.3 Nutrient overload, insulin resistance, and diabetes from a liver perspective
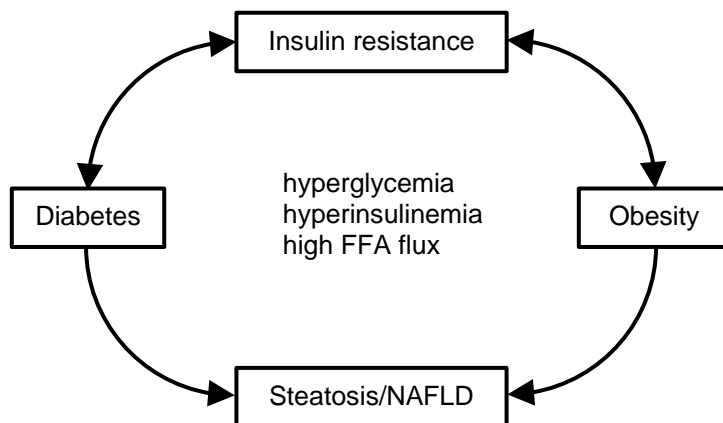
Figure 3: Pathophysiology of abnormal lipid and glucose metabolism in liver. (modified from Parekh, 2007)[25]

A pathological imbalance of the pathways described before can lead to excessive lipid accumulation in liver (steatosis)[26,27]. Increased glucose and insulin levels in circulation promote hepatic de novo lipogenesis and together with an increased flux of FFAs, this causes steatosis (Figure 3). The main cause for increased hepatic lipid accumulation is obesity, resulting from a discrepancy in food intake and energy expenditure[28]. Individuals with a body mass index (BMI) of 30 kg/m^2 or greater (calculated by dividing the body weight in kilograms by the square of the height in meters) are considered obese. The worldwide increase in obesity is associated with an increase in the prevalence of *non-alcoholic fatty liver disease* (NAFLD), which is defined by abnormal

fat accumulation in liver[29-31]. NAFLD may progress into *non-alcoholic steatohepatitis* (NASH) and eventually to cirrhosis and *hepatocellular carcinoma* (HCC) characterized by liver damage and inflammation, and fibrosis, respectively[32,33]. Lipid accumulation in NAFLD is closely associated with obesity, insulin resistance, and *type 2 diabetes* (T2D)[34,35]. In this context, hyperglycemia and hyperinsulinemia characterize insulin resistance, a physiological condition in which cells fail to respond to insulin[27]. Short term high-fat diet feeding of mice results in hepatic steatosis associated with impaired insulin sensitivity in hepatocytes identified by decreased tyrosine phosphorylation of *insulin receptor substrate* (IRS) 1 and 2 by the insulin receptor and the reduced ability of insulin to activate hepatic glycogen synthesis and to suppress hepatic glucose production[36]. In this model, hepatic insulin resistance is directly associated with an increase in hepatic DAG levels[37]. This correlation between hepatic DAG accumulation and hepatic insulin resistance is linked to an activation of the DAG-effector *protein kinase C* (PKC) ε, the predominantly activated PKC isoform in liver following fat feeding, which impairs the activation of the insulin receptor[34,36,37]. During healthy conditions, AKT is activated downstream of the insulin receptor which enhances lipid synthesis by activating the *mechanistic target of rapamycin* (mTOR) *complex* (mTORC) 1-SREBP1c pathway (reviewed in [38] and discussed later), and suppresses FOXO1-mediated gluconeogenesis[39,40]. However, during obesity, AKT fails to suppress FOXO1, leading to upregulated expression of gluconeogenic enzymes and increased glucose output[41,42] but AKT continues to activate de novo lipogenesis[43]. Taken together, the development of obesity correlates with the development of steatosis, insulin resistance, and diabetes in liver.

1.2 Protein Kinase D (PKD) family

Protein kinases are enzymes that covalently transfer a phosphate group from *adenosine triphosphate* (ATP) to free hydroxyl groups of a protein. Protein kinases are subdivided into groups and further into families based on sequence homology in the kinase domain and known functions[44]. One of these families is the protein kinase D family, which consists of 3 members: PKD1, PKD2, and PKD3. PKDs are serine/threonine kinases that belong to the *calcium/calmodulin-dependent protein kinases* (CAMK) superfamily. In 1994, PKD1 was identified as first member of the family in human and mouse. Initially, PKD1 was categorized as a member of the PKC

family and named PKCµ[45,46]. Subsequently, PKD3/PKCv and PKD2 were described, completing the PKD family[47,48].

1.2.1 Structure and Activation of PKDs

All three isoforms share structural and functional similarities with distinct differences between the three isoforms. The PKD isoforms consist of an N-terminal tandem repeat of zinc finger-like cysteine-rich motifs (*cysteine-rich domain*, CRD), an autoinhibitory *pleckstrin homology* (PH) domain, and a catalytic kinase domain (Figure 4)[49,50].

The PH domain is located in between the CRD and kinase domain of PKDs. The PH domain is present in numerous signaling proteins and binds to a plethora of lipids and other proteins[51]. For PKDs, the PH domain is essential for complex formation with PKCs[52]. Mutations in the PH domain or deletion of the PH domain markedly increased PKD activity, therefore the PH domain is considered to exhibit also an autoregulatory role[53].

The two CRD domains (C1a and C1b) bind DAG and phorbol esters with high affinity. This stimulates PKD activity in the presence of *phosphatidylserine* (PS)[54]. The CRD domain is highly homologous with DAG binding domains in PKCs, diacylglycerol kinases, *RAS guanyl-releasing proteins* (RasGRP), chimaerins, and Munc13s[55]. DAG as second messenger is generated through the key isoenzymes *phosphatidylinositol 4,5-bisphosphate (PIP$_2$)-specific phospholipases C* (PtdIns-PLC) β/γ/δ/ε that catalyze the hydrolysis of PIP$_2$ to DAG and *inositol trisphosphate* (IP$_3$). IP$_3$ binds to receptors on the ER, which leads to Ca^{2+} release into the cytosol. PLCs are activated by *G-protein-coupled receptor* (GPCR) and *receptor tyrosine kinases* (RTK). Alternatively, DAG is formed by the two-step hydrolysis of *phosphatidylcholine* (PC) to *phosphatidic acid* (PA) and choline by PC-specific *phospholipase D* (PLD) isoenzymes 1/2 and subsequently by the conversion of PA to DAG by *phosphatidic acid phosphohydrolase* (PAP). This reaction does not generate IP$_3$ and therefore does not lead to Ca^{2+} release[56]. *Conventional PKCs* (cPKCs), which include PKCα, PKCβ, and PKCγ, are activated by DAG and phospholipid binding in the C1 domain and Ca^{2+}-dependent phospholipid binding in the C2 domain, whereas *novel PKCs* (nPKCs) comprising PKCδ, PKCε, PKCθ and PKCη- are similarly activated but independent of *calcium* (Ca^{2+})[56,57]. Activation of PKCs mainly results in their translocation to the plasma membrane[57,58].

Introduction
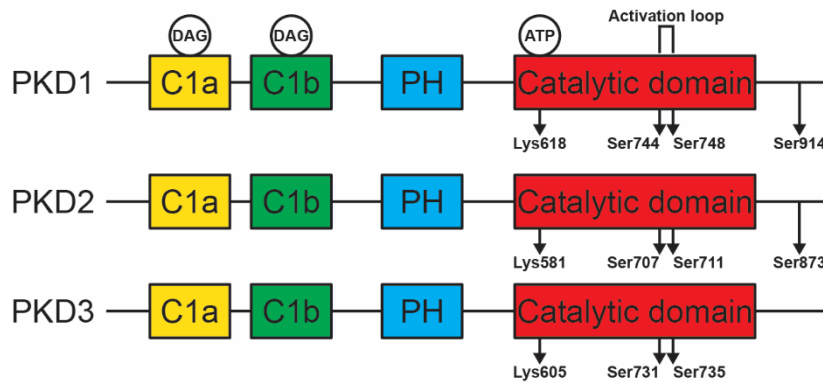
Figure 4: Structural domains of PKD isoforms. All three PKD isoforms (PKD1, PKD2, and PKD3) consist of 2 CRD domains (C1a and C1b) that bind DAG and phorbol esters, an autoinhibitory PH domain, and a catalytic domain. Two serine residues in the kinase domain can be phosphorylated, which activates the kinase and leads to an autophosphorylation of a C-terminal serine for PKD1 and PKD2 as indicated. ATP binds within the kinase domain and mutation of an indicated lysine eliminates binding of ATP (kinase dead mutation) (modified from Fu, 2011)[59]. *Protein kinase D* (PKD); *cysteine-rich domain* (C); *diacylglycerol* (DAG); *pleckstrin homology* (PH); *serine* (Ser); *lysine* (Lys).

PKCs rapidly activate PKDs via phosphorylation on two serine residues in the activation loop (PKD1: Ser744/748, PKD2: Ser707/711, PKD3: Ser731/735)[60-62], thereby stabilizing the activation loop in an active conformation. However, Ser744 is the predominant phosphorylation site for PKCs in PKD1 and Ser748 is thereafter autophosphorylated[63]. Subsequently, this activation in the kinase domain leads to an autophosphorylation of Ser914 on PKD1 or Ser873 on PKD2, whereas the phosphorylation site is absent in PKD3[49,64]. The carboxy-terminal phosphorylation of Ser914 in PKD1 is not required for kinase activity but for the autophosphorylation of Ser748[65].

Mutation studies were used to investigate the role of distinct amino acids for activation of PKDs. Substitution of both serine residues with glutamic acid (e.g. PKD3 S731E/S735E) results in a constitutive active form of PKD, whereas mutation of the serine residues to alanine (e.g. PKD3 S731A/S735A) prevents activation via phosphorylation[60]. Mutation of Lys618 in the ATP binding site results in a catalytically inactive/kinase dead version of PKD1 (K605A for PKD3)[64].

Upstream events that stimulate PKD activation through RTKs and GPCRs (G_q, G_{12}, G_i, and Rho)[66-70] include a variety of stimuli such as lipids (DAG), bioactive peptides (bombesin, bradykinin, endothelin, and vasopressin)[71,72], and growth factors [*platelet-derived growth factor* (PDGF), *vascular endothelial growth factor* (VEGF)][71,73], among other factors that further activate phospholipase Cs (PLCs) and c/nPKCs. The PKC-

dependent activation of PKDs is rapid and followed by a subsequent PKC-independent phosphorylation of PKDs[63,74,75].

The catalytic activity of all PKD isoforms can be inhibited by selective inhibitors such as the PKC/PKD inhibitor Gö6976[76] or the PKD-specific inhibitors CID755673[77] and CRT0066101[78].

1.2.2 Intracellular localization of PKDs

PKDs have been reported to localize to various cellular compartments. In unstimulated cells, PKD1 resides mainly in the cytoplasm[79,80] and to a lesser extent in the Golgi compartment[81,82]. Additionally, PKD1 shuttles between the cytoplasm and the nucleus[79]. Following PLC activation, PKD1 binds to the newly produced DAG with the C1b domain and translocates to the plasma membrane[79]. In vitro, this CRD-dependent translocation of PKD from the cytosol to the plasma membrane is also mediated by phorbol esters[83]. In contrast to C1a-mediated translocation, C1b-mediated translocation to the plasma membrane is only partial, but it is persistent for hours and the C1b domain can directly bind to $G_{\alpha q}$[84]. Following PKD phosphorylation through PKCs, PKDs reversely translocate back to the cytoplasm[79]. Then, the C1b domain in conjunction with a nuclear import receptor is required for the nuclear import, while the PH domain is essential for the nuclear export[79]. In contrast, the C1a domain is also required for the recruitment of PKD to the *trans-Golgi network* (TGN)[85,86]. Moreover, in response to mitochondrial *reactive oxygen species* (ROS), PKD1 localizes to mitochondria and activates NF-κB-dependent transcription in the nucleus[87].

The PKD isoforms have different binding affinities for phorbol esters and DAG in their respective C1 domains[88]. Furthermore, PKD2 is translocated to the plasma membrane and activated in the same way as PKD1; however, PKD2 does not further redistribute to the nucleus after its dissociation from the plasma membrane[89]. In contrast to PKD1 and PKD2 that are predominantly located in the cytoplasm, PKD3 is present in both the cytoplasm and the nucleus[90]. The intracellular distribution of PKDs is distinct suggesting that differential localization regulates their signaling properties.

Introduction

1.2.3 PKD functions in health and disease
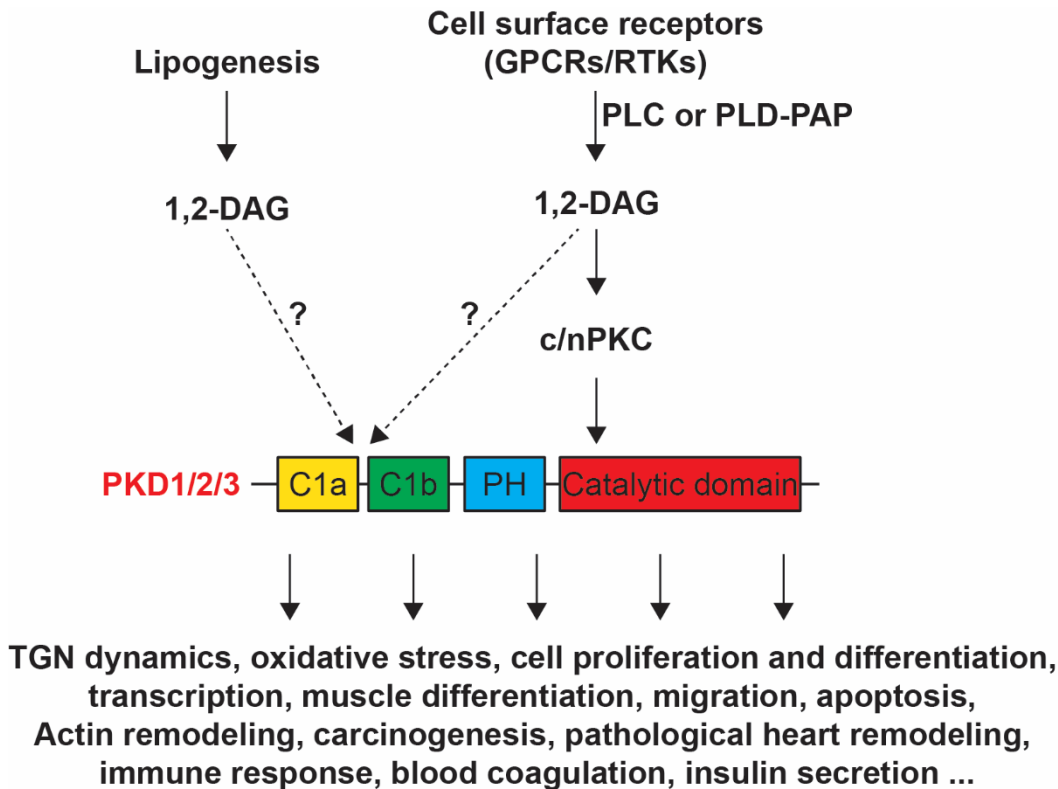
Figure 5: Activation and signaling pathways of PKD isoforms. PKD isoforms are activated in response to cell surface receptor ligand binding through c/nPKCs or directly by binding of DAG originating from different pools. PKDs are involved in various fundamental processes as indicated in the figure. *G-protein-coupled receptor* (GPCR); *receptor tyrosine kinase* (RTK); *phospholipase C* (PLC); *phospholipase D* (PLD); *phosphatidic acid phosphohydrolase* (PAP); *diacylglycerol* (DAG); *conventional/novel protein kinase C* (c/nPKC); *protein kinase D* (PKD); *cysteine-rich domain* (C); *pleckstrin homology* (PH); *trans-Golgi network* (TGN).

PKDs have tissue and cell specific functions, which is also reflected by a tissue-dependent differential co-expression of the isoforms[91], the upstream extra- or intracellular stimulus, the affinity for certain ligands such as DAG or phorbol esters, temporal/spatial localization, the isoform itself, and the substrate specificity[92].

PKD isoforms are involved in various fundamental cellular processes such as protein trafficking[82,85], oxidative stress[93], cell proliferation and differentiation[94], transcription[95], migration[96], apoptosis[97], actin remodeling[98-101], carcinogenesis[102], muscle differentiation[103,104], pathological heart remodeling[105,106], immune response[107], blood coagulation[108], and insulin secretion[109,110] (Figure 6).

PKDs regulate membrane fission at the TGN[82,85]. Thereby, dimeric PKD is required for the biogenesis of cell surface transport carriers at the TGN[111]. The complex formation of PKD isoforms is essential to modulate cofilin-driven directed cell migration, and the PKD dimer plays also a role in innate immunity[112,113]. At the TGN, PKD has various

other functions besides membrane fission, including the control of NLRP3 inflammasome activation[114].

Unlike classical PKD activation when DAG is produced at the plasma membrane, PKDs bind to DAG originating from mitochondria during oxidative stress conditions[115]. PKD1 is then phosphorylated at Tyr463 in the PH domain by Abl[116], leading to a conformational change followed by a Src-mediated N-terminal phosphorylation at Tyr95[117]. This tyrosine phosphorylation recruits PKCδ, resulting in the phosphorylation of the serine residues in the activation loop of PKDs, which in turn leads to *nuclear factor kappa-light-chain-enhancer of activated B cells* (NF-κB) translocation to the nucleus and its target gene expression[87,93,118].

Activation of PKDs by multiple growth-promoting GPCR agonists suggests a role for PKDs in mitogenic signaling. In Swiss 3T3 fibroblasts, overexpression of either PKD1 or PKD2 potentiated *deoxyribonucleic acid* (DNA) synthesis and cell proliferation stimulated by G_q-coupled receptor agonists[74,75,119,120]. Activated mitogenic signaling activates the *mitogen-activated protein kinase kinase* (MEK)/ *extracellular signal–regulated kinase* (ERK)/ *p90 ribosomal S6 kinase* (RSK) pathway leading to the accumulation of gene products that stimulate cell cycle progression such as c-Fos[74,119]. In epithelial cells, PKD phosphorylates specific residues in class II *histone deacetylase* (HDAC) 7 creating 14-3-3 binding sites, which facilitates the nuclear export of HDAC7. This in turn relieves target genes in the nucleus from HDAC repression, leading to VEGF expression that promotes proliferation and migration in endothelial cells, a key step in angiogenesis[96,121,122]. During osteoblast differentiation, BMP-2 induces PKD activation resulting in HDAC7 phosphorylation and its nuclear export, releasing Runx2 from repression[123,124]. Phosphorylation of HDAC5/7 by PKDs also occurs in lymphocytes in which the PKD-HDAC axis regulates Nur77 expression and apoptosis[95,125]. In cardiomyocytes, PKD-mediated HDAC phosphorylation is involved in cardiac remoldeling[126]. Mice with cardiac-specific deletion of PKD1 are partially protected from pathological heart remodeling. PKD phosphorylates HDACs leading to their dissociation from *myocyte enhancer factor* (MEF) 2 and consequently to the expression of MEF2 target genes[105]. Furthermore, PKD and several upstream kinases phosphorylate CREB on Ser133[127]. In the heart, CREB phosphorylation by PKD contributes to pathological cardiac remodeling[128] besides HDAC phosphorylation.

PKDs are involved in cell migration and actin remodeling. PKD1 directly phosphorylates cortactin[98,99], the cofilin phosphatase *slingshot* (SSH) 1L[100], and *p21-*

activated kinase (PAK) 4[101], and thereby decreases cell motility. Furthermore, PKD1 reduces cell migration by phosphorylating *Rab interactor* (Rin) 1[129]. During *epithelial-mesenchymal transition* (EMT), a process in which epithelial cells lose their polarity as well as their cell-cell adhesions and gain migratory and invasive properties, PKD1 phosphorylates the transcription factor Snail, a master regulator of EMT that represses expression of E-cadherin, resulting in decreased cell adhesion[130,131]. Moreover, PKD1 phosphorylates β-catenin, leading to increased nuclear localization of β-catenin[132]. Together, PKD1 decreases cell motility and EMT, indicating a tumor suppressive role of PKD1[133]. However, PKD isoforms have been reported to be involved in various cancer types, including prostate cancer[134-137], breast cancer[138-141], pancreatic cancer[142-147], skin cancer[148-150], gastric cancer[151,152], and HCC[153] among others[102] with tumor and PKD isoform specific functions. Whereas PKD1 has mainly tumor suppressive functions, PKD2 and PKD3 follow different regulations and functions[154]. For example, in prostate cancer, PKD1 negatively regulates cell proliferation of prostate cancer cells[135-137], whereas PKD2 and PKD3 promote cell proliferation and survival of prostate cancer cells by activating AKT/ERK[134] and NF-κB signaling pathways as well as by increasing the expression of *urokinase-type plasminogen activator* (uPA) and *matrix metalloproteinases 7/9* (MMP-7/9)[155], which mediate cell migration through ECM degradation[138]. Similarly, PKD2 promotes the expression and secretion of MMP7/9 in pancreatic cancer[147]. In contrast, PKD1 inhibits breast cancer cell invasion by suppressing the transcription of several MMPs[138].

PKDs have been described in various metabolic processes. In pancreatic β cells, *mitogen-activated protein kinase* (MAPK) p38δ catalyzes an inhibitory phosphorylation of PKD1, thereby attenuating stimulated insulin secretion through impaired membrane fission at the TGN[109]. In the same cells, PKD1 binds to *phosphatidylinositol 4-kinase* (PI4K) IIα and phosphorylates PI4KIIα at the TGN and thus negatively regulates its activity and insulin secretion[156,157]. PKD1 is activated downstream of GPR40 and is implicated in the second phase of insulin secretion in response to fatty acids in β cells[110]. In adipocytes, deletion of PKD1 promotes energy dissipation and suppresses lipogenesis which protects from diet-induced obesity[158].

However, PKD functions have not been investigated so far in a very important metabolic organ, the liver. Of particular interest is the expression of the PKD isoforms in the liver, since as described above, the individual isoforms have specific functions in different tissues.

1.3 *Mechanistic target of rapamycin* (mTOR)

1.3.1 *mTOR complex* (mTORC) components and downstream signaling

mTOR is a serine/threonine kinase that is a major regulator of cell growth by sensing nutrient availability and nutrient-evoked signals such as insulin, and thus controls many anabolic and catabolic processes (reviewed in [159]). mTOR is the catalytic subunit of mTORC1 and mTORC2. Both complexes consist of mTOR, *mammalian lethal with Sec13 protein 8* (mLST8; also known as GβL), and *DEP-domain-containing mTOR-interacting protein* (Deptor) (reviewed in [160]). *Regulatory-associated protein of mTOR* (Raptor) and *proline-rich AKT substrate 40 kDa* (PRAS40) are specific for mTORC1, whereas *rapamycin-insensitive companion of mTOR* (Rictor), *mammalian stress-activated protein kinase interacting protein* (mSIN1), and *protein observed with Rictor-1* (Protor-1) are exclusively found in mTORC2 (Figure 6) (reviewed in [160]). PRAS40 and Deptor bind to mTORC1 when its activity is reduced and promote its inhibition. Upon activation, mTORC1 directly phosphorylates PRAS40 on Ser183 and Deptor is phosphorylated in an mTORC-dependent manner, thereby reducing the binding affinities of PRAS40 and Deptor, thus further activating mTORC1[161-163]. Furthermore, Deptor can also inhibit mTORC2 activity[161]. mLST8 associates with the kinase domain in mTORC1[164]; however, its deletion does not affect mTORC1 activity, whereas mLST8 is essential in mTORC2 by maintaining Rictor-mTOR interaction[165]. Raptor binds to the mTOR signaling motif of mTORC1 substrates and recruits them, and Raptor regulates the subcellular localization of mTORC1 (reviewed in [166]). Rictor and mSIN1 bind to each other, resulting in a stabilization of the two components. Another binding partner of Rictor is Protor-1, whose physiological relevance is unclear (reviewed in [160]). mTORC1 is sensitive to acute rapamycin treatment, whereas mTORC2 is only sensitive to chronic rapamycin treatment, which was shown to disrupt its structure (reviewed in [160]).
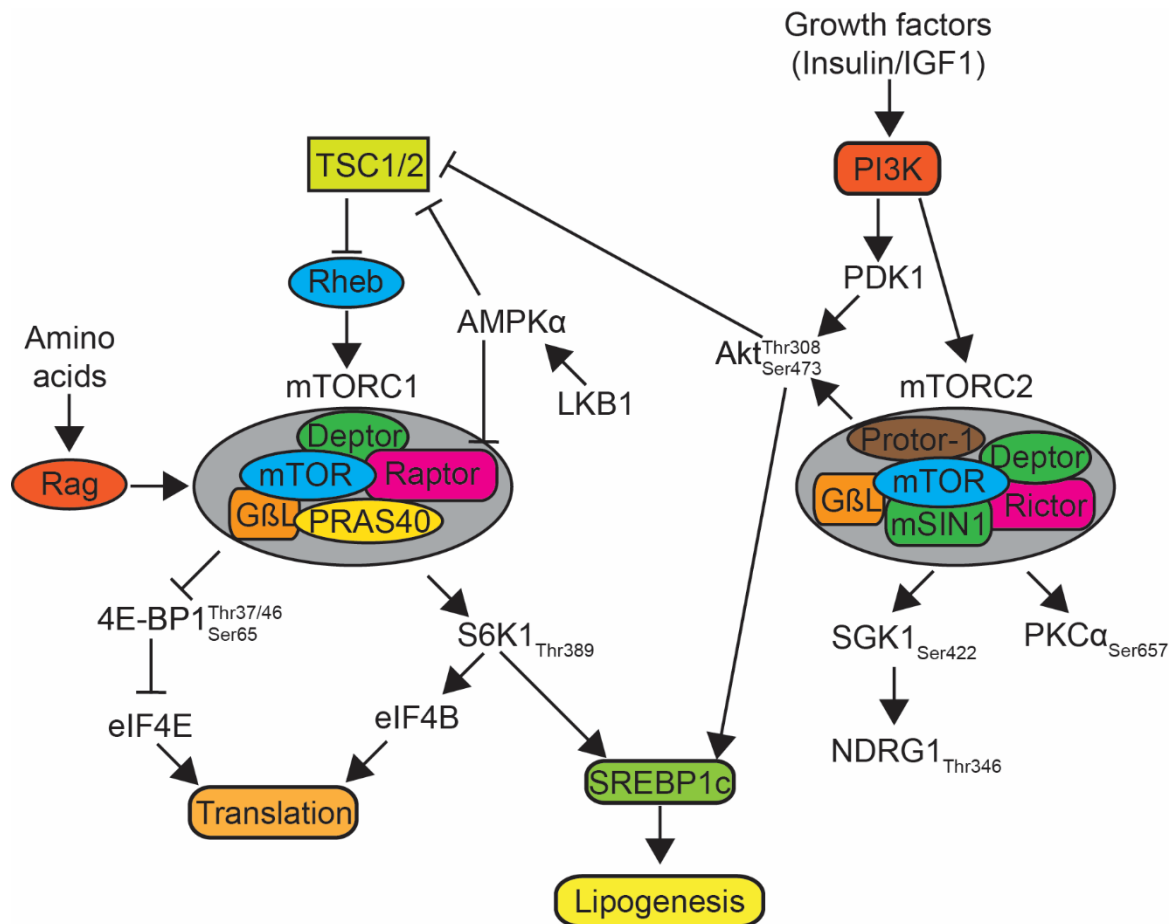
Figure 6: Schematic overview of mTORC signaling. Major components and regulators of mTORC1 and mTORC2 signaling as well as downstream targets. mTORC1 contains mTOR, Raptor, mLST8, PRAS40, and Deptor. mTORC2 contains mTOR, Rictor, mLST8, mSin1, Deptor, and Protor-1. Downstream effectors regulate lipogenesis, translation, autophagy, and lysosomal localization (not shown). *Phosphoinositide 3-kinase* (PI3K); *3-phosphoinositide-dependent protein kinase* (PDK); *protein kinase B* (AKT); *tuberous sclerosis complex* (TSC); *Ras homolog enriched in brain* (Rheb); *ras-related GTPase* (Rag); *liver kinase B* (LKB); *AMP-activated protein kinase* (AMPK); m*echanistic target of rapamycin* (mTOR); *mechanistic target of rapamycin complex* (mTORC); *regulatory associated protein of mTOR* (Raptor); *rapamycin-insensitive companion of mTOR* (Rictor); *mammalian lethal with Sec13 protein 8* (mLST8; also known as GβL); *DEP-domain-containing mTOR-interacting protein* (Deptor); *proline-rich AKT1 substrate 1* (PRAS40); *mammalian stress-activated protein kinase interacting protein 1* (mSIN1); *protein observed with Rictor-1* (Protor-1); *eIF4E-binding protein* (4E-BP); *eukaryotic translation initiation factor 4E* (eIF4E); *p70 ribosomal S6 kinase* (S6K); *eukaryotic translation initiation factor 4B* (eIF4B); *sterol regulatory element binding protein* (SREBP); *serum and glucocorticoid-regulated kinase* (SGK); *N-myc downstream regulated* (NDRG); *protein kinase C* (PKC).

During cell growth, nutrients are produced and anabolic processes such as autophagy are inhibited. These pathways are regulated by mTORC signaling (reviewed in[167]). Activation of mTORC1 leads to a direct phosphorylation of *p70 ribosomal S6 kinase* (S6K) 1 on Thr389 and *eukaryotic translation initiation factor 4E (eIF4E)-binding protein* (4E-BP) 1 on Thr37/46 and Ser65. S6K1 phosphorylates many substrates that promote *messenger ribonucleic acid* (mRNA) translation, including *eukaryotic translation initiation factor* (eIF4B) on Ser422[168], *ribosomal protein S6* (rPS6) on

Introduction

Ser235/236[169]; however, this mechanism has been challenged. It was proposed that rpS6 is rather phosphorylated by a MAPK-dependent kinase[170], and *programmed cell death protein* (PDCD) 4 on Ser67, an inhibitor of eIF4A, which undergoes degradation following the phosphorylation by S6K[171]. By contrast, S6K2 that is phosphorylated on Thr388 by mTORC1 appears to have other functions than promoting translation[172]. Hyperphosphorylation of 4E-BP1 on Thr37/46 and Ser65 by mTORC1 disrupts the binding with the translation initiation factor eIF4E, resulting in an activation of cap-dependent translation[173,174].

mTORC2 phosphorylates the AGC protein kinase family members PKC, AKT, and *serum and glucocorticoid-regulated kinase* (SGK) (reviewed in[167]). Phosphorylation of PKCα on Ser657[175], PKCδ[176], PKCζ[177], and possibly other PKCs (PKCγ and PKCε)[178] in the hydrophobic motif by mTORC2 regulates actin cytoskeleton reorganization and cell migration. SGK1, a kinase involved in ion transport and growth, is activated by mTORC2 through phosphorylation of Ser422 in the hydrophobic motif. Like S6K and other AGC kinases, SGK1 is phosphorylated by PDK1 in the T-loop[179]. SGK1 in turn phosphorylates the metastasis suppressor *N-myc downstream regulated* (NDRG) 1 on Thr346[180-182] which is involved in myelinating Schwann cells, lipogenesis, and adipogenesis[183,184]. Importantly, mTORC2 phosphorylates the key effector of insulin/PI3K signaling AKT on Ser473[185]. AKT in turn phosphorylates the mTORC1 inhibitor *tuberous sclerosis complex* (TSC) 2[186-188], FOXO1/3a transcription factors, and *glycogen synthase kinase* (GSK) 3β promoting cell survival, proliferation, and growth (reviewed in [167]).

Introduction
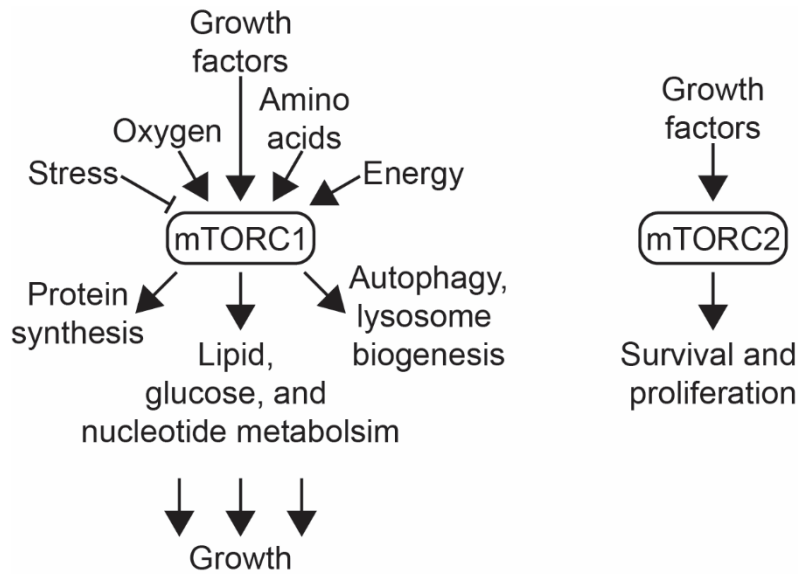
Figure 7: mTORC1 and mTORC2 signaling pathways. Upstream effectors of mTORC1 and mTORC2 as well as downstream pathways. *Mechanistic target of rapamycin complex* (mTORC). (modified from Saxton, 2017)[167]

Metabolites – such as lipids, glucose, and nucleotides – are also required for cell growth (Figure 7). mTORC1 promotes de novo lipogenesis in an S6K1-dependent manner by activating the maturation of SREBP[189,190], a master regulator of lipo- and sterolgenic gene transcription[15]. In addition, mTORC1-activated S6K1 phosphorylates *serine/threonine-protein kinase* (SRPK) 2 at Ser494, resulting in nuclear translocation of SRPK2 and in enhanced splicing of lipogenic pre-mRNAs by phosphorylated SR proteins[191]. Moreover, mTORC1 promotes lipogenesis by phosphorylating the phosphatidic acid phosphatase lipin 1, which prevents lipin 1 from repressing SREBP in the nucleus[22]. mTORC1 also promotes purine synthesis through activation of the transcription factor ATF4[192] and pyrimidine synthesis by phosphorylating CAD (*carbamoyl-phosphate synthetase 2, aspartate transcarbamoylase, dihydroorotase*) on Ser1859 in an S6K1-dependent manner[193]. Furthermore, mTORC1 stimulates glycolysis by promoting the translation of *hypoxia-inducible factor* (HIF) 1α, which activates the transcription of glycolytic genes[190]. To promote cell growth, mTORC1 also suppresses protein catabolism by regulating autophagy and liposomal biogenesis (reviewed in [166]). Under nutrient deprivation, mTORC1 directly phosphorylates and inhibits the autophagy-initiating kinase ULK1 (*Unc-51 like autophagy activating kinase 1*) on Ser757 as well as ULK1-associated ATG13 at multiple residues[194-196]. AMPK, a key activator regulating autophagy, activates ULK1 which is suppressed by mTORC1-mediated phosphorylation of ULK1[196]. In addition, mTORC1 directly phosphorylates

and inhibits other factors involved in autophagy induction such as *class III PtdIns 3-kinase* (PIK3C3, also known as VPS34)[197] and the *transcription factor EB* (TFEB) whose nuclear translocation is inhibited, resulting in suppressed expression of genes involved in autophagy and lysosomal biogenesis[198-201]. mTORC1 signaling also regulates proteasomal activity (reviewed in [167]). Acute mTORC1 inhibition increases overall protein ubiquitination and thus targeting them for proteasomal degradation[202], and mTORC1 induces the abundance of proteasomal chaperones and subunits by inhibiting ERK5[203], whereas chronic mTORC1 activation increases proteolysis by inducing the expression of proteasomal subunits downstream of NRF1[204] (Figure 7).

1.3.2   Upstream effectors of mTORC1 and mTORC2

Tuberous sclerosis complex (TSC), a heterotrimeric complex consisting of TSC1 (also known as hamartin), TSC2 (also known as tuberin), and TBC1D7, was identified as a key negative regulator of mTORC1 signaling[186,205,206]. TSC controls mTOR signaling by acting as a *GTPase activating protein* (GAP) towards inhibiting Rheb (*Ras homolog enriched in brain*) GTPase[205,207,208], a factor that directly binds to and activates mTORC1[209]. Various growth factors control the activity of TSC. The MAP kinase ERK and its effector *p90 ribosomal S6 kinase* (RSK) 1 phosphorylate and inhibit TSC2 in response to receptor tyrosine kinase-dependent Ras signaling[210,211]. Insulin and *insulin-like growth factor* (IGF)-1 stimulated AKT phosphorylation inhibits TSC2 by phosphorylating it on multiple sites[186,187] and thus promoting the dissociation of TSC from lysosomal membranes where Rheb localizes[212]. Alternatively, AKT directly phosphorylates PRAS40, which is crucial for insulin stimulation of mTOR activity[213]. Furthermore, *tumor necrosis factor* (TNF) α signaling-activated *IκB kinase* (IKK) β phosphorylates TSC1 at Ser487 and Ser511, resulting in suppression of TSC1 and ultimately activation of mTORC1[214], whereas TSC2 integrates Wnt and energy signals via AMPK and GSK3 to regulate mTORC1-mediated cell growth[215]. Generally, AMPK itself is activated in response to low energy levels (ATP, glucose) or stress (hypoxia, DNA damage), leading to mTORC1 inhibition through direct phosphorylation of Raptor or indirectly through phosphorylation and activation of TSC2[167,205,216,217]. However, glucose deprivation, hypoxia, and DNA-damage response can increase TSC activity also independent of AMPK (reviewed in [167]). Additionally, mTORC1 is also activated by an increased level of amino acids which is sensed through the *Ras-related GTPase* (Rag)[218,219]. Rags are heterodimers of RagA or RagB with RagC or RagD and are

bound to the lysosomal membrane through the Ragulator complex[167,220,221]. Upon amino acid stimulation, Rag is activated and binds to Raptor and thus recruits mTORC1 to the lysosomal membrane where Rheb also resides (reviewed in [166,167]).

mTORC1 senses cytosolic and intra-lysosomal amino acids through multiple mechanisms. Cytosolic leucine and arginine activate mTORC1 through the GATOR complex that has a GAP activity towards RagA and RagB[222]. GATOR consists of the tetrameric GATOR1 and the pentameric GATOR2 subcomplexes. Inhibition of GATOR1 makes mTORC1 signaling resistant to amino acid deprivation, whereas inhibition of GATOR2 suppresses mTORC1 signaling[222]. Moreover, the mTORC1 positive regulator GATOR2 is negatively regulated by the cytosolic leucine sensors Sestrin1 and 2[223-226]. During leucine deprivation, Sestrin2 binds and inhibits GATOR2 which is disrupted upon leucine binding to Sestrin2, resulting in mTORC1 activation[225,226]. Furthermore, the *cellular arginine sensor for mTORC1* (CASTOR) 1/2 is a cytosolic arginine sensor that binds to GATOR2 upon arginine deprivation[227,228]. In contrast, binding of arginine disrupts the CASTOR-GATOR association and thus leads to mTORC1 activation[227,228]. Similarly, *S-adenosylmethionine* (SAM) *sensor upstream of mTORC1* (SAMTOR) senses methionine in form of SAM[229]. Binding of SAM to SAMTOR disrupts the SAMTOR-GATOR1 interaction and thereby promotes mTORC1 activity[229]. Intra-lysosomal amino acids activate mTORC1 through Rag in a process that requires interaction of *vacuolar H^+-ATPase* (v-ATPase) with the Ragulator[221,230]. Lysosomal arginine activates mTORC1 through SLC38A9, a lysosomal amino acid transporter that interacts with the Rag-Ragulator-v-ATPase complex[231-233].

Unlike mTORC1, mTORC2 mainly functions as a downstream effector of insulin/PI3K signaling. PtdIns(3,4,5)P$_3$ interacts with the PH domain of mSIN1 to release its ability to inhibit mTOR[234]. In addition, partially phosphorylated AKT (Thr308) directly phosphorylates mSIN1 on Thr86, leading to mTORC2 activation and phosphorylation of AKT on Ser473 by mTORC2 (positive-feedback loop)[235]. Moreover, insulin-stimulated PI3K promotes mTORC2 activation through mTORC2-ribosome binding, suggesting that ribosomes directly activate mTORC2[236]. mTORC2 activity is also regulated through negative feedback-loops from mTORC1 and its substrates (reviewed in [167]). Activated S6K1 represses IRS gene expression and degradation through direct IRS phosphorylation[237,238] and mTORC1 phosphorylates the adaptor protein Grb10 that mediates inhibition of PI3K upstream of AKT and mTORC2[239,240].

1.3.3 Impact of mTOR signaling on liver physiology

Besides promoting cell growth and survival, mTOR signaling has multiple other functions in adipose tissue, muscle, and brain, as well as in immunity, aging, and cancer (reviewed in [167,241]). In the liver, mTOR signaling has many physiological roles. Active mTOR complexes promote SREBP-dependent de novo lipogenesis and HIF1α-dependent glycolysis to support cell growth[190]. However, this means at the same time that dysregulated mTOR signaling can have pathophysiological implications.

In the liver, active mTOR promotes glucose and ketone bodies production upon fasting. Liver-specific deletion of TSC1 results in constitutive active mTORC1, leading to a defect in ketogenesis upon fasting as hyperactivated mTORC1 suppresses the activity of *peroxisome proliferator activated receptor* (PPAR) α, the master regulator of ketogenic gene expression during fasting[242]. In addition, mTORC is a positive regulator of de novo lipogenesis (reviewed in [243]). Activated mTORC1 promotes lipogenic gene expression through SREBP[189,190]. In the liver, mTORC1 regulates the nuclear localization of the SREBP-effector lipin 1, thereby regulating lipo- and sterolgenic gene expression[22]. Alternatively, mTOR phosphorylates *CREB regulated transcription coactivator* (CRTC) 2 and attenuates its inhibitory effect on COPII-dependent SREBP1 maturation[244]. Other results suggest a mechanism in which mTORC1-independent ('free') Raptor negatively regulates hepatic AKT activity and lipogenesis through reduced degradation of the AKT phosphatase *PH domain and leucine rich repeat protein phosphatase* (PHLPP) 2 and decreased AKT activity, thus promoting lipogenesis[245]. Consistently, hepatocyte-specific deletion of TSC1 not only results in reduced hepatic triglyceride content but also in depletion of hepatic and plasma glutamine, leading to PGC-1α–dependent expression of *fibroblast growth factor* (FGF) 21 in the liver[246], a regulator of hepatic lipid levels[247]. Furthermore, stress-inducible Sestrins activate AMPK and suppress mTORC1-S6K activity in liver. Deletion of Sestrin2 and 3 provokes hepatic mTORC1-S6K activation, glucose intolerance, insulin resistance, and hepatosteatosis[248]. Similarly, pharmacological intervention with metformin inhibits hepatic mTORC1 signaling via dose-dependent mechanisms involving AMPK and the TSC complex[249].

Hepatic mTORC2 also regulates de novo lipogenesis and glycolysis[250,251]. Liver-specific Rictor knockout mice display reduced AKT phosphorylation on Ser473 as well as reduced glucokinase and SREBP1c activity in the liver, leading to constitutive gluconeogenesis, impaired glycolysis and lipogenesis, and ultimately to systemic

hyperglycemia, hyperinsulinemia, and hypolipidemia[250]. Prolonged treatment with rapamycin also inhibits mTORC2 signaling in vivo, because liver-specific Raptor knockout mice (despite lacking hepatic mTORC1 activity) display normal glucose tolerance and remain responsive to rapamycin treatment[252].

Taken together, mTORC1 and mTORC2 regulate lipid and glucose homeostasis in the liver through multiple mechanisms. Dysregulation of mTOR signaling can lead to the development of hepatosteatosis, hepatic insulin resistance, hyperglycemia and thus to T2D.

1.4 Phenylalanine and tyrosine metabolism

The liver plays a central role in the complex *amino acid* (AA) metabolism. AAs are used to form proteins or can be metabolized and used as substrates for other pathways. AAs are either glucogenic or ketogenic depending on their ability to be transformed into pyruvate and molecules of the TCA cycle to contribute to the production of glucose or into the ketone bodies acetyl-CoA and acetoacetyl-CoA. In addition, AAs undergo transaminations and deaminations, leading ultimately to ureagenesis (reviewed in [253]). An important step in the AA metabolism is the conversion from the essential AA phenylalanine to the conditionally essential AA tyrosine. The enzyme *phenylalanine hydroxylase* (PAH) catalyzes the hydroxylation on the aromatic side chain by using *tetrahydrobiopterin* (BH4) as cofactor for the reaction (Figure 8)[254,255].
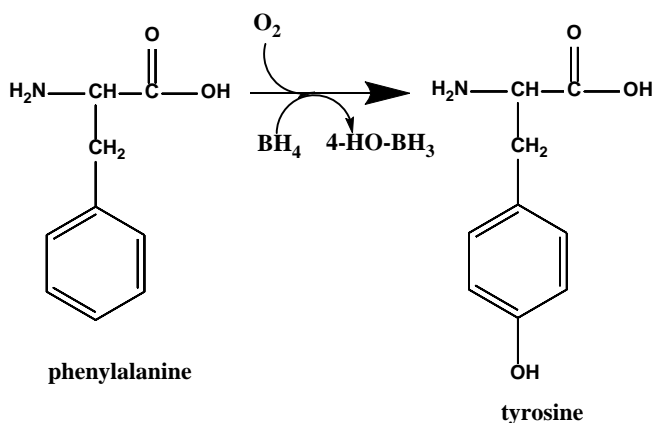
Figure 8: PAH catalyzes hydroxylation of phenylalanine leading to tyrosine.

PAH along with tyrosine hydroxylase, and tryptophan hydroxylase belong to the family of aromatic amino acid hydroxylases (reviewed in [255]), and is mainly found in liver and to a smaller extent in the kidney[256]. Deficiency or mutations in PAH are associated with

the metabolic disorders of classic *phenylketonuria* (PKU), mild PKU, or mild *hyperphenylalaninemia* (HPA) that are classified based on blood *phenylalanine* (Phe) concentrations (reviewed in [257,258]). The enzymatic activity of PAH is mainly regulated allosterically or by phosphorylation. Allosterically, PAH is activated by high phenylalanine concentrations and inhibited by BH_4 (reviewed in [259]). The other mode of regulation is phosphorylation of PAH, resulting in more active PAH[260]. Upstream of PAH, glucagon was shown to induce phosphorylation of PAH[261,262]. This is in line with the observation that glucagon regulates amino acid turnover in liver. Patients with glucagon-producing tumors (glucagonomas) have accelerated amino acid turnover and ureagenesis (reviewed in [253]). In vitro, a few kinases were reported to phosphorylate PAH on Ser16[263-266]. The most prominent among them is *cAMP-dependent protein kinase A* (PKA) as glucagon stimulation leads to the intracellular activation of PKA. Ser16 as phosphorylation site of PAH was confirmed by substituting serine with glutamic acid (S16E) in human or rat PAH, resulting in activated PAH at the same level as phosphorylated PAH[267,268]. Phosphorylation of PAH on Ser16 results in a moderate increase of PAH activity, which is by far not as highly induced as by Phe treatment[260]. However, it was shown that phosphorylation of PAH on Ser16 lowers the Phe concentration required for activation[149,269]. Other kinases phosphorylating PAH or upstream events activating PAH remain unclear.

1.5 Aim of the thesis

Hepatic insulin resistance is a hallmark of T2D characterized by dysregulated glucose and lipid metabolism in hepatocytes[11]. Briefly, hepatocytes fail to suppress gluconeogenesis and glycogenolysis in response to insulin, leading to hyperglycemia in circulation, and to increased lipogenesis rate and lipid accumulation in liver. In this context, correct nutrient sensing and signal transduction is essential and often requires the involvement of protein kinases. A family of protein kinases that has been shown to be involved in signaling cascades in metabolic organs are protein kinase D isoforms[92]. In particular, signaling of p38δ-PKD1 was shown to regulate glucose homeostasis and insulin secretion in pancreatic β cells by controlling membrane fission at the TGN[109]. More recently, it was reported that deletion of PKD1 in adipocytes protects from diet-induced obesity by suppressing lipogenesis and promoting energy dissipation[158]. During obesity or lipid overload, DAG accumulates in liver and besides being a second messenger, DAG is also an intermediate product of triglyceride synthesis (reviewed

in [37]). PKDs are DAG and PKC effectors that integrate various signaling inputs[57]. However, the impact of DAG-evoked signaling cascades and PKD signaling itself have not yet been investigated in a metabolic highly relevant organ: the liver.

For this reason, the aim of this study was to identify PKD function in liver metabolism by investigating whether PKD signaling has implications on glucose or lipid metabolism as well as on other metabolic pathways in liver. PKDs are differently expressed depending on cell type and tissue, and multiple upstream signaling events activate PKDs[49]. For this reason, the first aim of the thesis was to determine the expression level of the three PKD isoforms in liver and to identify their upstream effectors. In order to study PKD3 function on a physiological level, mice lacking PKD3 specifically in hepatocytes as well as mice that express constitutive active PKD3 in liver were generated. The mice were challenged with physiological and pathophysiological research diets such as *normal diet* (ND) and HFD (which promotes obesity and diabetes) and examined for metabolic alterations globally and in liver. For analyzing the role of PKD3 function in vitro, primary hepatocytes were isolated either from wild type and PKD3-deficient livers, or primary hepatocytes were transduced with adenovirus expressing EGFP control or PKD3ca. Finally, unbiased mass spectrometry-based approaches were applied to identify signaling pathways affected by PKD3 function and the direct substrate of PKD3.

2 Materials and Methods

2.1 Materials

2.1.1 Equipment

Table 1: List of equipment used in this thesis.

Equipment	Specification	Manufacturer/source
Animal ear punch	2 mm	Fine Science Tools
Autoclave	VX-120	Systec
Autoclave sterilizer	DX-100	Systec
Automated tissue processor	ASP200S	Leica
Bench-top homogenizer	PT 1600E	Polytron
Centrifuge	5424 R	Eppendorf
Centrifuge	5810 R; rotor: A-4-62	Eppendorf
Confocal microscope	TCS SP8	Leica
Dionex Ultimate 3000 UHPLC system	hyphenated with a *Q exactive mass spectrometer* (QEMS) equipped with a HESI probe	Thermo Fisher Scientific
Easy-nLC 1000		Thermo Fisher Scientific
Electrophoresis cell	Sub-Cell GT	Bio-Rad
Erlenmeyer flask	1000 mL	Simax
Evaporator	Reacti-Vap™; 9-port; 27-port	Thermo Fisher Scientific
Fluorescence microscope	DM5500 B; illuminator: X-Cite 200DC; camera: Leica DFC365 FX; power supply: CTR HS	Leica
Freezer (-20°C)	profi line GG4310	Liebherr
Freezer (-20°C)	Comfort	Liebherr
Freezer (-80°C)	HERAfreeze HFU666 basic	Thermo Fisher Scientific
Freezing chamber		Thermo Fisher Scientific
Fridge	profi line FKS5000	Liebherr
Fridge-freezer	CP3523-21	Liebherr
Gas burner	Type CFH	A. Hartenstein
Glass bottles	2000 mL; 1000 mL; 500 mL; 250 mL; 100 mL	Duran
Glucometer	Accu-Chek	Roche
Homogenizing pestle	PP-pestle; cone-shaped; 70 mm	Roth
Ice machine		Ziegra
Imager for Gels	Typhoon TRIO	GE Healthcare
Imager for Proteins	Amersham Imager 600	GE Healthcare
Incubator	C150	Binder
Incubator	Heracell 240	Heraeus
Incubator shaker	ISF-1-W	Kuhner
Inverted microscope	CKX31	Olympus
Inverted microscope	IX71	Olympus
Laminar flow cabinet	SB-1200	BDK Luft- und Reinraumtechnik
Liquid scintillation counter	Tri-Carb 2910 TR	Perkin Elmer
Magnetic rack		Thermo Fisher Scientific

Materials and Methods

Equipment	Specification	Manufacturer/source
Magnetic stirrer	MR Hei-Standard	Heidolph
Mass spectrometer	TOF/TOF™ 5800 System	SCIEX
Mechanical piece counter	T120	IVO
Metabolic cage	Indirect calorimetry system PhenoMaster	TSE systems
Mice cage	GM500PFS; lid: for water bottles; water bottle: 300 mL; lid: full length	Tecniplast
Mice cage rack system	Green Line IVC	Tecniplast
Micro scale	AB265-S	Mettler Toledo
Microcentrifuge	Galaxy Ministar	VWR
Microwave		Dynamic
MilliQ water purification system	X-CAD	Millipore
Multi-channel pipette	Transferpette S12 (20 – 200 µL)	Brand
Multimode microplate reader	Spark™ 10M	Tecan
Multiplex ELISA reader	Bio-Plex® MAGPIX™ Multiplex reader	Bio-Rad
Neubauer chamber	0.1 mm Depth	Hecht-Assistant
Nitrogen cell storage tank	Cryosytem 4000	MVE
Nitrogen storage tank	Cryotherm	Apollo
Nuclear magnetic resonance (NMR) analyzer	The minispec LF50	Bruker
Orbitrap analyzer	Orbitrap LC-MS	Thermo Fisher Scientific
Orbitrap fusion	Orbitrap Fusion™ Tribrid™ Mass spectrometer	Thermo Fisher Scientific
pH-meter	FiveEasy	Mettler Toledo
Photometer	BioPhotometer	Eppendorf
PicoView® ion source		New Objective
Pipette	Transferpette S (0.5 – 10 µL)	Brand
Pipette boy		Gilson
Pipette controller	Accu-Jet Pro	Brand
Power supply	PowerPac HC	Bio-Rad
QIAgility		Qiagen
Reacti-block for evaporator	A-1	Thermo Fisher Scientific
Real-time PCR system	QuantStudio 5 real-time PCR system	Thermo Fisher Scientific
Repetitive pipet	Repetman	Gilson
Rotation microtome	RM2255	Leica
Scissors (standard)	Blunt; 13 cm	Fine Science Tools
Scissors (tissue)	Spiky; 10.5 cm	Fine Science Tools
Spot Picker	Ettan	GE Healthcare
Thermal cycler	T100	Bio-Rad
Thermo block	Thermomixer Comfort	Eppendorf
Thermocycler	7900HT Fast Real Time PCR	Thermo Fisher Scientific
TLC adsorbent scraper	13 mm steel blade	Sigma-Aldrich
TLC developing tank		Roth
TLC glass cutter		A. Hartenstein
TLC immersion chamber for plates		Camag
Tweezer (fine)	Tip: 0.8 mm x 0.7 mm	Fine Science Tools
Tweezer (standard)	15.5 cm	Fine Science Tools

Materials and Methods

Equipment	Specification	Manufacturer/source
UV-/Vis-spectral photometer	Nanodrop 2000c	Thermo Fisher Scientific
UV-transilluminator	UVT-28 ME; camera: EASY 440K	Herolab
Vacuum concentrator	Concentrator 5301	Eppendorf
Vacuum pump	BVC 21	Vacuubrand
Volumetric flask	2000 mL; 1000 mL; 250 mL; 100 mL	Vitlab
Vortexer	RS-VA 10	Phoenix Instrument
Water bath	TW8	Julabo
Water bath	WB20	P-D Industriegesellschaft
X-ray film processor	Cawomat 2000 IR	CAWO

2.1.2 Consumables

Table 2: List of consumables used in this thesis.

Consumable	Specification	Manufacturer/source
384-well plate	MicroAmp Optical	Thermo Fisher Scientific
5 kDa MWCO spin column		GE Healthcare
96-well plate	Nunc-Immuno; MaxiSorp	Thermo Fisher Scientific
Adhesive film	PCR compatible	Thermo Fisher Scientific
Aluminium foil	15 µm	A. Hartenstein
Blotting and chromatography papers	Grade 3 mm CHR; 46 x 57 cm	Whatman
Capillary columns	PicoFrit, 30 cm x 150 µm ID	New Objective
Catheter	Vasofix Safety IV cannulae G22	B. Braun
Cell culture chamber	8-well on PCA detachable	Sarstedt
Cell scraper	24 cm	Techno Plastic Products
Cell strainer	100 µm	Corning
Collagen type I-coated plate	6-well; 12-well, 96-well	Corning
Cover slips	Round; 20 mm diameter	Roth
Cover slips	24 x 60 mm	Roth
Cryo tube	1.8 mL	Sarstedt
Cuvette	10 x 4 x 45 mm	Sarstedt
Filter papers	185 mm	Macherey-Nagel
Glucometer stripes	ACCU-CHEK Inform II test strips (50)	Roche
Immobilon-P transfer membrane [*polyvinylidene fluoride* (PVDF)]	0.45 µm	Millipore
IPG strip holder		GE Healthcare
Microcapillary pipette	Hirschmann; volume 1-5 µL	Sigma-Aldrich
Microscope slide	26 x 76 mm	Roth
Microscope slide	Superfrost; 26 x 76 mm	Thermo Fisher Scientific
Needle	26 *gauge* (G) x 3/8"; 0.45 mm x 10 mm	BD Microlane
Petri dish	92 x 16 mm	Sarstedt
Pipette	Serological; 2 mL; 5 mL; 10 mL; 25 mL	Sarstedt
Pipette filter tips	Biosphere; 20 µL; 200 µL; 1250 µL	Sarstedt
Pipette syringes	500 µL; 1250 µL; 2500 µL	VWR

Materials and Methods

Consumable	Specification	Manufacturer/source
Pipette tips	20 µL; 200 µL; 1000 µL	Sarstedt
Porous spherical silica	ReproSil-Pur 120 C18-AQ; 1.9 µm	Dr. Maisch
QIAgility tips	50 µL	Qiagen
Reaction tube	Conical; 15 mL, 50 mL	Sarstedt
Reaction tube	1500 µL; 2000 µL; 5000 µL	Sarstedt
Reaction tube	Multiply-µStrip; Pro8; 200 µL	Sarstedt
Reagent reservoir	Disposable; Pre-sterile; 50 mL	VWR
Repetative pipette tips	0.1 mL; 0.5 mL; 1.25 mL; 2.5 mL; 5 mL; 12 mL	VWR
Scintillation vial	Pony Vial, 6 mL	Perkin Elmer
Seal foil	Parafilm	Roth
Silica-matrix columns	Strata SI-1 Silica 100 mg/1 mL tubes	Phenomenex
Sterile filter	Filtropur; pore size: 0.2 µm; 0.45 µm	Sarstedt
Syringe	Omnifix; 1 mL; 5 mL; 10 mL; 20 mL	B. Braun
Syringe	Omnican; U-100 Insulin; 1 mL/100 I.U.; 30 G x 1/2"; 0.3 mm x 12 mm	B. Braun
Syringe	Tuberculin; 1 mL	Chirana T. Injecta
Tips used for desalting and concentrating peptides	Zip-tip C18	Merck
Tissue culture dishes	10 cm; 6 cm	Sarstedt
TLC plate	Silica gel 60	Merck
UPLC-column	Acclaim RSLC 120 C8 reversed-phase column (2.2 µm particles, 50 × 2.1 mm)	Thermo Fisher Scientific
Well plates	6-well; 12-well, 96-well	Sarstedt
X-ray films	Super RX-N	Fujifilm

2.1.3 Chemicals and reagents

Table 3: List of chemicals and reagents used in this thesis.

Chemicals and reagents	Manufacturer	Identifier
$[^3H]\text{-}H_2O$	Hartmann Analytic	#ART0194
1,4-Dithiothreitol (DTT)	Sigma-Aldrich	#10197777001
12-molybdophosphoric acid	Alfa Aesar	#56166
2'-deoxynucleoside 5'-triphosphate (dNTP) mix (2 mM each):	Thermo Fisher Scientific	#R0242
Acetic acid	Roth	#3738.1
Acetonitrile	Sigma-Aldrich	#271004
Acrylamide	AppliChem	#A4989
Agar	Sigma-Aldrich	#A1296
Agarose	Roth	#2267.4
Albumin fraction V	Roth	#8076.2
Ammonium bicarbonate (NH_4HCO_3)	Sigma-Aldrich	#09830
Ammonium chloride (NH_4Cl)	Sigma-Aldrich	#A9434
Ammonium peroxidisulphate (APS)	Roth	#9592.2
Ampicillin	Sigma-Aldrich	#A0166
Bovine serum albumin (BSA)	Sigma-Aldrich	#A7030
Bromophenol blue	Roth	#A512.1

Materials and Methods

Chemicals and reagents	Manufacturer	Identifier
Butanol	Merck	#8222622500
Calcium chloride (CaCl$_2$)	Roth	#CN93.1
Cerium (IV) sulfate	Sigma-Aldrich	#359009
CHAPS	Roth	#1479.3
Chloroform (CHCl$_3$)	Roth	#Y015.1
Cholesterol	Sigma-Aldrich	#C8867
Cholesteryl palmitate	Sigma-Aldrich	#C6072
Coomassie brilliant blue	Sigma-Aldrich	#B0770
Cy®3 Maleimide Mono-Reactive Dye	GE Healthcare	#PA23031
Cy®5 Maleimide Mono-Reactive Dye	GE Healthcare	#PA15131
Dimethylformamid (DMF)	Sigma-Aldrich	#33120-M
DNA loading dye solution, 6x	Sigma-Aldrich	#G2526
Dry milk; fat-free	Roth	#T145.4
Earle's balanced salt solution (EBSS) (without Ca^{2+}/Mg^{2+})	Thermo Fisher Scientific	#14155048
Enhanced chemiluminescence (ECL) substrate	Bio-Rad	#170-5061
Eosin G solution	Roth	#3139.2
Ethanol; absolute	Roth	#5054.1
Ethanol; denatured	Roth	#K928.3
Ethyl acetate	Sigma-Aldrich	#34858
Ethylenediaminetetraacetic acid (EDTA)	Roth	#8040.1
Formalin	Sigma-Aldrich	#HT501128
Formic acid	Sigma-Aldrich	#106526
Formic acid (98-100%) for LC/MS	Sigma-Aldrich	#5.33002
Free fatty acid (FFA) standard	Wako Diagnostics	#276-76491
GeneRuler 1 kbp DNA ladder	Thermo Fisher Scientific	#SM0311
GeneRuler 100 bp DNA ladder	Thermo Fisher Scientific	#SM0241
Glucose	Roth	#X997.2
Glycerol	Roth	#3783.1
Glycerol standard	Sigma-Aldrich	#G7793
Glycine	Roth	#3790.3
Glycine	Sigma-Aldrich	#G8790
Goat serum	Sigma-Aldrich	#G9023
Hank's balanced salt solution (HBSS) (with Ca^{2+}/Mg^{2+})	Biochrom (Merck)	#L2035
Heptane	Sigma-Aldrich	#32287-M
Hexane	Sigma-Aldrich	#34859-M
Hoechst 33342 dye	Thermo Fisher Scientific	#62249
Hydrochloric acid (HCl)	Sigma Aldrich	#30721
Hydrogen peroxide (H$_2$O$_2$)	Sigma-Aldrich	#31642
Hydrophobic pen; Roti®-Liquid barrier marker	Roth	#AN91.1
Ibuprofen	Sigma-Aldrich	#I110
Immersion liquid type G	Leica	#11513910
Insulin (100 I.E./mL)	Sanofi Aventis	Insuman rapid
Iodoacetamide	Sigma-Aldrich	#I6125
Isopropanol	Roth	#CP41.3
Kanamycin sulfate	Sigma-Aldrich	#K1377

Materials and Methods

Chemicals and reagents	Manufacturer	Identifier
Ketamine	Pharmacia (Pfizer)	Ketavet
Lamivudine	Sigma-Aldrich	#L1295
L-phenylalanine	Sigma-Aldrich	#P5482
L-serine	Sigma-Aldrich	#S4311
L-tyrosine	Sigma-Aldrich	#T8566
Lysine	Sigma-Aldrich	#62840
Magnesium chloride (MgCl$_2$)	Roth	#KK36.1
Magnesium sulfate (MgSO$_4$)	Sigma-Aldrich	#M2643
Mayer's hematoxylin solution	Sigma-Aldrich	#MHS16
Methanol (MeOH)	Sigma-Aldrich	#34860
Methanol (MeOH)	Roth	#4627.3
Midori green advance DNA stain	Nippon Genetics	#MG04
Mounting medium; Roti®-Mount	Roth	#HP68.1
NEBNext multiplex oligos for Illumina	NEB	#E7335
Nonadecanoic acid	Sigma-Aldrich	#N5252
Nonidet P-40 (NP-40)	Sigma-Aldrich	#74385
NuPAGE® *lithium dodecyl sulfate* (LDS) sample buffer	Thermo Fisher Scientific	#NP0007
NuPAGE® Novex® 4-12% Bis-Tris gels	Thermo Fisher Scientific	#NP0321PK2
NuPAGE™ MOPS SDS running buffer (20X)	Thermo Fisher Scientific	#NP0001
Oleic acid	Sigma-Aldrich	#O1008
PageRuler® prestained protein ladder	Thermo Fisher Scientific	#26619
Paraformaldehyde (PFA)	Roth	#0335.2
Pharmalytes	GE Healthcare	#17-0456-01
Phosphate-buffered saline (PBS)	Sigma-Aldrich	#P3813
Phosphatidylcholine	Sigma-Aldrich	#P3556
Phosphatidylethanolamine	Sigma-Aldrich	#P7943
Pierce™ IP Lysis Buffer	Thermo Fisher Scientific	#87787
Pierce™ Protein A/G Magnetic Beads	Thermo Fisher Scientific	#88803
Porcine trypsin protease	Promega	#V5280
PowerUp™ SYBR™ green master mix	Thermo Fisher Scientific	#A25742
ProLong Gold Antifade Mountant with *4',6-diamidino-2-phenylindole* (DAPI) mounting reagent	Thermo Fisher Scientific	#P36931
Protease and phosphatase inhibitor (PPI) cocktail (100x)	Thermo Fisher Scientific	#78442
QIAzol lysis reagent	Qiagen	#79306
Quick Start™ Bradford 1x dye reagent	Bio-Rad	#5000205
Scintillation fluid	Zinsser Analytic	#1008000
Simply Blue™ safe stain	Thermo Fisher Scientific	#LC6060
Sodium chloride (NaCl)	Roth	#3957.1
Sodium dodecyl sulfate (SDS) pellets	Roth	#CN30.2
Sodium hydroxide (NaOH)	Roth	#P031.1
Sulfuric acid (H$_2$SO$_4$)	Sigma-Aldrich	#30743-M
Tetramethylethylenediamine (TEMED)	Carl Roth	#2367.1
Thiourea	Sigma-Aldrich	#T7875
Tridecanoic acid	Sigma-Aldrich	#T0502
Trifluoroacetic acid	Sigma-Aldrich	#302031
Triolein	Sigma-Aldrich	#T7140

Materials and Methods

Chemicals and reagents	Manufacturer	Identifier
TRIS base	Roth	#AE15.4
Triton X-100	Roth	#3051.3
Trypton/Pepton from casein	Roth	#8952.2
Tween 20	Roth	#9127.1
Tyloxapol (Triton WR1339)	Sigma-Aldrich	#T0307
UltraPure™ distilled water (Dnase/Rnase Free)	Thermo Fisher Scientific	#10977-035
Urea	Sigma-Aldrich	#U0631
Xylazine	cp-pharma	Xylavet
Xylol	Roth	#9713.3
Yeast extract	AppliChem	#A1552.1
α-cyano-4-hydroxycinnamic acid	Sigma-Aldrich	#70990
β-mercaptoethanol	Sigma-Aldrich	#M3148

2.1.4 Buffers and solutions

All buffers and solutions were prepared in distilled, deionized water (ddH$_2$O) obtained from a MilliQ Water Purification System unless stated otherwise. pH was adjusted with HCl or NaOH, respectively.

Blocking buffer (WB)

	TRIS buffered saline with tween (TBST)
5%	BSA or fat-free dry milk

Blocking buffer (IF)

	PBS
0.5%	BSA
10%	Normal goat serum

Crystal violet staining solution

2%	Crystal violet (90%)
20%	Ethanol

Fixation solution

4%	PFA (in PBS)

5x Laemmli buffer (SDS-PAGE)

300 mM	TRIS, pH 6.8 (2 M stock)
10%	SDS
50%	Glycerol
25%	β-mercaptoethanol
spatual tip	Bromophenolblue

Lysis buffer (DNA Extraction)

100 mM	TRIS, pH 8.5 (1 mM stock)
5 mM	EDTA (0.5 M stock)
200 mM	NaCl (5 M stock)
0.2%	SDS (20% stock)

→ 0.1 mg/mL Proteinase K was added freshly before usage

Materials and Methods

Lysis buffer (WB)

20 mM	TRIS, pH 7.5 (1 M stock)
150 mM	NaCl (5 M stock)
20 mM	β-glycerophosphate
5 mM	$MgCl_2$
5%	Glycerol
0.2%	NP-40
0.2%	Triton X-100
1x	PPI (added before usage)

10x Running/Transfer buffer

250 mM	TRIS
1.92 M	Glycine

1x Running buffer

10%	10x Running buffer
0.5%	SDS (20% stock)

50x Tris-acetate-EDTA (TAE)

2 mM	TRIS
5.7%	Acetic acid
10%	EDTA (0.5 M stock)

1x TAE

2%	50x TAE

1x Transfer buffer

10%	10x Transfer buffer
20%	Methanol

10x Tris-buffered saline (TBS), pH 7.6

0.2 M	TRIS
1.4 M	NaCl

1x TBS

10%	10x TBS

1x TBST

10%	10x TBS
0.1%	Tween 20

10% separating gel (WB – 20 mL)

9.8 mL	ddH_2O
5 mL	TRIS, pH 8.6 (1.5 mM stock)
5 mL	Acrylamide (40% stock)
100 µL	SDS (20% stock)
200 µL	APS (10% stock)
20 µL	TEMED

4% stacking gel (WB – 10 mL)

8.2 mL	ddH_2O
620 µL	TRIS, pH 8.6 (1.5 mM stock)
946 µL	Acrylamide (40% stock)
50 µL	SDS (20% stock)
100 µL	APS (10% stock)
10 µL	TEMED

Materials and Methods

2.1.5 Kits

Table 4: List of kits used in this thesis.

Commercial kit	Manufacturer	Identifier
Bio-Plex Pro Mouse Diabetes 8-plex Assay	Bio-Rad	#171-F7001M
BCA Protein Assay Kit	Thermo Fisher Scientific	#23227
Enzyme Pretreatment Kit	Leica	#AR9551
First Strand cDNA Synthesis Kit	Thermo Fisher Scientific	#K1612
In Situ Cell Death Detection Kit, Fluorescein	Roche (Sigma-Aldrich)	#11684795910
LabAssay Cholesterol	Wako	#294-65801
Mouse Insulin ELISA Kit	Crystal Chem	#90080
NEBNext® Poly(A) mRNA Magnetic Isolation Module	NEB	#E7490S
NEFA Kit: NEFA-HR(2) R1 Set; NEFA-HR(2) R2 Set	Wako	#434-91795; #436-91995
NucleoBond® Xtra Midi	Macherey-Nagel	#740410.50
NucleoSpin® Gel and PCR Clean-up	Macherey-Nagel	#740609.250
NucleoSpin® Plasmid	Macherey-Nagel	#740588.250
Pierce™ Phosphoprotein Enrichment Kit	Thermo Fisher Scientific	#90003
RNeasy Plus Universal Tissue Mini Kit	Qiagen	#73404
Serum TG Determination Kit	Sigma-Aldrich	#TR0100
Serum TG Kit> Free Glycerol Reagent	Sigma-Aldrich	#F6428
Serum TG Kit> Triglyceride Reagent	Sigma-Aldrich	#T2449
Taq DNA Polymerase	Thermo Fisher Scientific	#EP0282
Tyrosine Assay Kit	Cell Biolabs (Biocat)	#MET-5073

2.1.6 Oligonucleotides

Table 5: List of RT-qPCR primers used in this thesis.

Full gene name	Gene name	Forward primer (5' - 3') (upper) Reverse primer (5' - 3') (lower)
3-Hydroxyl-3-methylglutaryl-CoA reductase	*Hmgcr*	CTTGTGGAATGCCTTGTGATTG AGCCGAAGCAGCACATGAT
3-Hydroxyl-3-methylglutaryl-CoA synthase 1	*Hmgcs1*	CCTGGACCGCTGCTAT TGAAAGATCATGAAGCCAAAATCA
7-Dehydrocholesterol reductase	*Dhcr7*	GACCCTCATTAACCTGTCCTTCG CCAGGTTTCATTCCAGAAGAAGTC
Acetyl-CoA carboxylase alpha	*Acaca*	TGGAGAGCCCCACACACA GACAGACTGATCGCAGAGAAAG
Farnesyl diphosphate synthase	*Fdps*	ATGGAGATGGGCGAGTTCTTC CCGACCTTTCCCGTCACA
Farnesyl-diphosphate farnesyltransferase 1	*Fdft1*	CCAACTCAATGGGTCTGTTCCT TGGCTTAGCAAAGTCTTCCAACT
Fatty acid synthase	*Fasn*	CAACATGGGACACCCTGAG GTTGTGGAAGTGCAGGTTAGG
Glucose-6-phosphatase catalytic-subunit	*G6pc*	CGACTCGCTATCTCCAAGTGA GTTGAACCAGTCTCCGACCA
Hypoxanthine phosphoribosyltransferase 1	*Hprt1*	TCCTCCTCAGACCGCTTTT

Materials and Methods

Full gene name	Gene name	Forward primer (5' - 3') (upper) Reverse primer (5' - 3') (lower)
		CCTGGTTCATCGCTAATC
Insulin-induced gene 1	*Insig1*	GAGGTGTCACAGTGGGAAACATAG
		TCTTCATCACACCCAGGACCA
Insulin-induced gene 2	*Insig2*	TGTATATTTTTTGCTGGAGGCATAAC
		TTCAGCAATAACTTTGCATTCATACAT
Lanosterol synthase	*Lss*	ATGAGTTGGGTCGGCAGAGAT
		GCGCTTTTGGTAAGTCCGTG
Mevalonate diphosphate decarboxylase	*Mvd*	ATGGCCTCAGAAAAGCCTCAG
		TGGTCGTTTTTAGCTGGTCCT
Mevalonate kinase	*Mvk*	GCTTCAGCGACTGGACACG
		ACAGGTAGAGAAAGGCAAGCAGA
Phosphoenolpyruvate carboxykinase 1	*Pck1*	CTGCATAACGGTCTGGACTTC
		CAGCAACTGCCCGTACTCC
Protein kinase D1 (in same exon)	*Pkd1*	ATGTGGGAGAAAACGTGGTT
		GGGGATGACGGGCATAAGAG
Protein kinase D2 (in same exon)	*Pkd2*	CTTCGAGATCATCACGGCCA
		CTGTCTCCCAACCCCGAAC
Protein kinase D3 (in same exon)	*Pkd3*	AGGCAGTAACCCACACTGTTT
		TCTGCGCCACATCTAGTCCC
Protein kinase D3	*Pkd3*	GTCTGTCAAATGTATCTCTGCCA
		GGTGAGTATGTGACTCTTCACTG
Ribosomal protein L13a	*Rpl13a*	CCCTCCACCCTATGACAAGA
		GCCCCAGGTAAGCAAACTT
Ribosomal protein lateral stalk subunit P0	*36B4*	GTGTTCGACAATGGCAGCAT
		GACACCCTCCAGGAAGCGA
Stearoyl-CoA desaturase	*Scd1*	CATCATTCTCATGGTCCTGCT
		CCCAGTCGTACACGTCATTTT
Sterol regulatory element binding transcription factor 2	*Srebp2*	GCGTTCTGGAGACCATGGA
		ACAAAGTTGCTCTGAAAACAAATCA
Sterol regulatory element binding transcription factor 1a	*Srebp1a*	CAGACACTGGCCGAGATGTG
		CTTGGTTGTTGATGAGCTGGAG
Sterol regulatory element binding transcription factor 1c	*Srebp1c*	GGAGCCATGGATTGCACATT
		GGCCCGGGAAGTCACTGT

Table 6: List of siRNAs used in this thesis.

siRNA	Manufacturer	Identifier
siGENOME Non-Targeting Control siRNA Pool #1, 5 nmol	GE Dharmacon	#D-001206-13-05
SMARTpool: siGENOME Srebf1 siRNA, 5 nmol	GE Dharmacon	#M-040814-01-0005
SMARTpool: siGENOME Srebf2 siRNA, 5 nmol	GE Dharmacon	#M-050073-01-0005

Materials and Methods

2.1.7 Plasmids

Table 7: List of vectors, plasmids and constructs used in this thesis.

Plasmids	Manufacturer	Identifier
pEGFP-C1	Clontech	#6084-1
pEX-K4 FLAG-mPKD3	synthesized by Eurofins	

2.1.8 Antibodies

2.1.8.1 Primary antibodies

Table 8: List of primary antibodies used in this thesis (for WB, IHC, IF and IP).

Antibody	Clone	Manufacturer	Reference no.
4E-BP1	53H11	Cell Signaling	9644
4E-BP1-pSer^{65}		Cell Signaling	9451
4E-BP1-pThr$^{37/46}$	236B4	Cell Signaling	2855
ACC	C83B10	Cell Signaling	3676
ACC-pSer^{79}	D7D11	Cell Signaling	11818
AKT (pan)	C67E7	Cell Signaling	4691
AKT-pSer^{473}	193H12	Cell Signaling	4058
AKT-pThr^{308}	C31E5E	Cell Signaling	2965
AKT-pThr^{450}		Cell Signaling	9267
AMPKα	D5A2	Cell Signaling	5831
AMPKα-pThr^{172}	40H9	Cell Signaling	2535
CD3		Zytomed	RBK024
CD45R/B220	RA3-6B2	BD Biosciences	553084
Cleaved Caspase-3		Cell Signaling	9661
Collagen type IV		Cedarlane	CL50451AP-1
CPS1		Proteintech	18703-1-AP
CPT2		Proteintech	18703-1-AP
Deptor/DEPDC6		Novus Biologicals	NBP1-49674
ERp72	D70D12	Cell Signaling	5033
Ezrin/Radixin/Moesin (ERM)		Cell Signaling	3142
F4/80	BM8	Linaris	T-2006
FDFT1		Proteintech	13128-1-AP
FLAG		Sigma	F1804/F3165
GAPDH		Sigma	G9545
HMGCS1	D1Q9D	Cell Signaling	42201
IRS-1	D23G12	Cell Signaling	3407
IRS-1-pSer^{612}	C15H5	Cell Signaling	3203
IRS-2		Cell Signaling	4502
Ki-67		Thermo Fisher Scientific	RM-9106-S1
LSS		Proteintech	13715-1-AP
LxRxx[S*/T*] motif		Cell Signaling	4381
mTOR		Cell Signaling	2972
mTOR-pSer^{2448}	D9C2	Cell Signaling	5536
mTOR-Ser^{2481}		Cell Signaling	2974

Materials and Methods

Antibody	Clone	Manufacturer	Reference no.
Myc-Tag	9B11	Cell Signaling	2276
NDRG1		Cell Signaling	5196
NDRG1-pThr^{346}		Cell Signaling	3217
PAH		Proteintech	16347-1-AP
PKD/PKDμ-pSer$^{744/748}$		Cell Signaling	2054
PKD3/PKDv	D57E6	Cell Signaling	5655
PMP70	70-18	Sigma	SAB4200181
Raptor	24C12	Cell Signaling	2280
RCAS1	D2B6N	Cell Signaling	12290
Rictor	53A2	Cell Signaling	2114
Rxx[S*/T*] motif	110B7E	Cell Signaling	9614
S6 Kinase (p70)		Cell Signaling	9202
S6 Kinase (p70)-pThr^{389}	1A5	Cell Signaling	9206
SGK1		Proteintech	23394-1-AP
SGK1-pSer^{422}		Thermo Fisher Scientific	PA5-35427
SREBP-1	2A4	Santa Cruz BT	sc-13551
Syntaxin 6	C34B2	Cell Signaling	2869
TSC1 (Hamartin)		Cell Signaling	4906
TSC2 (Tuberin)	D93F12	Cell Signaling	4308
YAP/TAZ	D24E4	Cell Signaling	8418
α-Tubulin		Cell Signaling	2144
β-Actin		Sigma	A5441

2.1.8.2 Secondary antibodies

Table 9: List of secondary antibodies used in this thesis (for WB and IF).

Antibody	Manufacturer	Reference no.
Donkey anti-Rabbit IgG Alexa Fluor 488	Thermo Fisher Scientific	#A21206
Goat anti-Mouse IgG Alexa Fluor 488	Thermo Fisher Scientific	#A11001
Goat anti-Mouse IgG Alexa Fluor 594	Thermo Fisher Scientific	#A11005
Goat Anti-Mouse IgG Atto 647N	Sigma-Aldrich	#50185
Goat anti-Rabbit IgG Alexa Fluor 594	Thermo Fisher Scientific	#A11012
Goat anti-Rabbit IgG-HRP	GE Healthcare	#RPN4301
Sheep anti-Mouse IgG-HRP	GE Healthcare	#RPN4201

2.1.9 Enzymes

Table 10: List of enzymes used in this thesis.

Enzymes	Manufacturer	Identifier
Collagenase type 1	Worthington	#LS004196
EcoRI	NEB	#R0101
Proteinase K	Thermo Fisher Scientific	#EO0491
SalI	NEB	#R0138
T4 DNA ligase (5 U/μl)	Thermo Fisher Scientific	#EL0014
XhoI	NEB	#R0146

Materials and Methods

2.1.10 Cell culture reagents and media

Table 11: List of cell culture reagents and media used in this thesis.

Cell culture reagents and media	Manufacturer	Identifier
[^{3}H]-acetic acid	Perkin Elmer	#NET003005MC
[^{3}H]-oleic acid	Perkin Elmer	#NET289001MC
1,2-Dioctanoyl-sn-glycerol	Enzo Life Sciences	#BML-DG112-0020
Adenosine triphosphate (ATP)	Sigma-Aldrich	#A2383
Akti-1/2	Sigma-Aldrich	#A6730
Bovine serum albumin (BSA)	Sigma-Aldrich	#A8806
Collagen I Rat Protein, Tail	Thermo Fisher Scientific	#A1048301
CRT0066101	Tocris	#4975
Dimethyl sulfoxide (DMSO)	Sigma-Aldrich	#D8418
DMEM (4.5 g/L D-glucose) w/o Phe and Tyr	US Biological (Biomol)	#D9803-06.25
DMEM (4.5 g/L D-glucose, 1 mM sodium pyruvate, 4.0 mM glutamine)	Thermo Fisher Scientific	#31966-021
DMEM (-glucose, -glutamine, -phenol red)	Thermo Fisher Scientific	#A1443001
Dulbecco's modified eagle media (DMEM) (1 g/L D-glucose) w/o amino acids	US Biological (Biomol)	#D9800-13.10
Dulbecco's phosphate-buffered saline (DPBS)	Thermo Fisher Scientific	#14190-094
Foetal bovine serum (FBS)	Thermo Fisher Scientific	#10270-106
FuGENE 6 Transfection Reagent	Promega	#E2691
Glucagon	Sigma-Aldrich	#G2044
Glucose solution (200 g/L)	Thermo Fisher Scientific	#A24940-01
GlutaMAX (100x)	Thermo Fisher Scientific	#35050-061
Insulin solution human (10 mg/mL)	Sigma-Aldrich	#I9278
KU0063794	Sigma-Aldrich	#SML0382
Lipofectamine RNAiMAX	Thermo Fisher Scientific	#13778075
MitoTracker Red CMXRos	Thermo Fisher Scientific	#M7512
Nonessential amino acids (NEAA) (100x)	Thermo Fisher Scientific	#11140-050
Oleic acid-Albumin from bovine serum	Sigma-Aldrich	#O3008
OptiMEM	Thermo Fisher Scientific	#31985-047
Penicillin/Streptomycin (P/S) (10000 U/mL/10000 µg/mL)	Thermo Fisher Scientific	#15140-122
Percoll PLUS	GE Healthcare	#GE17-5445-02
Rapamycin	Cayman Chemical	#13346
Sodium pyruvate (SP) (100 mM)	Thermo Fisher Scientific	#11360-039
Trypan blue stain	Thermo Fisher Scientific	#15250-061
Trypsin (0.05%)-EDTA	Thermo Fisher Scientific	#25300-054

<u>HEK293T maintenance medium</u>

DMEM (4.5 g/L D-Glucose)

10%	FBS
1%	P/S

<u>HEK293T freezing medium</u>

DMEM (4.5 g/L D-Glucose)

10%	FBS
1%	P/S
5%	DMSO

34

Materials and Methods

Primary hepatocytes maintenance medium	Serum starvation medium
DMEM (4.5 g/L D-Glucose)	DMEM (4.5 g/L D-Glucose)
10% FBS	1% P/S
1% P/S	0.25% BSA

2.1.11 Bacterial strains and media

One Shot™ TOP10 Chemically Competent *E. coli* bacteria were used for cloning (Thermo Fisher Scientific; #C404003).

Lysogeny broth (LB) medium, pH 7.0	LB plates
10 g/L Trypton/Pepton from casein	LB medium
	15 g/L Agar
10 g/L NaCl	Antibiotic
5 g/L Yeast extract	

2.1.12 Cell lines

Human embryonic kidney (HEK) 293T cells were a generous gift from Prof. Dr. Eilers.

2.1.13 Mice and diets

Table 12: List of mouse strains used in this thesis.

Mouse line	Manufacturer	Identifier
B6.loxP-mPKD3-loxP	Michael Leitges	
B6.loxP-STOP-loxP-Tg(mPKD3.S731E/S735E)\4	Made by Cyagen	
B6.Cg-Tg(Alb-cre)21Mgn/J	The Jackson Laboratory	#003574
C57BL/6JRj	Janvier Labs	

Table 13: List of research diets used in this thesis.

Experimental diets	Manufacturer	Identifier
High-fat diet (HFD) with 58 kcal% fat w/sucrose	ResearchDiets	#D12331i
Normal diet (ND)	sniff Spezialdiäten	#V1125-3

Materials and Methods

2.1.14 Software

Table 14: List of software used in this thesis.

Software and algorithms	Manufacturer	Identifier
DAVID functional annotation tool	*National Institutes of Health* (NIH), open source	https://david.ncifcrf.gov/
DeCyder	GE Healthcare	Version 6.5
FastQC script	Babraham Bioinformatics	
GPS Explorer	Applied Biosystems	Version 3.5
Illustrator CS6	Adobe	N/A
Image QuantTL	GE Healthcare	
ImageJ	NIH	https://imagej.nih.gov/ij/
LAS X	Leica	
Mascot search engine	Matrix science	
MaxQuant		Version 1.6.2.2
QIAgility	Qiagen	Version 4.13.5
QuantStudio™ Design & Analysis Software	Thermo Fischer Scientific	
Trace finder software	Thermo Fischer Scientific	

2.2 Methods

2.2.1 In vivo analysis

2.2.1.1 Animals

Conditional liver-specific PKD3-deficient mice (*PKD3^liverΔ/Δ*) were generated by intercrossing PKD3 floxed mice (*PKD3^f/f*) (exon 2 and 4 flanked by loxP sites)[270] with mice carrying the Cre recombinase under the control of the albumin promoter/enhancer (B6.Cg-Tg(Alb-cre)21Mgn/J)[271]. Conditional liver-specific PKD3ca transgenic mice (*TgPKD3ca^liver*) were generated by intercrossing loxP-STOP-loxP-(3xFlag)PKD3ca mice (generated by Cyagen with the PiggyBac transgenic method) with Alb-Cre mice. The two serine residues in the PKD3 kinase domain were mutated to glutamic acid (S731E/S735E), leading to *constitutive active* (ca) form of PKD3 (*PKD3ca*). C57BL/6JRj mice were bought from Janvier Labs and used for PKD inhibitor (CRT0066101) in vivo experiments. Thereby, the mice were randomly assigned to two groups that received either an *intraperitoneal* (i.p.) injection of vehicle or 10 mg/kg BW of CRT0066101 (in 5% DMSO) for 5 consecutive days.
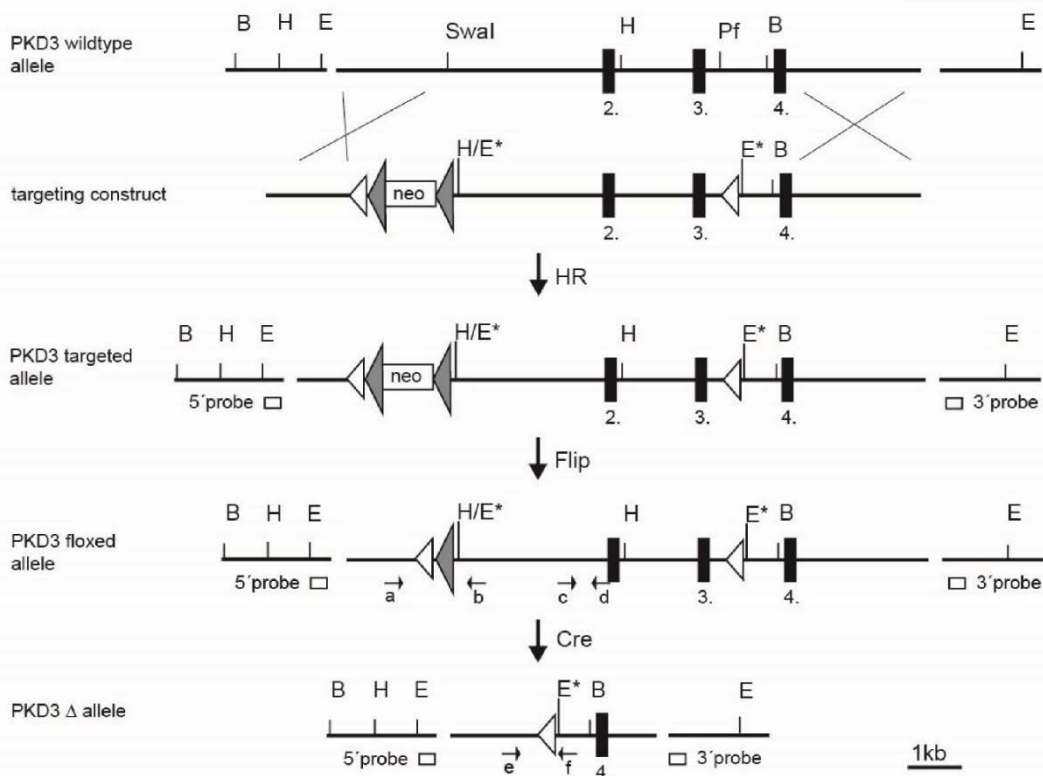
Figure 9: Scheme for generating conditional PKD3-deficient mice. Targeting strategy of the PKD3 mouse locus. The LoxP sites were inserted in the introns flanking exons 2 and 4 by HR with the targeting construct. Crossing of the mice with mice carrying transgenic FLP recombinase removed NEO selection cassette. Finally, conditional PKD3-deficient mice were generated by intercrossing the mice with mice carrying transgenic Cre recombinase. *Homologous recombination* (HR); *flippase* (FLP); *neomycin resistance cassette* (NEO). Picture courtesy of Michael Leitges

Materials and Methods

All animal studies were approved by the local animal welfare authorities (district government of Lower Frankonia, Regierung von Unterfranken) documented under the animal protocol numbers AK55.2-2531.01-124/13 and AK55.2.2-2532-2-741-13.

The mice were housed in groups of maximal five animals in cages (green line IVC-rack system, Tecniplast) with ad libitum supply of water and normal chow diet (ssniff Spezialdiaeten) in a 12 *hours* (h) light/dark cycle at a constant temperature of 23°C and 55% humidity. For HFD-feeding experiments (Research Diets, D12331i), the mice received a high calorie diet (58% kcal from fat) starting after weaning for a duration of 24 weeks, unless otherwise stated. *Body weight* (BW) gain was analyzed by weekly body weight measurements.

For tissue collecting, mice were sacrificed by cervical dislocation or by *carbon dioxide* (CO_2) euthanasia. Blood was withdrawn and organs (liver, gWAT, sWAT, BAT, and SKM) were removed, weighted, and snap frozen in liquid nitrogen or fixed in 10% formalin for histological analysis.

2.2.1.2 Mouse genotyping

2.2.1.2.1 DNA extraction from mouse tissue

Mouse ear tissue was lysed in 500 µL lysis buffer containing 0.1 mg/mL proteinase K overnight at 55°C with continuous shaking at 900 rpm on a thermomixer. The following day, 100 µL of 5 M NaCl was added to the samples, vortexed, and centrifuged at 13000 rpm for 10 min at 4°C. Subsequently, the upper aqueous phase containing the nucleic acids (~500 µL) was transferred to a new tube and supplemented with 500 µL of isopropanol followed by vortexing. Samples were placed at -20°C for 30 min, followed by centrifugation at 13000 rpm for 10 min at 4°C. Next, the supernatant was discarded and the precipitated nucleic acid pellet was washed with 1 mL of 70% ethanol and centrifuged again at 13000 rpm for 10 min at 4°C. The air-dried DNA pellet was solubilized in ddH_2O for 10 min at 55°C while constantly shaking. Genotyping of the mice was performed by a *polymerase chain reaction* (PCR) using specific primers.

Materials and Methods

2.2.1.2.2 PCR for mouse genotyping

2.2.1.2.2.1 Alb-cre mice

PCR mix (20 µL final volume):

2 µL	DNA
2 µL	Thermo buffer-MgCl$_2$
1.6 µL	MgCl$_2$
2 µL	dNTPs (2 mM stock)
1 µL	Primer 'wt' (10 µM)
1 µL	Primer 'common' (10 µM)
1 µL	Primer 'cre' (10 µM)
0.25 µL	Taq polymerase (5 U/µL)
9.15 µL	H$_2$O

PCR program:

Step 1	94°C	2 min
Step 2	94°C	20 s
Step 3	65°C	15 s
	(-0.5v per cycle)	
Step 4	68°C	10 s
→ go to step 2, 10x		
Step 5	94°C	15 s
Step 6	60°C	15 s
Step 7	72°C	10 s
→ go to step 6, 28x		
Step 8	72°C	2 min
Step 9	4°C	∞

Primers for genotyping of *Alb-cre* PCR:

Primer 'wt': 5' – TGC AAA CAT CAC ATG CAC AC – 3'

Primer 'common': 5' – TTG GCC CCT TAC CAT AAC TG – 3'

Primer 'cre': 5' – GAA GCA GAA GCT TAG GAA GAT GG – 3'

Resulting band sizes: WT: 351 bp, cre: 390 bp, cre artifact: 150 bp

2.2.1.2.2.2 PKD3$^{f/f}$ mice

PCR mix (20 µL final volume):

2 µL	DNA
2 µL	Thermo buffer-MgCl$_2$
1.6 µL	MgCl$_2$
2 µL	dNTPs (2 mM stock)
1 µL	Primer forward (10 µM)
1 µL	Primer reverse (10 µM)
0.25 µL	Taq polymerase (5 U/µL)
10.15 µL	H$_2$O

PCR program:

Step 1	94°C	2 min
Step 2	94°C	20 s
Step 3	63°C	15 s
	(-0.5°C per cycle)	
Step 4	68°C	10 s
→ go to step 2, 10x		
Step 5	94°C	15 s
Step 6	60°C	15 s
Step 7	72°C	40 s
→ go to step 6, 28x		
Step 8	72°C	2 min
Step 9	4°C	∞

Primers for genotyping of *PKD3$^{f/f}$* PCR:

Primer forward: 5' – GAT GAC CCT TAG AGT TAA AAC TCA CAG – 3'

Primer reverse: 5' – CAG ATC TGA ATT ACA TAG AAA GGA ACT G – 3'

Materials and Methods

Resulting band sizes: WT: lower band, Flox: upper band

2.2.1.2.2.3 TgPKD3ca mice

PCR mix (20 µL final volume):

2 µL	DNA
2 µL	Thermo buffer-MgCl$_2$
1.6 µL	MgCl$_2$
2 µL	dNTPs (2 mM stock)
1 µL	Primer 'Tg fwd' (10 µM)
1 µL	Primer 'Tg rev' (10 µM)
1 µL	Primer 'IL2 fwd' (10 µM)
1 µL	Primer 'IL2 rev' (10 µM)
0.25 µL	Taq polymerase (5 U/µL)
8.15 µL	H$_2$O

PCR program:

Step 1	94°C	2 min
Step 2	94°C	20 s
Step 3	65°C	15 s
	(-0.5°C per cycle)	
Step 4	68°C	10 s
→ go to step 2, 10x		
Step 5	94°C	15 s
Step 6	60°C	15 s
Step 7	72°C	10 s
→ go to step 6, 28x		
Step 8	72°C	2 min
Step 9	4°C	∞

Primers for genotyping of *TgPKD3ca* PCR:

Primer 'Tg fwd': 5' – CTG TGA TTT AAAGCC CGA AAA TGT TG – 3'

Primer 'Tg rev': 5' – CCA AGT CTG ATA ATC CTG TAG CCA – 3'

Primer 'IL2 fwd': 5' – CTA GGC CAC AGA ATT GAA AGA TCT – 3'

Primer 'IL2 rev': 5'– GTA GGT GGA AAT TCT AGC ATC ATC C – 3'

Resulting band sizes: Tg: 424 bp, IL2 (internal control): 324 bp

2.2.1.2.3 Agarose gel electrophoresis

The PCR products were separated on a 3% agarose gel. Briefly, the gel was made by adding 7.5 g of agarose to 250 mL 1x *TRIS-acetate-EDTA* (TAE) buffer and boiled in a microwave until the agarose was dissolved. After cooling down for 3 min, the DNA stain (Midori Green Advance) was added before pouring the gel into a mold with comb. Following polymerization, the PCR products were diluted in an appropriate amount of 6x loading dye and loaded together with the 100 bp DNA ladder onto the gel that was covered in 1x TAE. Separation of the samples and ladder was achieved at 120 V for 1 h followed by visualization using an *ultra violet* (UV) device.

2.2.1.3 Glucose and insulin tolerance tests

Glucose tolerance test (GTT) and *insulin tolerance test* (ITT) were performed with mice that were fasted for 4 h prior to the experiment. Briefly, the mice received i.p. a defined dose of glucose (2 g/kg BW) or insulin (0.8-1.5 U/kg BW, depending on mouse strain and diet) and the blood glucose concentration was monitored at several time points before injection (0) and 15, 30, 60, 90, and 120 min after injection with an Accu-chek glucometer.

2.2.1.4 Serum metabolite and HOMA-IR analysis

Serum cholesterol, glycerol, TG, FFA, and insulin concentrations were determined with commercially available kits and quantifications were performed according to the manufacturer's instructions.

For cholesterol, 300 µL of chromogen reagent was added to 2 µL of serum and incubated for 5 min at 37°C. A Spark 10M microplate reader was used to measure the absorption at 600 nm and the background absorption at 700 nm. For calculating the concentration, background absorption was subtracted from absorption at 600 nm as well as from blank and the concentration was calculated using a standard curve.

For glycerol and TG, 200 µL of free glycerol reagent was added to 2.5 µL of serum and incubated for 5 min at 37°C. A Spark 10M microplate reader was used to measure the absorption at 540 nm. Subsequently, 50 µL of triglyceride reagent was added for 5 min at 37°C and the measurement was repeated. For calculating the concentration, blank absorption was subtracted from sample absorption and the concentration was calculated using a standard curve. Similarly, TG were calculated by subtracting the 'glycerol concentration' from the 'total glycerides concentration' multiplied by 0.8 (dilution factor).

For FFA, 200 µL of reagent A was added to 2.5 µL of serum and incubated for 5 min at 37°C. A Spark 10M microplate reader was used to measure the absorption at 546 nm and the background absorption at 660 nm. Subsequently, 100 µL of reagent B was added for 5 min at 37°C and the measurement was repeated. For the calculation, background absorption was subtracted from absorption at 546 nm as well as from blank and the concentration was calculated using a standard curve.

For insulin, the concentration was quantified by using either a magnetic bead-based insulin *enzyme-linked immunosorbent assay* (ELISA) kit (Bio-Rad) or a conventional

insulin ELISA kit (ChrystalChem). For magnetic bead-based insulin ELISA kit, 50 µL of the diluted magnetic beads was added to the wells and washed twice before adding 50 µL of diluted serum and standards, and incubated for 1 h at *room temperature* (RT) with shaking at 850 rpm. After three washing steps, 25 µL of detection antibody was added and incubated for 30 min at RT and shaking at 850 rpm. Following three more washing steps, 50 µL of streptavidin-PE was added and incubated for 10 min at RT and shaking at 850 rpm. After three more washing steps, the beads were resuspended in 125 µL assay buffer before reading of the plate with a Bio-Plex MAGPIX system. For the conventional mouse insulin ELISA, 5 µL of serum was added to 95 µL of diluent and incubated for 2 h at 4°C. After washing, 100 µL of antibody solution was added and incubated for 30 min at RT. Following washing, 100 µL of substrate solution was added and incubated for 40 min at RT. After washing again, 100 µL of stop solution was added and the absorbance was measured at 450/630 with a Spark 10M microplate reader. HOMA-IR was calculated with the following formula: fasting insulin (mU/mL) x fasting glucose (mg/dL) divided by 405 (fasting= overnight for 16 h).

2.2.1.5 Metabolic measurements

Energy expenditure (EE), food intake, activity, *respiratory exchange ratio* (RER), oxygen consumption, and CO_2 production were measured in an automated indirect calorimetry system (Phenomaster) after 23 weeks of ND and HFD feeding. Because of different drinking bottles, the mice were allowed 4 days to adapt to the training drinking bottles before transferring them to the metabolic cages in the Phenomaster. Each mouse was housed in a separate cage in which they had ad libitum access to food and water, and the mice were kept in a 12 h light/dark cycle with a constant temperature of 23°C. Finally, the mice were allowed additional 3 days to adapt to the metabolic cages before starting the data acquisition.

2.2.1.6 Body composition

Lean and fat body mass analysis was performed by using body composition analyzer, which is based on *nuclear magnetic resonance* (NMR).

Materials and Methods

2.2.1.7 Fasting/refeeding protocol

Mice were fasted for 16 (overnight), 24, or 48 h depending on the experiment with free access to water. The food was restored for 4 or 24 h before blood or tissue sampling.

2.2.1.8 Insulin injections

The HFD-fed mice received an i.p. dose of 8 U/kg BW of insulin. After 15 min, the livers were collected according to standard procedures described above.

2.2.1.9 VLDL secretion

VLDL secretion was determined using tyloxapol (Triton WR1339) to inhibit *lipoprotein lipase* (LPL) and thus VLDL clearance from the plasma. Briefly, overnight fasted mice received a retro-orbital injection of 0.5 mg/g BW tyloxapol (10% solution in 0.9% NaCl). Blood was collected before injected and 1, 2, 4, and 6 h after injection. Quantification of serum TG and cholesterol concentrations were performed as described in 2.2.1.4.

2.2.1.10   In vivo lipogenesis assay

HFD-fed mice (for 8 weeks) were fasted overnight prior to the assay. The following day, the mice were refed with HFD for 4 h before they received an i.p. dose of 8 mCi $[^3H]$-H_2O/100 g BW (in 0.9% NaCl). After 2 h, the livers were excised and cut into three 80 mg pieces. The pieces were homogenized 1:5 in 0.1 N HCl and the lipids were extracted as described in 2.2.3.6.

2.2.2 Molecular cloning

For the cloning of the pEGFP-FLAG-mPKD3 plasmid, standard techniques for molecular cloning were applied.

2.2.2.1 Restriction digest

The plasmids for insert and backbone were double-digested with EcoRI and XhoI (pEX-K4-FLAG-mPKD3) and EcoRI and SalI (pEGFP-C1), respectively, in NEB3.1 buffer for 1 h at 37°C followed by thermal inactivation for 10 min at 70°C. Subsequently, the digested DNA was separated on a 1% agarose gel at 90 V for 30 min (see 2.2.1.2.3 for agarose gel electrophoresis).The 2725 bp FLAG-mPKD3 band and 4721 bp pEGFP-C1 backbone band were cut out and DNA was purified with

a kit according to the manufacturer's instructions (NucleoSpin Gel and PCR Clean-up, Macherey-Nagel).

2.2.2.2 Ligation

Ligations with several different insert/backbone rations were performed with T4 ligase for 1.5 h at RT.

2.2.2.3 Transformation

One Shot TOP10 chemically competent *E. coli* bacteria were used for transformation. Briefly, the ligated vector was added to the competent cells right after thawing of the cells on ice. The mixture was then incubated on ice for 30 min before a heat shock at 42°C in a water bath for 30 *seconds* (s). Thereafter, 250 μL LB-medium was added to the bacteria and incubated for 1 h at 37°C with continuous shaking at 250 rpm. The transformation mixture was plated on antibiotic-containing agar plates and incubated at 37°C overnight. Positive clones were picked and further cultured in LB-medium for Mini preps

2.2.2.4 Plasmid purification (Mini and Midi prep)

Clones were picked and cultured in 5 mL LB-medium supplemented with respective antibiotics at 37°C and 225 rpm overnight. 4 mL of the culture was used for plasmid purification using the mini prep kit (NucleoSpin Plasmid, Macherey-Nagel) according to the manufacturer's guidelines. Briefly, the cells were pelleted by centrifugation (30 s, 11000 rpm), resuspended in 250 μL buffer A1, and lysed by adding 250 μL buffer A2 (5 min). Lysis was stopped and neutralized by adding of 300 μL buffer A3, and the lysate was clarified from precipitated proteins by centrifugation for 10 min at 11000 rpm. The clear supernatant was loaded onto the column, and washed with 500 μL buffer AW and 600 μL buffer A4 (1 min, 11000 rpm, respectively). Finally, the plasmid was eluted with 300 μL buffer AE (1 min, 11000 rpm).

Sequencing confirmed successfully cloned plasmids (Eurofins). 1 mL from the positive mini cultures was used to inoculate 200 mL LB-medium for an overnight culture. Plasmid purification of midi cultures was performed according to the manufacturer's protocol (NucleoBond Midi, Macherey-Nagel). Briefly, the cells were pelleted by centrifugation [4500*g* (*gravitation force*), 10 min, 4°C], resuspended in 8 mL buffer

RES, and lysed by adding 8 mL buffer LYS (5 min). Lysis was stopped and neutralized by adding 8 mL buffer NEU, and the lysate was loaded on an equilibrated column with filter followed by washing steps with 5 mL buffer EQU (removal of filter afterwards) and 8 mL buffer WASH. Plasmids were eluted with 5 mL buffer ELU and precipitated by mixing with 3.5 mL isopropanol. After centrifugation ($4500g$, 1 h, 4°C), the DNA pellet was washed with 1 mL 70% ethanol, dried, and reconstituted in TE-Buffer.

2.2.3 In vitro analysis

2.2.3.1 HEK293T cell culture and transfection

The adherent HEK293T cell line was cultivated in DMEM (4.5 g/L D-glucose, 1 mM sodium pyruvate, 4.0 mM glutamine) supplemented with 10% FBS and 1% P/S.

For transfection, coverslips (in a 12-well plate) were precoated with Matrigel (0.1% in ice cold PBS) for 30 min at 37°C and washed once with PBS. For plating, 80.000 cells per well were seeded one day prior to the transfection (cells were 50-80% confluent at transfection). Transfection of the cells was carried out by using FuGENE 6 transfection reagent according to the manufacturer's instructions. In brief, 3 µL of the transfection reagent was mixed with OptiMEM followed by the addition of 1 µg plasmid. The plasmid/transfection reagent mixture was incubated for 15 min at RT before adding it dropwise to the wells containing cells in antibiotic-free growth medium. After overnight incubation, the transfection medium was replaced by standard growth medium containing 1% P/S. 24 h post transfection, the cells were washed twice in DPBS, fixed in 4% PFA (in PBS) for 10 min, washed in DPBS, and mounted using ProLong Gold Antifade Mountant with DAPI.

2.2.3.2 Primary hepatocyte isolation and culture

Primary mouse hepatocytes were isolated with the collagen perfusion method. 8- to 12-week-old male mice were anesthetized with ketamine/xylazine. For perfusion, the vena cava was cannulated, the portal vein was cut immediately afterwards, and the liver was perfused with 20 mL EBSS (without Ca^{2+}/Mg^{2+}) containing 0.5 mM EGTA. Next, the buffer was replaced to 50 mL HBSS (with Ca^{2+}/Mg^{2+}) supplemented with 100 U/mL type I collagenase. Following digestion, the liver was excised and the gall bladder was removed. The cells were liberated into DMEM supplemented with 10% FBS and 1% P/S, filtered through a 100 µm cell strainer, and centrifuged ($50g$, 3 min,

Materials and Methods

4°C). Subsequently, 22.5 mL Percoll was mixed with 2.5 mL 10x PBS, and 25 mL DMEM (containing the cells) was used to form a gradient allowing hepatocyte enrichment (50g, 10 min, 4°C), followed by three washes with 50 mL culture medium (50g, 3 min, 4°C). The primary hepatocytes were then plated either on precoated collagen type I 6- and 12-well plates or on self-coated rat collagen type I (50 µg/mL in 20 mM acetic, x µg/cm^2) for 1 h at RT, followed by 3 washes with PBS) 96-well seahorse plates, 6-, 8-, 12-well plates, and 6 or 10 cm dishes. After 4 to 6 h of attachment, the medium was replaced by fasting medium (DMEM supplemented with 0.2% FFA-free BSA and 1% P/S), and the cells were used the following day unless otherwise stated.

2.2.3.3 Adenovirus infection

Infection of primary hepatocytes was performed at 4 to 6 h after plating with adenoviruses expressing either *enhanced green fluorescent protein* (EGFP) (Ad-EGFP) or constitutive active PKD3 (Ad-mycPKD3ca) at a *multiplicity of infection* (MOI) of 10. Medium was replaced the following day and the cells were used for experiments 36 to 48 h after infection. Transduction efficiency was 100%, which was assessed by analyzing the expression of the EGFP reporter (present in all adenoviruses).

2.2.3.4 *Small interfering RNA* (siRNA) transfection

Transduction of primary hepatocytes was performed at 4 to 6 h after plating with *siNon-Targeting* (siNT) (30 nM), *siSrebp1* (30 nM), or *siSrebp2* (30 nM) using the Lipofectamine RNAiMAX transfection reagent according to the manufacturers' protocol. Medium was replaced the following day and cells were used for experiments 36 to 48 h after transduction.

2.2.3.5 Primary hepatocyte stimulation

Primary hepatocytes were incubated either with 1,2-dioctanoyl-sn-glycerol for 4, 6, and 8 h or with oleic acid (bound to albumin) for 4 and 20 h.

2.2.3.6 Lipogenesis assay

Primary hepatocytes were incubated in DMEM (25 mM glucose, 0.2% FFA-free BSA, and 1% P/S) supplemented with 0.5 mM sodium acetate and 4 µCi/mL ^{3}H-acetate at

basal or insulin (100 nM)–stimulated conditions for 4 to 6 h. Following incubation, the cells were washed twice with DPBS and scraped in 0.1 N HCl. Next, 0.8 volume of the homogenate was mixed stepwise with 3 volumes of MeOH/CHCl$_3$ (2:1, v/v), 1 volume of CHCl$_3$, and 1 volume of H$_2$O. The phases were separated by centrifugation (3000g, 10 min). The resulting lower phase was transferred to a new tube followed by a washing step with upper-phase MeOH/CHCl$_3$/H$_2$O (15:175:180, v/v/v) (3000g, 10 min). Finally, the lower phase was transferred to a scintillation tube and the lipids were dried under a stream of *nitrogen* (N$_2$). The lipids were resuspended in 4 mL of scintillation liquid and used for lipid scintillation counting. The lipogenesis rate was calculated as the amount of tritium incorporated into the newly formed lipids [measured in *disintegrations per minute* (dpm)] normalized to total protein (assessed with Bradford) per hour.

Alternatively, the extracted lipids were separated on a TLC plate as described in 2.2.5.1. The lipid spots were stained, scraped, and measured by lipid scintillation counting.

For inhibitor treatments, the medium was supplemented with 10 µM Akti-1/2, 0.7 µM KU0063794, and 0.7 µM rapamycin 4 to 6 h after plating (16 h before the experiment). In contrast, 1 µM CRT0066101 was added 1 h before the experiment.

2.2.3.7 FA oxidation assay

Primary hepatocytes were incubated in DMEM containing ^{3}H-oleic acid (2 µCi/mL) and 0.2 mM oleic acid (bound to albumin) at basal or insulin (100 nM)-stimulated conditions for 3 h. Afterwards, the supernatant was collected, the cells were washed twice with DPBS, and scraped in 0.1 N HCl which was used for determining protein concentration. To 0.5 volumes of the supernatant, 1 volume of MeOH/CHCl$_3$ (2:1, v/v) and 1 volume of 2 M KCl/2 M HCl (1:1, v/v) were added and mixed stepwise. Subsequently, centrifugation (3000g, 10 min) was used to separate the phases, the resulting upper phase was transferred to a new tube, and the extraction was repeated again. Finally, the two upper phases were combined, transferred to a scintillation tube, and 4 mL of scintillation liquid was added for scintillation counting. FA oxidation rate was calculated as the amount of tritium incorporated into ^{3}H$_2$O (measured in dpm) normalized to total protein (assessed with Bradford) per hour.

2.2.3.8 Phenylalanine conversion assay

Primary hepatocytes were fasted in DMEM without *phenylalanine* (Phe) and *tyrosine* (Tyr) for 1 h. Afterwards, the cells were stimulated with either 0, 0.01, 0.1, 1, or 2.5 mM Phe for 1 h (500 µL/well, 12-well plate). Next, the cells were lysed in 120 µL lysis buffer followed by centrifugation at 10000g for 10 min at 4°C. Tyrosine was quantified using the Tyrosine Assay Kit according to the manufacturer's protocol. Briefly, 50 µL of the cleared cell homogenate and standards were loaded into the wells of a 96-well microtiter plate. Subsequently, 50 µL of reaction mix was added, mixed thoroughly, and incubated for 10 min at RT on an orbital shaker. A Spark 10M microplate reader was used to measure the absorption at 490 nm and the concentration was calculated using a standard curve.

2.2.3.9 AA and glucagon stimulation

Primary hepatocytes were fasted in DMEM without AAs for 1 h. Afterwards, the cells were incubated with either no amino acids, all amino acids, all amino acids except Phe and Tyr, Phe exclusively, or Phe and Tyr exclusively for 1 h. For this reason, DMEM without AA and DMEM without Phe and Tyr were supplemented with respective amounts of glucose, serine, glycine, Phe, and Tyr. Cells were stimulated with glucagon for 0, 5, and 20 min. After stimulation, WB was performed as described in 2.2.5.2.

2.2.4 Histological analyses

Liver tissue was fixed in 10% formalin, dehydrated in an automated tissue processor, embedded in paraffin, cut in 2- to 4-µm liver sections and put on glass slides.

2.2.4.1 Histology

Hematoxylin and eosin (H&E) staining was performed according to standard laboratory procedures. In brief, sections were deparaffinized in xylol (2x 10 min) and rehydrated in an alcohol gradient (100%, 100%, 95%, 90%, 80%, 70%, and 50%, 5 min each), followed by 5 min in ddH$_2$O. Subsequently, the sections were stained with hematoxylin for 10 min, rinsed in tap water for 10 min, and put in ddH$_2$O for additional 5 min. Eosin counterstaining was performed for 2 min. Sections were dehydrated in an alcohol gradient (50%, 70%, 80%, 90%, 96%, 100%, and 100%, 2 min each) followed by xylol

(2x 10 min). Finally, the sections were mounted in a xylene-based mounting medium (RotiMount). Analysis was performed with an inverted microscope (Olympus CKX31).

Sirius red staining was performed in collaboration with the working group of Prof. Dr. Heikenwalder (protocol not available).

2.2.4.2 *Immunohistochemistry* (IHC)

Immunohistochemical stainings were performed in collaboration with the working group of Prof. Dr. Heikenwalder (detailed protocol not available). Antibodies against Ki-67 (H2, 95°C), cleaved caspase-3 (H2), B220 (H2), CD3 (H2, 95°C), F4/80 (E1), and collagen type IV (E1) were used in combination with either an EDTA pretreatment (H2) or an enzyme pretreatment kit (E1) (Leica), respectively.

For *TdT-mediated dUTP-biotin nick end labeling* (TUNEL) staining, a fluorescence in situ cell death detection kit was used according to the manufacturer's guidelines. Briefly, the sections were deparaffinized and rehydrated as described in 2.2.4.1. Next, the slides were washed twice with PBS and incubated with 50 µL TUNEL reaction mixture for 60 min at 37°C in a humidified chamber in the dark followed by the washes with PBS. Analysis (excitation 488 nm, emission 540 nm) was performed with a fluorescent microscope (Leica DM5500 B).

2.2.4.3 *Immunofluorescence* (IF)

Immunofluorescent stainings were performed according to standard lab procedures. In brief, cells were permeabilized in 0.5% Tritron X-100 (in PBS) for 5 min at RT followed by blocking with 10% *normal goat serum* (NGS) and 0.5% BSA in PBS for 1 h. Next, the cells were washed twice with PBS and incubated with primary antibody solution (in PBS with 1% NGS) overnight in a humidified chamber at 4°C. The following day, the cells were washed twice with PBS and incubated with fluorophore-conjugated secondary antibody solution (in PBS with 1% NGS) for 1 h at 4°C. Subsequently, the cells were washed twice with PBS and mounted using ProLong Gold Antifade Mountant with DAPI. Analysis was performed using a confocal microscope (Leica TCS SP8).

2.2.4.4 Mitochondrial staining

For mitochondrial staining, 300 nM MitoTracker Red CMXRos was added to the growth medium for 30 min at 37°C. Cells were washed in DPBS, fixed in 4% PFA (in PBS) for 10 min, washed twice with PBS, and mounted using ProLong Gold Antifade Mountant with DAPI. Analysis was performed using a confocal microscope (Leica TCS SP8).

2.2.5 Molecular biology/biochemical methods

2.2.5.1 Lipid extraction and *thin-layer chromatography* (TLC)

Extraction of hepatic lipids was performed according to the protocol of Bligh and Dyer with modifications[272]. In brief, 0.5 volumes of liver homogenate [1:100 in *phosphate-buffered saline* (PBS)] were acidified with 0.3 volumes of 0.2 N HCl. Afterwards, 3 volumes of MeOH/CHCl$_3$ (2:1, v/v), 1 volume of CHCl$_3$, and 1 volume of H$_2$O were added and mixed stepwise. Separation of the phases was achieved by centrifugation, the lower phase was transferred to a new tube, and the CHCl$_3$ was evaporated under a N$_2$ stream. The lipids were either resuspended in MeOH/CHCl$_3$ (1:1, v/v) for TLC-based separation on a silica gel 60 plate or in DMSO/H$_2$O for TG and cholesterol quantification as described in 2.2.1.4.

For TLC, the lipids were separated in the solvent mixtures CHCl$_3$/MeOH/20% acetic acid (65:25:5, v/v/v), hexane/ethyl acetate/acetic acid (59:10:1, v/v/v), and pure hexane. Cholesteryl palmitate (for CE), triolein (for TG), oleic acid (for FFA), cholesterol (for FC), phosphatidylethanolamine (for PE), and phosphatidylcholine (for PL) were used as standards (in MeOH/CHCl$_3$, 1/1, v/v, 1 mg/mL each) to identify the lipid classes on the TLC plate. The lipids were visualized with a hydrous solution of 2.5% 12-molybdophosphoric acid, 1% cerium (IV) sulfate, and 6% H$_2$SO$_4$ by quickly dipping in the plate and heating it at 200°C until the bands appear.

2.2.5.2 Immunoblotting

Protein lysates were obtained either from tissue or cells in lysis buffer supplemented with *protease and phosphatase inhibitor* (PPI) cocktail. Tissue pieces were homogenized with a homogenizing pestle, and cells were scraped from cell culture plates and forced through a 26 G syringe needle for homogenization. Next, cell fragments were pelleted by centrifugation (13000 rpm, 10 min at 4°C) and the supernatant (protein lysate) was transferred to a new tube. Protein concentration was

determined with the BCA Protein Assay Kit according the manufacturer's instructions. Protein concentrations were adjusted with lysis buffer to an equal volume, mixed with a corresponding amount of 5x Laemmli buffer, and boiled for 5 min at 95°C.

Western blot (WB) was performed according to standard lab procedures. Briefly, 20 µg of protein lysates were separated on a 10% *sodium dodecyl sulfate-polyacrylamide gel electrophoresis* (SDS-PAGE) and transferred on a *polyvinylidene fluoride* (PVDF) membrane (330 mA, A const., 3.5 h, 4°C). The membrane was washed in TBST, blocked in blocking buffer (1 h, 4°C), and probed with primary antibodies (Table 8) in 5% BSA in TBST (unless otherwise stated) overnight at 4°C. The following day, the membrane was washed 3x with TBST for 5 min and incubated in corresponding mouse or rabbit *horseradish peroxidase* (HRP)–conjugated secondary antibody (Table 9) for 1 h. Subsequently, the membrane was washed 3x in TBST for 20 min and once in TBS for 5 min before visualizing the proteins with *enhanced chemiluminescence* (ECL) substrate for digital or X-ray film-based imaging.

2.2.5.3 *Real-time quantitative PCR* (RT-qPCR) analysis

Total *ribonucleic acid* (RNA) was extracted from tissue or cells using QIAzol Lysis Reagent according to the manufacturer's guidelines. In brief, cells were scraped with 1 mL QIAzol Lysis Reagent and tissues were homogenized in the same amount of QIAzol Lysis Reagent using a bench top homogenizer, and incubated for 5 min at RT. Next, 0.2 mL $CHCl_3$ was added and incubated for 2-3 min at RT followed by phase separation ($12000g$, 15 min, 4°C). The resulting upper aqueous phase was transferred to a new tube, mixed with 0.5 mL isopropanol, and incubated for 10 min at RT. After centrifugation (12000g, 15 min, 4°C), the supernatant was aspirated and the pellet was washed in 1 mL 75% Ethanol. Following centrifugation ($7500g$, 5 min, 4°C), the supernatant was removed and the pellet was air-dried for 10 min. An appropriate amount of of RNase-free water were added and the RNA concentration and quality were assessed using a NanoDrop spectral photometer.

For *complementary DNA* (cDNA) synthesis, First Strand cDNA Synthesis Kit was used according to the manufacturer's instructions. For this reason, two different master mixes were prepared for cDNA synthesis:

Materials and Methods

Master mix 1:

1 µg   RNA

1 µL   random hexamer primer

x µL   RNase-free water (up to a total volume of 11 µL)

Master mix 2:

4 µL   5x Reaction Buffer

1 µL   RiboLock RNase Inhibitor (20 U/µL)

2 µL   10 mM dNTP mix

2 µL   M-MuLV Reverse Transcriptase (20 U/µL)

Master mix 1 was heated up to 65°C in a thermal cycler for 5 min and cooled on ice afterwards. Next, 9 µL of master mix 2 was added, incubated for 5 min at 25°C, and followed by 60 min at 37°C in a thermal cycler. Finally, the reaction was terminated with a heating step for 5 min at 70°C.

cDNA of cells was diluted 1:5 and from tissues 1:10 – 1:15 in RNase-free water. RT-qPCR was performed using PowerUp SYBR Green Master Mix. The RT-qPCR samples and master mix were pipetted by a QIAgility and analyzed on a QuantStudio 5 Real-Time PCR System.

RT-qPCR mix:

2 µL   cDNA (diluted)

5 µL   PowerUp SYBR Green Master Mix

0.4 µL   forward primer (1:10 in H_2O, stock: 1 µg/mL)

0.4 µL   reverse primer (1:10 in H_2O, stock: 1 µg/mL)

2.2 µL   RNase-free water

RT-qPCR program:

Step 1   95°C   10 min

Step 2   95°C   15 s

Step 3   60°C   1 min

→go to step 2, 40x

Step 4   95°C   15 s

Step 5   60°C   1 min

Step 6   95°C   15 s   (step 4-6 for melting curve)

Materials and Methods

Relative amounts of all mRNAs were calculated using comparative C_T method normalized to the reference gene *Rpl13a*, *36B4*, or *Hprt1*. The mouse primer sequences (sense and antisense) are listed in Table 5.

Absolute quantification of PKD isoform copy numbers was performed according to a standard protocol from Applied Biosystems. In brief, primers were designed to be located within same exons and genomic DNA of known concentration was used for creating a standard curve reflecting copy numbers.

2.2.5.4 *Immunoprecipitation* (IP)

Cells were lysed in Pierce IP Lysis Buffer supplemented with PPI, and protein content was quantified as described in 2.2.5.2. IP was performed with Pierce Protein A/G Magnetic Beads according to the manufacturer's protocol. Briefly, 4 mg of protein (2 mg/mL) was incubated with 30 µL of antibody on a rotary device overnight at 4°C (all steps were carried out at 4°C unless otherwise stated). The following day, 200 µL of magnetic protein A/G beads were washed once with TBST, mixed with the antibody/protein mixture, and incubated for 1.5 h on a rotary device. Next, beads were collected on a magnetic stand and supernatant was collected for later WB analysis. Beads were washed with TBST for 5 min four times, followed by washing with ddH$_2$O once. Samples were eluted in 1x NuPAGE *lithium dodecyl sulfate* (LDS) sample buffer supplemented 60 mM DDT for 10 min at 95°C. Beads were magnetically separated from the immunoprecipitated product, which was further analyzed on WB or by MS.

2.2.6 *Mass spectrometry* (MS)-based methods

2.2.6.1 Lipidomics

2.2.6.1.1 DAG content

Hepatic DAG content was determined with the help of the working group of Prof. Dr. Schulze. 50 mg of liver tissue was homogenized in 7-fold volume of 1% acetic acid using a stirring plastic pistil. 280 µL of the liver homogenate, 70 µL methanol, 210 µL n-butanol and 20 µL of 10 mM 1,2-dioctanoyl-sn-glycerol [in n-butanol/methanol (3/1, v/v)] were mixed vigorously. Subsequently, 200 µL n-heptane and 100 µL ethyl acetate were added followed by centrifugation for 2 min at 13000 rpm. The resulting upper phase was transferred to a new tube and the lower phase was extracted with another

Materials and Methods

200 µL n-heptane and 100 µL ethyl acetate. The phases were combined and evaporated at 45°C under a stream of N_2.

For lipid class separation, the dried extract containing DAG was resuspended in 150 µL hexane and applied on a silica matrix column. Washing was performed by adding 750 µL hexane, 750 µL hexane/ethyl acetate (18/1, v/v) and 1.5 mL hexane/ethyl acetate (9/1, v/v) to the column. DAGs were eluted with 750 µL hexane/ ethyl acetate (9/4, v/v) and the eluate evaporated to at 45°C under a stream of N_2.

For *liquid chromatography* (LC)/MS-analysis, DAGs were dissolved in 250 µL mobile phase A/mobile phase B (70/30, v/v) [mobile phase A: acetonitrile/water/formic acid (10/89.9/0.1, v/v/v), mobile phase B: acetonitrile/water/formic acid (90/9.9/0.1, v/v/v)]. A Thermo Scientific Dionex Ultimate 3000 UHPLC system hyphenated with a *Q exactive mass spectrometer* (QEMS) equipped with a HESI probe and UPLC column was used. 5 µL of the sample were injected to the C8 column at 40°C with the following gradient program:

20% solvent B	2 min
100% solvent B	5 min (linear increase)
100% solvent B	22 min
20% solvent B	1 min
20% solvent B	5 min (for column equilibration before each injection)

The flow rate was maintained at 350 µL/min and the eluent was directed to the HESI source of the QEMS.

MS parameters:

Heater temperature	120°C
Sheath gas	30 L/min
Auxiliary gas	10 L/min
Sweep gas	3 L/min
Spray voltage	3.6 kV
Capillary temperature	320°C
S-lens	55 (RF level)
Full scan range	300 to 700 (m/z) in positive ion mode
Resolution	70000 nm
Maximum injection time	200 *milliseconds* (ms)

Peak corresponding to the calculated DAG masses (MIMOH ± 2 mMU) were integrated using TraceFinder software.

2.2.6.1.2 Liver FA composition

Hepatic total FA content was determined with the help of the working group of Prof. Dr. Schulze. Liver tissue was homogenized in 1:100 PBS using a stirring plastic pistil. 100 µL of the liver homogenate was mixed stepwise with 20 µL standard-mix [containing lamivudine, tridecanoic acid, nonadecanoic acid, and ibuprofen in MeOH/CHCl3 (1/1, v/v), 5 mM each], 30 µL 0.2 M HCl, 90 µL $CHCl_3$, 100 µL $CHCl_3$, and 100 µL ddH_2O. Phases were separated by centrifugation, the lipid-containing lower phase was transferred to a new tube, and dried under a stream of N_2. Residue was resuspended in 0.5 mL of freshly prepared 0.3 M KOH in $MeOH/H_2O$ (9/1, v/v) and heated for 1 h at 80°C. Neutral lipids were extracted twice with 0.5 mL hexane, centrifuged, and the upper phase was discarded. Lower phases were acidified with 50 µL formic acid and the total fatty acids were extracted twice with 0.5 mL hexane. After centrifugation, the upper phase was transferred to a new tube and dried at 45°C under N_2 (residue contained total free fatty acids).

For LC/MS-analysis, the dried eluated samples were redissolved in 100 µL isopropanol and centrifuged for 2 min. 20 µL supernatant were transferred into sampler-vials. Mobile phase A consisted of acetonitrile/water/formic acid (5/95.9/0.1, v/v/v), and mobile phase B consisted of acetonitrile/water/formic acid (90/9.9/0.1, v/v/v). A Thermo Scientific Dionex Ultimate 3000 UHPLC system hyphenated with a QEMS equipped with a HESI probe and UPLC column was used. 3 µL of the sample were injected to the C8 column at 40°C with the following gradient program:

30% solvent B	1 min
100% solvent B	15 min (linear increase)
100% solvent B	13 min
30% solvent B	1 min
30% solvent B	5 min (for column equilibration before each injection)

The flow rate was maintained at 350 µL/min. The eluent was directed to the ESI source of the QE-MS from 3 min to 27 min after sample injection.

Materials and Methods

MS Scan Parameters:	HESI Source Parameters:
Scan type: Full MS in Negative Mode	Sheath gas flow rate: 30
Run time: 3 min - 27 min	Auxiliary gas flow rate: 10
Scan range: 160.0 - 460.0 m/z	Sweep gas flow rate: 3
Resolution: 70,000	Spray voltage: 2.5 kV
Microscans: 1	Capillary temperature: 320°C
AGC-target: 3E6	S-lens RF level: 55.0
Maximum injection Time: 400 ms	Auxiliary gas heater temp.: 120°C

Peak corresponding to the calculated masses (MIMOH ± 2 mMU) were integrated using TraceFinder software.

2.2.6.2 Proteomics

2.2.6.2.1 *Two-dimensional difference gel electrophoresis* (2D-DIGE)

MS analysis was performed in collaboration with Applied Biomics. Phosphoproteins were enriched by using Pierce Phosphoprotein Enrichment Kit according to the manufacturer's instructions. Afterwards, the buffer was replaced with 2 *dimensional* (D) cell lysis buffer [30 mM Tris-HCl (pH 8.8), containing 7 M urea, 2 M thiourea, and 4% CHAPS] using 5 kDa *molecular weight cut off* (MWCO) spin column. Then, the samples were centrifuged at 25000g for 30 min at 4°C and the supernatant (protein lysate) was collected. Protein concentration was determined using Bradford Reagent. Next, the lysate samples were diluted with the 2D cell lysis buffer to the same protein concentration at 6 μg/μL. For minimal CyDye labeling, 30 μg of protein lysate were mixed with 1 μL of diluted CyDye (1:5 diluted in DMF), followed by incubation in the dark on ice for 30 min. Next, 1 μL of 10 mM lysine was added to each of the samples, vortexed, and incubated in the dark on ice for additional 15 min. Afterwards, Cy3 and Cy5 labeled samples were mixed, and added to the non-labeled sample (300 μg each) together with 2x 2D sample buffer (8 M urea, 4% CHAPS, 20 mg/mL DTT, 2% pharmalytes, and traces of bromophenol blue), followed by adding 100 μL of DeStreak rehydration solution (7 M urea, 2 M thiourea, 4% CHAPS, 20 mg/mL DTT, 1% pharmalytes, and traces of bromophenol blue) to 250 μL for the 13 cm *immobilized pH gradient* (IPG) strip.

For *isoelectric focusing* (IEF), the labeled samples were mixed, loaded into the strip holder (strip facing down, mineral oil on top of the strip), and the IEF was run in the

dark at RT according to the manufacturer's protocol. Upon finishing the IEF, the IPG strips were incubated in freshly made equilibration buffer 1 [50 mM Tris-HCl (pH 8.8), containing 6 M urea, 30% glycerol, 2% SDS, traces of bromophenol blue, and 10 mg/mL DTT] for 15 min with gentle shaking. Then, the strips were rinsed in the freshly made equilibration buffer 2 [50 mM Tris-HCl (pH 8.8), containing 6 M urea, 30% glycerol, 2% SDS, traces of bromophenol blue, and 45 mg/mL iodoacetamide) for 10 min with gentle shaking. Subsequently, the IPG strips were rinsed once in SDS-gel running buffer, before they were transferred into the SDS-Gel (12% SDS-gel prepared using low florescent glass plates) and sealed with 0.5% (w/v) agarose solution (in SDS-gel running buffer). The SDS-gels were run until the dye front was about to run out.

For data analysis, the SDS-gel was scanned using a Typhoon TRIO. Then, the scanned images were analyzed by using Image QuantTL software, followed by in-gel and cross-gel analysis using DeCyder software for determining the ratio change of differential protein expression.

For spot picking and trypsin digestion, the spots of interest were picked up by Ettan Spot Picker. The gel spots were washed and digested in-gel with modified porcine trypsin protease. The digested tryptic peptides were desalted by Zip-tip C18 and the peptides were eluted from the Zip-tip with 0.5 µL of matrix solution (α-cyano-4-hydroxycinnamic acid, 5 mg/mL in 50% acetonitrile, 0.1% trifluoroacetic acid, 25 mM NH_4HCO_3), followed by spotting on the MALDI plate.

For MS, a 5800 mass spectrometer was used for MALDI-TOF (MS) and TOF/TOF (tandem MS/MS). For database search, both the resulting peptide mass and the associated fragmentation spectra were analyzed with GPS Explorer in combination with Mascot search engine to searching the *National Center for Biotechnology Information non-redundant* (NCBInr) or Swiss Protein database. Candidates with either protein score C.I.% or Ion C.I.% greater than 95 were considered significant.

2.2.6.2.2 MS following up IP with PKD substrate-motif antibody

MS analysis was performed in collaboration with the working group of Prof. Dr. Schlosser. Gel electrophoresis and In-gel digestion were carried out according to the standard procedures. Protein precipitation was performed overnight at -20°C with 4x the volume of acetone. Pellets were washed three times with acetone at -20°C. Pellets were washed 3x with acetone at -20°C. Precipitated proteins were dissolved in NuPAGE LDS sample buffer, reduced with 50 mM DTT at 70°C for 10 min, and

alkylated with 120 mM iodoacetamide for 20 min at RT. Samples were separated on a NuPAGE Novex 4-12% Bis-Tris gel using *3-(N-Morpholino) propansulfonsäure* (MOPS) buffer following the manufacturer's instructions. Gels were washed with ddH$_2$O three times for 5 min and stained for 45 min with Simply Blue Safe Stain. After washing with ddH$_2$O for 2 h, each gel band was cut into 16 slices.

The excised gel bands were destained with 30% acetonitrile (in 0.1 M NH$_4$HCO$_3$, pH 8), shrunk with 100% acetonitrile, and dried in a vacuum concentrator. Digests were performed with 0.1 µg trypsin per gel band (in 0.1 M NH$_4$HCO$_3$, pH 8) overnight at 37°C. Peptides were extracted from the gel slices with 5% formic acid and pooled with the supernatant.

An Orbitrap Fusion equipped with a PicoView ion source and coupled to an EASY-nLC 1000 were used for NanoLC-MS/MS analyzes. Peptides were loaded on capillary columns self-packed with 1.9 µm porous spherical silica and separated with a 30 min 3% to 30% linear gradient of acetonitrile and 0.1% formic acid with a flow rate of 500 nL/min.

MS and MS/MS scans were both obtained using an Orbitrap analyzer. The raw data was processed, analyzed, and quantified using the MaxQuant software[273]. *Label-free quantification* (LFQ) intensities were used for protein quantification[274]. Proteins with less than two identified razor and unique peptides were excluded. Data imputation was performed with values from a standard normal distribution with a mean of the 5% quantile of the combined log10-transformed LFQ intensities and a standard deviation of 0.1. Log2 transformed protein ratios of sample versus control with values outside a 1.5x (potential) or 3x (extreme) *interquartile range* (IQR), respectively, were considered as significantly enriched.

2.2.7 Statistical analysis

The results are presented as mean values ± *standard error of the mean* (SEM). Significances were assessed by using two-tailed Student's t test for independent groups, or by using one-way or two-way *analysis of variance* (ANOVA), followed by a post hoc Tukey's test for multiple comparisons. P values of 0.05 or lower were considered as statistically significant (*p<0.05, **p<0.01, and ***p<0.001).

3 Results

3.1 Activation of PKD3 in liver

3.1.1 PKD3 is activated by stimulation with DAG and extracellular purines as well as in response to HFD feeding

PKDs have been reported to be involved in various fundamental and cellular processes with a cell and tissue specific expression (reviewed in [49,92]). In the context of metabolism, PKDs have major roles in the regulation of adipose tissue function and pancreatic insulin secretion among many others[109,158]. However, a potential role in the liver has been neglected so far, why this study aimed to address this question.
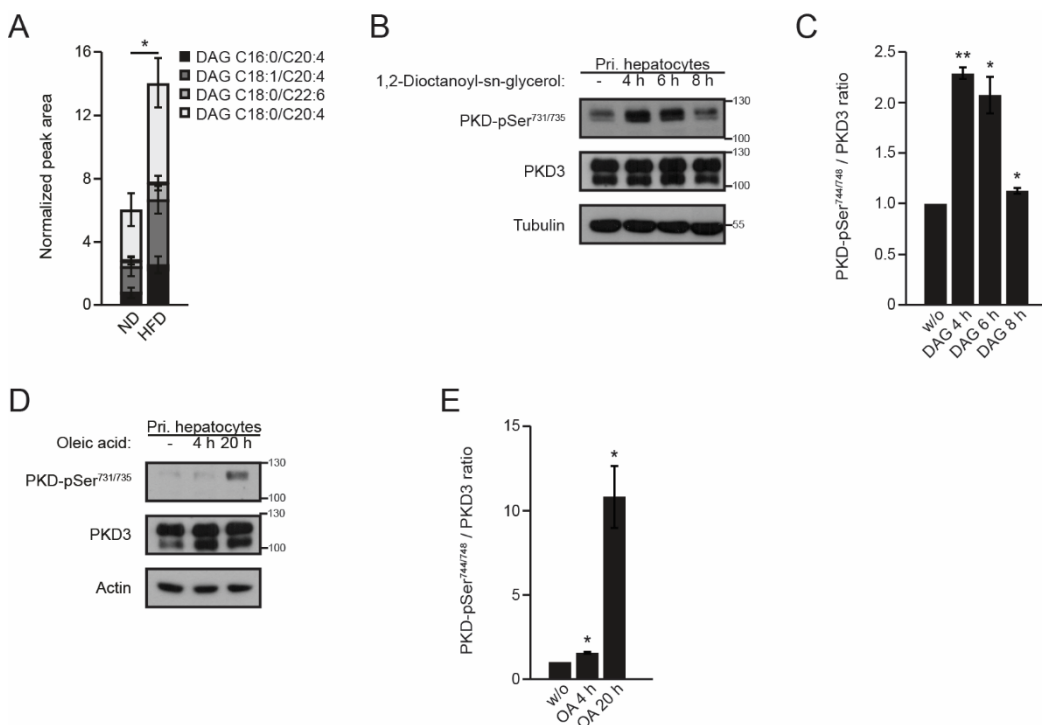
Figure 10: PKD3 is activated by DAG and oleic acid in primary mouse hepatocytes. (A) DAG content in livers of ND and HFD-fed mice assessed by lipid isolation followed by LC/MS and quantification of the four most abundant DAG species (n=7 mice/diet). This experiment was performed in collaboration with the working group of Prof. Dr. Schulze. (B, C) WB analysis and corresponding densitometric quantification of protein lysates from primary hepatocytes stimulated with 100 µM 1,2-Dioctanoyl-sn-glycerol for 4, 6, and 8 h using antibodies against PKD-pSer731/735, PKD3, and Tubulin as loading control (n=3 independent experiments). (D, E) WB analysis and corresponding densitometric quantification of protein lysates from primary hepatocytes stimulated with 750 µM oleic acid for 4 and 20 h using antibodies against PKD-pSer731/735, PKD3, and Actin as loading control (n=3 independent experiments). Data are presented as mean ± SEM. *P>0.05, **P>0.01 [unpaired two-tailed Student's t test (A) or one way ANOVA with post hoc Tukey's test (C, E)]. *Diacylglycerol* (DAG); *normal diet* (ND); *high-fat diet* (HFD); p*rotein kinase D* (PKD); *phospho* (p); *serine* (Ser); *oleic acid* (OA). (Mayer et al., 2019)[275]

Results

PKDs bind DAG with their cysteine-rich domains C1a and C1b. This regulates PKD localization and PKD activation via autophosphorylation of the two serine residues in the kinase domain[57]. DAG content in liver can be increased due to enhanced delivery of chylomicron remnants, increased uptake of fatty acids originating from adipocytes, increased hepatic de novo lipogenesis induced by skeletal muscle insulin resistance, or due to decreased mitochondrial function (summarized in [37]). DAG levels in liver are elevated during the pathological condition of NAFLD[276,277], which induces insulin resistance by DAG-mediated activation of PKCε[34].

The first aim of this study was to confirm that DAG accumulates in liver during high caloric intake and to identify upstream activators of PKDs. For this reason, livers from mice that were fed either an ND or HFD over a prolonged period (24 weeks) were used to analyze the DAG content by *liquid chromatography/mass spectrometry* (LC/MS). HFD feeding of mice results in lipid accumulation in liver with accompanied pathological consequences, which provides a tool for studying obesity in the context of liver diseases (reviewed in [278]). Indeed, DAG levels of the four most abundant DAG species (C16:0/C20:4, C18:1/C20:4, C18:0/C22:6, and C18:0/C20:4) were significantly increased in livers from HFD-fed mice compared to livers from ND-fed mice (Figure 10A). To examine whether DAG leads to an activation of PKD in liver, the culture media of primary mouse hepatocytes was supplemented with the cell permeable DAG analog 1,2-dioctanoyl-sn-glycerol for 4, 6, or 8 hours, resulting in a significantly enhanced activation of PKD, which can be measured by phosphorylation of the serine residues 731 and 735 in the catalytic domain of PKD (Figure 10B, C). Similarly, incubation of primary hepatocytes with oleic acid (OA) (C18:1), a fatty acid that is as a precursor for DAG synthesis, induced phosphorylation of PKD (Ser731/735) after 20 hours of incubation (Figure 10D, E).

Interestingly, while DAG accumulates during obesity[37], stimulation of primary hepatocytes with 1,2-dioctanoyl-sn-glycerol resulted in decreased expression of genes involved in de novo lipogenesis (*Srebp1c*, *Srebp2*, *Fasn*, *Hmgcs*, *Hmgcr*, *Fdps*) (Figure 11A). This suggests a negative feedback mechanism in which DAG might impair the expression of lipogenic genes in liver.
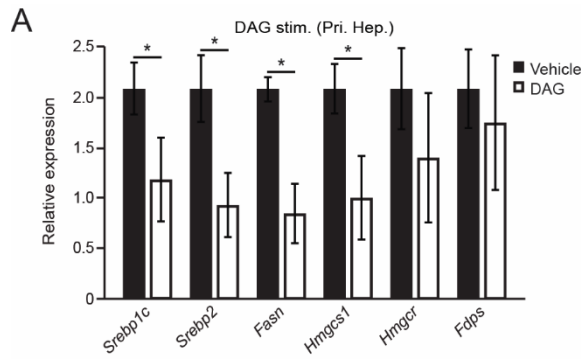
Results

Figure 11: DAG stimulation of primary hepatocytes decreases lipogenic gene expression. (A) RT-qPCR analysis of indicated genes in primary hepatocytes stimulated with 100 μM DAG in lipogenic conditions (100 nM insulin) (n=3 biological replicates/condition). Data are presented as mean ± SEM. *P>0.05 (unpaired two-tailed Student's t test. *Sterol regulatory element binding protein* (Srebp); *fatty acid synthase* (Fasn); *3-hydroxyl-3-methylglutaryl-CoA synthase* (Hmgcs); *3-hydroxyl-3-methylglutaryl-CoA reductase* (Hmgcr); *farnesyl diphosphate synthase* (Fdps). (Mayer et al., 2019)[275]

As stated above, hepatic DAG levels are elevated during obesity and lipid overload, which can be mimicked by HFD feeding in mice. Thereby, consistent with the in vitro experiments, PKD is highly significantly activated in mice livers that were fed an HFD compared to livers from ND-fed mice, indicated by an increased level of Ser731/735 phosphorylation of PKD (Figure 12A, B). This makes HFD-feeding a useful tool for studying the role of PKD function on liver metabolism.
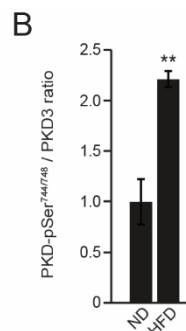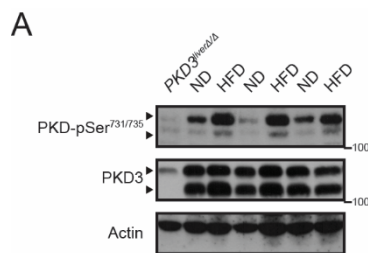

Figure 12: PKD3 is activated in liver upon HFD feeding. (A, B) WB analysis and corresponding densitometric quantification of protein lysates from livers of mice fed an ND or HFD using antibodies against PKD-pSer731/735, PKD3, and Actin as loading control (n=3 mice/diet). Data are presented as mean ± SEM. **P>0.01 (unpaired two-tailed Student's t test). P*rotein kinase D* (PKD); *phospho* (p); *serine* (Ser); *adenosine triphosphate* (ATP). (Mayer et al., 2019)[184]

Several studies reported that purinergic signaling affects liver metabolism in health and disease[279,280]. Furthermore, purinergic receptors have been shown to activate PKDs in other cell types[281,282]. In order to test whether purinergic signaling activates PKD in liver, primary hepatocytes were stimulated with *adenosine triphosphate* (ATP) for 30 s, 2 min, and 5 min, which led to a moderate increase in phosphorylation of Ser731/735 at all analyzed time points making ATP to an upstream activator of PKD (Figure 13).
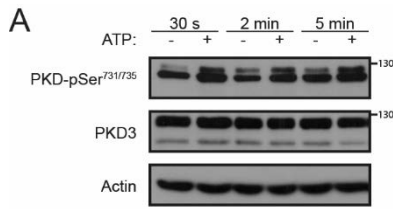
Results

Figure 13: ATP stimulation activates PKD3 in primary hepatocytes. (A) WB analysis of protein lysates from primary hepatocytes stimulated with 100 μM ATP for 30 s, 2 min, and 5 min using antibodies against PKD-pSer731/735, PKD3, and Actin as loading control (n=1 independent experiment). *Protein kinase D* (PKD); *phospho* (p); *serine* (Ser); *adenosine triphosphate* (ATP). (unpublished observation)

Taken together, PKD is activated in hepatocytes by stimulation with DAG and the fatty acid oleate, and physiologically by lipid overload in general through prolonged HFD-feeding of mice. Additionally, purinergic stimulation with ATP results in activation of PKD.

3.1.2 PKD3 is the predominant expressed isoform in liver

So far, three PKD isoforms have been described, namely PKD1, PKD2, and PKD3[92]. However, the expression level of the PKD isoforms has not yet been studied in liver in detail. To assess this, absolute quantification revealed that PKD1 is almost not (or at a very low level) expressed, and PKD2 transcripts were only marginally present in hepatocytes. Nevertheless, PKD3 is robustly expressed why it is considered as the predominantly expressed isoform in liver. Hence, further studies were focusing mainly on PKD3.
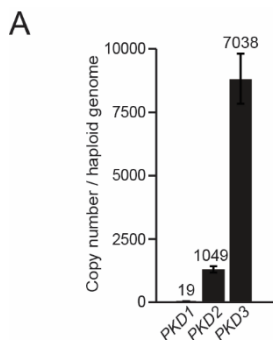

Figure 14: PKD isoform expression in liver. (A) Absolute quantification of PKD isoform expression in liver by using RT-qPCR with in-exon primers and normalizing it to a genomic DNA standard (n=8 mice). Data are presented as mean ± SEM. ***P>0.001 (one way ANOVA with post hoc Tukey's test). P*rotein kinase D* (PKD) (Mayer et al., 2019)[275]

3.2 Depletion of PKD3 promotes lipid accumulation but improves insulin sensitivity in liver

3.2.1 Hepatic deletion of PKD3 promotes glucose and insulin tolerance

The next step was to investigate PKD3 function on liver metabolism in vivo. Therefore, mice lacking PKD3 specifically in hepatocytes (*PKD3^{liverΔ/Δ}*) were generated by

crossing PKD3 floxed mice (*PKD3^f/f^*)[270] with mice expressing the Cre recombinase under the control of the albumin promoter (B6.Cg-Tg(Alb-cre)21Mgn/J)[271].
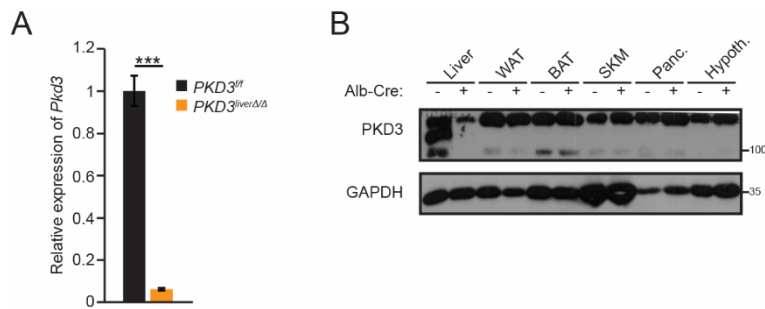

Figure 15: PKD3 deletion efficiency in liver. (A) RT-qPCR analysis of *Pkd3* expression in livers of control and *PKD3^liverΔ/Δ^* mice (n=7 mice/group). (B) WB analysis of PKD3 expression in indicated tissues from control and *PKD3^liverΔ/Δ^* mice (n=2 independent experiments). Data are presented as mean ± SEM. ***P>0.001 (unpaired two-tailed Student's t test). *Protein kinase D* (PKD); *white adipose tissue* (WAT); *brown adipose tissue* (BAT); *skeletal muscle* (SKM); *pancreas* (Panc.); *hypothalamus* (Hypoth.). (Mayer et al., 2019)[275]

A RT-qPCR analysis was performed to confirm that *Pkd3* mRNA is successfully silenced in livers of *PKD3^liverΔ/Δ^* mice in comparison to the expression level of control mice. The transcript level of *Pkd3* was significantly reduced by more than 90% (Figure 15A). The specific deletion of PKD3 was also confirmed on protein level by WB analysis and the deletion is restricted to liver and not to any other analyzed organ such as *white adipose tissue* (WAT), *brown adipose tissue* (BAT), *skeletal muscle* (SKM), *pancreas* (Panc.), and *hypothalamus* (Hypoth.) (Figure 15B). Notably, PKD3 appeared as three bands in the WB and all of them seem to be specific as they were all deleted by the Cre recombinase (Figure 15B). However, the reason and the relevance of the three bands remains unclear and needs to be further investigated. In addition, the three bands showed that PKD3 is mainly expressed in liver compared to the other organs.

Since DAG and oleic acid stimulation led to an activation of PKD3 (Figure 10B-E) and DAG accumulates during obesity, control and *PKD3^liverΔ/Δ^* mice received an HFD (the model diet for inducing obesity in mice) directly after weaning over a prolonged period of 24 weeks and body weight gain of the mice was assessed every 2 weeks. *PKD3^liverΔ/Δ^* mice did not differ in body weight gain over 24 weeks of HFD-feeding compared to control mice (Figure 16A). This was also reflected by no difference between control and *PKD3^liverΔ/Δ^* mice in lean and fat body mass measured by a specific mouse NMR (Figure 16B). However, when determining the weight of several organs such as liver *gonadal white adipose tissue* (gWAT), *subcutaneous white adipose tissue* (sWAT), *brown adipose tissue* (BAT), or *skeletal muscle* (SKM), the liver weight was

moderately, but significantly increased in livers from mice lacking PKD3 in hepatocytes compared to control mice, whereas the organ weight of other organs did not differ between the genotypes (Figure 16C). In contrast, control and *PKD3*$^{liver\Delta/\Delta}$ mice fed an ND for 24 weeks, did not differ in body weight gain (Figure 16D), lean and fat body composition (Figure 16E), or organ weights (Figure 16F). Importantly, prolonged HFD-feeding significantly increased body weight gain, total body fat mass, and the organ weight of liver, gWAT, and sWAT compared to ND-fed mice (P values not shown, Figure 16A-F).
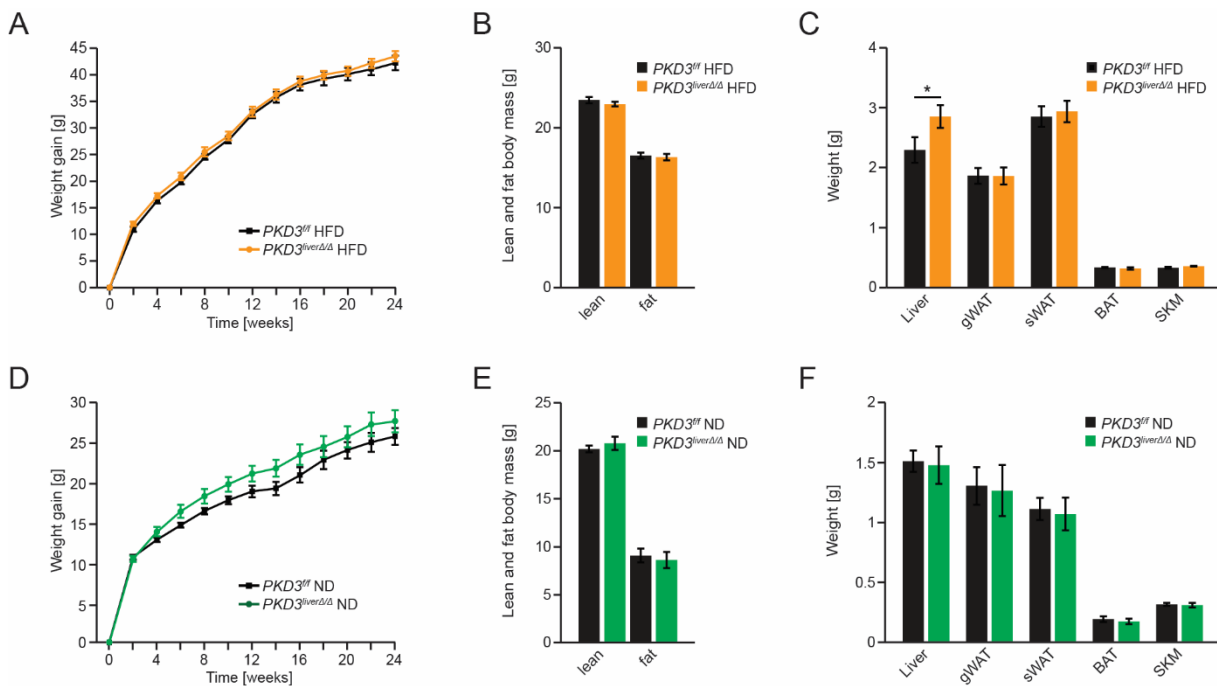

Figure 16: Weight gain, body fat composition, and organ weights in control and *PKD3*$^{liver\Delta/\Delta}$ mice. Control (*PKD3*$^{f/f}$) and *PKD3*$^{liver\Delta/\Delta}$ mice fed an HFD for 24 weeks were analyzed for body weight gain evolution over 24 weeks (A), lean and fat body mass assessed by NMR analysis (B), and organ weights (C) [n=8 mice (WT) and n=15 mice (KO)]. Control (*PKD3*$^{f/f}$) and *PKD3*$^{liver\Delta/\Delta}$ mice fed an ND for 24 weeks were analyzed for body weight gain evolution over 24 weeks (D), lean and fat body mass assessed by NMR analysis (E), and organ weights (F) [n=9 mice (WT) and n=8 mice (KO)]. Data are presented as mean ± SEM. *P>0.05 [unpaired two-tailed Student's t test (C, F) or two way ANOVA with post hoc Tukey's test (A, B, D, E)]. *Protein kinase D* (PKD); *flox/flox* ($^{f/f}$); *high-fat diet* (HFD); *normal diet* (ND); *gonadal white adipose tissue* (gWAT); *subcutaneous white adipose tissue* (sWAT); *brown adipose tissue* (BAT); *skeletal muscle* (SKM). (Mayer et al., 2019; A, C, D, F)[275], (unpublished observation; B, E)

Despite there being no differences in body weight gain and body fat composition but increased liver weight, the mice were analyzed more broadly for other relevant metabolic parameters by using metabolic cages. The mice were housed individually for one week in metabolic cages after 23 weeks of HFD and ND feeding, respectively. The mice were allowed to adapt to the new environment/metabolic cages for 3 days before data acquisition was performed for 4 days. The analyzed parameters included

energy expenditure, food intake, activity, *respiratory exchange rate* (RER), oxygen consumption, and carbon dioxide production for which the HFD-fed *PKD3^{liverΔ/Δ}* mice did not differ in any of these parameters compared to control mice (Figure 16A-F). This was also observed for ND-fed control and *PKD3^{liverΔ/Δ}* mice (Figure 16G-H, J-L), except for decreased daytime activity of mice lacking PKD3 in liver (Figure 16I).

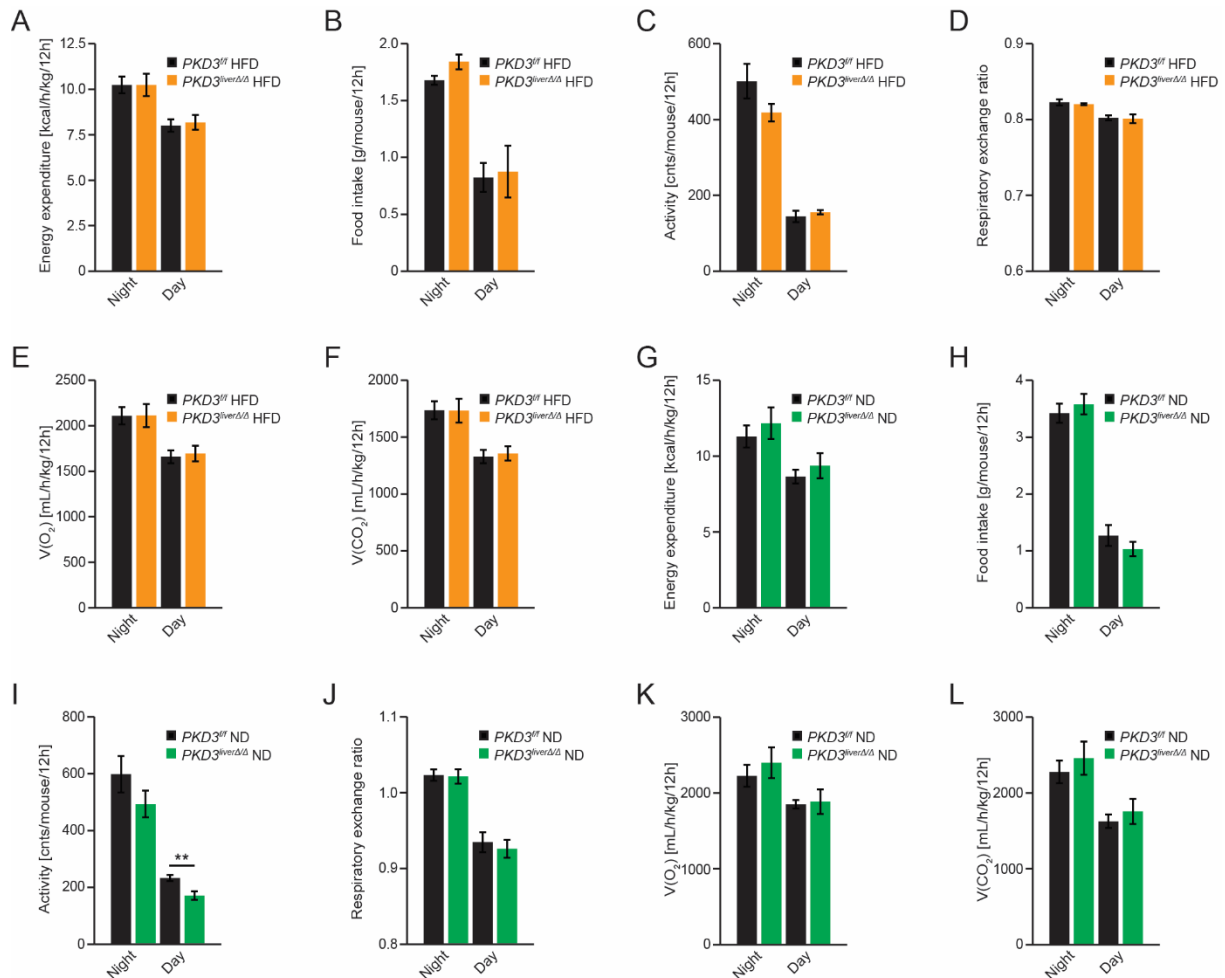**Figure 17: Hepatic deletion of PKD3 does not affect food intake, activity, or other calorimetric parameters.** Control and *PKD3^{liverΔ/Δ}* mice were analyzed in metabolic cages after 24 weeks of HFD-feeding for energy expenditure (A), food intake (B), activity (C), respiratory exchange ratio (D), oxygen consumption (E), and carbon dioxide production (F) [n=8 mice (WT) and n=15 mice (KO)]. Control and *PKD3^{liverΔ/Δ}* mice were analyzed in metabolic cages after 24 weeks of ND-feeding for energy expenditure (G), food intake (H), activity (I), respiratory exchange ratio (J), oxygen consumption (K), and carbon dioxide production (L) [n=9 mice (WT) and n=8 mice (KO)]. Data are presented as mean ± SEM. **P>0.01 (two way ANOVA with post hoc Tukey's test). *Protein kinase D* (PKD); *flox/flox* (^{f/f}); *high-fat diet* (HFD); *normal diet* (ND); *oxygen* (O_2); *carbon dioxide* (CO_2). (Mayer et al., 2019; A-D, G-J)[275], (unpublished observation; E, F, K, L)

The results showed that the increase in liver weight of *PKD3^{liverΔ/Δ}* mice was not due to changes in energy expenditure, food intake, activity, or RER (Figure 17), which was accompanied by no alterations in total body weight and fat depot mass (Figure 16).

Results

The liver is crucial for maintaining glucose homeostasis[11,283]. During fasting, the liver produces glucose by gluconeogenesis and glycogenolysis, and lowers postprandially blood glucose levels through glycolysis and glycogen synthesis[11,283]. To check whether PKD3 is involved in regulating glucose homeostasis, mice were challenged with a *glucose tolerance test* (GTT) for which the fasted mice received i.p. a defined dose of glucose and the glucose levels were monitored over 2 h at defined time points before and after injection. As shown in Figure 18A, B, HFD-fed *PKD3^(liverΔ/Δ)* mice displayed significantly improved glucose tolerance as the glucose concentration in circulation was lowering in these mice at much faster rates than for control mice. This observation was complemented by significantly improved insulin sensitivity of *PKD3^(liverΔ/Δ)* mice compared to control littermates as assessed by *insulin tolerance test* (ITT) (Figure 18C, D). For this assay, fasted mice received i.p. a defined dose of insulin and the blood glucose concentrations were monitored at the same time points as for GTT. As a response of the insulin challenge, the blood glucose concentrations of mice lacking PKD3 in liver dropped at much faster rates compared to controls, indicating that these mice responded to insulin in a much more sensitive fashion and thus, were less HFD-induced insulin resistant. Consistent with these results, HFD-fed *PKD3^(liverΔ/Δ)* mice presented significantly reduced serum insulin levels compared to control mice, thereby underlining the improved insulin sensitivity in these mice (Figure 18E). In case of ND-feeding, the glucose challenge of control and *PKD3^(liverΔ/Δ)* mice had no impact on the clearing rates of glucose from the circulation (Figure 18F, G). Additionally, there was no difference in ITT (Figure 18H, I) or serum insulin levels (Figure 18J) in control and *PKD3^(liverΔ/Δ)* mice fed an ND, emphasizing the importance of HFD-feeding for PKD activation and thus for physiologically improving glucose and insulin tolerance.
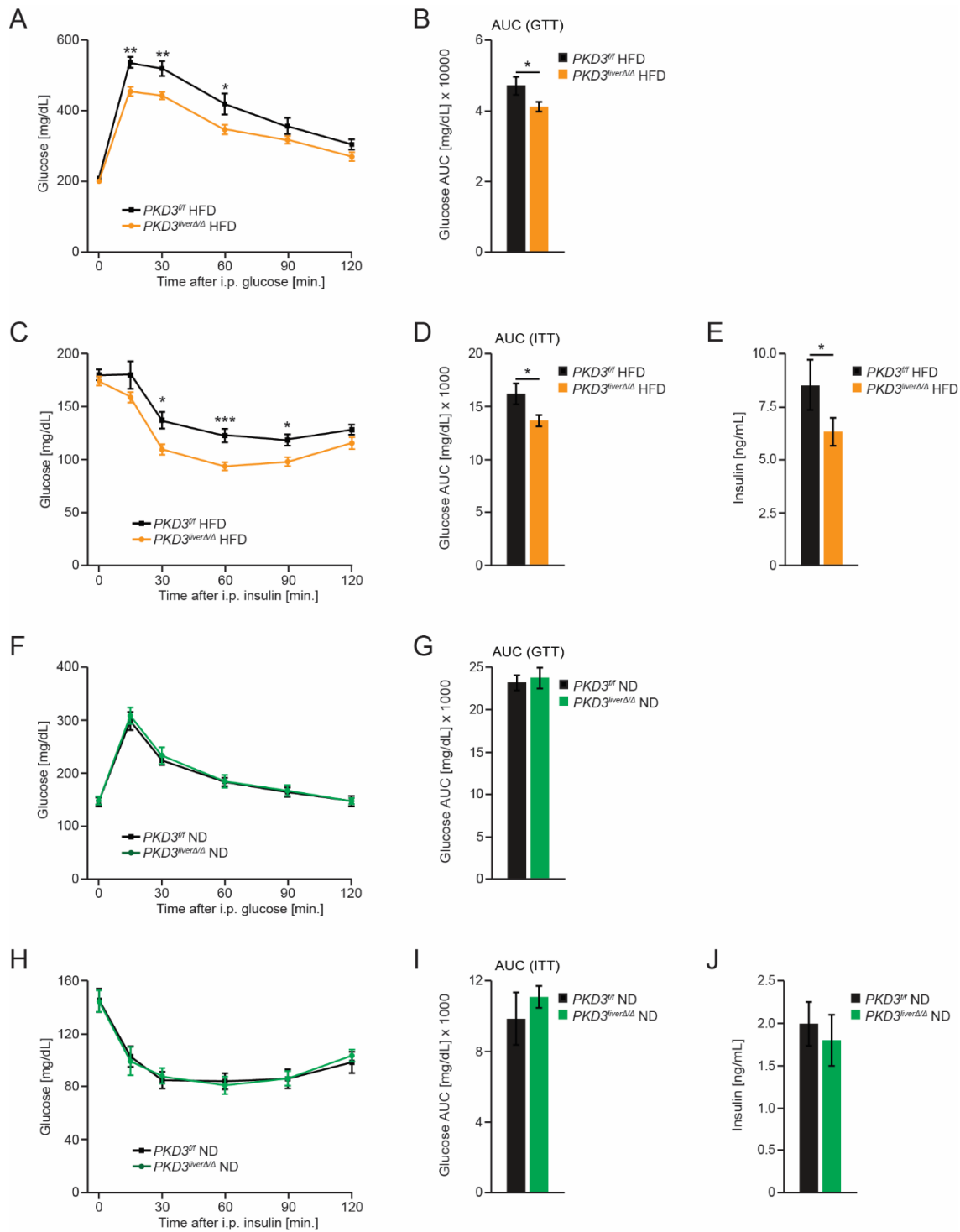
Results

Figure 18: PKD3 promotes glucose intolerance and insulin resistance. Control and *PKD3*$^{liver\Delta/\Delta}$
mice were analyzed for glucose tolerance (2 g/kg BW) with calculated AUC (A, B), and insulin tolerance
(1.5 U/kg BW) with calculated AUC (C, D), as well as for insulin levels in serum (E) after HFD feeding
for 16, 18, and 24 weeks, respectively [n=8 mice (WT) and n=15 mice (KO)]. Control and *PKD3*$^{liver\Delta/\Delta}$
mice were analyzed for glucose tolerance (2 g/kg BW) with calculated AUC (F, G), and insulin tolerance
(0.8 U/kg BW) with calculated AUC (H, I), as well as for insulin levels in serum (J) after ND feeding for
16, 18, and 24 weeks, respectively [n=9 mice (WT) and n=8 mice (KO)]. For all tolerance tests, the mice
received after 4 hours of fasting an intraperitoneal dose of glucose or insulin, respectively, and the blood
glucose levels were monitored at 0, 15, 30, 60, 90, and 120 min after injection. Data are presented as
mean ± SEM. *$P > 0.05$, **$P > 0.01$, ***$P > 0.001$ [unpaired two-tailed Student's t test (B, D, E, G, I, J) or
two way ANOVA with post hoc Tukey's test (A, C, F, H)]. *Protein kinase D* (PKD); *flox/flox* ($^{f/f}$); *high-fat
diet* (HFD); *normal diet* (ND); *glucose tolerance test* (GTT); *insulin tolerance test* (ITT); *intraperitoneal*
(i.p.); *area under the curve* (AUC). (Mayer et al., 2019; A-I)[275], (unpublished observation; J)

Results

In order to further investigate the physiologically improved insulin sensitivity in HFD-fed *PKD3^liverΔ/Δ* mice on a molecular level, the phosphorylation status of protein kinase B (AKT) was analyzed at basal conditions and in response to excess insulin. The level of AKT phosphorylation is a useful tool to study insulin signaling intracellularly because the binding of insulin to the insulin receptor leads to an IRS-PI3K-PDK mediated phosphorylation of AKT on Thr308 (reviewed in [284]). Experimentally, control and *PKD3^liverΔ/Δ* mice were fed an HFD for 24 weeks followed by an i.p. injection of vehicle or insulin (8 U/kg body weight) for 15 min. Analysis of AKT phosphorylation by WB revealed that mice lacking PKD3 in liver presented significantly increased levels of AKT phosphorylation on Thr308 and Ser473 compared to controls in response to insulin (Figure 19A, B). Together with improved ITT and lower serum insulin levels in *PKD3^liverΔ/Δ* mice, this outlines enhanced insulin sensitivity in the liver of these mice.
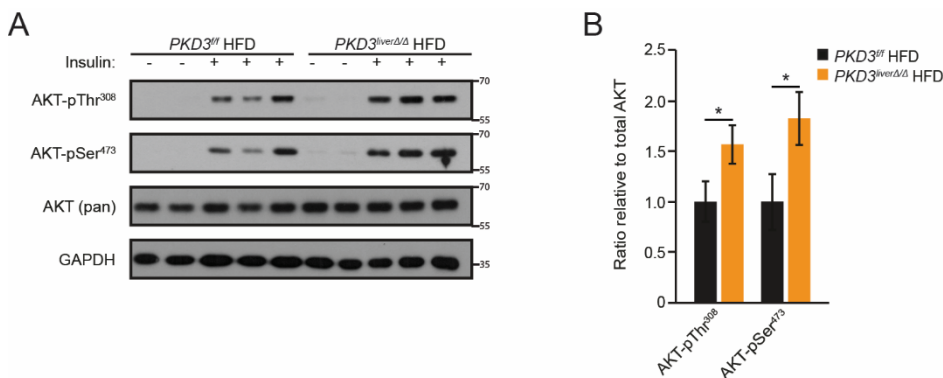

Figure 19: *PKD3^liverΔ/Δ* mice respond more sensitive to insulin on a molecular level in liver. (A, B) WB analysis and corresponding densitometric quantification of protein lysates from livers of control and *PKD3^liverΔ/Δ* mice fed an HFD for 24 weeks that received an intraperitoneal dose of the vehicle or insulin (8 U/kg body weight) for 15 min using antibodies against AKT-pThr308, AKT-pSer473, AKT (pan), and GAPDH as loading control (n=5 mice/group). Data are presented as mean ± SEM. **$P>0.05$ (one way ANOVA with post hoc Tukey's test). *Protein kinase D* (PKD); *flox/flox* ($^{f/f}$); *high-fat diet* (HFD); *protein kinase B* (AKT); *glyceraldehyde 3-phosphate dehydrogenase* (GAPDH); *phospho* (p); *threonine* (Thr); *serine* (Ser). (Mayer et al., 2019)[275]

3.2.2 PKD3 suppresses lipid accumulation in liver

A reason for the increased liver weight in HFD-fed *PKD3^liverΔ/Δ* mice might be due to the increased accumulation of lipids. To examine this possibility, H&E staining was performed to identify potential histological differences in the livers of the respective genotypes. Hematoxylin stains cell nuclei blue and eosin stains the extracellular matrix and cytoplasm pink. Liver sections from *PKD3^liverΔ/Δ* mice fed an HFD had qualitatively more and larger lipid droplets compared to controls, which can be seen by more white circular shaped droplets as H&E does not stain lipids (Figure 20A). To quantify this,

lipids were extracted by the method of Bligh and Dyer[272]. The lack of PKD3 in hepatocytes resulted in significantly increased accumulation of TG and especially of cholesterol in liver (Figure 20B, C). In contrast, liver sections from control and *PKD3^{liverΔ/Δ}* mice fed an ND did not show qualitatively any histological differences (Figure 20A), nor significant alterations in liver TG or cholesterol content (Figure 20D, E).
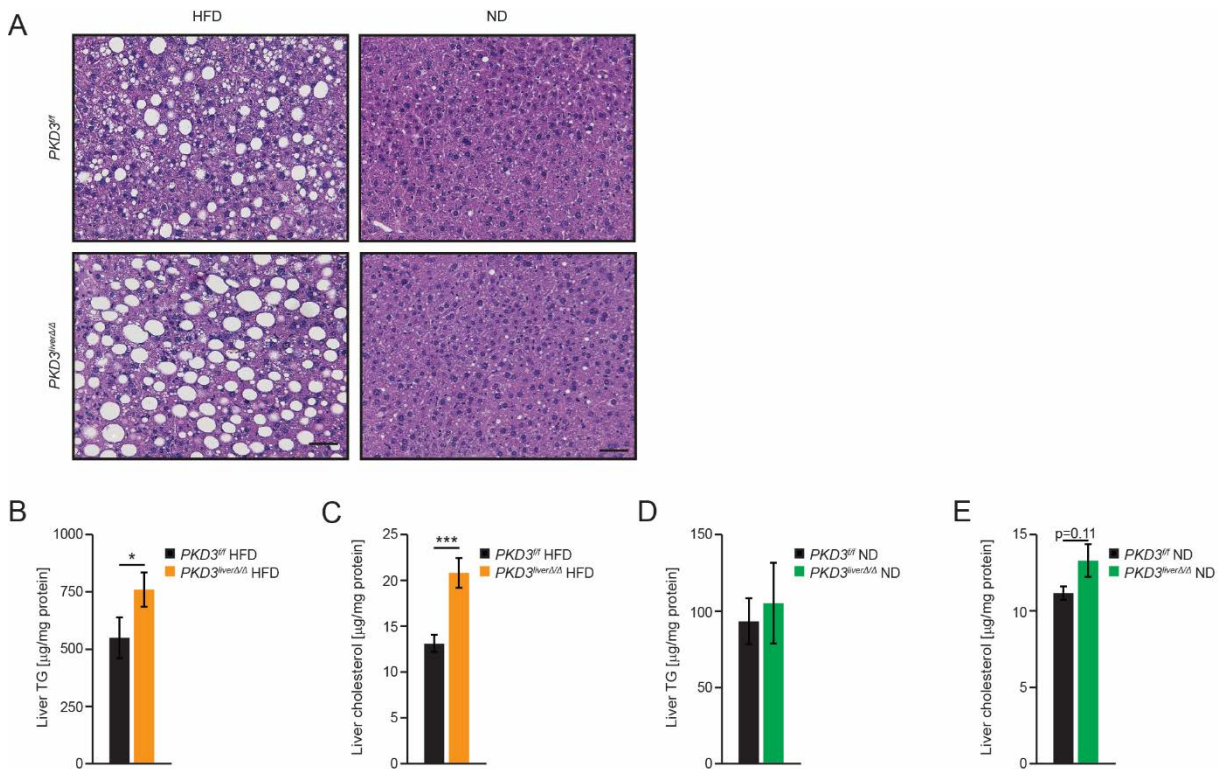

Figure 20: Lack of PKD3 promotes TG and cholesterol accumulation in liver. (A) Representative microscopy pictures of H&E stained liver sections from control and *PKD3^{liverΔ/Δ}* mice fed an HFD for 24 weeks (scale bar = 50 µm; representative picture of 6 mice/group). (B, C) Quantification of TG and cholesterol content, respectively, in extracted lipids from livers of control and *PKD3^{liverΔ/Δ}* mice fed an HFD for 24 weeks and normalized to protein level (n=10 mice/group). (D, E) Quantification of TG and cholesterol content, respectively, in extracted lipids from livers of control and *PKD3^{liverΔ/Δ}* mice fed an ND for 24 weeks and normalized to protein level (n=10 mice/group). Data are presented as mean ± SEM. *P>0.05, ***P>0.001 (unpaired two-tailed Student's t test). *Protein kinase D* (PKD); *flox/flox* (^{f/f}); *high-fat diet* (HFD); *normal diet* (ND); *triglycerides* (TG). (Mayer et al., 2019)[275]

Since total hepatic TG levels were enriched in mice that lack PKD3 in hepatocytes, the composition of FFAs and their level of saturation was measured. For this reason, lipids were extracted again from HFD-fed control and *PKD3^{liverΔ/Δ}* mice and subsequently saponified in order to quantify total hepatic FFAs (bound and unbound) by LC/MS. Among the eleven most present FFAs, oleic acid (C18:1) was the only significantly enriched FFA in livers of HFD-fed and *PKD3^{liverΔ/Δ}* mice (Figure 21A). In liver, intracellular FFAs originate either from endogenous de novo synthesis, or are taken

up from chylomicrons and peripheral tissues[285,286]. The high concentration of oleic acid implies that the fed HFD was extremely rich in this FFA.
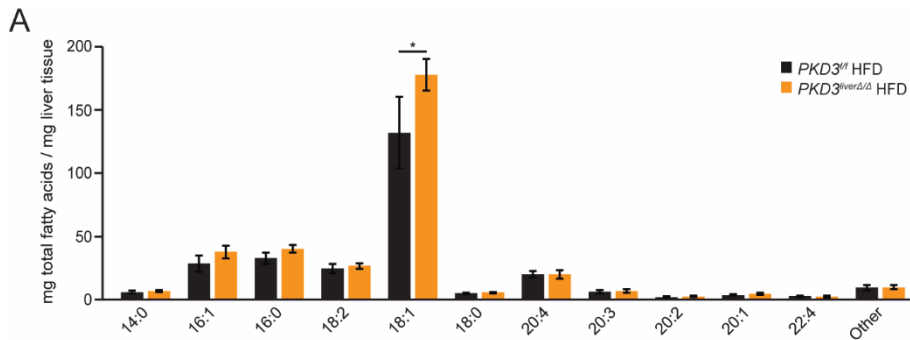

Figure 21: Oleic acid is the predominantly enriched FFA in livers of HFD-fed *PKD3^liverΔ/Δ* mice. (A) Total free fatty acid distribution (free and bound FFA) in livers from control and *PKD3^liverΔ/Δ* mice fed an HFD for 24 weeks. The isolated lipid phase was saponified in order to quantify total fatty acids by LC/MS (n=10 mice/group). This experiment was performed in collaboration with the working group of Prof. Dr. Schulze. Data are presented as mean ± SEM. *P>0.05 (unpaired two-tailed Student's t test). *Protein kinase D* (PKD); *flox/flox* (^f/f); *high-fat diet* (HFD). (unpublished observation)

There are many classes of lipids in hepatocytes beside TG and cholesterol. To check whether there are also differences in other classes of lipids, a *thin-layer chromatography* (TLC)-based separation of extracted hepatic lipids was used to analyze also the abundancy of CE, TG, FFA, *free cholesterol* (FC), *phosphatidylethanolamine* (PE), and PL qualitatively and quantitatively by identifying and comparing them with standards of known concentrations. The results showed that CE and TG appeared to be enriched in livers of HFD-fed *PKD3^liverΔ/Δ* mice compared to control mice (Figure 22A), which was confirmed by densitometric quantification (Figure 22B, C), whereas other classes of lipids such as FFA, FC, PE, and PL did not show any differences between the genotypes as detected with this method.
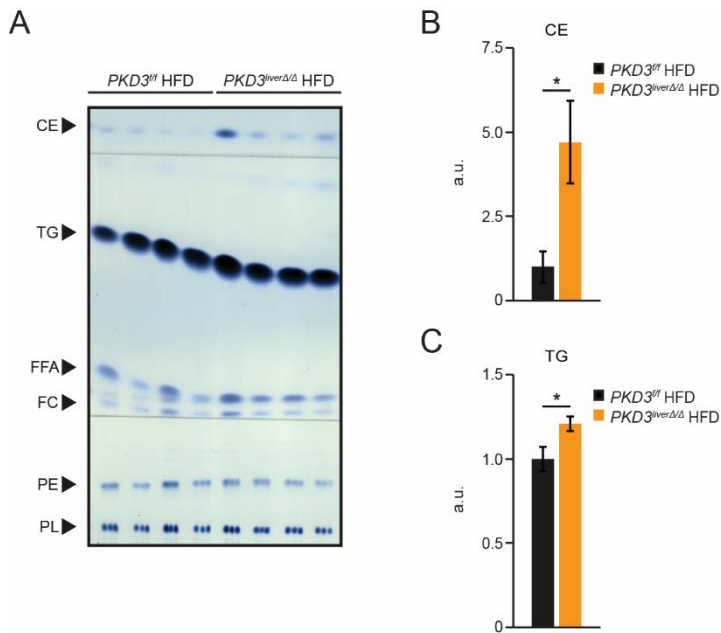
Figure 22: PKD3 suppresses the accumulation of cholesterol esters and TGs in liver. (A) TLC-mediated separation of lipids isolated from livers of control and $PKD3^{liver\Delta/\Delta}$ mice fed an HFD. Standards were used to localize CE, TG, FFA, FC, PE, and PL on the TLC plate (n=8 mice/group). (B, C) Corresponding densitometric quantification of CE and TG, respectively, by using standards of known concentrations (n=8 mice/group). Data are presented as mean ± SEM. *P>0.05 (unpaired two-tailed Student's t test). *Protein kinase D* (PKD); *flox/flox* ($^{f/f}$); *high-fat diet* (HFD); *arbitrary units* (a.u.); *cholesteryl ester* (CE); *triglycerides* (TG); *free fatty acids* (FFA); *free cholesterol* (FC); *phosphatidylethanolamine* (PE); *phospholipids* (PL). (Mayer et al., 2019)[275]

In addition to storing lipids in lipid droplets, the liver also uses them to form other lipids, uses them for β-oxidation in mitochondria, or packs and secrets them as VLDLs into the blood stream. For this reason, the concentrations of various metabolites were determined in serum of control and $PKD3^{liver\Delta/\Delta}$ mice. Serum cholesterol was significantly increased in serum of mice lacking PKD3 in hepatocytes (Figure 23A), whereas concentrations of TG, FFA, and glycerol were unaffected by hepatic PKD3 deletion (Figure 23B-D). Similarly to the results obtained before, there were no differences observed for serum cholesterol, TG, FFA, or glycerol between control and $PKD3^{liver\Delta/\Delta}$ mice fed an ND (Figure 23E-H).
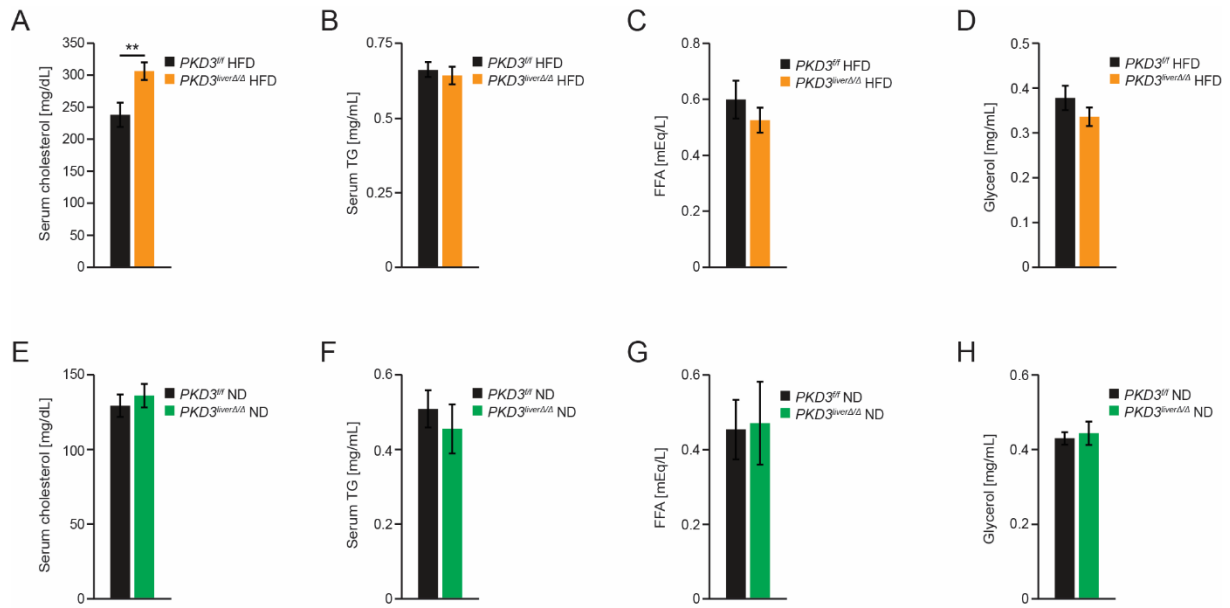
Figure 23: Determination of serum cholesterol, TG, FFA, and glycerol concentrations of control and *PKD3$^{liverΔ/Δ}$* mice. (A-D) Quantification of serum cholesterol (A), TG (B), FFA (C), and glycerol (D) concentrations of control and *PKD3$^{liverΔ/Δ}$* mice fed an HFD for 20 weeks (n=8 mice/group). (E-F) Quantification of serum cholesterol (E), TG (F), FFA (G), and glycerol (H) concentrations of control and *PKD3$^{liverΔ/Δ}$* mice fed an ND for 20 weeks (n=8 mice/group). Data are presented as mean ± SEM. **P>0.01 (unpaired two-tailed Student's t test). *Protein kinase D* (PKD); *flox/flox* (f/f); *high-fat diet* (HFD); *normal diet* (ND); *triglycerides* (TG); *free fatty acid* (FFA). (Mayer et al., 2019; A, B, E, F)[275], (unpublished observation; C, D, G, H)

3.2.3   PKD1 does not affect liver metabolism

PKD1 has been reported to be involved in various metabolic processes such as in the regulation of insulin secretion in pancreatic β cells[109] or the lack of PKD1 in adipocytes protects mice from the development of diet-induced obesity due to elevated energy expenditure[158]. To investigate a potential role of PKD1 on liver metabolism, mice lacking PKD1 specifically in hepatocytes (*PKD1$^{liverΔ/Δ}$*) were generated by crossing PKD1 floxed mice (*PKD1$^{f/f}$*)[105] with mice expressing the Cre recombinase under the control of the albumin promoter (B6.Cg-Tg(Alb-cre)21Mgn/J)[271]. The Cre recombinase-mediated deletion of *Pkd1* in liver was confirmed by RT-qPCR, while *Pkd1* expression was unaffected in gWAT and SKM (Figure 24A). Body weight gain of control and *PKD1$^{liverΔ/Δ}$* mice fed either an ND or an HFD was monitored over 24 weeks and subsequently organ weights were analyzed. In short, there were no differences observed for weight gain nor for organ weights regardless of the diet (Figure 24B, C). Control and liver-specific PKD1-deficient did also not differ in the response to the stimulus of i.p. glucose or insulin (Figure 24D, E), nor were there any differences in the concentration of serum metabolites such as glucose, TG, FFA, or glycerol between the genotypes independent of ND or HFD-feeding (Figure 24F-I).
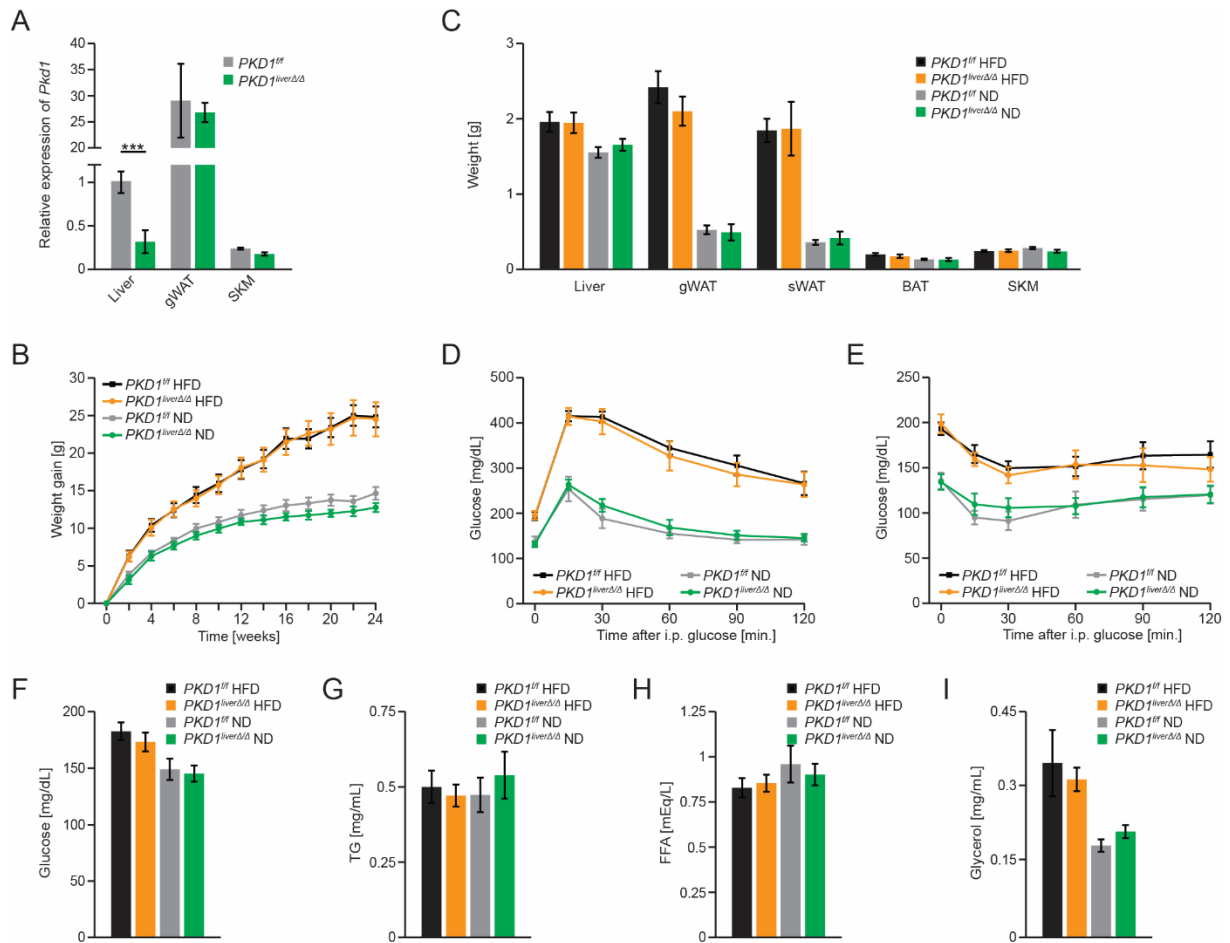
Figure 24: Deletion of PKD1 in liver does not affect organ weights, weight gain, or other metabolic parameters. RT-qPCR analysis of *Pkd3* expression in liver, epiWAT, and SKM of control (*PKD1^{f/f}*) and *PKD1^{liverΔ/Δ}* mice (n=4 mice/group). (B, C) Control and *PKD1^{liverΔ/Δ}* mice fed either an ND or HFD for 24 weeks were analyzed for body weight gain evolution (B) and organ weights (C). (D, E) The same mice were analyzed for glucose tolerance (1.5 g/kg BW) and insulin tolerance (0.25 U/kg BW) after feeding of indicated diets for 16 and 18 weeks, respectively (n=6-8 mice/group). (F-G) Quantification of serum cholesterol (F), TG (G), FFA (H), and glycerol (I) concentrations in control and *PKD1^{liverΔ/Δ}* mice fed an ND or HFD for 22 weeks (n=6-8 mice/group). Data are presented as mean ± SEM. *P>0.05, **P>0.01, ***P>0.001 [unpaired two-tailed Student's t test (A, B, F-I) or two way ANOVA with post hoc Tukey's test (C-E)]. *Protein kinase D* (PKD); *flox/flox* (^{f/f}); *high-fat diet* (HFD); *normal diet* (ND); *gonadal white adipose tissue* (gWAT); *subcutaneous white adipose tissue* (sWAT); *brown adipose tissue* (BAT); *skeletal muscle* (SKM); *triglycerides* (TG); *free fatty acid* (FFA). (unpublished observation)

3.2.4 Proliferation and fibrosis are unaffected by PKD3 deletion in hepatocytes

Immunohistological stainings for proliferation and apoptosis markers were used to exclude alterations in these processes for being responsible for the increased liver weight of HFD-fed *PKD3^{liverΔ/Δ}* mice, other than the increased accumulation of lipids in liver. There were no differences observed for proliferation between livers of HFD-fed control and *PKD3^{liverΔ/Δ}* mice assessed by Ki-67 staining (Figure 25A, B). For apoptosis, which was tested by staining of cleaved caspase-3 and TUNEL staining, deletion of PKD3 in hepatocytes did not alter this process (Figure 25A, C, D). The

pathological accumulation of lipids in liver leads to the development of steatosis and NAFLD, which might progress into NASH and ultimately to cirrhosis and HCC. In this context, NASH is characterized by steatosis, liver damage, and inflammation, and cirrhosis is further characterized by fibrosis[32]. For this reason, the infiltration of immune cells was studied to see whether PKD3 is involved in the transitioning of steatosis to NASH and cirrhosis. However, there was no difference observed for immune cells infiltration determined by specific immunohistological staining's (F4/80 for macrophages; CD3 for T cells; and B220 for B cells) between control and $PKD3^{liver\Delta/\Delta}$ HFD-fed mice. Additionally, these mice had a similar extent in collagen type IV and sirius red (collagen stain) stainings which are indicators for fibrosis (Figure 25A). Taken together, deletion of PKD3 did not affect apoptosis or proliferation of hepatocytes, neither did it promote the transition from steatosis to NASH and cirrhosis.
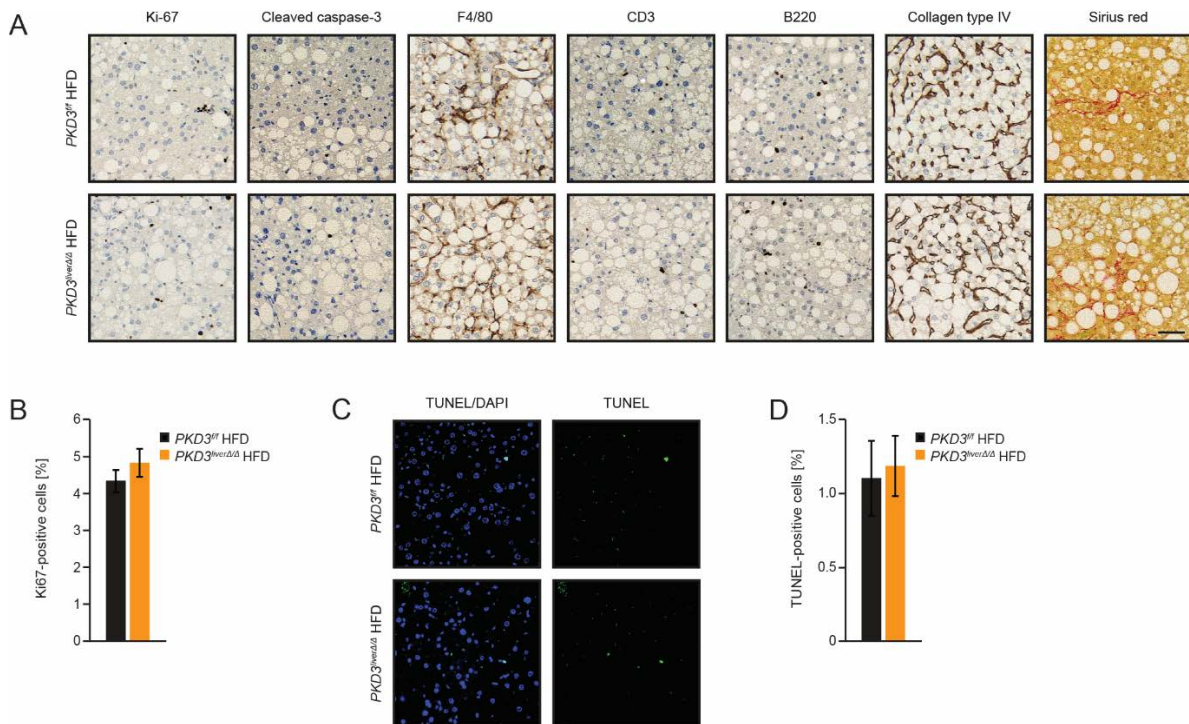
Figure 25: Proliferation, apoptosis, immune cell infiltration, and fibrosis are not affected by PKD3 deletion in liver. Representative microscopy pictures of Ki-67, cleaved caspase-3, F4/80, CD3, B220, and collagen type IV immunohistochemical and sirius red stained liver sections from control and $PKD3^{liver\Delta/\Delta}$ mice fed an HFD for 24 weeks (scale bar = 50 µm; images are representative of n=8 mice/group). (B) Quantification of Ki-67-positive cells from figure A. (C, D) Representative fluorescent images of TUNEL stained liver sections from control and $PKD3^{liver\Delta/\Delta}$ mice fed an HFD for 24 weeks and corresponding quantification of TUNEL-positive cells (Scale bar = 50 µm). This experiment was performed in collaboration with the working group of Prof. Dr. Heikenwalder. Data are presented as mean ± SEM with n>5000 cells counted per section and n=8 mice/group (unpaired two-tailed Student's t test). *Terminal deoxynucleotidyl transferase* (TdT); *deoxyuridine triphosphate* (dUTP); *TdT-mediated dUTP-biotin nick end labeling* (TUNEL). (Mayer et al., 2019)[275]

Results

The hippo pathway coactivators *yes-associated protein* (YAP) and *transcriptional coactivator with PDZ-binding motif* (TAZ) are involved in different hepatic processes. Among them, YAP drives tumorigenesis in liver (reviewed in [287]) and TAZ promotes inflammation and fibrosis in the liver[288] allowing an exploration of these features of NASH on a molecular level in PKD3-deficient livers. In contrast to the results obtained in Figure 25A, YAP/TAZ total protein level was increased in HFD-fed *PKD3^{liverΔ/Δ}* mice compared to controls (Figure 26A, B), suggesting that *PKD3^{liverΔ/Δ}* mice are prone to develop tumors and NASH. The liver damage markers *alanine transaminase* (ALT) and *aspartate transaminase* (AST) among other parameters can be used to calculate the NAFLD fibrosis score[289] allowing a prediction of liver damage in the context of fibrosis. However, ALT and AST activity was unaltered in serum of HFD-fed *PKD3^{liverΔ/Δ}* mice compared to control mice (Figure 26C, D), suggesting that alterations in YAP/TAZ protein level alone are not sufficient for developing liver fibrosis.
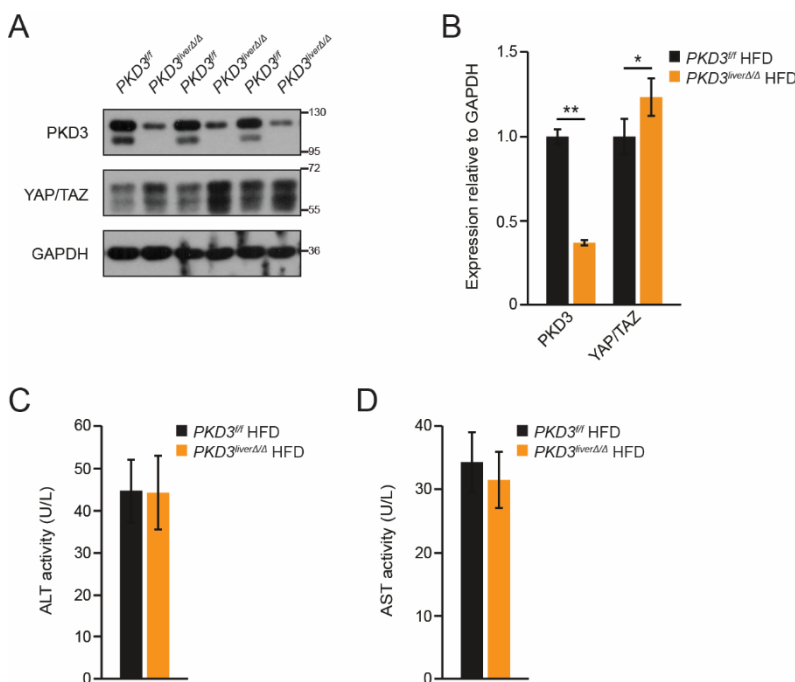
Figure 26: PKD3 suppresses YAP/TAZ protein content in liver without resulting in liver damage.
(A, B) WB analysis and corresponding densitometric quantification of protein lysates from livers of control and *PKD3^{liverΔ/Δ}* mice fed an HFD for 24 weeks using antibodies against PKD3, YAP/TAZ, and GAPDH as loading control (n=9 mice/group). (C, D) Analysis of liver damage markers ALT and AST in serum of control and *PKD3^{liverΔ/Δ}* mice fed an HFD for 24 weeks (n=9 mice/group). Data are presented as mean ± SEM. **P>0.05, **P>0.01 [unpaired two-tailed Student's t test (C, D), one way ANOVA with post hoc Tukey's test (B)]. *Protein kinase D* (PKD); *flox/flox* (^{f/f}); *high-fat diet* (HFD); *yes-associated protein* (YAP); *transcriptional coactivator with PDZ-binding motif* (TAZ); *glyceraldehyde 3-phosphate dehydrogenase* (GAPDH); *alanine transaminase* (ALT); *aspartate transaminase* (AST). (unpublished observation)

3.3 Lack of PKD3 in hepatocytes promotes de novo lipogenesis in an SREBP-dependent manner

There are several potential processes that might explain the increased lipid accumulation in livers of HFD-fed $PKD3^{liver\Delta/\Delta}$ mice, namely de novo lipogenesis, fatty acid oxidation, and VLDL secretion. Firstly, de novo lipogenesis rate was compared in primary hepatocytes isolated from control and $PKD3^{liver\Delta/\Delta}$ mice by incubating them with tritium-labeled acetate and insulin (if indicated) under lipogenic conditions (high glucose and acetate in the cell medium). Following incubation, lipids were isolated and the amount of incorporated tritium-labeled acetate into newly formed lipids was measured. The rate of de novo lipogenesis was significantly increased at basal and insulin-induced conditions in PKD3-deficient hepatocytes compared to control hepatocytes (Figure 27A). This difference in lipid synthesis rate resulted in higher levels of free cholesterol, TG, and cholesteryl esters, whereas other classes of lipids were not changed in hepatocytes isolated from $PKD3^{liver\Delta/\Delta}$ mice compared to controls (Figure 27B). Despite enhanced lipid synthesis rate and lipid accumulation in livers of $PKD3^{liver\Delta/\Delta}$ mice, the level of *fatty acid oxidation* (FAO) was moderately increased in PKD3-deficient hepatocytes compared to controls (Figure 27C). To investigate VLDL secretion, mice were i.v. injected with tyloxapol (a lipoprotein lipase inhibitor), resulting in blocked peripheral lipid uptake. Control and $PKD3^{liver\Delta/\Delta}$ mice did not display alterations in serum TG accumulation independent of ND and HFD-feeding (Figure 27D, E), meaning that elevated lipid level in livers of $PKD3^{liver\Delta/\Delta}$ mice are mainly a result of increased de novo lipogenesis.
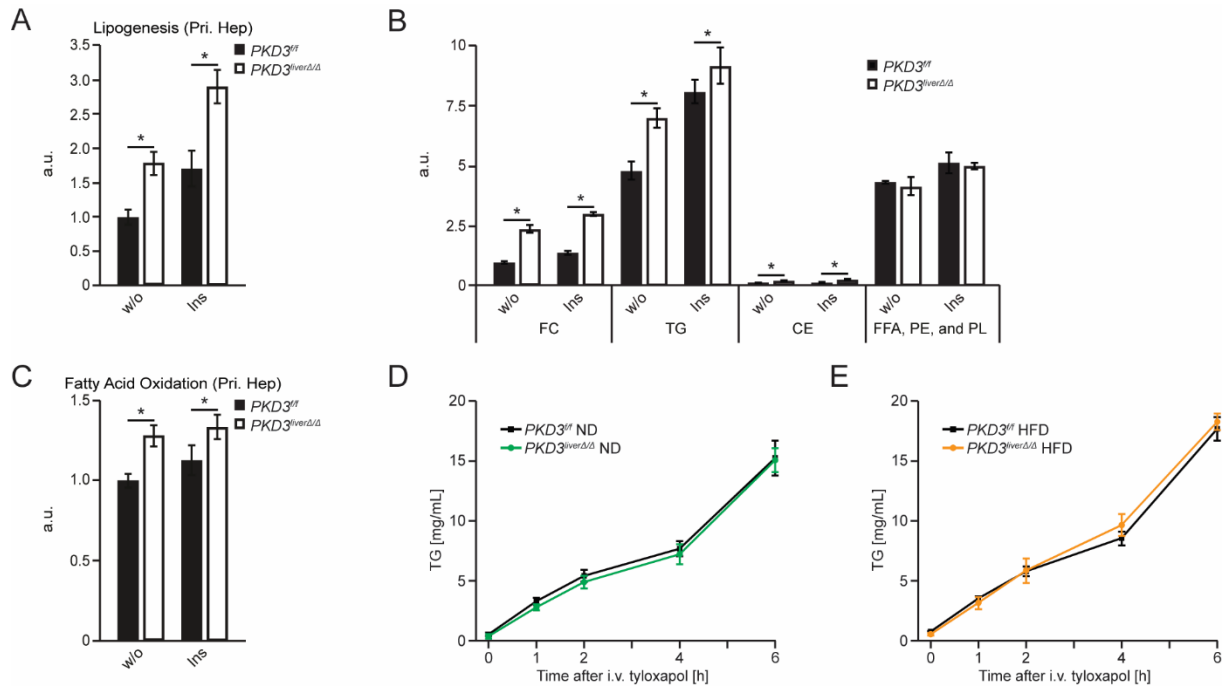
Results

Figure 27: Lack of PKD3 promotes de novo lipogenesis in hepatocytes. (A) Basal and insulin-stimulated total de novo lipogenesis rate during lipogenic conditions (serum deprived, 25 mM glucose, 0.5 mM sodium acetate, and 100 nM insulin, if indicated) in primary hepatocytes isolated from control and *PKD3^{liverΔ/Δ}* mice (n=3 biological replicates/group). (B) Quantification of TLC-separated lipid classes such as FC, TG, CE, and other lipids (FFA, PE, PL) from primary hepatocytes of indicated genotypes (n=3 biological replicates/group). (C) Basal and insulin-stimulated (100 nM) fatty acid oxidation rate in primary hepatocytes isolated from mice of indicated genotypes (n=3 biological replicates/group). (D, E) VLDL secretion assessed by measuring serum TG concentration at given time points after *intravenous* (i.v.) injection of 0.5 mg/g BW tyloxapol in mice of indicated genotypes that were either fed an ND (D) or an HFD (E) for 8 weeks [n=7 mice/group (D) and n=5 mice/group (E)]. Data are presented as mean ± SEM. *P>0.05, ***P>0.001 [one way ANOVA with post hoc Tukey's test (A-C), or two way ANOVA with post hoc Tukey's test (D, E)]. *Protein kinase D* (PKD); *flox/flox* (^{f/f}); *high-fat diet* (HFD); *normal diet* (ND); *arbitrary units* (a.u.); *free cholesterol* (FC); *triglycerides* (TG); *cholesteryl ester* (CE); *free fatty acids* (FFA); *phosphatidylethanolamine* (PE); *phospholipids* (PL). (Mayer et al., 2019)[275]

Transcriptional activation of lipogenic gene expression in liver is regulated by transcription factors such as USF, SREBP1c, ChREBP, and LXR, being SREBP the most prominent one[14]. The three SREBP isoforms (SREBP-1a, 1c, and 2) have some functional overlap; however, SREBP-1c is primarily responsible for the expression of lipogenic genes and SREBP2 for the expression of genes required for cholesterol synthesis[14]. SREBPs reside as larger precursors at the ER membrane and are cleaved by SCAP upon stimulation, resulting in the translocation to the nucleus of the mature SREBP protein, and thus leading to induction of lipogenic and its own gene expression[14].
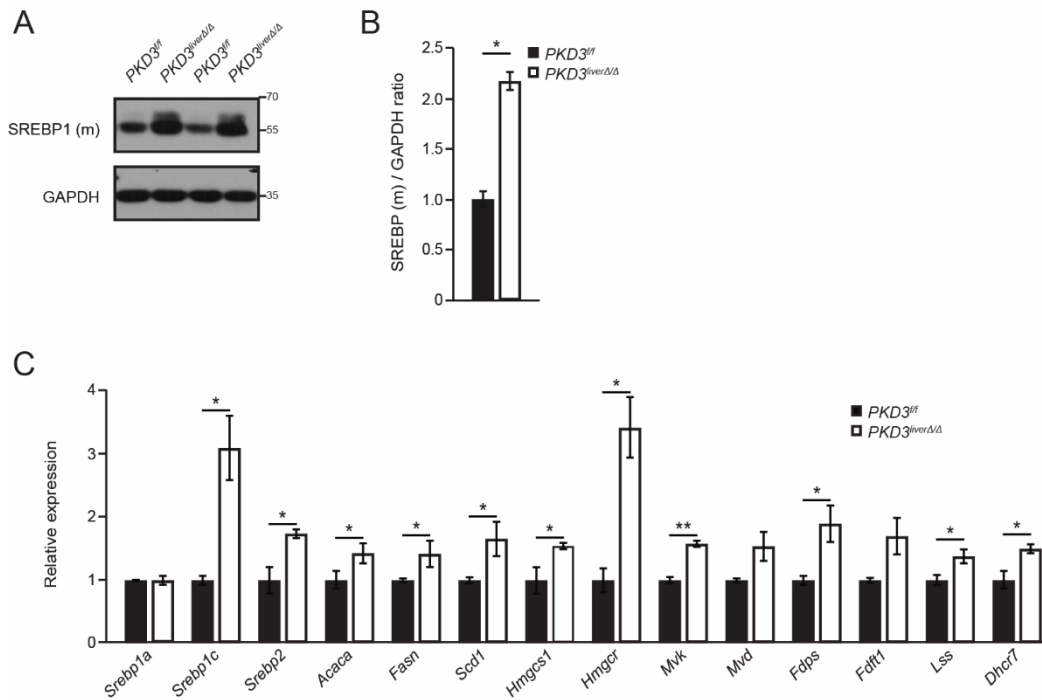
Figure 28: PKD3 mediates suppression of de novo lipogenesis through SREBP. (A, B) WB analysis and corresponding quantification of mature SREBP1 in primary hepatocytes isolated from mice of indicated genotypes after lipogenic stimulation (serum deprived, 25 mM glucose, 0.5 mM sodium acetate, and 100 nM insulin) using antibodies against SREPB1, and GAPDH as loading control (n=3 mice/group). (C) RT-qPCR analysis of Srebp gene and target genes expression in primary hepatocytes of indicated genotypes after lipogenic stimulation as in A (n=3 biological replicates/group). Data are presented as mean ± SEM. *P>0.05, **P>0.01 (unpaired two-tailed Student's t test (B, C). *Protein kinase D* (PKD); *flox/flox* ($^{f/f}$); *Sterol regulatory element-binding protein* (SREBP); *mature* (m); *glyceraldehyde 3-phosphate dehydrogenase* (GAPDH); *sterol regulatory element binding protein* (Srebp); *acetyl-CoA carboxylase alpha* (Acaca); *fatty acid synthase* (Fasn); *stearoyl-CoA desaturase* (Scd); *3-hydroxyl-3-methylglutaryl-CoA synthase* (Hmgcs); *3-hydroxyl-3-methylglutaryl-CoA reductase* (Hmgcr); *mevalonate kinase* (Mvk); *mevalonate diphosphate decarboxylase* (Mvd); *farnesyl diphosphate synthase* (Fdps); *farnesyl-diphosphate farnesyltransferase* (Fdft); *lanosterol synthase* (Lss); *7-dehydrocholesterol reductase* (Dhcr7). (Mayer et al., 2019)[275]

Primary hepatocytes isolated from control and *PKD3$^{liverΔ/Δ}$* mice were subjected to lipogenic conditions in the cell medium to stimulate SREBP activation. PKD3-deficient hepatocytes displayed elevated protein levels of the mature (cleaved) form of SREBP1 compared to wild type hepatocytes (Figure 28A, B). Consistently, transcriptional analysis confirmed increased levels of *Srebp1c* and *Srebp2* as well as their target genes (*Acaca, Fasn, Scd1, Hmgcs1, Hmgcr, Mvk, Mvd, Fdps, Fdft1, Lss*, and *Dhcr7*) in PKD3-deficienct hepatocytes compared to controls (Figure 28C).

Results
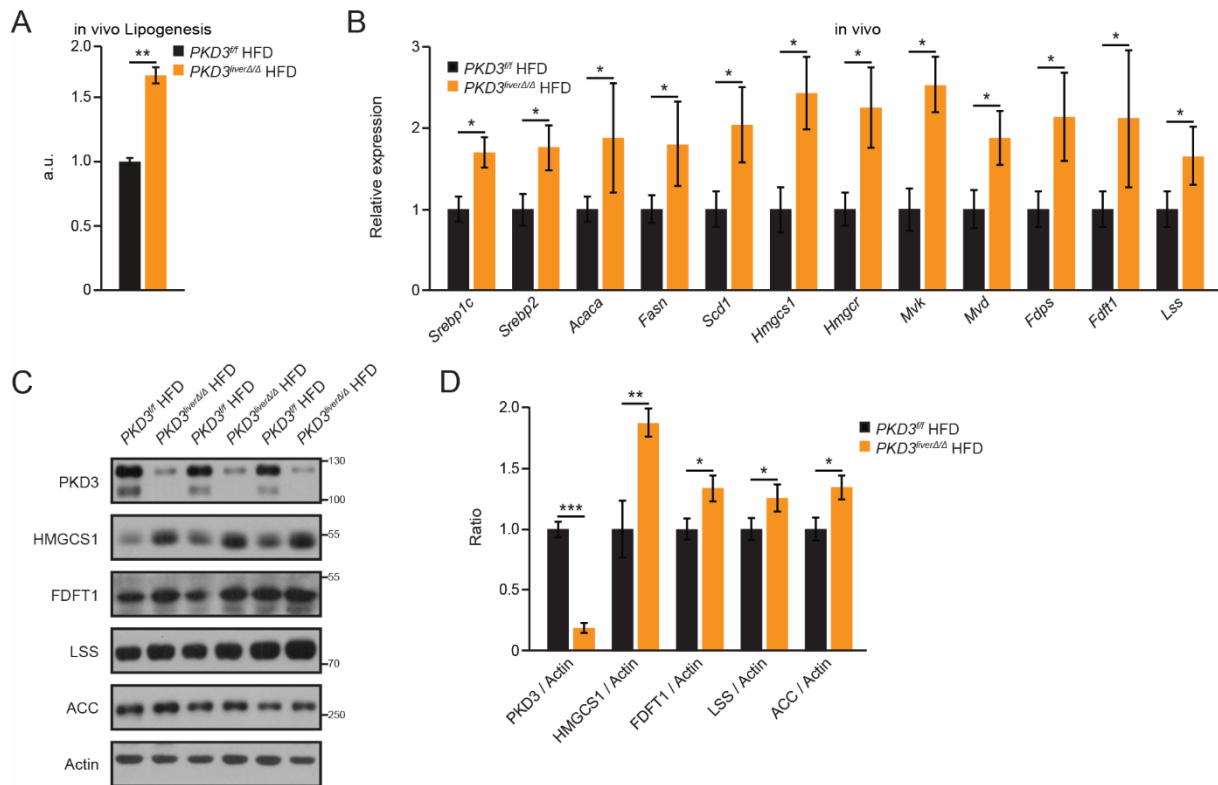
Figure 29: PKD3 suppresses lipogenesis in vivo. (A) In vivo de novo lipogenesis rate in livers from control and *PKD3^{liverΔ/Δ}* mice fed an HFD for 8 weeks, fasted overnight and refed for 4 hours prior to the experiment (n=5 mice/group). (B) RT-qPCR analysis of *Srebp* gene and target genes expression in livers from control and *PKD3^{liverΔ/Δ}* mice fed an HFD for 20 weeks, fasted overnight and refed for 4 hours (n=6 mice/group). (C, D) WB analysis and corresponding densitometric quantification of lipogenic enzymes in livers from the same mice as in B using antibodies against PKD3, HMGCS1, FDFT1, LSS, ACC, and Actin as loading control (n=3 mice/group). Data are presented as mean ± SEM. *P>0.05, **P>0.01, ***P>0.001 (unpaired two-tailed Student's t test). *Protein kinase D* (PKD); *flox/flox* (^{f/f}); *sterol regulatory element binding protein* (Srebp); *acetyl-CoA carboxylase alpha* (Acaca); *fatty acid synthase* (Fasn); *stearoyl-CoA desaturase* (Scd); *3-hydroxyl-3-methylglutaryl-CoA synthase* (Hmgcs); *3-hydroxyl-3-methylglutaryl-CoA reductase* (Hmgcr); *mevalonate kinase* (Mvk); *mevalonate diphosphate decarboxylase* (Mvd); *farnesyl diphosphate synthase* (Fdps); *farnesyl-diphosphate farnesyltransferase* (Fdft); *lanosterol synthase* (Lss); *acetyl-CoA carboxylase alpha* (ACC); *glyceraldehyde 3-phosphate dehydrogenase* (GAPDH). (Mayer et al., 2019)[275]

The increased rate of de novo lipogenesis in livers of PKD3-deficient hepatocytes was also observed in vivo. HFD-fed *PKD3^{liverΔ/Δ}* mice incorporated significantly more i.p. injected tritiated water ([^3H]-water) into newly formed lipids in response to a fasting/refeeding protocol compared to control littermates (Figure 29A). Consequently, the expression of *Srebp1* and *Srebp2* as well as their target genes was significantly upregulated in livers of *PKD3^{liverΔ/Δ}* mice compared to control mice after prolonged HFD feeding followed by a fasting/refeeding protocol (Figure 29B). In addition, the livers of these mice were used for determining the protein levels of several of these enzymes. The results showed an increase in the protein level for the enzymes HMGCS1, FDFT1, LSS, and ACC in PKD3-deficient livers compared to the control livers (Figure 29C, D).

Results
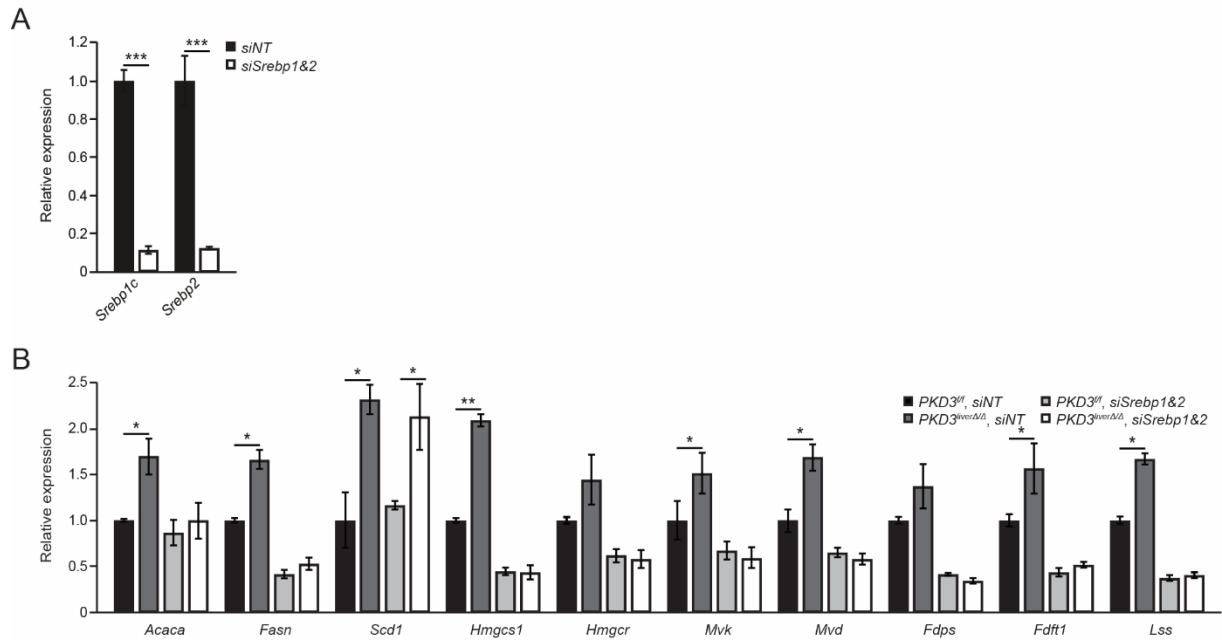
Figure 30: Silencing of Srebp1&2 abolishes the significant difference in lipogenic gene expression between control and PKD3-deficient hepatocytes. (A) RT-qPCR analysis of *Srebp1* and *Srebp2* gene expression in hepatocytes (n=3 biological replicates/condition). (B) RT-qPCR analysis of lipogenic genes expression in primary hepatocytes isolated from control and *PKD3$^{liverΔ/Δ}$* mice during lipogenic conditions (insulin stimulation for 4 h) that were either transfected with siNon-Targeting (siNT) or with the combination of siSrebp1 and siSrebp2 for 36 h prior to the experiment (n=3 biological replicates/condition). Data are presented as mean ± SEM. *P>0.05, **P>0.01 [unpaired two-tailed Student's t test (B), or one way ANOVA with post hoc Tukey's test (A)]. *Protein kinase D* (PKD); *flox/flox* (f/f); *non-targeting (*NT*); sterol regulatory element binding protein* (Srebp); *acetyl-CoA carboxylase alpha* (Acaca); *fatty acid synthase* (Fasn); *stearoyl-CoA desaturase* (Scd); *3-hydroxyl-3-methylglutaryl-CoA synthase* (Hmgcs); *3-hydroxyl-3-methylglutaryl-CoA reductase* (Hmgcr); *mevalonate kinase* (Mvk); *mevalonate diphosphate decarboxylase* (Mvd); *farnesyl diphosphate synthase* (Fdps); *farnesyl-diphosphate farnesyltransferase* (Fdft); *lanosterol synthase* (Lss). (Mayer et al., 2019)[275]

To investigate whether PKD really signals through SREBP, or whether SREBP is activated in response to another factor regulated by PKD3, a small interfering RNA (siRNA)-mediated silencing approach was used to silence *Srebp1* and *Srebp2* in primary hepatocytes. Firstly, deletion of *Srebp1c* and *Srebp2* was confirmed in siRNA-transfected primary hepatocytes after 36 h post transfection (Figure 30A). Next, wild type and PKD3-deficient hepatocytes were transfected with siSrebp1&2 again and subjected to a lipogenic stimulation with high glucose, high acetate, and insulin in the media for 4 h. In PKD3-deficient hepatocytes, the lipogenic gene expression was induced at a higher level compared to controls, which was blunted to the same level in both genotypes for *Acaca*, *Fasn*, *Hmgcs1*, *Hmgcr*, *Mvk*, *Mvd*, *Fdps*, *Fdft*, and *Lss*, except for *Scd1* (Figure 30B).

Results
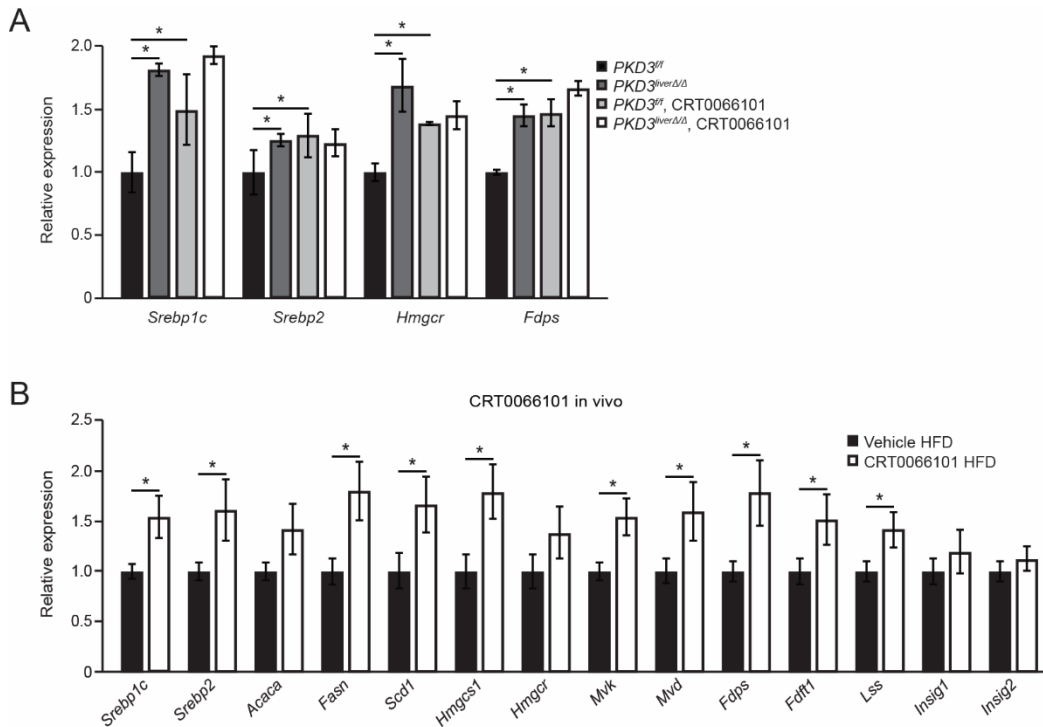
Figure 31: Inhibition of PKD increases lipogenic gene expression in isolated hepatocytes and in vivo. (A) RT-qPCR analysis of *Srebp1c*, *Srebp2*, *Hmgcr*, and *Fdps* expression in hepatocytes of indicated genotypes treated with vehicle or PKD Inhibitor CRT0066101 (0.1 µM) (n=3 biological replicates/condition). (B) RT-qPCR analysis of *Srebp* and target gene expression in livers of 8 weeks HFD-fed C57BL/6JRj mice that received either an i.p. injection of vehicle or CRT0066101 inhibitor (10 mg/kg BW) for five consecutive days. The mice were fasted overnight and refed for 4 hours before excising the livers (n=8 mice/group). Data are presented as mean ± SEM. *P>0.05 (unpaired two-tailed Student's t test). *Protein kinase D* (PKD); *flox/flox* (f/f); *high-fat diet* (HFD); *sterol regulatory element binding protein* (Srebp); *3-hydroxyl-3-methylglutaryl-CoA reductase* (Hmgcr); *farnesyl diphosphate synthase* (Fdps); *acetyl-CoA carboxylase alpha* (Acaca); *fatty acid synthase* (Fasn); *stearoyl-CoA desaturase* (Scd); *3-hydroxyl-3-methylglutaryl-CoA synthase* (Hmgcs); *mevalonate kinase* (Mvk); *mevalonate diphosphate decarboxylase* (Mvd); *farnesyl-diphosphate farnesyltransferase* (Fdft); *lanosterol synthase* (Lss); *insulin induced gene* (Insig). (Mayer et al., 2019)[275]

Moreover, the treatment of wild type and PKD3-deficient hepatocytes with the PKD-inhibitor CRT0066101 resulted in an increase of *Srebp1c*, *Srebp2*, *Hmgcr*, and *Fdps* expression under insulin-stimulated conditions regardless of the genotype and brought the expression to the same level between PKD3-deficient and wild type hepatocytes (Figure 31A). Consistent with previous findings, administration of the PKD-inhibitor for five consecutive days increased *Srebp1c* and *Srebp2* as well as their target gene expression in mice compared to vehicle administered control mice fed an HFD (Figure 31B). Altogether, pharmacological inhibition of PKD function promotes lipogenic gene expression in vitro and in vivo in hepatocytes.

Results
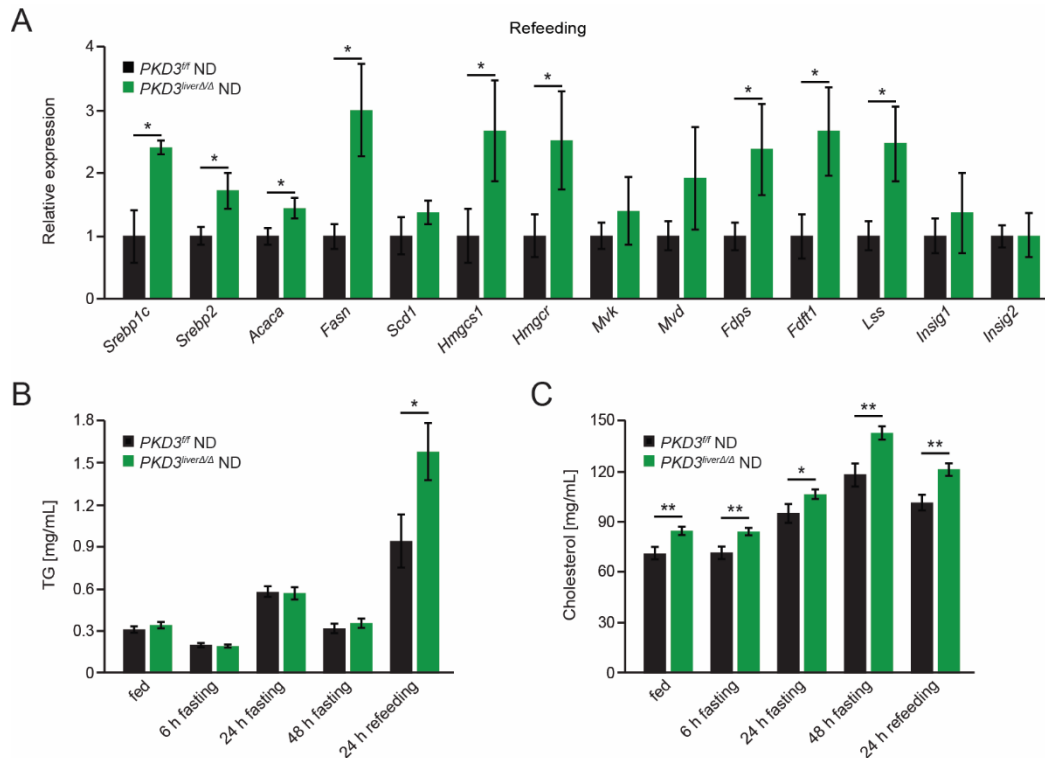
Figure 32: Refeeding augments lipogenic gene expression and lipid production in *PKD3^liverΔ/Δ* mice compared to control mice. (A) RT-qPCR analysis of *Srebp* and target gene expression in livers of control and *PKD3^liverΔ/Δ* mice that were fasted overnight and refed for 4 hours before excising the livers (n=4 mice/group; combined data from two individual experiments). (B, C) Quantification of TG (B) and cholesterol (C) concentrations in serum of control and *PKD3^liverΔ/Δ* mice fed an ND for 7 weeks that were fasted and refed for indicated time points (n=12 mice/group). Data are presented as mean ± SEM. *P>0.05, **P>0.01 [unpaired two-tailed Student's t test (A) or two way ANOVA with post hoc Tukey's test (B, C)]. *Protein kinase D* (PKD); *flox/flox* (^f/f); *normal diet* (ND); *sterol regulatory element binding protein* (Srebp); *acetyl-CoA carboxylase alpha* (Acaca); *fatty acid synthase* (Fasn); *stearoyl-CoA desaturase* (Scd); *3-hydroxyl-3-methylglutaryl-CoA synthase* (Hmgcs); *3-hydroxyl-3-methylglutaryl-CoA reductase* (Hmgcr); *mevalonate kinase* (Mvk); *mevalonate diphosphate decarboxylase* (Mvd); *farnesyl diphosphate synthase* (Fdps); *farnesyl-diphosphate farnesyltransferase* (Fdft); *lanosterol synthase* (Lss); *insulin induced gene* (Insig); *triglyceride* (TG). (Mayer et al., 2019)[275]

Insulin stimulation promotes SREBP activation and lipogenic gene expression in vitro and in vivo. Physiologically, the expression of lipogenic genes and de novo lipogeneses are induced upon food intake and subsequent insulin release[42]. To study the effect of the lipogenic program activation more broadly than by stimulating with insulin, differences in hepatic lipogenesis and the expression of genes promoting this process were analyzed between wild type and *PKD3^liverΔ/Δ* mice in response to a fasting/refeeding protocol. For this reason, mice were fasted overnight and refed for 4 hours, resulting in increased expression of *Srebp1c*, *Srebp2*, and some of their target genes in PKD3-deficient livers compared to control livers (Figure 32A). Furthermore, expression of *Insig1* and *Insig2* (*insulin induced gene*), which block the SCAP-SREBP complex in the ER and thus SREBP activation (reviewed in[290]), were unaffected by the

deletion of PKD3 in liver compared to control livers (Figure 32A). Consistent with the results obtained before, TG concentration was increased in serum after 48 h of prolonged fasting followed by 24 h of refeeding in $PKD3^{liver\Delta/\Delta}$ mice compared to controls (Figure 32B). This observation is in line with elevated serum cholesterol levels in mice lacking PKD3 in liver, nevertheless, cholesterol was increased in $PKD3^{liver\Delta/\Delta}$ mice at all studied conditions (fed, fasted, and refed) (Figure 32B).
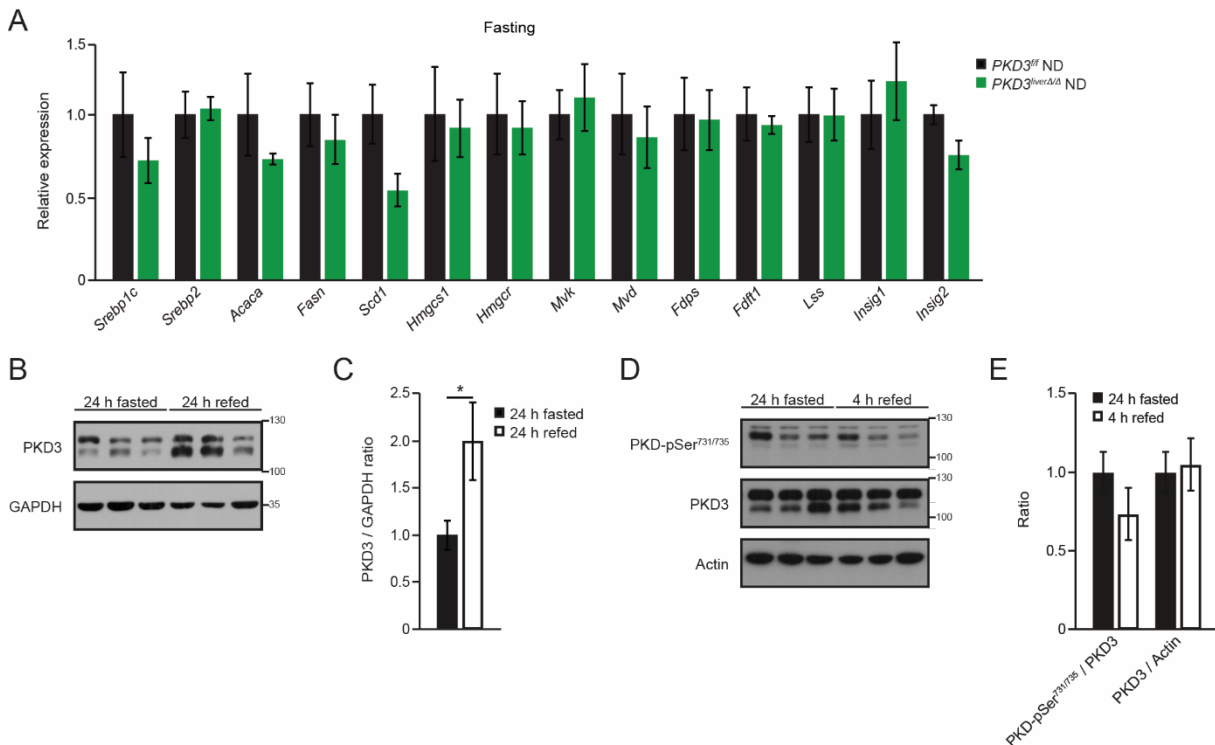
Figure 33: Fasting does not induce differences in lipogenic gene expression between control and $PKD3^{liver\Delta/\Delta}$ mice. (A) RT-qPCR analysis of *Srebp* and target gene expression in livers of control and $PKD3^{liver\Delta/\Delta}$ mice that were fasted overnight for 12 hours before excising the livers (n=4 mice/group). (B, C) WB analysis and corresponding densitometric quantification of PKD3 in livers of 24 h fasted and 24 h fasted/24 h refed C57BL/6JRj mice (n=3 mice/group). (D, E) WB analysis and corresponding densitometric quantification of PKD3 in livers of 24 h fasted and 24 h fasted/4 h refed C57BL/6JRj mice (n=3 mice/group). Data are presented as mean ± SEM. *P>0.05 (unpaired two-tailed Student's t test). *Protein kinase D* (PKD); *flox/flox* ($^{f/f}$); *normal diet* (ND); *sterol regulatory element binding protein* (Srebp); *acetyl-CoA carboxylase alpha* (Acaca); *fatty acid synthase* (Fasn); *stearoyl-CoA desaturase* (Scd); *3-hydroxyl-3-methylglutaryl-CoA synthase* (Hmgcs); *3-hydroxyl-3-methylglutaryl-CoA reductase* (Hmgcr); *mevalonate kinase* (Mvk); *mevalonate diphosphate decarboxylase* (Mvd); *farnesyl diphosphate synthase* (Fdps); *farnesyl-diphosphate farnesyltransferase* (Fdft); *lanosterol synthase* (Lss); *insulin induced gene* (Insig); *glyceraldehyde 3-phosphate dehydrogenase* (GAPDH). (Mayer et al., 2019)[275]

Refeeding induced lipogenic gene expression in livers of $PKD3^{liver\Delta/\Delta}$ mice to a higher expression level compared to control mice and consequently led to elevated serum TG and cholesterol levels in these mice; however, fasting alone did not result in differential lipogenic gene expression between wild type and $PKD3^{liver\Delta/\Delta}$ mice (Figure 33A). Notably, the protein level of PKD3 in liver was increased after 24 h of refeeding (Figure

33B, C). This was only observed after prolonged refeeding, whereas acute refeeding of 4 h was not sufficient to increase PKD3 protein content in liver (Figure 33D, E). Taken together, fasting followed by prolonged refeeding led to elevated hepatic PKD3 protein levels. In addition, lipogenic gene expression as well as serum TG and cholesterol levels were increased in mice lacking PKD3 in liver in response to refeeding.

3.4 PKD3 suppresses lipogenesis in an AKT and mTORC1/2-dependent manner in liver

Many studies described the interplay of the AKT pathway with SREBP-dependent lipogenic gene expression by manipulating the PI3K/AKT pathway and observing effects on SREBP signaling, indicating that PI3K/AKT activates SREBP[291-294]. Stimulation with insulin canonically leads to the activation of PI3K and thus to PIP_3 production and AKT phosphorylation on Thr308 and Ser473 through PDK1 and mTORC2, respectively, resulting in full activation (reviewed in [284]). For this reason, primary hepatocytes were isolated from control and $PKD3^{liver\Delta/\Delta}$ livers and stimulated with insulin. Indeed, insulin-induced AKT phosphorylation was more pronounced for AKT residues Thr308 and Ser473 in hepatocytes lacking PKD3 shown by WB and corresponding quantification (Figure 34A, B). PKD3 expression was fully silenced in KO hepatocytes compared to controls and PKD was phosphorylated and activated in response to insulin stimulation, which was not observed for PKD3-deficient hepatocytes (Figure 34A, B).
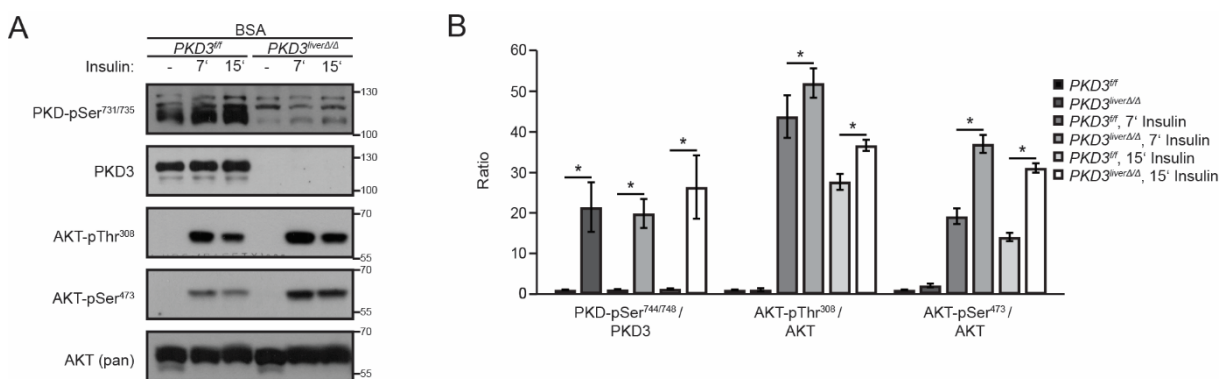
Figure 34: Lack of PKD3 augments insulin-stimulated AKT phosphorylation in primary hepatocytes. (A, B) WB analysis and corresponding densitometric quantification of indicated proteins in extracts from control and PKD3-deficient primary hepatocytes stimulated with 100 nM insulin for indicated time points using antibodies against PKD-pSer731/735, PKD3, AKT-pThr308, AKT-pSer473, and AKT (pan) (n=3 independent experiments). Data are presented as mean ± SEM. *$P>0.05$ (one way ANOVA with post hoc Tukey's test). *Protein kinase D* (PKD); *flox/flox* (f/f); *bovine serum albumin* (BSA); *phospho* (p); *threonine* (Thr); *serine* (Ser); *protein kinase B* (AKT). (Mayer et al., 2019)[275]

Results

In order to investigate the effect of PKD3 overexpression on AKT signaling, adenoviral transduction of primary hepatocytes was established for PKD3 overexpression. For this reason, primary hepatocytes were transduced with either an *adenovirus* (Ad) expressing EGFP control (Ad-EGFP) or a constitutive active form of PKD3 (Ad-mycPKD3ca), in which the two serine residues in the catalytic domain are mutated to glutamic acid (S731/S735E)[128]. This mutation leads to an activation of PKD3 independent of upstream effectors. The level of PKD3 overexpression was strongly elevated for the tested *multiplicity of infections'* (MOIs') of 5, 10, 30, 60, and 100 (Figure 35A, B). Therefore, a MOI of 10 was chosen for further adenoviral transductions unless otherwise stated.
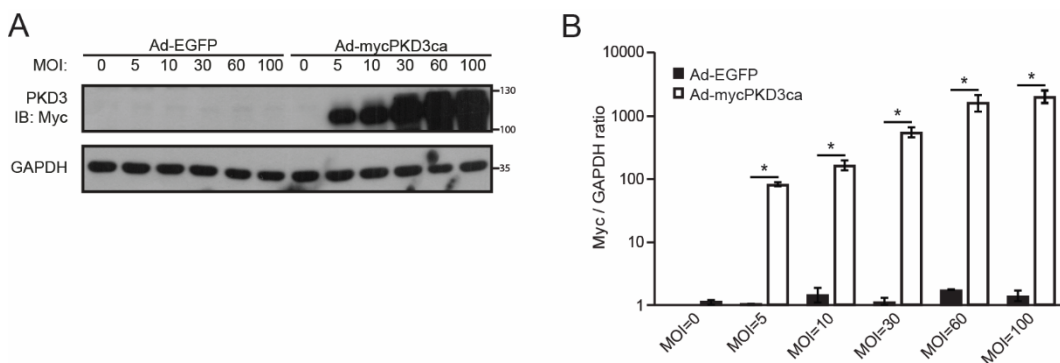
Figure 35: Adenoviral mediated overexpression of constitutive active PKD3 in hepatocytes. (A, B) WB analysis and corresponding densitometric quantification of Myc-tag in primary hepatocytes transduced with either adenovirus expressing EGFP control (Ad-EGFP) or constitutive active PKD3 (Ad-mycPKD3ca) at indicated MOIs (n=3 independent experiments). Data are presented as mean ± SEM. *P>0.05 (two way ANOVA with post hoc Tukey's test). *Adenovirus* (Ad); *enhanced green fluorescent protein* (EGFP); *protein kinase D* (PKD); *immunoblot* (IB); *constitutive active* (ca); *glyceraldehyde 3-phosphate dehydrogenase* (GAPDH); *multiplicity of infection* (MOI). (Mayer et al., 2019)[275]

Adenoviral-mediated overexpression of PKD3 in hepatocytes resulted not only in strongly elevated levels of PKD3ca, but also in increased levels of phosphorylated PKD at Ser731/Ser735 compared to control EGFP-expressing hepatocytes (Figure 36A, B). Expression of PKD3ca in hepatocytes impaired AKT activation following insulin stimulation, which can be seen by a markedly lower level of phosphorylated AKT at Ser473 and Thr308 as well as for a lower extent also for Thr450 (Figure 36A, B).

Together, lack of PKD3 in hepatocytes enhanced AKT phosphorylation. Conversely, overexpression of PKD3ca markedly suppressed AKT activation upon insulin stimulation.
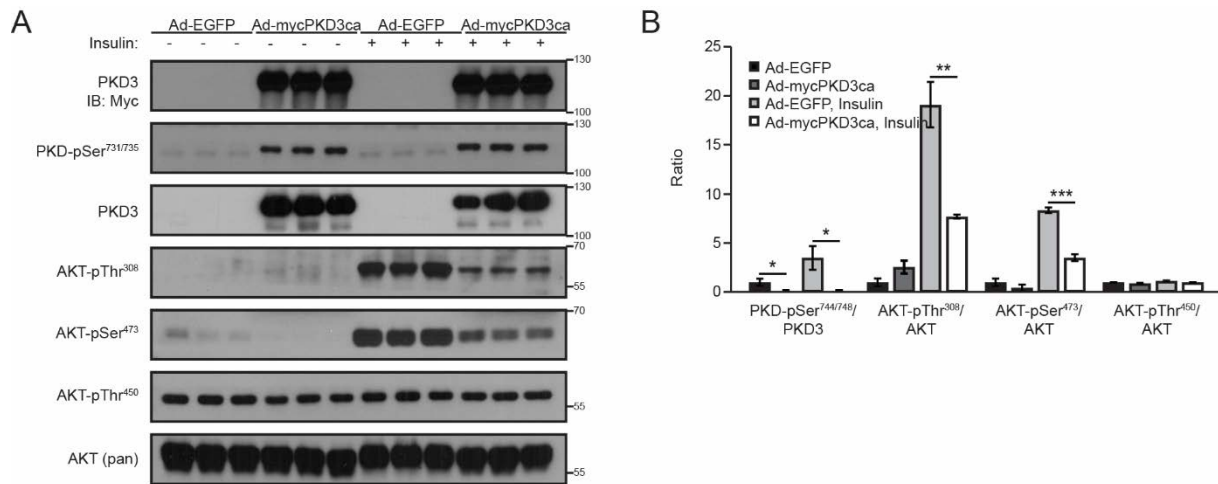
Figure 36: Expression of PKD3ca blocks insulin-induced phosphorylation of AKT in primary hepatocytes. (A, B) WB analysis and corresponding densitometric quantification of indicated proteins in extracts from PKD3-deficient primary hepatocytes transduced with either adenovirus expressing control EGFP (Ad-EGFP) or constitutive active PKD3 (Ad-mycPKD3ca) and stimulated with 100 nM insulin for 15 min, if indicated, using antibodies against Myc, PKD-pSer731/735, PKD3, AKT-pThr308, AKT-pSer473, AKT-pThr450, and AKT (pan) (n=3 independent experiments). Data are presented as mean ± SEM. *$P>0.05$, **$P>0.01$, ***$P>0.001$ (one way ANOVA with post hoc Tukey's test). *Adenovirus* (Ad); *enhanced green fluorescent protein* (EGFP); *protein kinase D* (PKD); *constitutive active* (ca); *immunoblot* (IB); *phospho* (p); *threonine* (Thr); *serine* (Ser); *protein kinase B* (AKT). (Mayer et al., 2019)[275]

Insulin-stimulated PI3K/AKT signaling induces lipogenesis in liver via activation of the mTOR complexes 1 and 2 (mTORC1 and mTORC2), leading to SREBP-dependent lipogenic gene expression[189,250,295,296]. Consistent with the previous results, PKD3 deletion in hepatocytes enhanced the phosphorylation of mTORC1 downstream substrates S6K1 on Thr389, as well as 4E-BP1 on Thr37/46 and Ser65 upon insulin stimulation compared to control hepatocytes (Figure 37A, B). Furthermore, phosphorylation of NDRG1 on Thr346 and SGK1 on Ser422 was increased in PKD3 deficient hepatocytes compared to wild type hepatocytes (Figure 37A, B). Another downstream substrate of mTORC2, AKT on residue Ser473, was also phosphorylated at a higher level compared to control hepatocytes (Figure 34A, B). In other words, hepatic deletion of PKD3 leads to the activation of mTOR complex 1 and 2 seen by an increased level of phosphorylation of respective downstream targets of the two mTOR complexes.
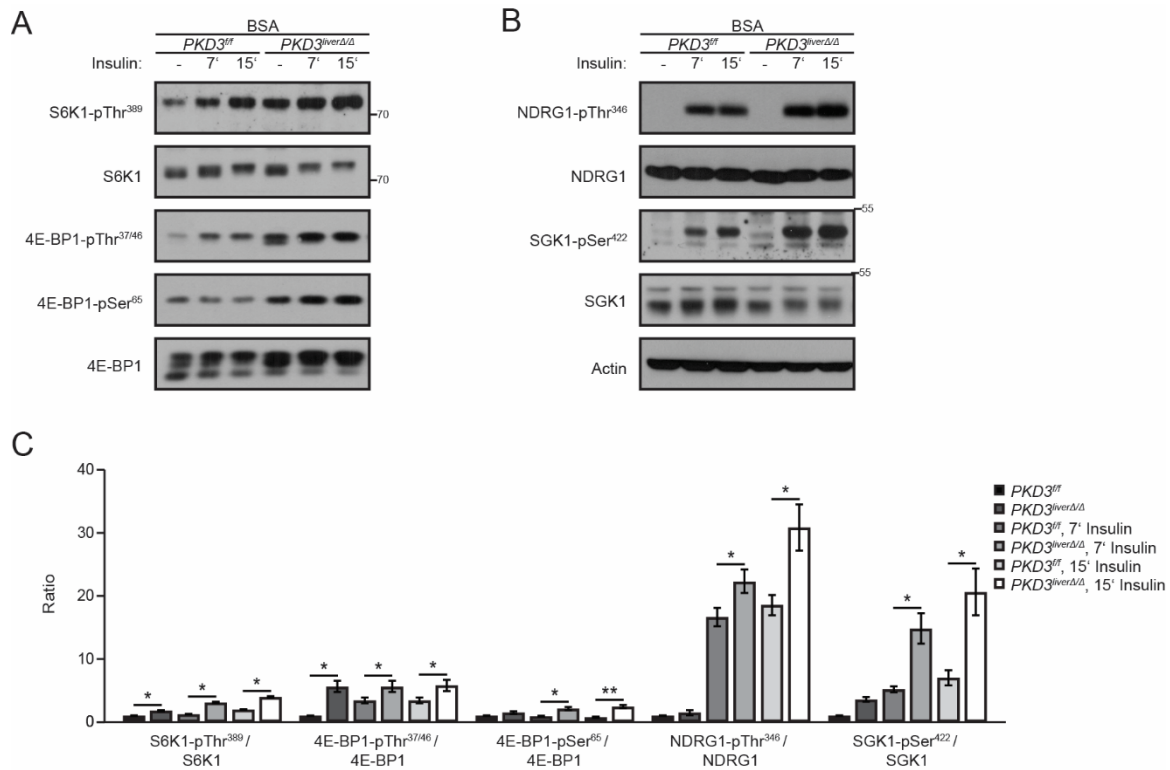
Figure 37: PKD3 deletion enhances mTORC1/2 substrate phosphorylation. (A-C) WB analysis and corresponding densitometric quantification of indicated proteins in extracts from control and PKD3-deficient primary hepatocytes stimulated with 100 nM insulin for indicated time points using antibodies against S6K1-pThr389, S6K1, 4E-BP1-pThr37/46, 4E-BP1-pSer65, 4E-BP1, NDRG1-pThr346, NDRG1, SGK1-pSer422, SGK1, and Actin as loading control (n=3 independent experiments). Data are presented as mean ± SEM. *P>0.05, **P>0.01 (one way ANOVA with post hoc Tukey's test). *Protein kinase D* (PKD); *flox/flox* (f/f); *bovine serum albumin* (BSA); *phospho* (p); *threonine* (Thr); *serine* (Ser); *p70 ribosomal S6 kinase* (S6K); *eIF4E-binding protein* (4E-BP); *N-myc downstream regulated* (NDRG); *serum and glucocorticoid-regulated kinase* (SGK). (Mayer et al., 2019)[275]

Conversely, adenoviral-mediated overexpression of PKD3ca in hepatocytes resulted in impaired phosphorylation of mTORC1 downstream targets such as S6K1 on Thr389, and 4E-BP1 on Thr37/46 and Ser65 at basal and insulin stimulated conditions compared to EGFP expressing control hepatocytes (Figure 38A, B). The level of phosphorylation of mTORC2 downstream targets was also increased for AKT on Ser473 (Figure 36A, B), and for NDRG1 on Thr346 despite an increase of total NDRG1 protein level (Figure 38A, B)

Taken together, PKD3 deletion in hepatocytes enhanced phosphorylation of mTORC1/2 substrates in response to insulin compared to control hepatocytes. This was reversed by expressing PKD3ca in primary hepatocytes, in which case mTORC1/2 substrates were less phosphorylated than in the control gepatocytes.
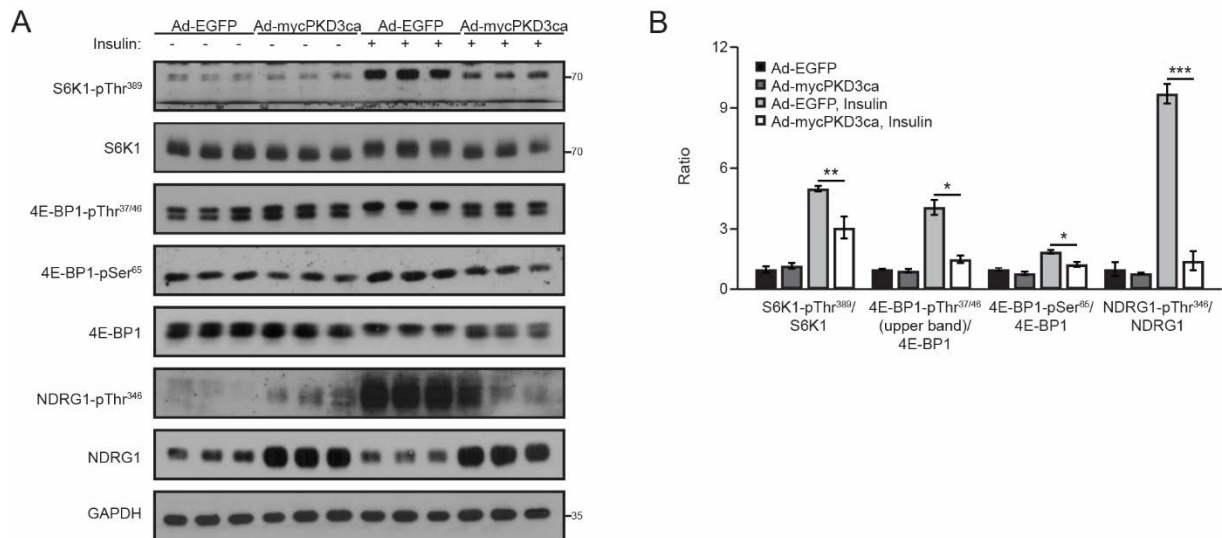
Figure 38: Overexpression of PKD3ca impairs mTORC1/2 substrate phosphorylation. (A, B) WB analysis and corresponding densitometric quantification of indicated proteins in extracts from PKD3-deficient primary hepatocytes transduced with either adenovirus expressing control EGFP (Ad-EGFP) or constitutive active PKD3 (Ad-mycPKD3ca) and stimulated with 100 nM insulin for 15 min, if indicated, using antibodies against S6K1-pThr389, S6K1, 4E-BP1-pThr37/46, 4E-BP1-pSer65, 4E-BP1, NDRG1-pThr346, NDRG1, and GAPDH as loading control (n=3 independent experiments). Data are presented as mean ± SEM. *P>0.05, **P>0.01, ***P>0.001 (one way ANOVA with post hoc Tukey's test). *Adenovirus* (Ad); *enhanced green fluorescent protein* (EGFP); *protein kinase D* (PKD); *constitutive active* (ca); *phospho* (p); *threonine* (Thr); *serine* (Ser); *p70 ribosomal S6 kinase* (S6K); *eIF4E-binding protein* (4E-BP); *N-myc downstream regulated* (NDRG); *glyceraldehyde 3-phosphate dehydrogenase* (GAPDH). (Mayer et al., 2019)[275]

Other components of mTORC1 and mTORC2 were not affected by the deletion of PKD3 in hepatocytes in regard to abundancy and phosphorylation. Namely, mTOR phosphorylation at Ser2448 and Ser2481, as well as the abundancy of mTOR, Raptor, and Rictor were unaltered by deleting PKD3 in primary hepatocytes (Figure 39A, B). mTOR and mLST8 are found in both complexes. Raptor and the non-core components PRAS40 and Deptor are exclusively found in mTORC1, whereas Rictor and mSIN1 in are specific for mTORC2.

Results
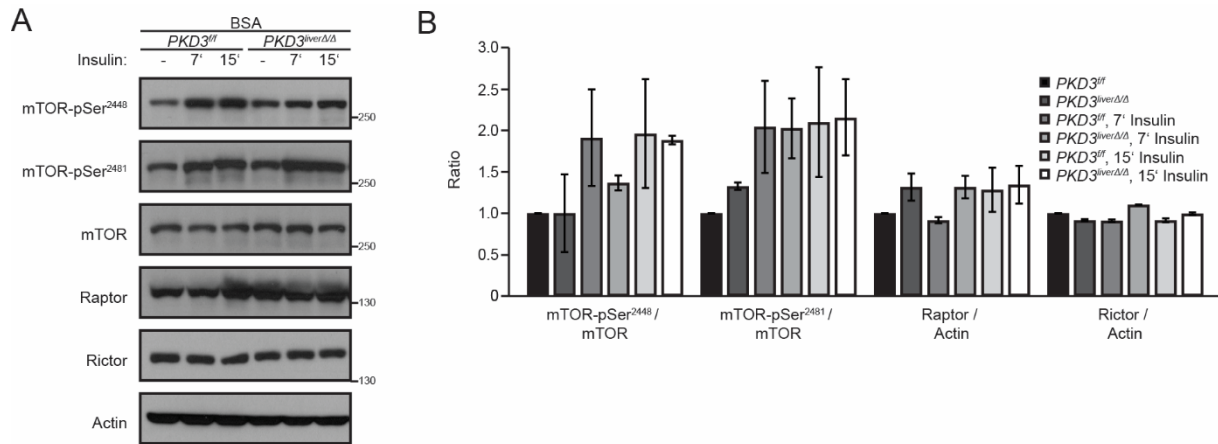
Figure 39: PKD3 deletion does not affect abundance and activity of mTORC1/2 components. (A, B) WB analysis and corresponding densitometric quantification of indicated proteins in extracts from control and PKD3-deficient primary hepatocytes stimulated with 100 nM insulin for indicated time points using antibodies against mTOR-pSer2448, mTOR-pSer2481, mTOR, Raptor, Rictor, and Actin as loading control (n=3 independent experiments). Data are presented as mean ± SEM. (one way ANOVA with post hoc Tukey's test). *Protein kinase D* (PKD); *flox/flox* (f/f); *bovine serum albumin* (BSA); *phospho* (p); *threonine* (Thr); *serine* (Ser); *mechanistic target of rapamycin* (mTOR); *regulatory associated protein of mTOR* (Raptor); *rapamycin-insensitive companion of mTOR* (Rictor). (Mayer et al., 2019)[275]

Similarly, phosphorylation and abundance of mTORC1 and mTORC2 components were unchanged after overexpressing PKD3ca in hepatocytes. Specifically, mTOR phosphorylation on Ser2448 and on Ser2481 was unaffected by expressing PKD3ca in primary hepatocytes compared to controls regardless of insulin stimulation (Figure 40A, C). The total protein levels of mTOR, Raptor, Rictor, TSC1, TSC2, and Deptor remained also unchanged despite expressing PKD3ca (Figure 40A, C).

Insulin binds to the insulin receptor leading to a tyrosine phosphorylation of IRS (reviewed in [284]); however, mTOR complexes and its effectors provide several feedback loops to IRS by directly phosphorylating IRS or by regulating the abundance of IRS[237,297-299]. Phosphorylation of IRS-1 on Ser612 was significantly increased as well as protein levels of IRS-1 and IRS-2 were moderately increased in PKD3ca-expressing hepatocytes compared to wild type hepatocytes (Figure 40B, D). AMPKα is another prominent effector of mTORC signaling by directly phosphorylating TSC2 and Raptor (reviewed in [300]). In addition, PKD1 promotes lipogenesis in adipocytes through phosphorylating AMPK and thereby suppresses its activity towards *acetyl-CoA carboxylase* (ACC)[158]. In primary hepatocytes, there were no differences in levels of phosphorylated AMPKα on Thr172 nor for ACC on Ser79 between control EGFP and PKD3ca-expressing hepatocytes (Figure 40B, D), excluding this mechanism for PKD3-mediated suppression of de novo lipogenesis in hepatocytes.
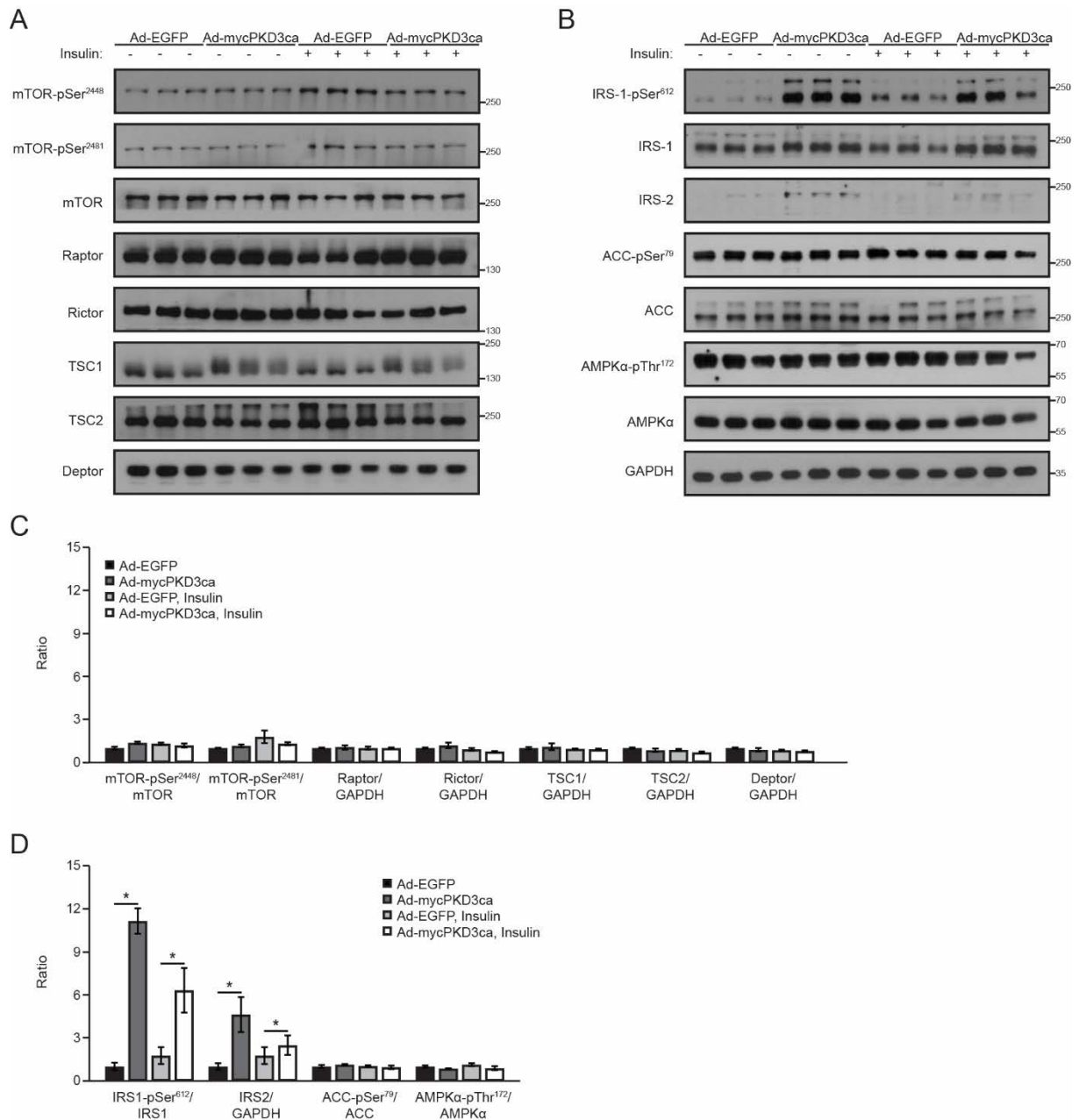
Figure 40: Overexpression of PKD3ca does not affect abundance and activity of mTORC1/2 components and upstream effectors. (A-D) WB analysis and corresponding densitometric quantification of indicated proteins in extracts from PKD3-deficient primary hepatocytes transduced with either adenovirus expressing control EGFP (Ad-EGFP) or constitutive active PKD3 (Ad-mycPKD3ca) and stimulated with 100 nM insulin for 15 min, if indicated, using antibodies against mTOR-pSer2448, mTOR-pSer2481, mTOR, Raptor, Rictor, TSC1, TSC2, Deptor, IRS1-pSer612, IRS-1, IRS-2, ACC-pSer79, ACC, AMPKα-pThr172, AMPKα, and GAPDH as loading control (n=3 independent experiments). Data are presented as mean ± SEM. *P>0.05, (one way ANOVA with post hoc Tukey's test). *Adenovirus* (Ad); *enhanced green fluorescent protein* (EGFP); *protein kinase D* (PKD); *constitutive active* (ca); *phospho* (p); *threonine* (Thr); *serine* (Ser); *mechanistic target of rapamycin* (mTOR); *regulatory associated protein of mTOR* (Raptor); *rapamycin-insensitive companion of mTOR* (Rictor); *tuberous sclerosis complex* (TSC); *insulin receptor substrate* (IRS); *acetyl-CoA carboxylase alpha* (ACC); *AMP-activated protein kinase* (AMPK); *glyceraldehyde 3-phosphate dehydrogenase* (GAPDH). (Mayer et al., 2019)[275]

Results
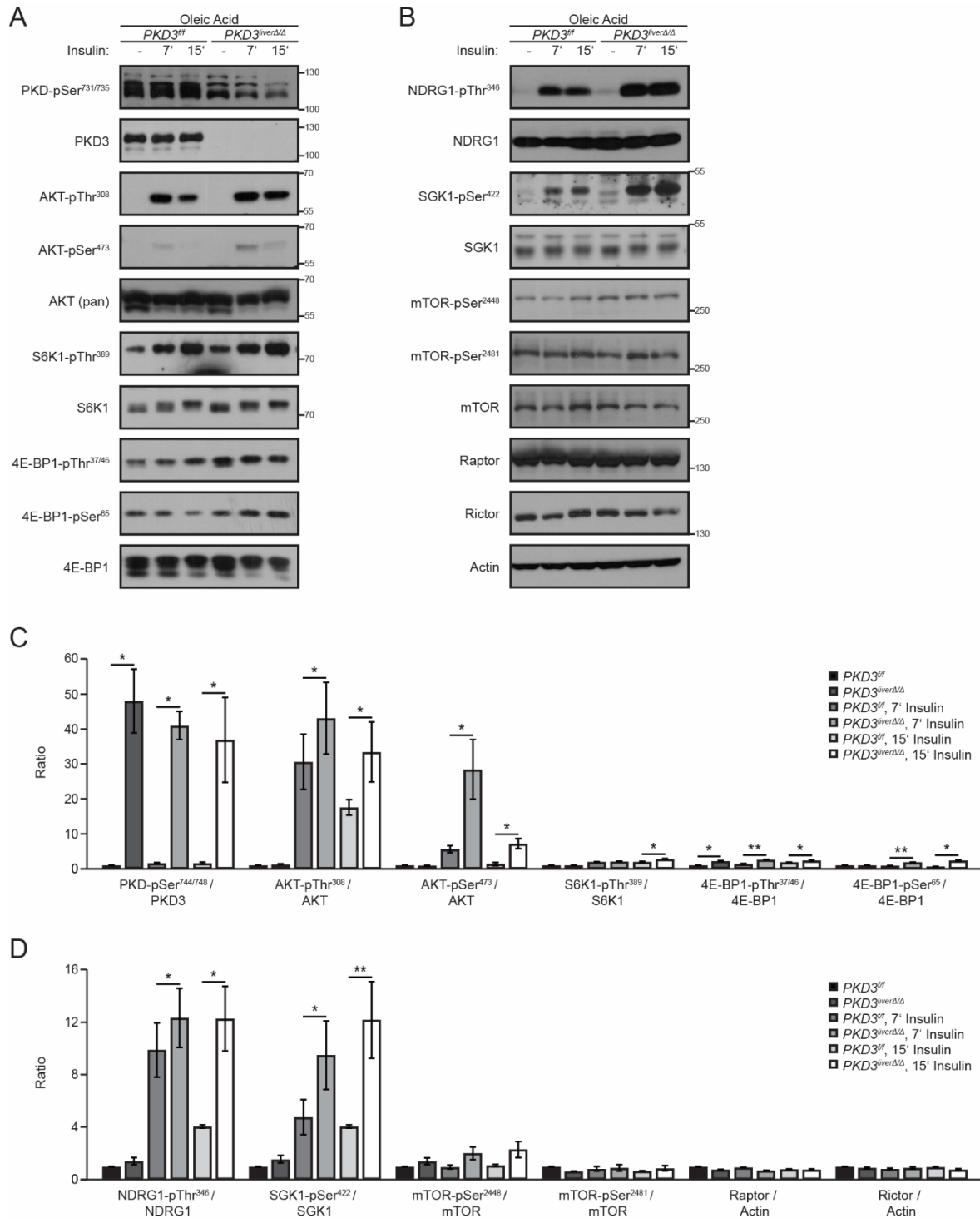
Figure 41: PKD3 deletion enhances AKT and mTORC1/2 substrate phosphorylation during lipid overload. (A-D) WB analysis and corresponding densitometric quantification of indicated proteins in extracts from control and PKD3-deficient primary hepatocytes stimulated with 100 nM insulin for indicated time points using antibodies against PKD-pSer731/735, PKD3, AKT-pThr308, AKT-pSer473, AKT (pan), S6K1-pThr389, S6K1, 4E-BP1-pThr37/46, 4E-BP1-pSer65, 4E-BP1, NDRG1-pThr346, NDRG1, SGK1-pSer422, SGK1, mTOR-pSer2448, mTOR-pSer2481, mTOR, Raptor, Rictor, and Actin as loading control (n=3 independent experiments). Data are presented as mean ± SEM. *P>0.05, **P>0.01 (one way ANOVA with post hoc Tukey's test). *Protein kinase D* (PKD); *flox/flox* ($^{f/f}$); *oleic acid* (OA); *phospho* (p); *threonine* (Thr); *serine* (Ser); *protein kinase B* (AKT); *p70 ribosomal S6 kinase* (S6K); *eIF4E-binding protein* (4E-BP); *N-myc downstream regulated* (NDRG); *serum and glucocorticoid-regulated kinase* (SGK); *mechanistic target of rapamycin* (mTOR); *regulatory associated protein of mTOR* (Raptor); *rapamycin-insensitive companion of mTOR* (Rictor). (Mayer et al., 2019)[275]

91

Results

Improved glucose tolerance and insulin resistance was observed in *PKD3^liverΔ/Δ* mice fed an HFD. However, previous in vitro experiments, showing that PKD3 signals through mTORC1/2 pathway, were performed in hepatocytes isolated from ND-fed mice. To mimic HFD-feeding of mice in vitro, primary hepatocytes were incubated with oleic acid in the culture medium to induce lipid accumulation. Oleic acid-loaded hepatocytes showed an increased level of phosphorylated AKT on Ser473 and Thr308, S6K1 on Thr389, 4E-BP1 on Thr37/46 and Ser65, NDRG1 on Thr346, as well as SGK1 on Ser422 for hepatocytes isolated from *PKD3^liverΔ/Δ* mice compared to control hepatocytes, whereas phosphorylation of mTOR on Ser2448 and Ser2481 as well as total protein levels of mTOR, Raptor, and Rictor were unaffected by the deletion of PKD3 in liver compared to controls (Figure 41A-D).
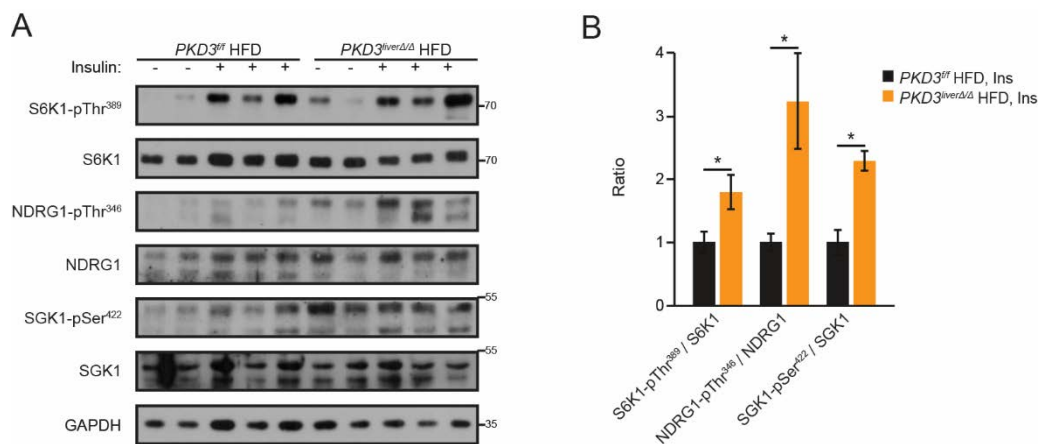
Figure 42: Insulin-mediated activation of mTORC1/2 substrates is increased in vivo in the absence of PKD3 in liver. (A, B) WB analysis and corresponding densitometric quantification of protein lysates from livers of control and *PKD3^liverΔ/Δ* mice fed an HFD for 24 weeks that received an intraperitoneal dose of the vehicle or insulin (8 U/kg body weight) for 15 min using antibodies against S6K1-pThr389, S6K1, NDRG1-pThr346, NDRG1, SGK1-pSer422, SGK1, and GAPDH as loading control (n=3 independent experiments). Data are presented as mean ± SEM. *P>0.05, **P>0.01 (one way ANOVA with post hoc Tukey's test). *Protein kinase D* (PKD); *flox/flox* (f/f); *high-fat diet* (HFD); *phospho* (p); *threonine* (Thr); *serine* (Ser); *p70 ribosomal S6 kinase* (S6K); *N-myc downstream regulated* (NDRG); *serum and glucocorticoid-regulated kinase* (SGK); *glyceraldehyde 3-phosphate dehydrogenase* (GAPDH). (Mayer et al., 2019)[275]

Phosphorylation of mTORC1/2 targets was also increased in vivo in HFD-fed *PKD3^liverΔ/Δ* mice compared to wild type (Figure 42A, B). In detail, phosphorylation of S6K1 on Thr389, NDRG1 on Thr346, and SGK1 on Ser422 was elevated in response to insulin injections in livers of *PKD3^liverΔ/Δ* mice compared to controls (Figure 42A, B). This were the same samples as used before to examine insulin sensitivity on a molecular level, which showed an increased level of phosphorylated AKT on Ser473 and Thr308 (Figure 19A, B), and Ser473 is known to be a direct substrate of mTORC2.

Results

Taken together, this result shows that mTORC1/2 signaling pathway is activated in vivo in the absence of PKD3 in lipid-loaded livers.
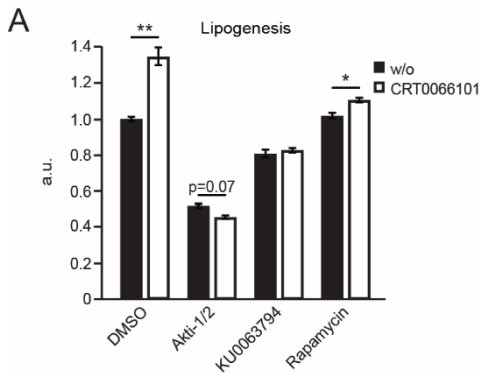
Figure 43: PKD3 deletion promotes de novo lipogenesis through AKT and mTORC pathways in liver. (A) Insulin-stimulated total de novo lipogenesis rate during lipogenic conditions (serum deprived, 25 mM glucose, 0.5 mM sodium acetate) in primary hepatocytes treated either with vehicle or CRT0066101 (1 µM) and in combination with DMSO (control), Akti-1/2 (10 µM), KU0063794 (0.7 µM), and Rapamycin (0.7 µM) treatment for 5 hours (n=3 biological replicates/group). Data are presented as mean ± SEM. *P>0.05, **P>0.01 (one way ANOVA with post hoc Tukey's test). *Dimethyl sulfoxide* (DMSO); *AKT inhibitor* (Akti); *arbitrary units* (a.u.). (Mayer et al., 2019)[275]

In short, lack of PKD3 promotes de novo lipogenesis in a pathway that requires AKT, mTORC1, and mTORC2 activation. To ultimately prove that this is true, de novo lipogenesis rate was measured in wild type and CRT0066101-treated primary hepatocytes in combination with treating the cells with specific inhibitors that block the activity of AKT (Akti-1/2), mTORC1/2 (KU0063794), and mTORC1 (Rapamycin) (Figure 43A). As shown before, inhibition of PKD by CRT0066101 increased de novo lipogenesis rate, which was reduced to the same extent by inhibiting AKT activity (Akti-1/2) in control and CRT0066101-treated cells (Figure 43A). Accordingly, the mTORC1/2 inhibitor KU0063794 decreased lipogenesis rate in control and CRT0066101-treated hepatocytes to the same level (Figure 43A). In contrast, incubation of control and CRT0066101 hepatocytes with Rapamycin only marginally reduced lipogenesis rate, which was still significant between control and CRT0066101-treated hepatocytes (Figure 43A).

3.5 PKD3ca localizes to a specific subcellular compartment

PKDs have been reported to localize to various cellular compartments[79-82,85,86]. Localizing PKDs within the cells might help to identify pathways and processes in which PKDs are involved in. For this reason, a PKD3-EGFP fusion protein was expressed in HEK293T cells and the subcellular localization of PKD3 was determined. As a result, PKD3 was found to reside in the trans-Golgi compartment identified by Syntaxin6 co-staining in HEK293T cells (Figure 44A). Expression of ectopic PKD3 was chosen for staining of PKD3 as staining of endogenous PKD3 was not assessable. For primary

hepatocytes, expression of PKD3ca was used to localize PKD3 (identified by myc-tag staining) (Figure 44B). Expression of PKD3ca appeared as small circular dots in primary hepatocytes, which was different to HEK293T cells (Figure 44A, B). This is consistent with the observation that PKD3ca did not co-localize with the TGN-marker *receptor-binding cancer-associated surface antigen* 1 (RCAS1) in primary hepatocytes (Figure 44B). Furthermore, PKD3ca did not co-localize with the ER marker *ER stress protein 72* (ERp72), mitotracker, or the peroxisome marker *peroxisomal membrane protein70* (PMP70), indicating that PKD3ca does not reside in the analyzed subcellular compartments (Figure 44B).
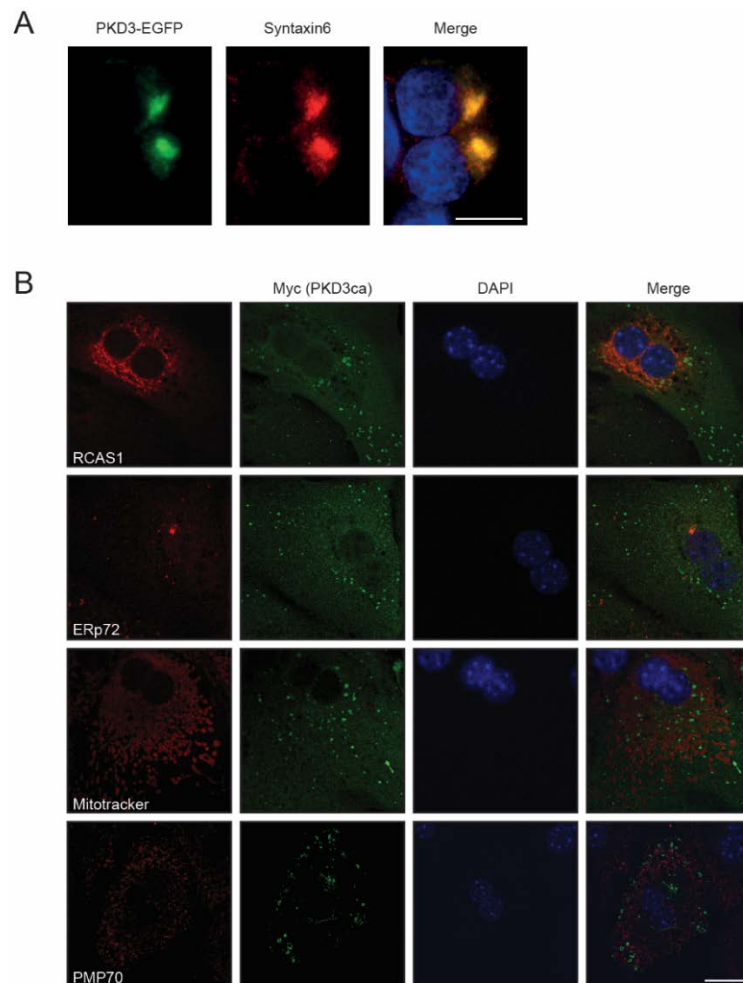
Figure 44: PKD3ca does not reside in TGN, ER, mitochondria, or peroxisomes. (A) Representative immunofluorescent microscopy pictures of HEK293T cells transiently transfected with a plasmid expressing PKD3-EGFP fusion protein that were stained with Syntaxin6 (TGN marker) and with DAPI for staining nuclei. Cells were visualized under a fluorescent microscope (Leica DM5500 B) at 63x magnification. Scale bar = 10 µm. (B) Representative immunofluorescent microscopy pictures of primary hepatocytes transduced with adenovirus expressing mycPKD3ca and stained with RCAS1 (TGN marker), ERp72 (ER marker), mitotracker (mitochondria marker), PMP70 (peroxisome marker), and DAPI for staining nuclei. Cells were visualized under a confocal fluorescent microscope (Leica TCS SP8) at 40x magnification. Scale bar = 20 µm. *Protein kinase D* (PKD); *constitutive active* (ca); *enhanced green fluorescent protein* (EGFP); *receptor-binding cancer-associated surface antigen* (RCAS); *ER stress protein* (ERp); *peroxisomal membrane protein* (PMP); *trans-Golgi network* (TGN); *endoplasmic reticulum* (ER). (unpublished observation)

3.6 PKD3 signaling influences gluconeogenesis in liver
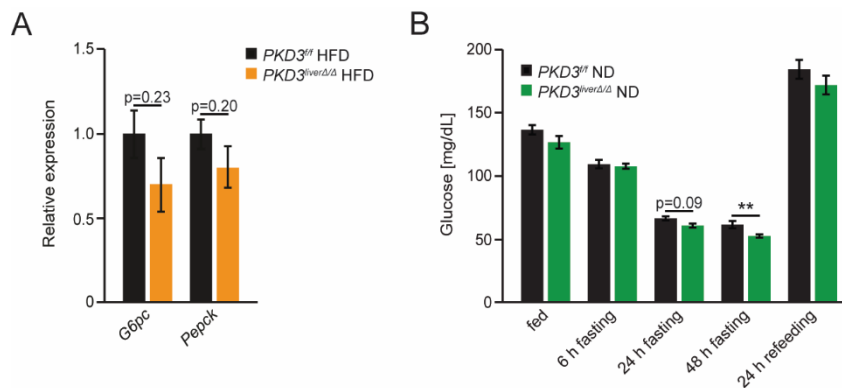
Figure 45: PKD3 promotes gluconeogenesis in vivo. (A) RT-qPCR analysis of *G6pc* and *Pepck* gene expression in mice of indicated genotypes that were fed an HFD for 24 weeks (n=8 mice/group). (B) Determination of blood glucose concentrations in control and *PKD3$^{liverΔ/Δ}$* mice fed an ND for 7 weeks that were fasted and refed for indicated time points (n=12 mice/group). Data are presented as mean ± SEM. *P>0.05, **P>0.01 [unpaired two-tailed Student's t test (A), or two way ANOVA with post hoc Tukey's test (B)]. *Protein kinase D* (PKD); *flox/flox* (f/f); *high-fat diet* (HFD); *normal diet* (ND); *glucose-6-phosphatase catalytic-subunit* (G6pc); *phosphoenolpyruvate carboxykinase* (Pepck). (unpublished observation)

Lipid and glucose metabolism are tightly co-regulated in the liver. Under lipogenic conditions, glycolysis is promoted leading to increased levels of pyruvate which provides a carbon source for lipogenesis, and, this in turn, links glycolysis to lipogenesis (reviewed in [5]). During the pathological conditions of diabetes mellitus, hepatocytes fail to respond to insulin, leading to increased net glucose production and thus to hyperglycemia (reviewed in [11]). mTORC2 signaling activates both - glycolysis and lipogenesis[250], whereas mTORC1 signaling is required for stimulation of lipogenesis, but not for the inhibition of gluconeogenesis in response to insulin[301]. For this reason, the rate of gluconeogenesis in respect to altered PKD3 signaling was determined in hepatocytes. In vivo, the expression of the two key enzymes for gluconeogenesis (*G6pc* and *Pepck*) was not significantly decreased in livers of *PKD3$^{liverΔ/Δ}$* mice compared to control mice fed an HFD for 24 weeks (ad libitum) (Figure 45A). Nevertheless, fasting blood glucose levels were significantly reduced in *PKD3$^{liverΔ/Δ}$* mice fed an ND after prolonged fasting compared to control mice (Figure 45B). Taken together, the results show that lack of PKD3 in hepatocytes suppresses gluconeogenesis in vivo, which is in line with the increased rate of de novo lipogenesis observed in PKD3-deficient hepatocytes.

3.7 Constitutive active PKD3 promotes insulin resistance in liver by impairing AKT activation

The results acquired from *PKD3^{liverΔ/Δ}* mice clearly demonstrated an activation of AKT and mTORC signaling, leading to improved insulin sensitivity in livers of mice lacking PKD3 compared to controls (results described before). In vitro, adenoviral-mediated overexpression of PKD3ca in primary hepatocytes reversed the results obtained with PKD3-deficient hepatocytes, including improved AKT activation in response to insulin treatment (results described before).
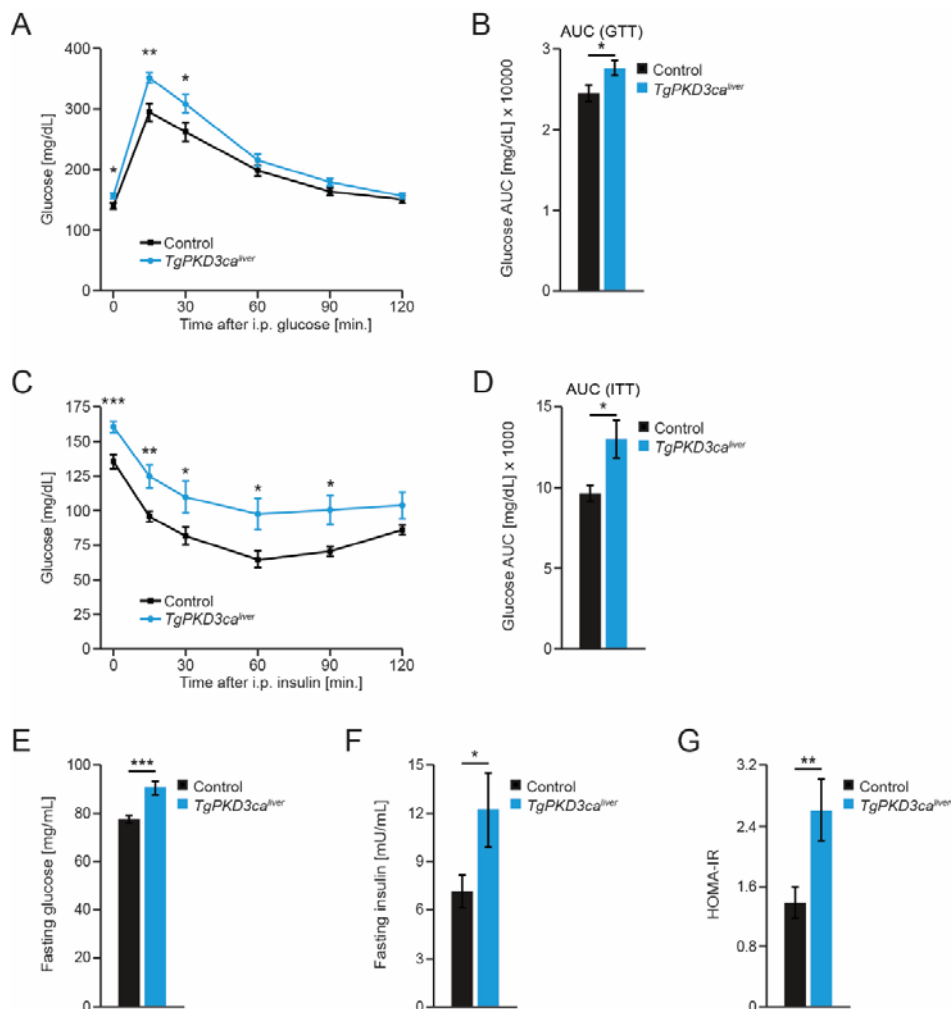
Figure 46: Constitutive active PKD3 impairs glucose tolerance and insulin sensitivity in liver. (A-D) Control and *TgPKD3ca^{liver}* mice were analyzed for glucose tolerance (2 g/kg BW) with calculated AUC fed an ND for 12 weeks (A, B) and analyzed for insulin tolerance (1 U/kg BW) with calculated AUC fed an ND for 10 weeks (C, D) [n=11 mice (Control) and n=13 mice (Tg)]. For all tolerance tests, the mice received after 4 hours of fasting an intraperitoneal dose of glucose or insulin, respectively, and the blood glucose levels were monitored at 0, 15, 30, 60, 90, and 120 min after injection. (E-G) Following an overnight fast, blood glucose (E) and insulin (F) were determined and used for calculating HOMA-IR (G) of control and *TgPKD3ca^{liver}* mice [n=11 mice (Control) and n=13 mice (Tg)]. Data are presented as mean ± SEM. *P>0.05, **P>0.01, ***P>0.001 [unpaired two-tailed Student's t test (B, D, E-G) or two way ANOVA with post hoc Tukey's test (A, C)]. *Protein kinase D* (PKD); *constitutive active* (ca); *transgenic* (Tg); *glucose tolerance test* (GTT); *insulin tolerance test* (ITT); *intraperitoneal* (i.p.); *area under the curve* (AUC); *homeostasis model assessment of insulin resistance* (HOMA-IR). (Mayer et al., 2019)[275]

Results

However, PKD3ca-mediated altered AKT phosphorylation and activation in vitro does not necessarily mean that insulin sensitivity is impaired in vivo as well. For this reason, the effect of PKD3ca expression on insulin signaling was also studied in vivo. To test this, liver-specific transgenic PKD3ca mice (*TgPKD3ca^liver*) were generated by crossing loxP-STOP-loxP-FlagPKD3ca mice with mice expressing the Cre recombinase under the control of the albumin promoter[271]. The *TgPKD3ca^liver* mice presented significantly impaired glucose tolerance compared to control mice (Figure 46A, B). Accordingly, *TgPKD3ca^liver* mice showed a significantly impaired response to insulin injections compared to wild type mice, which was assessed by insulin tolerance test (Figure 46C, D). These results go in line with increased overnight fasting blood glucose and serum insulin concentrations in *TgPKD3ca^liver* mice compared to controls (Figure 46E, F). Notably, increased fasting blood glucose concentrations were also observed for the 0 time point in GTT and ITT after 4 hours of fasting (Figure 46A, C). These parameters (fasting glucose and fasting insulin) were then used to calculate a *homeostasis model assessment of insulin resistance* (HOMA-IR)[302] value of 2.5, indicating that *TgPKD3ca^liver* mice were considered as borderline of being insulin resistant (Figure 46G). Importantly, these results were obtained from control and *TgPKD3ca^liver* mice fed an ND, why it was not required to study the effects of HFD-feeding on this mouse line.
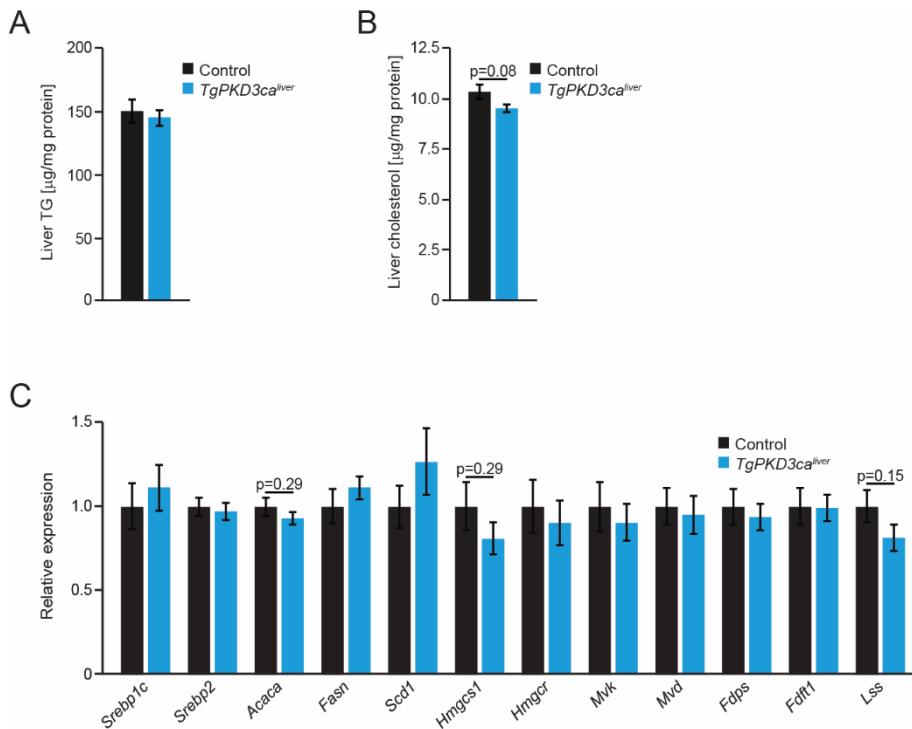
Figure 47: Hepatic PKD3ca does not lower liver lipid concentrations. (A, B) Quantification of TG (A) and cholesterol content (B) in extracted lipids from livers of control and *TgPKD3ca^liver^* mice fed ND for 24 weeks and normalized to protein level [n=11 mice (Control) and n=13 mice (Tg)]. (C) RT-qPCR analysis of *Srebp* and target gene expression in livers of control and *TgPKD3ca^liver^* mice that were fasted overnight and refed for 4 hours before excising the livers (n=11 mice/group). Data are presented as mean ± SEM. (unpaired two-tailed Student's t test). *Protein kinase D* (PKD); *constitutive active* (ca); *transgenic* (Tg); *triglyceride* (TG), *sterol regulatory element binding protein* (Srebp); *acetyl-CoA carboxylase alpha* (Acaca); *fatty acid synthase* (Fasn); *stearoyl-CoA desaturase* (Scd); *3-hydroxyl-3-methylglutaryl-CoA synthase* (Hmgcs); *3-hydroxyl-3-methylglutaryl-CoA reductase* (Hmgcr); *mevalonate kinase* (Mvk); *mevalonate diphosphate decarboxylase* (Mvd); *farnesyl diphosphate synthase* (Fdps); *farnesyl-diphosphate farnesyltransferase* (Fdft); *lanosterol synthase* (Lss). (Mayer et al., 2019)[275]

On the other hand, liver triglyceride content was unchanged between livers of *TgPKD3ca^liver^* and control mice (Figure 47A), whereas liver cholesterol content was marginally reduced in livers expressing PKD3ca compared to controls (p=0.08) (Figure 47B). On mRNA level, lipogenic gene expression was not significantly reduced in livers of *TgPKD3ca^liver^* mice compared to control livers (Figure 47C).

Results
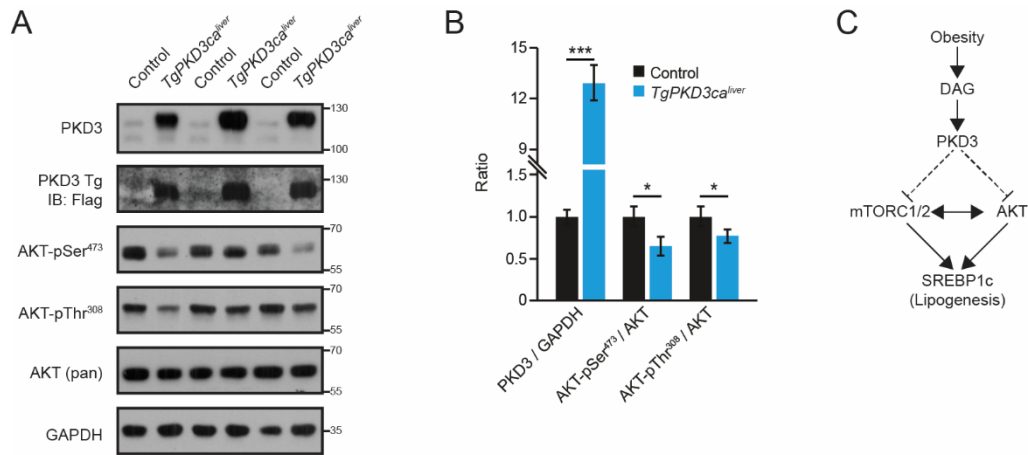
Figure 48: PKD3ca impairs refeeding-stimulated AKT phosphorylation in liver. (A, B) WB analysis and corresponding densitometric quantification of indicated proteins in extracts from control and *TgPKD3ca^liver^* mice fed ND for 24 weeks that were fasted overnight and refed for 4 hours before excising the livers using antibodies against PKD3, Flag, AKT-pSer473, AKT-pThr308, AKT (pan), and GAPDH as loading control (n=3 mice/group). (G) Graphical summary of proposed PKD3 action liver. Data are presented as mean ± SEM. *P>0.05, ***P>0.001 (unpaired two-tailed Student's t test). *Protein kinase D* (PKD); *constitutive active* (ca); *transgenic* (Tg); *phospho* (p); *serine* (Ser); *threonine* (Thr); *protein kinase B* (AKT); *glyceraldehyde 3-phosphate dehydrogenase* (GAPDH); *diacylglycerol* (DAG); *mechanistic target of rapamycin complex* (mTORC). (Mayer et al., 2019)[275]

In order to investigate the impaired insulin tolerance of *TgPKD3ca^liver^* mice at a molecular level, control and *TgPKD3ca^liver^* mice were fasted overnight and refed for 4 hours before the livers were used to check AKT phosphorylation. Firstly, expression of PKD3ca was 13 times higher than the endogenous level of PKD3 (Figure 48A, B). Secondly, AKT phosphorylation was reduced for Ser473 and Thr308 in livers of *TgPKD3ca^liver^* mice compared to controls in response to the fasting/refeeding protocol (Figure 48A, B).

In conclusion, PKD3ca expression was sufficient to impair insulin sensitivity in vivo. This was further confirmed on a molecular level seen by a decreased level of AKT phosphorylation. The combined in vitro and in vivo results together propose a model in which DAG accumulation (resulting from obesity) leads to an activation of PKD3 and to a suppression of AKT signaling in liver. Conversely, lack of PKD3 in liver promotes AKT and mTORC activation and thus to increased lipogenesis (Figure 48C).

3.8 Studies for identifying the direct substrate of PKD3 in hepatocytes

In the prior results, one question remained unanswered: What is the direct substrate of the kinase PKD3 in liver? In order to address this question experimentally, two

different unbiased mass spectrometry-based approaches were chosen to identify the direct target, as well as signaling events downstream of PKD3.

3.8.1 2D-DIGE-based approach

For this method, primary hepatocytes isolated from *PKD3^{liverΔ/Δ}* mice were again transduced with either adenovirus expressing control EGFP (Ad-EGFP) or constitutive active PKD3 (Ad-mycPKD3ca). 48 hours post transduction, protein lysates were made and enriched for phosphoproteins, which were then labeled with either Cy3 (EGFP) or Cy5 (mycPKD3ca) (Figure 49A), and analyzed by *two-dimensional fluorescence difference gel electrophoresis* (2D-DIGE). In the 2D-gel, the phosphoproteins are separated in 2 dimensions according to *molecular weight* (MW) and *potentia hydrogenii* (pH). The *isoelectric point* (pI) of a protein is defined by the amino acid sequence/composition and posttranslational modifications such phosphorylation. For this reason, proteins that are phosphorylated as a result of PKD3 expression have a different pI than the unphosphorylated proteins and migrate to a different pI beside the separation based on the MW. Separated spots that appear 'red' were phosphorylated in PKD3ca expressing hepatocytes compared to EGFP expressing control hepatocytes ('green') (Figure 49B). 40 of the most prominent 'red' spots were picked and subjected to mass spectrometry-based identification (Figure 49C). CPS1, EEA1, ACTN1, EEF2, VCP, GFM1, CPT2, RDX, MSN, HACL1, HSPD1, ALDH7A1, CNDP2, SELENBP2, KRT16, NADK2, DDX39b, DLST, PDIA6, CALR, IVD, BHMT1, ALDOA, CRYZ, NPM1, ALAD, C1QBP, PRDX3, and TIMM9 were identified as putative downstream targets of PKD3 signaling in hepatocytes (Figure 49C).

C

Spot No.	UniProt	Gene names	Protein names	Calc. MW	Calc. pI	Prot. Score	Ion Score
1-7	8QC196	Cps1 (*)	Carbamoyl-phosphate synthase [ammonia], mito.	164,514	6,48	520	412
8	Q8BL66	Eea1	Early endosome antigen 1	160,817	5,59	386	311
9	Q7TPR4	Actn1	Alpha-actinin-1	103,004	5,23	321	296
10	P58252	Eef2	Elongation factor 2	95,253	6,41	654	613
11,12	Q01853	Vcp	Transitional endoplasmic reticulum ATPase	89,266	5,14	160	127
13	Q8K0D5	Gfm1	Elongation factor G, mito.	83,497	6,48	154	143
14	P52825	Cpt2	Carnitine O-palmitoyltransferase 2, mito.	73,934	8,59	287	245
15,16	P26043	Rdx	Radixin	68,500	5,91	716	578
17	P26041	Msn	Moesin	67,725	6,22	483	393
18	Q9QXE0	Hacl1	2-hydroxyacyl-CoA lyase 1	63,619	5,89	686	663
19	P63038	Hspd1	60 kDa heat shock protein, mito.	60,917	5,91	126	89
20	Q9DBF1	Aldh7a1	Alpha-aminoadipic semialdehyde dehydrogenase	58,824	7,16	123	104
21	Q9D1A2	Cndp2	Cytosolic non-specific dipeptidase	52,734	5,43	546	540
22	Q63836	Selenbp2	Selenium-binding protein 2	52,576	5,78	146	126
23	Q9Z2K1	Krt16 (*)	Keratin, type 1 cytoskeletal 16	51,574	5,13	54	24
24	Q8C5H8	Nadk2	NAD kinase 2, mito.	50,827	8,31	646	588
25	Q9Z1N5	Ddx39b	Spliceosome RNA helicase Ddx39b	49,004	5,44	664	587
26-28	Q9D2G2	Dlst	Dihydrolipoyllysine-residue succinyltransferase comp. of OGDC, mito.	48,964	9,11	629	604
29	Q922R8	Pdia6	Protein disulfide-isomerase A6	48,070	5,00	556	546
30	P14211	Calr	Calreticulin	47,965	5,33	71	38
31	Q9JHI5	Ivd	Isovaleryl-CoA dehydrogenase, mito.	46,286	8,53	105	91
32	O35490	Bhmt1	Betaine--homocysteine S-methyltransferase 1	44,992	8,01	653	609
33	P05064	Aldoa	Fructose-bisphosphate aldolase A	39,331	8,31	662	615
34	P47199	Cryz	Quinone oxidoreductase	35,246	8,18	624	298
35	Q61937	Npm1	Nucleophosmin	32,540	4,62	247	229
36	P10518	Alad	Delta-aminolevulinic acid dehydratase	36,000	6,32	101	86
37	O35658	C1qbp	Complement comp. 1 Q subcomp.-binding protein, mito.	30,994	4,82	112	112
38,39	P20108	Prdx3	Thioredoxin-dependent peroxide reductase, mito.	28,109	7,15	283	278
40	Q9WV98	Timm9	Mito. import inner membrane translocase subunit Tim9	10,337	6,71	85	75

Figure 49: 2D-DIGE method reveals putative PKD3 targets in hepatocytes. (A) Experimental outline: Primary hepatocytes were isolated from *PKD3^liverΔ/Δ* mice and transduced with either adenovirus expressing control EGFP (Ad-EGFP) or constitutive active PKD3 (Ad-mycPKD3ca). Phosphoproteins were enriched and labeled with Cy3 (EGFP) or Cy5 (PKD3ca), and used for 2D-difference gel electrophoresis. (B) Gel image of 2D-DIGE separated phosphoproteins based on molecular weight and pH from EGFP expressing PKD3wt-deficient hepatocytes (Cy3-labeled; green) and PKD3ca expressing PKD3wt-deficient hepatocytes (Cy5-labeled, red). Red spots are indicated by arrowheads for spot 1 to 40. (C) List of identified spots/proteins by mass spectrometry showing spot number, UniProt accession number, gene names, protein names, calculated MW, calculated pI, protein score, and ion score. *Protein kinase D* (PKD); *adenovirus* (Ad); *enhanced green fluorescent protein* (EGFP); *constitutive active* (ca); *molecular weight* (MW); *potentia hydrogenii* (pH); *calculated* (calc.); *protein* (prot.); *isoelectric point* (pI). (unpublished observation)

A basic method to examine whether the phosphorylation level of a protein is altered, is to separate the proteins on a very long (20 cm) SDS-PAGE gel and to check for a mobility shift. For this purpose, primary hepatocytes deficient for PKD3 were

transduced again with adenovirus expressing either EGFP control or PKD3ca. Indeed, detection of *ezrin/radixin/moesin* (ERM) showed an upshift in the PKD3ca-expressing hepatocytes compared to the EGFP control, which disappeared after treatment with alkaline phosphatase, indicating that the upshifted band in the WB was due to differential phosphorylation (Figure 50A). *Carbamoyl phosphate synthetase* (CPS) 1 also showed a shift in the WB in response to PKD3ca expression; however, as a downshift (Figure 50A). For the third analyzed protein *carnitine palmitoyltransferase* (CPT) 2, no shifts were observed in the WB, which does not exclude phosphorylation of CPT2 induced by PKD3ca signaling, because this method can lead to false negative results, for example when the protein is only partially phosphorylated/not sufficient for a shift in the WB (Figure 50A).
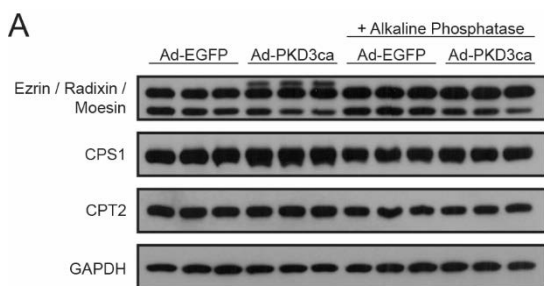
Figure 50: Hepatic PKD3ca expression shifts ERM and CPS1 in WB. (A) WB analysis of selected hits in extracts from PKD3-deficient primary hepatocytes transduced with either adenovirus expressing control EGFP (Ad-EGFP) or constitutive active PKD3 (Ad-mycPKD3ca) and treated with alkaline phosphatase (if indicated) using antibodies against ERM, CPS1, CPT2, and GAPDH as loading control (n=2 independent experiments). *Adenovirus* (Ad); *enhanced green fluorescent protein* (EGFP); *Protein kinase D* (PKD); *constitutive active* (ca); *ezrin/radixin/moesin* (ERM); *carbamoyl phosphate synthetase* (CPS); *carnitine palmitoyltransferase* (CPT); *glyceraldehyde 3-phosphate dehydrogenase* (GAPDH). (unpublished observation)

3.8.2 Immunoprecipitation with substrate motif antibody-based approach

Kinases are either serine/threonine or tyrosine kinases with preferences for specific amino acids within their consensus sequence (motif). PKDs are serine/threonine kinases with the substrate motif [L/V/I]xRxx[S*/T*] (x= random amino acid). For PKDs, *arginine* (R) in -3 position is almost essential, whereas *leucine* (L) in -5 position is preferred among other possible amino acids such as *valine* (V) or *isoleucine* (I). A phospho-(Ser/Thr) PKD substrate (LxRxx[S*/T*]) antibody was used for immunoprecipitation to enrich proteins that have a phosphorylated PKD motif in lysates from primary hepatocytes expressing either EGFP or PKD3ca. These immunoprecipitated proteins were then identified by mass spectrometry. First, it was confirmed that overexpression of PKD3ca led to an increase in proteins that have a phosphorylated PKD motif and that the antibody can be used for IP (Figure 51A, B).
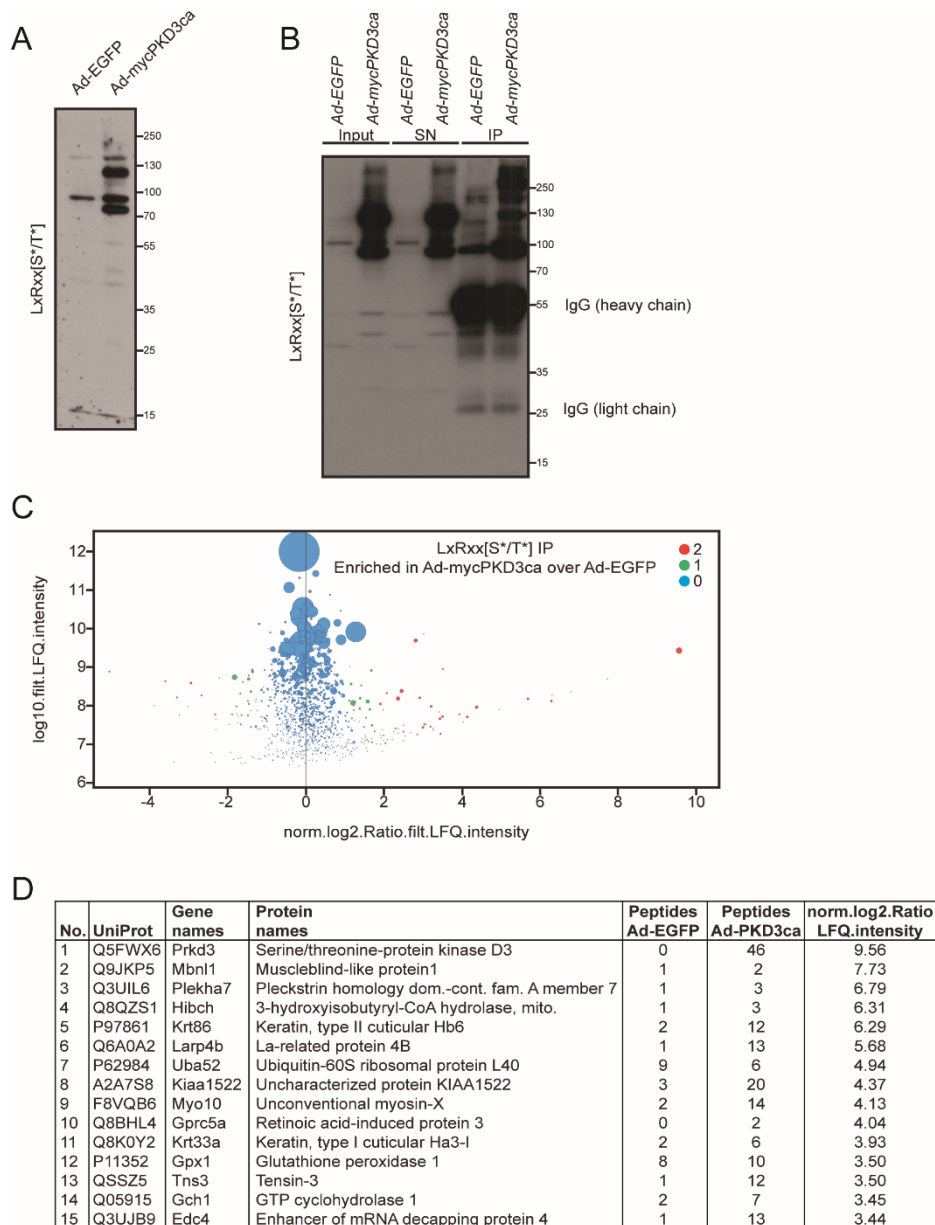
Figure 51: Putative PKD3 targets in hepatocytes identified by mass spectrometry following IP with LxRxx[S*/T*] antibody. (A) WB analysis of proteins with phosphorylated PKD motifs in lysates from PKD3-deficient primary hepatocytes transduced with either adenovirus expressing control EGFP (Ad-EGFP) or constitutive active PKD3 (Ad-mycPKD3ca) using a PKD-substrate motif (LxRxx[S*/T*])-specific antibody (n=3 independent experiments). (B) WB analysis of immunoprecipitated proteins with phosphorylated PKD motif from the same lysates as in (A) using a PKD-substrate motif (LxRxx[S*/T*]) antibody for IP and detection (n=3 independent experiments). (C) Volcano plot of the statistical significance of log2 transformed protein ratios versus log10-transformed LFQ intensities between control and PKD3ca expressing hepatocytes. Boxplot outliers with log2 transformed protein ratios versus control with values outside 1.5x or 3x of the IQR, respectively, were considered as significantly enriched indicated by blue (0), green (1) and red (2) dots, respectively (n=1 independent experiment). (D) List of the 15 most enriched proteins identified by mass spectrometry showing number, UniProt accession number, gene names, protein names, peptide count in EGFP and PKD3ca samples, respectively, and log2 transformed LFQ protein ratio. This experiment was performed in collaboration with the working group of Prof. Dr. Schlosser. *Protein kinase D* (PKD); *adenovirus* (Ad); *enhanced green fluorescent protein* (EGFP); *constitutive active* (ca); *supernatant* (SN); *immunoprecipitation* (IP); *immunoglobulin G* (IgG); *logarithm* (log); *label-free quantitation* (LFQ); *interquartile range* (IQR). (unpublished observation)

| No.	UniProt	Gene names	Protein names	Peptides Ad-EGFP	Peptides Ad-PKD3ca	norm.log2.Ratio LFQ.intensity
1	Q8BQZ4	Ralgapb	Ral GTPase-activating protein subunit beta	1	3	10.24
2	P63260	Actg1	Actin, cyto. 2	48	44	8.04
3	Q9JKP5	Mbnl1	Muscleblind-like protein 1	1	2	7.53
4	P35700	Prdx1	Peroxiredoxin-1	3	11	7.19
5	K9J7B2	Ugta6b	UDP-glucuronosyltransferase	1	13	6.35
6	Q62426	Cstb	Cystatin-B	1	6	6.22
7	P70275	Sema3e	Semaphorin-3E	1	14	5.85
8	Q62266	Sprr1a	Cornifin-A	2	9	5.45
9	Q5FWX6	Prkd3	Serine/threonine-protein kinase D3	3	42	5.38
10	P54823	Ddx6	Probable ATP-depended RNA helicase DDX6	2	14	5.33
11	P63168	Dynll1	Dynein light chain 1, cyto.	0	3	5.26
12	P01887	B2m	Beta-2-microglobulin	1	2	5.24
13	Q80TV8	Clasp1	CLIP-associating protein 1	0	30	5.04
14	O54962	Banf1	barrier-to-autointegration factor	1	3	5.00
15	Q80U30	Clec16a	Protein CLEC16A	1	2	4.96

Figure 52: Putative PKD3 targets in hepatocytes identified by mass spectrometry following IP with Rxx[S*/T*] antibody. (A) WB analysis of proteins with phosphorylated Rxx[S*/T*] motifs in lysates from PKD3-deficient primary hepatocytes transduced with either adenovirus expressing control EGFP (Ad-EGFP) or constitutive active PKD3 (Ad-mycPKD3ca) using a Rxx[S*/T*]-specific motif antibody (n=3 independent experiments). (B) WB analysis of immunoprecipitated proteins with phosphorylated Rxx[S*/T*] motif from the same lysates as in (A) using a Rxx[S*/T*]-specific motif antibody for IP and detection (n=3 independent experiments). (C) Volcano plot of the statistical significance of log2 transformed protein ratios versus log10-transformed LFQ intensities between control and PKD3ca expressing hepatocytes. Boxplot outliers with log2 transformed protein ratios versus control with values outside 1.5x or 3x of the IQR, respectively, were considered as significantly enriched indicated by blue (0), green (1) and red (2) dots, respectively (n=1 independent experiment). (D) List of the 15 most enriched proteins identified by mass spectrometry showing number, UniProt accession number, gene names, protein names, peptide count in EGFP and PKD3ca samples, respectively, and log2 transformed LFQ protein ratio. This experiment was performed in collaboration with the working group of Prof. Dr. Schlosser *Protein kinase D* (PKD); *adenovirus* (Ad); *enhanced green fluorescent protein* (EGFP); *constitutive active* (ca); *supernatant* (SN); *immunoprecipitation* (IP); *immunoglobulin G* (IgG); *logarithm* (log); *label-free quantitation* (LFQ); *interquartile range* (IQR). (unpublished observation)
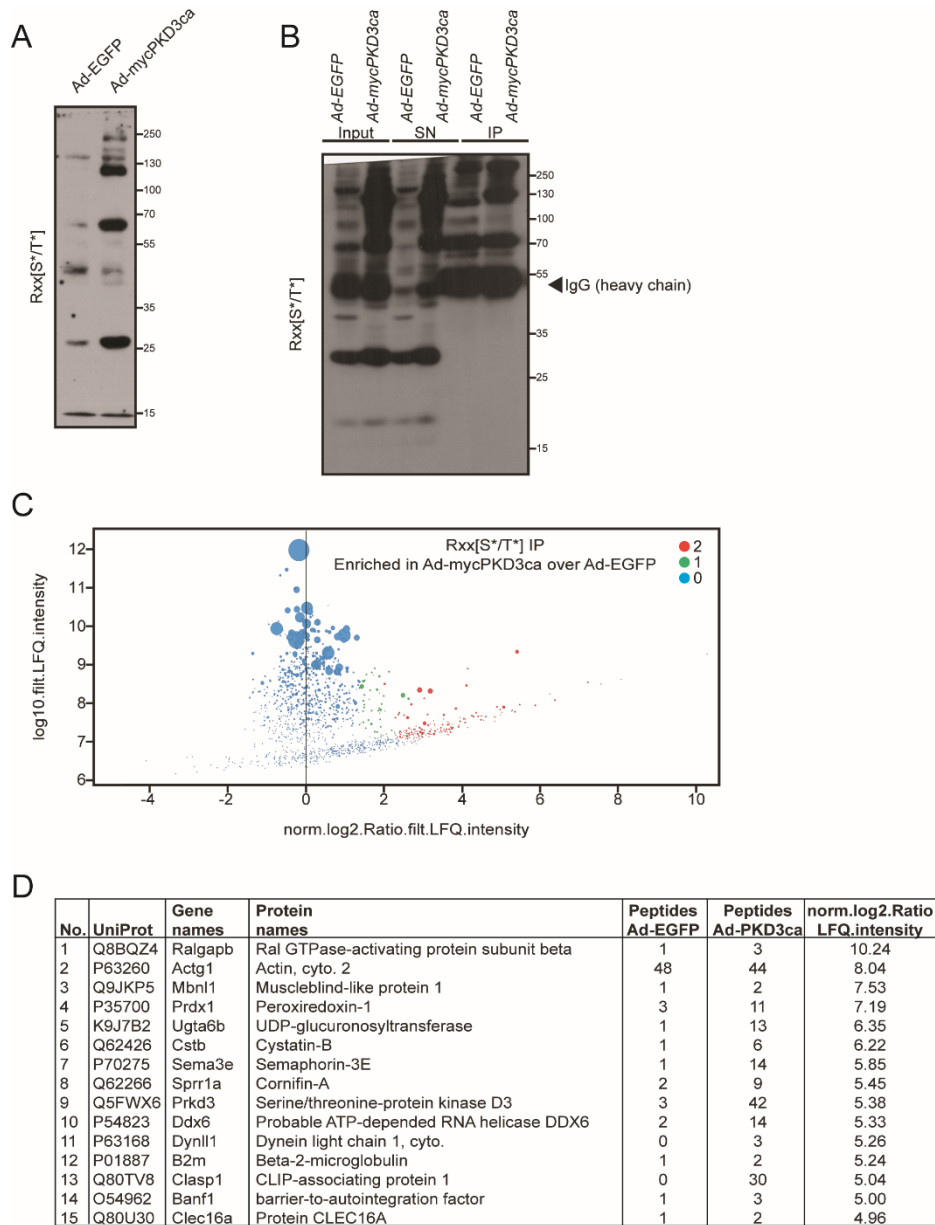
Results

Second, immunoprecipitated proteins with phosphorylated PKD motif were identified by mass spectrometry. 84 proteins were significantly enriched (significance of 1 or 2) in PKD3ca expressing hepatocytes compared to EGFP expressing hepatocytes (Figure 51C and Appendix 6.1.1). As a result, the 15 most enriched proteins by PKD3ca expression were PKD3 itself, MBNL1, PLEKHA7, HIBCH, KRT86, LARP4B, UBA52, KIAA1522, MYO10, GPRC5A, KRT33A, GPX1, TNS3, GCH1, and EDC4 (Figure 51D).

As mentioned before, *leucine* (L) in -5 position of the PKD substrate motif is the most frequently found amino acid in the PKD motif; however, many PKD motifs also contain *valine* (V), *isoleucine* (I), or other amino acids in the -5 position of the PKD substrate motif. In order to not exclude targets of PKD3 signaling in hepatocytes, a less PKD-specific motif antibody (Rxx[S*/T*]) was used in the same experimental design to enrich serine/threonine-phosphorylated proteins that have an *arginine* (R) in -3 position. Overexpression of PKD3ca confirmed an increase in proteins that have a phosphorylated Rxx[S*/T*] motif and that the antibody can be used for IP (Figure 52A, B). Next, the antibody was used for immunoprecipitation from protein lysates of EGFP and PKD3ca expressing hepatocytes, respectively, followed by protein identification using mass spectrometry. As a result, 236 proteins were significantly enriched (significance of 1 or 2) in primary hepatocytes expressing PKD3ca compared to EGFP-expressing hepatocytes (Figure 52C and Appendix 6.1.2). The 15 most enriched proteins by PKD3ca expression were RALGAPB, ACTG1, MBNL1, PRDX1, UGTA6B, CSTB, SEMA3E, SPRR1A, PKD3 itself, DDX6, DYNLL1, B2M, CLASP1, BANF1, and CLEC16A (Figure 52D).

Results
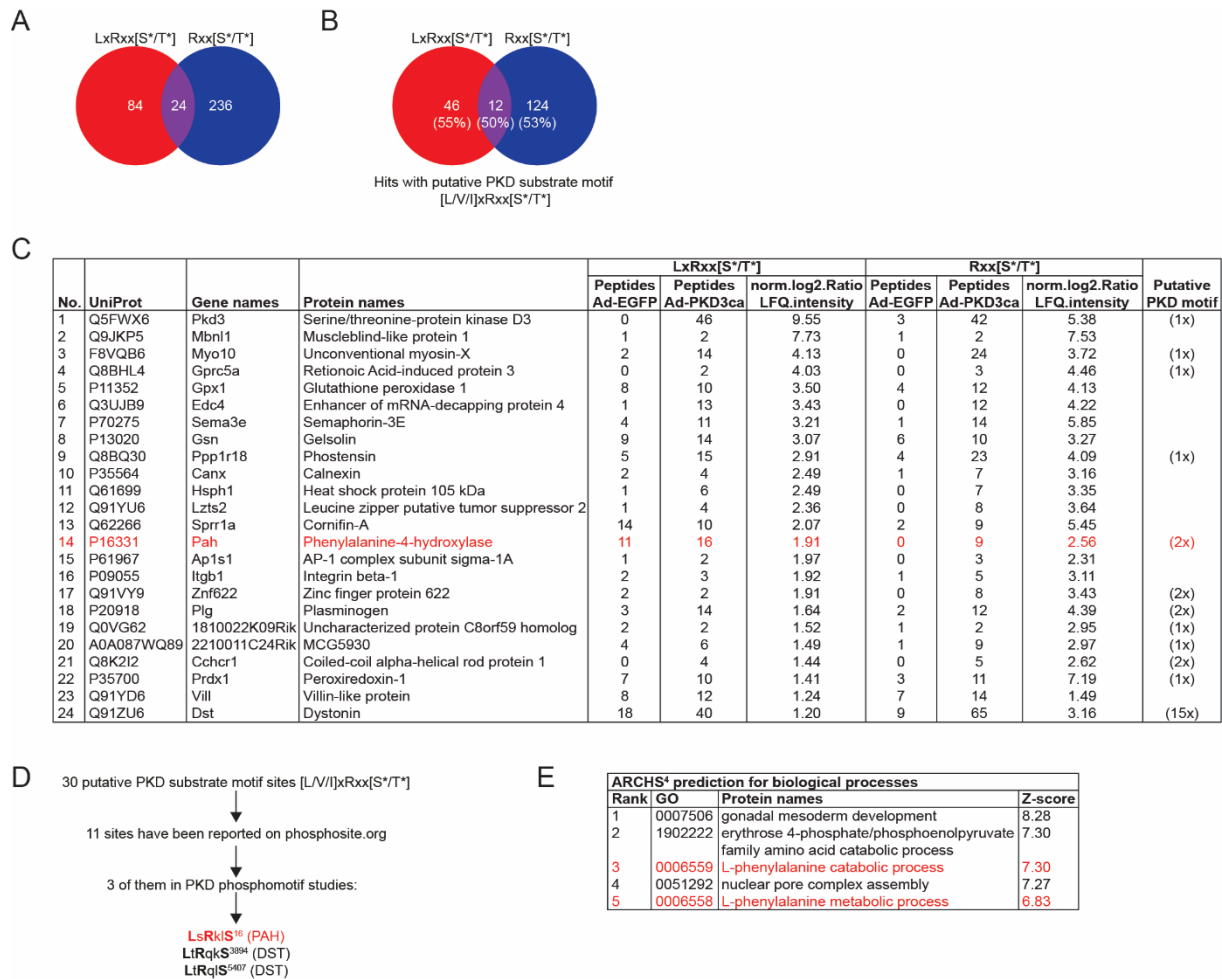
Figure 53: PKD motif and comparison analysis of LxRxx[S*/T*] and Rxx[S*/T*]-based screenings.
(A) Identification of common hits that were significantly enriched in both LxRxx[S*/T*] and Rxx[S*/T*] substrate motif antibodies-based screenings. (B) In silico identification of putative PKD motifs [L/V/I]xRxx[S*/T*] within the list of significantly enriched hits of both screenings (amount of proteins that have a putative site as percentage in brackets) by using Expasy ScanProsite tool. (C) List of the 24 common hits that were significantly enriched in LxRxx[S*/T*] and Rxx[S*/T*] screenings showing number, UniProt accession number, gene names, protein names, peptide count and log2 transformed LFQ protein ratio for LxRxx[S*/T*] and Rxx[S*/T*] screenings, respectively, and the amount of putative PKD motifs for each protein. (D) Scheme for computational hit selection by comparing the putative PKD substrate motifs with phosphosite.org repository. (E) ARCHS[4] prediction for biological processes in which PKD3 might be implicated[303]. *Protein kinase D* (PKD); *adenovirus* (Ad); *enhanced green fluorescent protein* (EGFP); *constitutive active* (ca); *immunoprecipitation* (IP); *logarithm* (log); *label-free quantitation* (LFQ); *phenylalanine hydroxylase* (PAH); *dystonin* (DST). (unpublished observation)

The LxRxx[S*/T*] screening identified 84 proteins and the Rxx[S*/T*] screening identified 236 proteins significantly enriched (phosphorylated) in hepatocytes expressing PKD3ca compared to controls. 24 proteins were enriched (phosphorylated) in both screenings by PKD3ca expression (Figure 53A). Among them, in silico analysis revealed that 12 proteins have at least one putative PKD motif [L/V/I]xRxx[S*/T*] (Figure 53B). The 24 proteins significantly enriched (phosphorylated) in both screenings by PKD3ca were MBNL1, MYO10, GPRC5A, GPX1, EDC4, SEMA3E,

Results

GSN, PPP1R18, CANX, HSPH1, LZTS2, SPRR1A, PAH, AP1S1, ITGB1, ZNF622, PLG, 1010022K09RIK, 2210011C24RIK, CCHCR1, PRDX1, VILL, and DST (Figure 53C). The 12 hits with a putative PKD motif have in total 30 putative motifs identified by in silico analysis. The 30 putative PKD motifs were then compared with the phosphosite.org repository in order to determine whether or not they had been reported before. Indeed, 11 sites were found on phosphosite.org database and among them, 3 sites were reported in PKD studies, namely, LsRklS16 for PAH and LtRqkS3894 as well as LtRqlS5407 for *dystonin* (DST) (Figure 53D). PAH was of particular interest because ARCHS4 prediction tool for biological processes claims that 'L-phenylalanine catabolic process' and 'L-phenylalanine metabolic process' are likely influenced by PKD3 signaling (Figure 53E).

DAVID Functional Annotation Clustering (Rxx[S*/T*])		
Cluster	Term	Enrichment Score
1	cell-cell adhesion	8.50
2	mitochondrion	8.16
3	oxidation-reduction process	8.05
4	actin binding	6.54
5	nucleotide or ATP binding	6.13
6	GTP binding	4.36
7	RNA binding	4.13
8	protein binding/folding	3.48
9	flavonoid glucuronidation	3.32
10	endoplasmatic reticulum	3.09
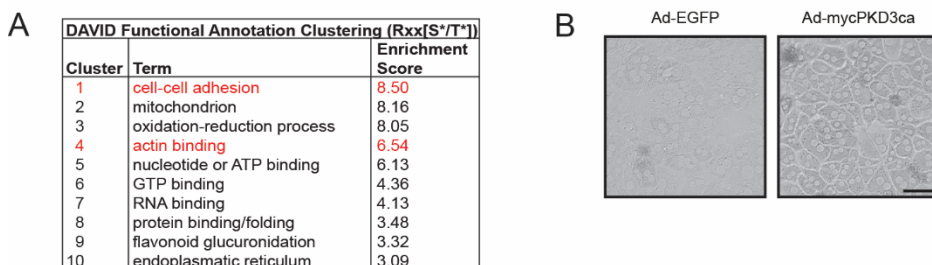
Figure 54: PKD3ca expression promotes processes such as cell-cell adhesion and actin binding. (A) List of enriched processes featured by PKD3ca expression in hepatocytes determined by functional annotation clustering (DAVID) of Rxx[S*/T*] enriched phosphoproteins showing cluster number, term and enrichment score. (B) Representative light microscopy pictures of PKD3-deficient primary hepatocytes transduced with either adenovirus expressing control EGFP (Ad-EGFP) or constitutive active PKD3 (Ad-mycPKD3ca) (n=3 independent experiments). *Adenovirus* (Ad); *protein kinase D* (PKD); *enhanced green fluorescent protein* (EGFP); *constitutive active* (ca). (unpublished observation)

DAVID functional annotation clustering[304] was applied to unravel pathways and processes influenced by PKD3ca expression by clustering the results of the board Rxx[S*/T*] screening. For this reason, GOTERM BP, GOTERM CC, and GOTERM MF, as well as UP KEYWORDS enriched by PKD3ca were clustered in groups and ranked according to their enrichment score (Figure 54A). Among the enriched processes, cell-cell adhesion and actin binding are of particular interest as the morphology of primary hepatocytes transduced with adenovirus expressing PKD3ca appeared qualitatively altered compared to EGFP expressing hepatocytes (Figure 54B). Together, computational DAVID analysis revealed upregulation of cell-cell adhesion and actin binding by PKD3ca expression, making these processes a promising target for further investigations.

Results

3.8.3 PAH is a target of PKD3 in liver

Figure 55: Expression of PKD3ca activates PAH in hepatocytes. (A) WB analysis of PAH expression (and shifting) in primary hepatocytes transduced with either adenovirus ex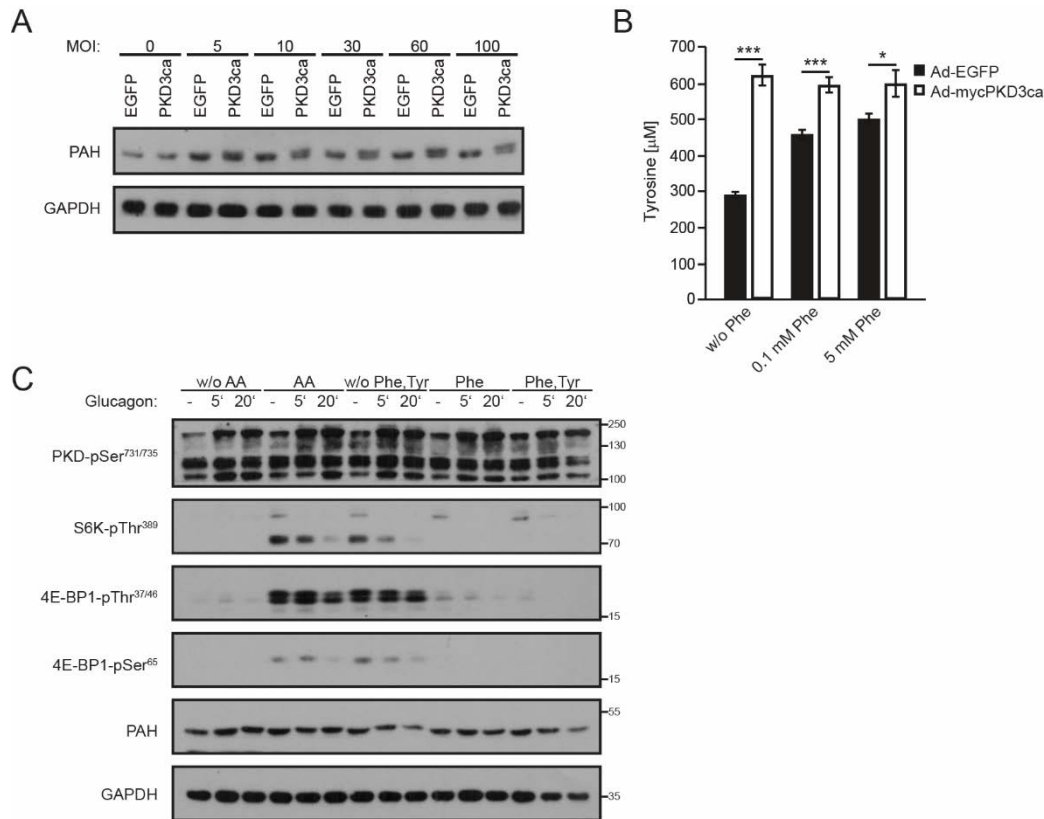pressing EGFP control (Ad-EGFP) or constitutive active PKD3 (Ad-mycPKD3ca) at indicated MOIs (n=2 independent experiments). (B) Intracellular phenylalanine to tyrosine conversion assay in primary hepatocytes transduced with either adenovirus expressing EGFP control (Ad-EGFP) or constitutive active PKD3 (Ad-mycPKD3ca) that were depleted from Phe and Tyr in the medium for 1 h before stimulation with 0, 0.1, or 5 mM Phe for 1 h (n=1 independent experiment). (C) WB analysis of indicated proteins in primary hepatocytes cultured in DMEM with either no amino acids (w/o AA), all amino acids (AA), all amino acids except phenylalanine and tyrosine (w/o Phe, Tyr), phenylalanine exclusively (Phe), or phenylalanine and tyrosine exclusively (Phe, Tyr) in combination with glucagon stimulation for 0, 5, and 20 min using antibodies against PKD-pSer731/735, S6K1-pThr389, 4E-BP1-pThr37/46, 4E-BP1-pSer65, PAH, and GAPDH as loading control (n=1 independent experiment). Data are presented as mean ± SEM. *P>0.05, ***P>0.001 (one way ANOVA with post hoc Tukey's test). *Adenovirus* (Ad); *enhanced green fluorescent protein* (EGFP); *protein kinase D* (PKD); *constitutive active* (ca); *multiplicity of infection* (MOI); *phenylalanine* (Phe); *tyrosine* (Tyr); *amino acid* (AA); *phospho* (p); *threonine* (Thr); *serine* (Ser); *p70 ribosomal S6 kinase* (S6K); *eIF4E-binding protein* (4E-BP); *phenylalanine hydroxylase* (PAH); *glyceraldehyde 3-phosphate dehydrogenase* (GAPDH). (unpublished observation)

PKD3 was predicted to be involved in phenylalanine metabolism (Figure 53E). Moreover, phenylalanine hydroxylase was significantly enriched in both screenings (LxRxx[S*/T*] and Rxx[S*/T*]) in PKD3ca expressing hepatocytes (Figure 53A-E). Additionally, computational analysis revealed the LsRklS16 of PAH is a putative PKD motif, which was described on phosphosite.org in a PKD substrate screening (Figure 53A-E). Ser16 of PAH was reported before as a target of glucagon and PKA

stimulation[261,263]. Phosphorylated PAH on Ser16 was shown to be more active at lower phenylalanine concentrations[263,265]. For these reasons, PAH was chosen for further experiments to investigate whether Ser16 of PAH is a substrate of PKD3. Mechanistically, phenylalanine hydroxylase catalyzes the conversion of phenylalanine to tyrosine by hydroxylating the aromatic side chain in a reaction that requires *tetrahydrobiopterin* (BH$_4$) as cofactor[254,255]. First, protein lysates from primary hepatocytes that were transduced with increasing amounts of adenovirus expressing either EGFP or PKD3ca, were used for detecting PAH expression. Interestingly, there was an upshift of PAH in lysates from hepatocytes expressing PKD3ca. This upshift appeared as two bands suggesting that PKD3ca expression leads to a phosphorylation of PAH (Figure 55A). As PAH catalyzes to conversion of Phe to Tyr, primary hepatocytes expressing either EGFP or PKD3ca were deprived from Phe and Tyr in the medium before adding certain concentrations of Phe to the medium. The results showed that there was highly significant more intracellular Tyr already at unstimulated conditions in hepatocytes expressing PKD3ca compared to controls (Figure 55B). Stimulation with 0.1 and 5 mM Phe increased the amount of intracellular Tyr in EGFP expressing hepatocytes, whereas intracellular Tyr concentrations were significantly higher in PKD3ca expressing hepatocytes independent of Phe stimulation (Figure 55B). As mentioned before, glucagon stimulation leads to an activation of PAH[261,305]. In order to determine whether glucagon stimulates PKD activity or whether this suppresses amino acid-mediated stimulation of S6K and 4E-BP1 activation, primary hepatocytes were cultured in media containing either no amino acids (w/o AA), all amino acids (AA), all amino acids except phenylalanine and tyrosine (w/o Phe, Tyr), phenylalanine exclusively (Phe), or phenylalanine and tyrosine exclusively (Phe, Tyr) and stimulated with glucagon. The results showed that PKD3 was phosphorylated by glucagon independent of the presence of amino acids (Figure 55C). Furthermore, stimulation of primary hepatocytes with media containing either all AAs or all AAs except Phe and Tyr were sufficient to induce a robust phosphorylation of S6K on Thr389 and a phosphorylation of 4E-BP1 on Thr37/46 and Ser65, which was suppressed by glucagon in a timely manner after 5 and 20 min of stimulation (Figure 55C). Taken together, this preliminary data suggests that PKD3 activation leads to a phosphorylation and activation of PAH, and PKD3 might integrate the signaling cascade of glucagon stimulation towards PAH.

4 Discussion

The liver is a key metabolic organ and a central hub for numerous physiological processes including blood filtration, blood glucose regulation, lipid and cholesterol homeostasis, endocrine control of growth signaling pathways, and breakdown of xenobiotic compounds[306]. These processes are regulated by a variety of hormonal and nutritional inputs. In this context, precise sensing of nutrient concentrations and fast adaptation to changes in nutrient availability is essential. Signaling through hormones like insulin and glucagon as well as through other signaling molecules initiates signaling cascades that lead to alterations in respective metabolic pathways. For example, the liver is a key target for the pancreatic hormones insulin and glucagon, thereby regulating glucose homeostasis. Insulin lowers postprandially the blood glucose concentration, whereas its counterpart glucagon increases the blood glucose concentration upon fasting[11]. Binding of these extracellular signaling molecules to membrane-bound receptors induces an intracellular signaling cascade that frequently involves protein kinases. Protein kinase C family members are of particular interest because they can both positively and negatively modulate insulin action[307]. PKCs have been reported to play a role in the development of peripheral insulin resistance[37]. Conventional and novel PKCs are activated upon DAG binding dependent or independent of Ca^{2+}-mediated phospholipid binding[56]. In the liver, accumulation and binding of DAG to the predominantly expressed PKC isoform PKCε inhibits the activation of the insulin receptor kinase[34-37]. Hepatic DAG accumulation is a result of an increased level of long-chain fatty acids originating from enhanced de novo lipogenesis, increased uptake (from chylomicrons and adipose tissues), and decreased β-oxidation[37,308]. Obesity and insulin resistance were directly linked with an increase in hepatic DAG content[36].

Closely related protein kinase D family members (PKD1, PKD2, and PKD3) are DAG and PKC effectors[57] that are involved in numerous physiological processes, including insulin secretion in pancreatic β-cells, and in the regulation of adipose tissue function[109,158]. However, the role of PKDs in liver metabolism and their implications in liver diseases remained elusive. For this reason, the aim of this thesis was to study PKD function in the liver by manipulating PKD signaling and analyzing its physiological and pathophysiological consequences.

Discussion

4.1 Obesity and DAG activate PKD3 in liver

The PKD isoforms are differently expressed depending on the cell type, indicating tissue-specific functions[91]. Database analysis of *Pkd1*, *Pkd2*, and *Pkd3* expression among several tissues revealed that *Pkd3* has the highest expression levels among different PKD isoforms in liver[91]. To assess this question in a quantitative manner that allows the comparison of the *Pkd* transcript level of the isoforms relative to each other, absolute expression of the three PKD isoforms in liver was quantified using an internal genomic DNA standard. The results showed that *Pkd1* is barely expressed, *Pkd2* is expressed moderately, and *Pkd3* is by far the most abundantly expressed isoform in liver (Figure 14). In addition, PKD3 abundancy is largely restricted to the liver compared to other metabolically relevant organs (Figure 15), suggesting a role of PKD3 in liver function. However, it remains unclear which cellular mechanisms control the differential PKD isoform expression in different tissues[91]. Moreover, previous studies reported that PKDs form heterodimers, which control secretory vesicle biogenesis and fission at the TGN as well as F actin-based directed motility in HeLa cells[111-113]. Absolute quantification of PKD isoform expression revealed a PKD3 abundancy of more than 86%, suggesting that PKD3 possibly forms besides PKD2-PKD3 hetero-complexes also PKD3 homodimers, or remains as monomer.

Importantly, identifying upstream signaling events and factors activating hepatic PKD3 is crucial for studying PKD3 function in liver and the identification of the upstream effectors might provide insights into pathways in which PKD3 is involved. PKDs are known to be PKC and DAG effectors that bind DAG with their two cysteine-rich domains, which mediate the translocation of inactive PKDs from the cytosol to the plasma membrane[49]. DAG simultaneously activates PKCs at the plasma membrane, which mediates transphosphorylation of PKDs on Ser731 (PKD3)[92]. Then, DAG and PKC synergistically induce catalytic activation of PKD by promoting autophosphorylation on Ser735 (PKD3)[92]. For this reason, primary hepatocytes were incubated with a cell-permeable DAG analog to analyze whether this mode of activation is preserved in liver. Indeed, DAG induced a robust activation of PKDs seen by phosphorylation on Ser731/735 (Figure 10), which is in line with previous findings in other cell types[92]. DAG accumulates in liver following an increase in long-chain fatty acids arising from enhanced delivery of chylomicron remnants, increased fatty acid uptake from adipocytes, increased hepatic de novo lipogenesis induced by skeletal muscle insulin resistance, or from decreased mitochondrial β-oxidation[37]. Oleic acid

Discussion

(C18:1) is a fatty acid that is frequently used as substrate for DAG synthesis. Oleic acid-loading of primary hepatocytes also activated PKD3 indicated by the phosphorylation of two serine residues in the activating loop in the kinase domain (Figure 10). Oleic acid was shown before to induce PKD activation through the binding to the cell membrane fatty acid receptor GPR40 in β-cells, leading to an intracellular Gαq-PLC-mediated increase in DAG content, which in turn activated PKD[110]. However, the response in PKD activation in oleic acid-loaded hepatocytes was much slower after a prolonged period of DAG loading (20 h), suggesting that PKD3 is not only activated by the membrane-bound secondary messenger DAG but also from DAG that arises from endogenous de novo synthesis. Physiologically, it was reported that hepatic DAG content is increased during obesity[36,37], as well as during the pathological condition of NAFLD[276,277]. Experimentally, feeding mice with an HFD induces obesity, steatosis, and peripheral insulin resistance[309]. For this reason, it was worthwhile to study whether HFD-feeding of mice affected PKD3 activation in liver. First, it was successfully confirmed that the used HFD increased DAG content in livers of mice that were fed an HFD for 24 weeks compared to mice that were fed an ND for the same time (Figure 10). Quantification of DAG content was assessed in liver lysates; however, a previous study showed that membrane and particularly cytosolic DAG is responsible for induction of muscle insulin resistance[310]. Therefore, it might be of interest to do subcellular fractionation and measuring DAG abundancy within the subcellular fractions. Importantly, HFD-feeding of mice resulted in a significant activation of PKD3 indicated by increased Ser731/735 phosphorylation in livers of HFD-fed mice compared to livers of ND-fed mice (Figure 12), suggesting a role for PKD3 in liver during lipid accumulation.

Multiple studies described the influence of purinergic signaling on regulating liver metabolism in health and disease[279,280]. In liver, purinergic receptors mediate bile secretion, glycogen, and lipid metabolism[280]. ATP is released either from sympathetic nerves as co-transmitter or from hepatocytes and Kupffer cells due to mechanic stress[279]. Ligand binding to purinergic receptors has been reported to increase intracellular DAG levels[311]. ATP stimulation for 15 s increased the DAG concentration of about 80% in rat renal mesangial cells[311]. In addition, extracellular ATP rapidly increased the activity and phosphorylation of PKD in rat parotid acinar salivary cells[281] and astrocytes[282]. In this thesis, stimulation of primary hepatocytes with ATP induced fast phosphorylation of PKD3 on Ser731/735 (Figure 13), which is in line with the

previous observations. However, the exact upstream signal transduction and in particular, the distinct purinergic receptor activating PKD3 in hepatocytes in response to ATP stimulation remains unclear.

Finally, PKD3 was activated in primary hepatocytes in response to glucagon stimulation (Figure 55). Previous studies reported a PMA-mediated inhibition of glucagon-stimulated adenylate cyclase activity in hepatocytes[312,313], which was dependent on PMA-bound PKD[314]. Together, this suggests a feedback-loop of glucagon-activated PKD3 back to the glucagon receptor in hepatocytes. The physiological relevance of the glucagon-mediated PKD activation will be discussed later (see 4.4).

In conclusion, PKD3 was activated in hepatocytes by various upstream signaling effectors/events, including obesity accompanied with increases in intrahepatic DAG and FA content, as well as in response to glucagon and purinergic signaling.

4.2 Lack of PKD3 promotes hepatic lipid accumulation

As already elaborated, DAG accumulates in liver during obesity, leading to an activation of PKD3 in hepatocytes, therefore HFD-feeding of mice was used to analyze the role of activated hepatic PKD3 on whole body physiology. For this reason, mice lacking PKD3 in liver were generated by crossing PKD3 floxed mice with mice expressing the Cre recombinase under the control of the albumin promoter and fed an HFD for 24 weeks. Depletion of PKD3 in liver did not affect body weight gain during 24 weeks of HFD-feeding; however, it significantly increased the liver weight (Figure 15 and Figure 16). The observed increase in liver weight despite no difference in body weight reflects the rather small liver-to-body-weight ratio in general and has been described in various other hepatic genetic models. For example, hepatic depletion of HDAC3 resulted in severe hepatosteatosis and increased liver weight without any changes in body weight compared to controls when fed an HFD[315]. Generally, the weight of the liver can be increased due to promoted cell cycle progression and increased proliferation[316] among other causes. However, the level of proliferation assessed by Ki-67 staining, apoptosis (staining of cleaved caspase-3 and TUNEL), as well as immune cell infiltration was unaffected by depleting PKD3 in hepatocytes (Figure 25), suggesting that the increased liver weight resulted from an accumulation of certain metabolites. Indeed, lack of PKD3 in hepatocytes promoted TG and cholesterol accumulation in liver (Figure 20 and Figure 22), which is a feature of hepatic

Discussion

steatosis and NALFD[7,317]. A recent study described the implications of PKD1 signaling on adipose tissue function, including the regulation of lipolysis and lipogenesis[158]. In contrast to liver, ablation of PKD1 in murine adipocytes resulted in decreased TG accumulation in an AMPK-dependent manner[158]. The accumulation of TG in adipose tissues might be differently controlled as TG levels are regulated by numerous pathways in the adipose tissue[318]. Together, PKDs control lipogenesis differently in adipocytes and hepatocytes. The phosphorylation of AMPK as well as of the AMPK-target ACC was not influenced by expressing PKD3ca in hepatocytes, suggesting a different set of substrates and tissue-specific roles for the PKD isoforms. Deletion of PKD1 in hepatocytes did not alter any analyzed parameters of hepatic physiology (Figure 24), which is supported by the fact that PKD1 expression was very low in liver (Figure 14)[91].

In the liver, the non-physiological accumulation of lipids can result from different processes: increased uptake from chylomicron remnants and peripheral tissues, increased synthesis (de novo lipogenesis), decreased catabolism (β-oxidation), or decreased VLDL secretion[286]. These processes were analyzed whether they are differently regulated in response to PKD3 deletion in hepatocytes (Figure 27). First, hepatic steatosis is accompanied by increased VLDL secretion[319], which occurs via the Golgi[320,321]. Inhibition of PKD1 activity was shown to impair the membrane fission at the TGN and thus reduces its secretory capacity[82,111]. A study showed that the PKD inhibitor Gö6976 suppressed VLDL secretion in human Huh7.5.1 cells[322]. In this thesis, VLDL secretion rate did not differ in mice lacking PKD3 in hepatocytes compared to control mice neither when fed an ND nor an HFD (Figure 27). This discrepancy might be explained by the Gö6976 inhibitor itself, which does not only inhibit PKDs but also PKCs, which could have been avoided by using one of the PKD-specific inhibitors CID755673 or CRT0066101[77,78]. Moreover, an FAO assay was used to determine the rate of β-oxidation. PKD3-deficient hepatocytes oxidized significantly more ^{3}H-oleate compared to wild type hepatocytes, but alterations in FAO rate did not explain the origin of increased lipid accumulation. Finally, de novo lipogenesis was identified in this thesis as the primary process leading to increased lipid accumulation in PKD3-deficient hepatocytes. Previous studies showed that PKDs regulate lipid accumulation; however, overexpression of PKD1 in cardiomyocytes prevented lipid accumulation[323], whereas overexpression of PKD1 in adipocytes promoted de novo lipogenesis and lipid accumulation[158]. Again, this inconsistency might be due to different roles of the

Discussion

PKD isoforms in different tissues. In addition, this also suggests that PKDs regulate de novo lipogenesis and fat accumulation through different processes.

Taken together, deletion of PKD3 in hepatocytes promotes lipid accumulation due to increased de novo lipogenesis.

4.3 PKD3 regulates insulin signaling and SREBP-driven lipogenesis through AKT and mTORC1/2

Hepatic lipid accumulation leads to the development of hepatic insulin resistance (reviewed in [324]) through a mechanism in which DAG-activated PKCε impairs the activation of the IR[34,35,325]. Unexpectedly, despite an increased level of intrahepatic lipids, mice lacking PKD3 in liver showed improved glucose tolerance and insulin sensitivity (Figure 16). Conversely, mice overexpressing PKD3ca in hepatocytes displayed impaired glucose tolerance and reduced insulin sensitivity even when fed an ND, leading to insulin resistance assessed by HOMA-IR index (Figure 46).

A pathway that features both increased lipid accumulation and improved sensitivity at the same time is mTORC signaling (reviewed in [166,167]). Both mTOR complexes 1 and 2 have been shown to regulate de novo lipogenesis through the transcription factors SREBP1c and SREBP2, and insulin sensitivity by phosphorylating AKT and providing feedback loops back to the IR and IRS (reviewed in [166,167,326]). Hepatic ablation of Rictor, a major component of mTORC2, resulted in loss of AKT phosphorylation on Ser473 and reduced SREBP1c activity, leading to decreased lipid accumulation and impaired insulin sensitivity[250]. Moreover, activation of mTORC1 was shown to stimulate SREBP-dependent lipogenic gene expression and thus promotes de novo lipogenesis[189,190,296]. In this thesis, ablation of PKD3 in liver promoted de novo lipogenesis through activation of AKT and mTORC1/2, leading to SREBP1c and SREBP2-mediated lipogenic gene expression. Importantly, DAG stimulation of primary hepatocytes decreased lipogenic gene expression (Figure 11), which is in line with a previous study reporting that stimulation with the same DAG analog resulted in a modest reduction in SREBP1 levels shown by Western blot[327]. Insulin stimulation of hepatocytes deficient for PKD3 resulted in reduced phosphorylation of AKT and mTORC1 targets S6K1 and 4E-BP1 as well as of the mTORC2 substrates SGK1 and AKT (Figure 34; Figure 37; Figure 39; Figure 41). In contrast, adenoviral mediated overexpression of constitutive active PKD3ca in hepatocytes reversed the results

Discussion

obtained in PKD3 KO hepatocytes, revealing that AKT phosphorylation was impaired as well as phosphorylation of mTORC1 and mTORC2 substrates was reduced (Figure 36; Figure 38; Figure 40). mTORC1 was shown to regulate SREBP maturation and activity through lipin 1[22] and S6K1[328,329]. Lipin 1 is a phosphatidic acid phosphatase that catalyzes the conversation of PA to DAG and therefore potentially also provides a feedback activation of PKD3 as shown for the maturation of autolysosomes in muscle cells[330]. A previous study revealed that PKD3 can directly phosphorylate and activate S6K1 in an mTOR-independent manner, which contributed to breast cancer cell growth[331]; however, the lipogenesis rate or SREBP activation was not analyzed in this study. Furthermore, another study showed that the PKD-related protein kinase PKCβ is a mediator of insulin-mediated activation of SREBP1c and expression of its lipogenic target genes through directly activating the SREBP1c promoter[332]. However, in contrast to these two studies, the results obtained in this thesis clearly indicate that PKD3 signals through mTOR since the phosphorylation of all analyzed mTORC1 and mTORC2 downstream substrates was influenced by manipulating PKD3. Yet, there might be also an mTOR-independent regulation of lipogenesis by PKD3 in hepatocytes under certain conditions. In this thesis, total protein level of YAP/TAZ was increased in livers of HFD-fed *PKD3*$^{liverΔ/Δ}$ mice (Figure 26). PKDs were reported to mediate YAP activation in response to insulin[333,334]. In the liver, TAZ promotes inflammation and fibrosis in NASH[288], but YAP protects against ER stress-induced cell death and liver injury[335], and ER stress promotes SREBP cleavage and consequently lipogenesis[20,336]. Notably, quantification of the indicators of liver damage ALT and AST as well as staining for the fibrosis markers collagen type IV and collagen fibers (sirius red) was not affected by hepatic PKD3 deletion (Figure 25; Figure 26), indicating that PKD3 does not promote TAZ-mediated inflammation and fibrosis. In this hypothesized model, the primary effect of PKD3 would be to block YAP action and thus promote ER stress, leading to SREBP maturation and ultimately to steatosis. For this reason, it would be worth determining TAZ and YAP protein levels separately of each other in order to see whether YAP protein level is indeed increased in livers lacking PKD3. Other mechanisms that regulate lipogenesis which might be influenced by PKD3 signaling include USF or *DNA-dependent protein kinase* (DNA-PK). They are known to promote lipogenic gene expression[14]. Oxidative stress might present an upstream condition that induces PKD3 activity in liver because stress-activated *death-associated protein kinase* (DAPK) was reported to interact and activate PKD[93,337], which might be

the reason for increased SREBP-mediated lipogenesis in hepatocytes[338]. In addition, the phosphorylation of the mTORC2 downstream effector NDRG1 was increased in the absence of PKD3 (Figure 37). NDRG1 was shown to promote lipogenesis in a PPARγ-dependent manner in adipocytes, implicating that PKD3 might regulate lipogenesis through other transcription factors than SREBP[184]. Nevertheless, silencing of SREPP1 and SREBP2 in hepatocytes abolished the elevated lipogenesis rate in hepatocytes lacking PKD3 (Figure 30) demonstrating that PKD3 suppresses lipogenesis in an SREBP-dependent manner. Similarly, inhibition of either AKT, mTORC1, or mTORC2 activity confirmed that PKD3 suppresses de novo lipogenesis through these factors (Figure 43).

Although it is clear that PKD3 suppresses SREBP-mediated lipogenesis in an AKT and mTOR-dependent manner, the exact mechanism how PKD3 controls AKT and mTORC1/2 activity, and the direct substrate of PKD3 in hepatocytes remained unclear. Previous studies showed that stimulation with PMA or with a GPCR agonist markedly increased PKD1-mediated phosphorylation of the PI3K regulatory subunit p85α, leading to a feedback inhibition of PIP_3/AKT activation[339,340]. PKD1 directly phosphorylates p85α on Ser154 to enhance its interaction with PTEN, resulting in an activation of PTEN, which inhibits the conversion of PIP_3 to PIP_2 and thus impairs the phosphorylation of AKT downstream of PIP_3[341,342]. This would fit with the results obtained in this thesis in which PKD3 deletion led to impaired AKT phosphorylation in vitro and in vivo (Figure 19; Figure 34). Another potential target of PKD3 in hepatocytes might be *Src homology region 2 domain-containing phosphatase-1* (SHP-1). SHP-1 was shown to be directly phosphorylated on Ser557 by PKD2 and PKD3 in thymocytes[343]. The tyrosine phosphatase SHP-1 dephosphorylates the regulatory p85 subunit of PI3K on Tyr688, leading to a decrease in PI3K activity[344,345]. This suggests that the putative phosphorylation of SHP-1 by PKD3 might be an inhibitory phosphorylation, resulting in inactive SHP-1 and thus active PI3K, PDK1 and AKT. This hypothesis is supported by the observation that hepatic insulin sensitivity is heightened in mice lacking SHP-1 in liver[346], which also emphasizes its relevance in hepatic insulin resistance. Furthermore, PKD3 might also provide the negative feedback on insulin signaling by directly phosphorylating the IR similar to PKCε[34,35] or factors downstream of the IR such as IRS or PDK. Unexpectedly, phosphorylation of IRS1 at Ser612 was increased in hepatocytes overexpressing PKD3ca (Figure 40),

Discussion

indicating that also other signaling pathways (e.g. MAPK pathway[347]) might be activated in response to PKD3ca expression.

As elaborated before, PKD3 ablation in liver resulted in hepatic lipid accumulation but protected the mice from developing hepatic insulin resistance. These processes are intertwined with hepatic glucose metabolism[5,11]. Canonically, insulin directly inhibits hepatic gluconeogenesis through activation of AKT, resulting in phosphorylation of FOXO1 and suppression of gluconeogenic gene expression[348]. In this thesis, ablation of PKD3 in hepatocytes promoted glucose production in vitro but suppressed glucose output in vivo (Figure 45), suggesting different mechanisms of regulation. In addition, net hepatic glucose production is the summation of glucose originating from gluconeogenesis and glycogenolysis, as well as from decreased glycolysis and glycogen synthesis[11]. However, the preliminary data provided in this thesis on the regulation of hepatic glucose metabolism is limited. Hepatic glucose metabolism is also strongly influenced by the whole body metabolism, food intake and the type of diet, as well as by other environmental factors[11], which have to be taken into account. Rictor-deficient hepatocytes produced more glucose at basal and insulin-stimulated conditions, which is due to increased FOXO1-mediated expression of gluconeogenic genes[250]. Considering that PKD3 ablation in hepatocytes promoted mTORC2 activation, this means that the results obtained from the in vivo experiments, in which the lack of PKD3 suppressed glucose output, are in line with PKD3 inhibiting mTORC2 function. Correspondingly, activation mTORC1 due to TSC2-deletion resulted in enhanced HIF1α-driven expression of glycolytic genes[190], which fits again with the observed decreased glucose concentrations in mice lacking hepatic PKD3 after prolonged fasting (Figure 45). However, this might also be due to impaired gluconeogenesis. In cancer cells, it was demonstrated that PKD1 regulates hypoxic glycolytic metabolism by increasing the expression of HIF-1α and glycolytic enzymes[349]. Notably, during insulin resistance, direct liver insulin signaling is required for lipogenesis, while it is dispensable for the suppression of glucose production[42]. Nevertheless, PKD3 might also regulate glucose output from hepatocytes independent of mTOR. PKD1 regulates contraction-induced GLUT4 translocation and consequently glucose uptake in cardiomyocytes[350,351]. For this reason, PKD3 might suppress the translocation of GLUT2 in hepatocytes, leading to increased glucose concentrations during fasting. This hypothesis is supported by the observation that overexpression of wild-type PKD3 significantly enhanced basal and insulin-stimulated glucose uptake in

Discussion

L6 myotubes[352]. Moreover, PKD1 phosphorylates CREB at Ser133, which contributes to pathological cardiac remodeling[127,128]. In liver, CREB regulates hepatic gluconeogenesis through the coactivator PGC-1 and hepatic lipid metabolism through nuclear hormone receptor PPARγ[353,354], suggesting that PKD3 potentially might phosphorylate CREB also in liver and thereby regulating hepatic glucose metabolism.

PKDs have distinct intracellular localizations in different cell types and in response to numerous stimuli, indicating that the differential distribution regulates their signaling properties. For this reason, determination of the intracellular localization of PKD3 in hepatocytes might help to unravel the mechanism of PKD3 action in hepatocytes. PKDs have been described to reside in the cytoplasm[79,80], nucleus[79,90], Golgi[81,82,85,86], mitochondria[87,355], and might translocate to the plasma membrane upon activation[79,83]. However, expression of PKD3ca in primary hepatocytes did not result in TGN, mitochondria, or ER localization of PKD3ca (Figure 44). PKD3ca was found in punctate structures that might be peroxisomes or endosomes/lysosomes as shown previously[356]. However, expression of a kinase inactive form of PKD (PKD-K618N) did not affect protein transport from ER to the endosomes via the TGN nor was PKD localized to endosomes in HeLa cells[82]. PKD3ca did also not localize to peroxisomes, which would have been of particular interest, as TSC was reported to reside on peroxisome membranes, which controls mTORC1 activity[357,358], and hence, TSC might be a potential substrate of PKD3 in hepatocytes. For this reason, co-staining of PKD3ca with a lysotracker would be insightful as the lysosome is a major site of mTORC1 activation (reviewed in[359]).

In conclusion, hepatic PKD3 suppresses SREBP-depended de novo lipogenesis through impairing the activation of AKT, mTORC1, and mTORC2. In addition, PKD3 provides a negative feedback on insulin sensitivity.

4.4 Proteomics identified PAH as a target of PKD3 in liver

Three different mass spectrometry-based approaches were used to identify substrates of PKD3 in hepatocytes. EGFP (as control) and PKD3ca were expressed in PKD3-deficient hepatocytes and either enriched for phosphoproteins and separated on a 2D-DIGE gel or used for immunoprecipitation with motif-specific antibodies (LxRxx[S*/T*] and Rxx[S*/T*]). For all approaches, the putative PKD3 targets were identified by MS.

Discussion

The 2D-DIGE-based approach, among the others, identified the closely related actin-binding proteins Ezrin/Radixin/Moesin (ERM) as potential targets of PKD3 in hepatocytes (Figure 49; Figure 50). Furthermore, Moesin was also identified as a potential PKD3 target by MS following immunoprecipitation with the Rxx[S*/T*]-motif antibody in hepatocytes expressing PKD3ca (Table 16). The proteins of the ERM family are cross-linkers between the plasma membrane and the actin filament, which is important for the formation of microvilli, cell adhesion, and membrane ruffling[360]. At the plasma membrane, ERM proteins are activated by binding to *phosphatidylinositol 4,5-bisphosphate* (PtdIns(4,5)P$_2$) followed by phosphorylation of conserved threonine residues (Ezrin at Thr567, Radixin at Thr564, Moesin at Thr558, respectively) by specific kinases, which in turn allows the ERM proteins to unfold the F-actin domain and bind to the cytoskeleton (reviewed in [361]). Among the kinases phosphorylating the conserved threonine in ERM proteins are the PKD-related kinases PKCα and PKCι, which were shown to phosphorylate Ezrin at Thr567[362,363]. In addition, the ERM family members are bound to the scaffold protein *ERM binding phosphoprotein* (EBP) 50 (also known as NHERF-1)[364], which is directly phosphorylated by PKCs on Ser337/Ser338[365]. In this context, activated PKDs were reported to transiently associate with EBP50, suggesting that PKDs may act as a regulator of proteins at the EBP50 scaffold[366]. This would be in line with the results obtained in this thesis in which expression of PKD3ca led to a phosphorylation of one or multiple ERM proteins (Figure 49; Figure 50). However, PKD3 lacks the C-terminal *postsynaptic density-95/discs large/zonula occludens* (PDZ)-binding motif, which has been shown to be required for the interaction with EBP50[366], suggesting a different mechanism for PKD3. In addition, neither Ezrin, Radixin, nor Moesin have a putative PKD substrate motif. This observation does not exclude a direct phosphorylation of PKD3, but it might be possible that the ERM proteins are phosphorylated in a signaling cascade by other factors that are activated by PKD3. An in vitro kinase assay with PKD3 and the ERM proteins might help to unravel the question whether PKD3 directly phosphorylates ERM proteins.

MS following a Rxx[S*/T*]-motif antibody-based IP identified *Ral GTPase activating protein non-catalytic beta subunit* (RalGAPβ) as the most enriched hit in hepatocytes expressing PKD3ca (Figure 52). RalGAPα is a GAP for the RalA and RalB small GTPases[367]. The catalytic subunit RalGAPα forms a heterodimer with the regulatory subunit RalGAPβ and both RalGAP subunits share sequence and structural similarity with TSC1-TSC2[367]. RalGAPs are activated in response to insulin[367] and RalGAP

Discussion

signaling controls mTORC1 activity[368]. In this context, physical interaction between RalGAPβ and RalGAPα is required for maximal stability of the subunits and for acitivity[367]. Insulin inhibits the RalGAP heterodimer through an AKT-catalyzed phosphorylation of RalGAPα on Thr718, which triggers the binding of the negative regulator 14-3-3[367,369]. In this thesis, computational analysis identified four putative PKD phosphorylation sites (PKD substrate motif: [L/V/I]xRxx[S*/T*]) of RalGAPβ (LaReSS156, IsRprS357, InRdnS470, and LvRgmS971) that might be phosphorylated by PKD3 in hepatocytes leading to an inhibitory phosphorylation of RalGAPβ that possibly promotes the dissociation of the RalGAP complex.

Moreover, expression of PKD3ca also increased the abundancy of immunoprecipitated TSC1 (n.s.) and TSC2 (IP with Rxx[S*/T*]-motif antibody) (Appendix 6.1.2). Similarly to RalGAPα/β, the TSC complex regulates mTOR activity by inhibiting the GTPase Rheb[205,207,208], a factor that binds to and activates mTORC1[209]. AKT directly inhibits the TSC complex by phosphorylating TSC2 on several residues, leading to mTORC1 activation[186-188,370]. In contrast, the direct or indirect phosphorylation of TSC1/2 through PKD3 might stabilize TSC1/2, as expression of PKD3ca in hepatocytes impaired mTORC1 activation (Figure 38). However, stabilization of TSC1/2 does not explain the decreased level of phosphorylation of other upstream regulators of TSC and mTORC1, such as AKT at Thr308 and Ser473 in response to PKD3ca expression (Figure 36). Computational analysis identified one putative PKD phosphorylation site for TSC1 (LfRnkS1094) and seven putative PKD phosphorylation sites for TSC2 (IlRelS49, LlRadS625, IyRcaS802, LvRrpT1203, LpRsnT1270, LhRsvS1291, IeRaiS1365).

MS following the LxRxx[S*/T*]-motif antibody-based IP identified *Tensin* (TNS) 3 as a potential target of PKD3 in hepatocytes (Figure 51). Tensin3 belongs together with Tensin1, Tensin2, and *C-terminal tensin-like protein* (CTEN) to the Tensin family of focal adhesion molecules[371,372]. Tensins link integrins with the actin cytoskeleton, thereby contributing to focal adhesion assembly[372]. In this context, Tensins are involved in fundamental processes such as cell attachment and migration at focal adhesions[372]. In addition, Tensins influence the activity of Rho GTPases such as RhoA or Rac1 by interacting with GTPase-activating proteins (such as *deleted in liver cancer* (DLC) 1) or guanine nucleotide exchange factors (such as *dedicator of cytokinesis* (DOCK) 5)[372,373]. For mammary cell migration, EGF was shown to induce a switch in the expression from TNS3 to CTEN, thereby easing the integrin linkage to the cytoskeleton, as CTEN lacks an actin-binding domain in contrast to the other Tensin

Discussion

family members[374-376]. EGF stimulation promotes Tyr phosphorylation of TNS3, leading to an TNS3–PI3K complex formation and subsequently to Rac1 activation at the leading edge of a migrating cell[377], a cell compartment where PKDs are also found[378]. Rac1 is known to regulate the activity of both mTOR complexes; however, independent of PI3K[379]. Therefore, PKD3 might phosphorylate TNS3 (putative PKD phosphorylation sites: LiRwdS332, LlRkpS571, VqRgiS648) in liver, resulting in mTORC activation through pathways that possibly require Rac1 or PI3K/AKT signaling.

Both screenings with MS following immunoprecipitation with motif antibodies (LxRxx[S*/T*] and Rxx[S*/T*]) identified phenylalanine hydroxylase (PAH) to be enriched in hepatocytes expressing PKD3ca (Figure 53). Moreover, PKD3 was predicted to be involved in phenylalanine metabolism (Figure 53). PAH has two putative PKD motifs (LsRklS16 and IpRpfS411), of which Ser16 has been reported to be phosphorylated in response to glucagon and PKA stimulation[261,263]. However, the classical PKA motif is RRx[S*/T*][380] and in -2 position of Ser16 is lysine (K) and not arginine (R), meaning that it is not the most common PKA motif; nevertheless, it is a classical PKD motif. For this reason, the results obtained in this thesis suggest a model in which glucagon activates PAH in a mechanism that requires PKD3-mediated phosphorylation of PAH on Ser16. In fact, glucagon stimulation led to an activation of PKD3 in hepatocytes. Physiologically, phosphorylation of PAH on Ser16 lowers the concentration of Phe required for activation[149,269]. Indeed, expression of PKD3ca in hepatocytes increased Tyr concentrations (Figure 55) due to increased activity of PAH. Furthermore, AA catabolism is tightly connected with the excretion of ammonia in form of urea. A key enzyme in this context is *carbamoyl phosphate synthetase* (CPS) 1, which catalyzes the ATP-dependent synthesis of carbamoyl phosphate from ammonia and bicarbonate[381]. Interestingly, CPS1 was found to be enriched in lysates from PKD3 expressing hepatocytes in the 2D-DIGE (Figure 49; Figure 50), suggesting that PKD3-altered phenylalanine metabolism affects the phosphorylation of CPS1. However, CPS1 activity has not been reported so far to be regulated by phosphorylation. A recent study showed that the activity of CPS1 is regulated by SIRT5-dependent deacetylation[382].

All three different MS-based approaches identified numerous potential targets of PKD3 in liver. However, almost all of them have not been reported as PKD substrates before. Various studies described PKD substrates, including CREB[127,128], HDACs[95], cortactin[98,99], SSH1L[100], PAK4[101], Rin1[129], Snail[130,131], β-catenin[132], PI4KIIα[156,157], and

Discussion

AMPKα[383], among multiple other substrates. In this context, the substrates can be phosphorylated by PKD1, PKD2, PKD3 or by a combination of the two or three PKD isoforms. Alternatively, there are isoform exclusive substrates for the PKD isoforms. For instance, PKD3 regulates paxillin trafficking and cellular protrusive activity by phosphorylating GIT1[384]. Nevertheless, PKD1 and PKD2 are the most studied PKD isoforms and only a few targets are known to be phosphorylated by PKD3. Therefore, the potential targets of PKD3 in this study cannot be compared with studies presenting global PKD1-dependent phosphorylation events[385]. However, in this study, the MS experiment was repeated three times which might help to avoid false positive results. In this thesis, a different approach was used by performing screenings with two different motif antibodies (LxRxx[S*/T*] and Rxx[S*/T*]). In this way, PAH was identified in both screenings. Notably, only 53-55% of the identified proteins possess a putative PKD motif, which can have several reasons, for example, due to unspecific binding of the antibody, or due to co-immunoprecipitation. Last, the results from the screenings in this thesis cannot be compared with other studies since they were not performed in hepatocytes or hepatic cell lines.

Taken together, RalGAPβ and especially PAH might be promising targets of PKD3 in hepatocytes that might give new insights into the regulation of hepatic mTOR signaling and phenylalanine metabolism, respectively.

4.5   Conclusions and perspectives

The findings presented in this thesis provide new insights into PKD signaling in liver. PKDs have been reported to be involved in various physiological processes including insulin secretion in β pancreatic cells and the regulation of adipose tissue function[109,158]. Until now, the physiological role of PKDs in liver remained elusive. The findings in this thesis showed that PKD3 is the predominantly expressed PKD isoform in liver, and it was activated by lipid overload. Deletion of PKD3 in hepatocytes promoted AKT, mTORC1, and mTORC2 activity in response to insulin treatment. Furthermore, hepatic deletion of PKD3 improved glucose tolerance and insulin sensitivity in mice. At the same time, lack of hepatic PKD3 promoted SREBP-mediated de novo lipogenesis, leading to increased hepatic TG and cholesterol content in livers of PKD3-deficient mice fed an HFD. In contrast, overexpression of PKD3ca impaired insulin sensitivity and caused insulin resistance.

Discussion

Of note, unraveling the exact mechanism of PKD3 signaling requires further studies. Furthermore, PAH was identified as a promising target of PKD3 in liver. In this context, additional studies on the hepatic phenylalanine metabolism and its potential effector PKD3 will help to understand the role of PKDs in liver.

In conclusion, the findings in this thesis show that PKD3 provides a negative feedback on insulin signaling and suppresses hepatic lipid content. For this reason, targeting PKD3 signaling might be a promising strategy for improving hepatic insulin sensitivity or decreasing hepatic lipid production.

5   References

1   Lautt, W. W. & Greenway, C. V. Conceptual review of the hepatic vascular bed. *Hepatology* **7**, 952-963 (1987).

2   Kalra, A. & Tuma, F. in *StatPearls*   (2019).

3   Kmiec, Z. Cooperation of liver cells in health and disease. *Adv Anat Embryol Cell Biol* **161**, III-XIII, 1-151 (2001).

4   Sasse, D., Spornitz, U. M. & Maly, I. P. Liver architecture. *Enzyme* **46**, 8-32 (1992).

5   Rui, L. Energy metabolism in the liver. *Compr Physiol* **4**, 177-197, doi:10.1002/cphy.c130024 (2014).

6   Dardevet, D., Moore, M. C., Remond, D., Everett-Grueter, C. A. & Cherrington, A. D. Regulation of hepatic metabolism by enteral delivery of nutrients. *Nutr Res Rev* **19**, 161-173, doi:10.1017/S0954422407315175 (2006).

7   Cohen, J. C., Horton, J. D. & Hobbs, H. H. Human fatty liver disease: old questions and new insights. *Science* **332**, 1519-1523, doi:10.1126/science.1204265 (2011).

8   De Chiara, F. *et al.* Urea cycle dysregulation in non-alcoholic fatty liver disease. *J Hepatol* **69**, 905-915, doi:10.1016/j.jhep.2018.06.023 (2018).

9   Chiang, J. Y. L. Bile acid metabolism and signaling in liver disease and therapy. *Liver Res* **1**, 3-9, doi:10.1016/j.livres.2017.05.001 (2017).

10   Kubes, P. & Jenne, C. Immune Responses in the Liver. *Annu Rev Immunol* **36**, 247-277, doi:10.1146/annurev-immunol-051116-052415 (2018).

11   Petersen, M. C., Vatner, D. F. & Shulman, G. I. Regulation of hepatic glucose metabolism in health and disease. *Nat Rev Endocrinol* **13**, 572-587, doi:10.1038/nrendo.2017.80 (2017).

12   Roden, M. Mechanisms of Disease: hepatic steatosis in type 2 diabetes--pathogenesis and clinical relevance. *Nat Clin Pract Endocrinol Metab* **2**, 335-348, doi:10.1038/ncpendmet0190 (2006).

13   Rines, A. K., Sharabi, K., Tavares, C. D. & Puigserver, P. Targeting hepatic glucose metabolism in the treatment of type 2 diabetes. *Nat Rev Drug Discov* **15**, 786-804, doi:10.1038/nrd.2016.151 (2016).

14   Wang, Y., Viscarra, J., Kim, S. J. & Sul, H. S. Transcriptional regulation of hepatic lipogenesis. *Nat Rev Mol Cell Biol* **16**, 678-689, doi:10.1038/nrm4074 (2015).

15   Horton, J. D., Goldstein, J. L. & Brown, M. S. SREBPs: activators of the complete program of cholesterol and fatty acid synthesis in the liver. *J Clin Invest* **109**, 1125-1131, doi:10.1172/JCI15593 (2002).

16   Shao, W. & Espenshade, P. J. Expanding roles for SREBP in metabolism. *Cell Metab* **16**, 414-419, doi:10.1016/j.cmet.2012.09.002 (2012).

17   Madison, B. B. Srebp2: A master regulator of sterol and fatty acid synthesis. *J Lipid Res* **57**, 333-335, doi:10.1194/jlr.C066712 (2016).

18   Horton, J. D. *et al.* Combined analysis of oligonucleotide microarray data from transgenic and knockout mice identifies direct SREBP target genes. *Proc Natl Acad Sci U S A* **100**, 12027-12032, doi:10.1073/pnas.1534923100 (2003).

19   Osborne, T. F. & Espenshade, P. J. Evolutionary conservation and adaptation in the mechanism that regulates SREBP action: what a long, strange tRIP it's been. *Genes Dev* **23**, 2578-2591, doi:10.1101/gad.1854309 (2009).

References

20   Kammoun, H. L. *et al.* GRP78 expression inhibits insulin and ER stress-induced SREBP-1c activation and reduces hepatic steatosis in mice. *J Clin Invest* **119**, 1201-1215, doi:10.1172/JCI37007 (2009).

21   Walker, A. K. *et al.* A conserved SREBP-1/phosphatidylcholine feedback circuit regulates lipogenesis in metazoans. *Cell* **147**, 840-852, doi:10.1016/j.cell.2011.09.045 (2011).

22   Peterson, T. R. *et al.* mTOR complex 1 regulates lipin 1 localization to control the SREBP pathway. *Cell* **146**, 408-420, doi:10.1016/j.cell.2011.06.034 (2011).

23   Li, Y. *et al.* AMPK phosphorylates and inhibits SREBP activity to attenuate hepatic steatosis and atherosclerosis in diet-induced insulin-resistant mice. *Cell Metab* **13**, 376-388, doi:10.1016/j.cmet.2011.03.009 (2011).

24   Walker, A. K. *et al.* Conserved role of SIRT1 orthologs in fasting-dependent inhibition of the lipid/cholesterol regulator SREBP. *Genes Dev* **24**, 1403-1417, doi:10.1101/gad.1901210 (2010).

25   Parekh, S. & Anania, F. A. Abnormal lipid and glucose metabolism in obesity: implications for nonalcoholic fatty liver disease. *Gastroenterology* **132**, 2191-2207, doi:10.1053/j.gastro.2007.03.055 (2007).

26   Bechmann, L. P. *et al.* The interaction of hepatic lipid and glucose metabolism in liver diseases. *J Hepatol* **56**, 952-964, doi:10.1016/j.jhep.2011.08.025 (2012).

27   Czech, M. P. Insulin action and resistance in obesity and type 2 diabetes. *Nat Med* **23**, 804-814, doi:10.1038/nm.4350 (2017).

28   Spiegelman, B. M. & Flier, J. S. Obesity and the regulation of energy balance. *Cell* **104**, 531-543, doi:10.1016/s0092-8674(01)00240-9 (2001).

29   Feldstein, A. E. Novel insights into the pathophysiology of nonalcoholic fatty liver disease. *Semin Liver Dis* **30**, 391-401, doi:10.1055/s-0030-1267539 (2010).

30   Browning, J. D. *et al.* Prevalence of hepatic steatosis in an urban population in the United States: impact of ethnicity. *Hepatology* **40**, 1387-1395, doi:10.1002/hep.20466 (2004).

31   Loomba, R. & Sanyal, A. J. The global NAFLD epidemic. *Nat Rev Gastroenterol Hepatol* **10**, 686-690, doi:10.1038/nrgastro.2013.171 (2013).

32   Hashimoto, E., Taniai, M. & Tokushige, K. Characteristics and diagnosis of NAFLD/NASH. *J Gastroenterol Hepatol* **28 Suppl 4**, 64-70, doi:10.1111/jgh.12271 (2013).

33   Petta, S. & Craxi, A. Hepatocellular carcinoma and non-alcoholic fatty liver disease: from a clinical to a molecular association. *Curr Pharm Des* **16**, 741-752, doi:10.2174/138161210790883787 (2010).

34   Samuel, V. T. *et al.* Inhibition of protein kinase Cepsilon prevents hepatic insulin resistance in nonalcoholic fatty liver disease. *J Clin Invest* **117**, 739-745, doi:10.1172/JCI30400 (2007).

35   Samuel, V. T., Petersen, K. F. & Shulman, G. I. Lipid-induced insulin resistance: unravelling the mechanism. *Lancet* **375**, 2267-2277, doi:10.1016/S0140-6736(10)60408-4 (2010).

36   Samuel, V. T. *et al.* Mechanism of hepatic insulin resistance in non-alcoholic fatty liver disease. *J Biol Chem* **279**, 32345-32353, doi:10.1074/jbc.M313478200 (2004).

37   Jornayvaz, F. R. & Shulman, G. I. Diacylglycerol activation of protein kinase Cepsilon and hepatic insulin resistance. *Cell Metab* **15**, 574-584, doi:10.1016/j.cmet.2012.03.005 (2012).

References

38   Caron, A., Richard, D. & Laplante, M. The Roles of mTOR Complexes in Lipid Metabolism. *Annu Rev Nutr* **35**, 321-348, doi:10.1146/annurev-nutr-071714-034355 (2015).

39   Nakae, J., Barr, V. & Accili, D. Differential regulation of gene expression by insulin and IGF-1 receptors correlates with phosphorylation of a single amino acid residue in the forkhead transcription factor FKHR. *EMBO J* **19**, 989-996, doi:10.1093/emboj/19.5.989 (2000).

40   Gross, D. N., van den Heuvel, A. P. & Birnbaum, M. J. The role of FoxO in the regulation of metabolism. *Oncogene* **27**, 2320-2336, doi:10.1038/onc.2008.25 (2008).

41   Qu, S. *et al.* Aberrant Forkhead box O1 function is associated with impaired hepatic metabolism. *Endocrinology* **147**, 5641-5652, doi:10.1210/en.2006-0541 (2006).

42   Titchenell, P. M. *et al.* Direct Hepatocyte Insulin Signaling Is Required for Lipogenesis but Is Dispensable for the Suppression of Glucose Production. *Cell Metab* **23**, 1154-1166, doi:10.1016/j.cmet.2016.04.022 (2016).

43   Brown, M. S. & Goldstein, J. L. Selective versus total insulin resistance: a pathogenic paradox. *Cell Metab* **7**, 95-96, doi:10.1016/j.cmet.2007.12.009 (2008).

44   Manning, G., Whyte, D. B., Martinez, R., Hunter, T. & Sudarsanam, S. The protein kinase complement of the human genome. *Science* **298**, 1912-1934, doi:10.1126/science.1075762 (2002).

45   Valverde, A. M., Sinnett-Smith, J., Van Lint, J. & Rozengurt, E. Molecular cloning and characterization of protein kinase D: a target for diacylglycerol and phorbol esters with a distinctive catalytic domain. *Proc Natl Acad Sci U S A* **91**, 8572-8576, doi:10.1073/pnas.91.18.8572 (1994).

46   Johannes, F. J., Prestle, J., Eis, S., Oberhagemann, P. & Pfizenmaier, K. PKCu is a novel, atypical member of the protein kinase C family. *J Biol Chem* **269**, 6140-6148 (1994).

47   Hayashi, A., Seki, N., Hattori, A., Kozuma, S. & Saito, T. PKCnu, a new member of the protein kinase C family, composes a fourth subfamily with PKCmu. *Biochim Biophys Acta* **1450**, 99-106, doi:10.1016/s0167-4889(99)00040-3 (1999).

48   Sturany, S. *et al.* Molecular cloning and characterization of the human protein kinase D2. A novel member of the protein kinase D family of serine threonine kinases. *J Biol Chem* **276**, 3310-3318, doi:10.1074/jbc.M008719200 (2001).

49   Rozengurt, E., Rey, O. & Waldron, R. T. Protein kinase D signaling. *J Biol Chem* **280**, 13205-13208, doi:10.1074/jbc.R500002200 (2005).

50   Steinberg, S. F. Regulation of protein kinase D1 activity. *Mol Pharmacol* **81**, 284-291, doi:10.1124/mol.111.075986 (2012).

51   Cozier, G. E., Carlton, J., Bouyoucef, D. & Cullen, P. J. Membrane targeting by pleckstrin homology domains. *Curr Top Microbiol Immunol* **282**, 49-88 (2004).

52   Waldron, R. T., Iglesias, T. & Rozengurt, E. The pleckstrin homology domain of protein kinase D interacts preferentially with the eta isoform of protein kinase C. *J Biol Chem* **274**, 9224-9230, doi:10.1074/jbc.274.14.9224 (1999).

53   Iglesias, T. & Rozengurt, E. Protein kinase D activation by mutations within its pleckstrin homology domain. *J Biol Chem* **273**, 410-416, doi:10.1074/jbc.273.1.410 (1998).

54   Van Lint, J. V., Sinnett-Smith, J. & Rozengurt, E. Expression and characterization of PKD, a phorbol ester and diacylglycerol-stimulated serine

protein kinase. *J Biol Chem* **270**, 1455-1461, doi:10.1074/jbc.270.3.1455 (1995).

55 Brose, N., Betz, A. & Wegmeyer, H. Divergent and convergent signaling by the diacylglycerol second messenger pathway in mammals. *Curr Opin Neurobiol* **14**, 328-340, doi:10.1016/j.conb.2004.05.006 (2004).

56 Newton, A. C., Bootman, M. D. & Scott, J. D. Second Messengers. *Cold Spring Harb Perspect Biol* **8**, doi:10.1101/cshperspect.a005926 (2016).

57 Wang, Q. J. PKD at the crossroads of DAG and PKC signaling. *Trends Pharmacol Sci* **27**, 317-323, doi:10.1016/j.tips.2006.04.003 (2006).

58 Newton, A. C. Protein kinase C: structural and spatial regulation by phosphorylation, cofactors, and macromolecular interactions. *Chem Rev* **101**, 2353-2364 (2001).

59 Fu, Y. & Rubin, C. S. Protein kinase D: coupling extracellular stimuli to the regulation of cell physiology. *EMBO Rep* **12**, 785-796, doi:10.1038/embor.2011.139 (2011).

60 Iglesias, T., Waldron, R. T. & Rozengurt, E. Identification of in vivo phosphorylation sites required for protein kinase D activation. *J Biol Chem* **273**, 27662-27667, doi:10.1074/jbc.273.42.27662 (1998).

61 Waldron, R. T. *et al.* Activation loop Ser744 and Ser748 in protein kinase D are transphosphorylated in vivo. *J Biol Chem* **276**, 32606-32615, doi:10.1074/jbc.M101648200 (2001).

62 Waldron, R. T. & Rozengurt, E. Protein kinase C phosphorylates protein kinase D activation loop Ser744 and Ser748 and releases autoinhibition by the pleckstrin homology domain. *J Biol Chem* **278**, 154-163, doi:10.1074/jbc.M208075200 (2003).

63 Jacamo, R., Sinnett-Smith, J., Rey, O., Waldron, R. T. & Rozengurt, E. Sequential protein kinase C (PKC)-dependent and PKC-independent protein kinase D catalytic activation via Gq-coupled receptors: differential regulation of activation loop Ser(744) and Ser(748) phosphorylation. *J Biol Chem* **283**, 12877-12887, doi:10.1074/jbc.M800442200 (2008).

64 Matthews, S. A., Rozengurt, E. & Cantrell, D. Characterization of serine 916 as an in vivo autophosphorylation site for protein kinase D/Protein kinase Cmu. *J Biol Chem* **274**, 26543-26549, doi:10.1074/jbc.274.37.26543 (1999).

65 Rybin, V. O., Guo, J. & Steinberg, S. F. Protein kinase D1 autophosphorylation via distinct mechanisms at Ser744/Ser748 and Ser916. *J Biol Chem* **284**, 2332-2343, doi:10.1074/jbc.M806381200 (2009).

66 Yuan, J., Slice, L. W. & Rozengurt, E. Activation of protein kinase D by signaling through Rho and the alpha subunit of the heterotrimeric G protein G13. *J Biol Chem* **276**, 38619-38627, doi:10.1074/jbc.M105530200 (2001).

67 Paolucci, L., Sinnett-Smith, J. & Rozengurt, E. Lysophosphatidic acid rapidly induces protein kinase D activation through a pertussis toxin-sensitive pathway. *Am J Physiol Cell Physiol* **278**, C33-39, doi:10.1152/ajpcell.2000.278.1.C33 (2000).

68 Yuan, J., Slice, L. W., Gu, J. & Rozengurt, E. Cooperation of Gq, Gi, and G12/13 in protein kinase D activation and phosphorylation induced by lysophosphatidic acid. *J Biol Chem* **278**, 4882-4891, doi:10.1074/jbc.M211175200 (2003).

69 Yuan, J., Rey, O. & Rozengurt, E. Activation of protein kinase D3 by signaling through Rac and the alpha subunits of the heterotrimeric G proteins G12 and G13. *Cell Signal* **18**, 1051-1062, doi:10.1016/j.cellsig.2005.08.017 (2006).

70 Waldron, R. T., Innamorati, G., Torres-Marquez, M. E., Sinnett-Smith, J. & Rozengurt, E. Differential PKC-dependent and -independent PKD activation by

References

G protein alpha subunits of the Gq family: selective stimulation of PKD Ser(7)(4)(8) autophosphorylation by Galphaq. *Cell Signal* **24**, 914-921, doi:10.1016/j.cellsig.2011.12.014 (2012).

71   Zugaza, J. L., Waldron, R. T., Sinnett-Smith, J. & Rozengurt, E. Bombesin, vasopressin, endothelin, bradykinin, and platelet-derived growth factor rapidly activate protein kinase D through a protein kinase C-dependent signal transduction pathway. *J Biol Chem* **272**, 23952-23960, doi:10.1074/jbc.272.38.23952 (1997).

72   Guo, J., Gertsberg, Z., Ozgen, N., Sabri, A. & Steinberg, S. F. Protein kinase D isoforms are activated in an agonist-specific manner in cardiomyocytes. *J Biol Chem* **286**, 6500-6509, doi:10.1074/jbc.M110.208058 (2011).

73   Wong, C. & Jin, Z. G. Protein kinase C-dependent protein kinase D activation modulates ERK signal pathway and endothelial cell proliferation by vascular endothelial growth factor. *J Biol Chem* **280**, 33262-33269, doi:10.1074/jbc.M503198200 (2005).

74   Sinnett-Smith, J. *et al.* Protein kinase D mediates mitogenic signaling by Gq-coupled receptors through protein kinase C-independent regulation of activation loop Ser744 and Ser748 phosphorylation. *J Biol Chem* **284**, 13434-13445, doi:10.1074/jbc.M806554200 (2009).

75   Sinnett-Smith, J., Rozengurt, N., Kui, R., Huang, C. & Rozengurt, E. Protein kinase D1 mediates stimulation of DNA synthesis and proliferation in intestinal epithelial IEC-18 cells and in mouse intestinal crypts. *J Biol Chem* **286**, 511-520, doi:10.1074/jbc.M110.167528 (2011).

76   Gschwendt, M. *et al.* Inhibition of protein kinase C mu by various inhibitors. Differentiation from protein kinase c isoenzymes. *FEBS Lett* **392**, 77-80, doi:10.1016/0014-5793(96)00785-5 (1996).

77   Sharlow, E. R. *et al.* Potent and selective disruption of protein kinase D functionality by a benzoxoloazepinolone. *J Biol Chem* **283**, 33516-33526, doi:10.1074/jbc.M805358200 (2008).

78   Harikumar, K. B. *et al.* A novel small-molecule inhibitor of protein kinase D blocks pancreatic cancer growth in vitro and in vivo. *Mol Cancer Ther* **9**, 1136-1146, doi:10.1158/1535-7163.MCT-09-1145 (2010).

79   Rey, O., Sinnett-Smith, J., Zhukova, E. & Rozengurt, E. Regulated nucleocytoplasmic transport of protein kinase D in response to G protein-coupled receptor activation. *J Biol Chem* **276**, 49228-49235, doi:10.1074/jbc.M109395200 (2001).

80   Matthews, S. A., Iglesias, T., Rozengurt, E. & Cantrell, D. Spatial and temporal regulation of protein kinase D (PKD). *EMBO J* **19**, 2935-2945, doi:10.1093/emboj/19.12.2935 (2000).

81   Hausser, A. *et al.* Structural requirements for localization and activation of protein kinase C mu (PKC mu) at the Golgi compartment. *J Cell Biol* **156**, 65-74, doi:10.1083/jcb.200110047 (2002).

82   Liljedahl, M. *et al.* Protein kinase D regulates the fission of cell surface destined transport carriers from the trans-Golgi network. *Cell* **104**, 409-420 (2001).

83   Matthews, S., Iglesias, T., Cantrell, D. & Rozengurt, E. Dynamic re-distribution of protein kinase D (PKD) as revealed by a GFP-PKD fusion protein: dissociation from PKD activation. *FEBS Lett* **457**, 515-521, doi:10.1016/s0014-5793(99)01090-x (1999).

84   Oancea, E., Bezzerides, V. J., Greka, A. & Clapham, D. E. Mechanism of persistent protein kinase D1 translocation and activation. *Dev Cell* **4**, 561-574 (2003).

References

85   Baron, C. L. & Malhotra, V. Role of diacylglycerol in PKD recruitment to the TGN and protein transport to the plasma membrane. *Science* **295**, 325-328, doi:10.1126/science.1066759 (2002).

86   Maeda, Y., Beznoussenko, G. V., Van Lint, J., Mironov, A. A. & Malhotra, V. Recruitment of protein kinase D to the trans-Golgi network via the first cysteine-rich domain. *EMBO J* **20**, 5982-5990, doi:10.1093/emboj/20.21.5982 (2001).

87   Storz, P., Doppler, H. & Toker, A. Protein kinase D mediates mitochondrion-to-nucleus signaling and detoxification from mitochondrial reactive oxygen species. *Mol Cell Biol* **25**, 8520-8530, doi:10.1128/MCB.25.19.8520-8530.2005 (2005).

88   Chen, J., Deng, F., Li, J. & Wang, Q. J. Selective binding of phorbol esters and diacylglycerol by individual C1 domains of the PKD family. *Biochem J* **411**, 333-342, doi:10.1042/BJ20071334 (2008).

89   Rey, O., Reeve, J. R., Jr., Zhukova, E., Sinnett-Smith, J. & Rozengurt, E. G protein-coupled receptor-mediated phosphorylation of the activation loop of protein kinase D: dependence on plasma membrane translocation and protein kinase Cepsilon. *J Biol Chem* **279**, 34361-34372, doi:10.1074/jbc.M403265200 (2004).

90   Rey, O., Yuan, J., Young, S. H. & Rozengurt, E. Protein kinase C nu/protein kinase D3 nuclear localization, catalytic activation, and intracellular redistribution in response to G protein-coupled receptor agonists. *J Biol Chem* **278**, 23773-23785, doi:10.1074/jbc.M300226200 (2003).

91   Matthews, S. A. *et al.* Unique functions for protein kinase D1 and protein kinase D2 in mammalian cells. *Biochem J* **432**, 153-163, doi:10.1042/BJ20101188 (2010).

92   Rozengurt, E. Protein kinase D signaling: multiple biological functions in health and disease. *Physiology (Bethesda)* **26**, 23-33, doi:10.1152/physiol.00037.2010 (2011).

93   Storz, P. & Toker, A. Protein kinase D mediates a stress-induced NF-kappaB activation and survival pathway. *EMBO J* **22**, 109-120, doi:10.1093/emboj/cdg009 (2003).

94   Zhukova, E., Sinnett-Smith, J. & Rozengurt, E. Protein kinase D potentiates DNA synthesis and cell proliferation induced by bombesin, vasopressin, or phorbol esters in Swiss 3T3 cells. *J Biol Chem* **276**, 40298-40305, doi:10.1074/jbc.M106512200 (2001).

95   Matthews, S. A. *et al.* Essential role for protein kinase D family kinases in the regulation of class II histone deacetylases in B lymphocytes. *Mol Cell Biol* **26**, 1569-1577, doi:10.1128/MCB.26.4.1569-1577.2006 (2006).

96   Ha, C. H., Jhun, B. S., Kao, H. Y. & Jin, Z. G. VEGF stimulates HDAC7 phosphorylation and cytoplasmic accumulation modulating matrix metalloproteinase expression and angiogenesis. *Arterioscler Thromb Vasc Biol* **28**, 1782-1788, doi:10.1161/ATVBAHA.108.172528 (2008).

97   Zhang, W., Zheng, S., Storz, P. & Min, W. Protein kinase D specifically mediates apoptosis signal-regulating kinase 1-JNK signaling induced by H2O2 but not tumor necrosis factor. *J Biol Chem* **280**, 19036-19044, doi:10.1074/jbc.M414674200 (2005).

98   Eiseler, T., Hausser, A., De Kimpe, L., Van Lint, J. & Pfizenmaier, K. Protein kinase D controls actin polymerization and cell motility through phosphorylation of cortactin. *J Biol Chem* **285**, 18672-18683, doi:10.1074/jbc.M109.093880 (2010).

References

99   De Kimpe, L. *et al.* Characterization of cortactin as an in vivo protein kinase D substrate: interdependence of sites and potentiation by Src. *Cell Signal* **21**, 253-263, doi:10.1016/j.cellsig.2008.10.015 (2009).

100   Peterburs, P. *et al.* Protein kinase D regulates cell migration by direct phosphorylation of the cofilin phosphatase slingshot 1 like. *Cancer Res* **69**, 5634-5638, doi:10.1158/0008-5472.CAN-09-0718 (2009).

101   Spratley, S. J., Bastea, L. I., Doppler, H., Mizuno, K. & Storz, P. Protein kinase D regulates cofilin activity through p21-activated kinase 4. *J Biol Chem* **286**, 34254-34261, doi:10.1074/jbc.M111.259424 (2011).

102   Roy, A., Ye, J., Deng, F. & Wang, Q. J. Protein kinase D signaling in cancer: A friend or foe? *Biochim Biophys Acta Rev Cancer* **1868**, 283-294, doi:10.1016/j.bbcan.2017.05.008 (2017).

103   Kleger, A. *et al.* Protein kinase D2 is an essential regulator of murine myoblast differentiation. *PLoS One* **6**, e14599, doi:10.1371/journal.pone.0014599 (2011).

104   Kim, M. S. *et al.* Protein kinase D1 stimulates MEF2 activity in skeletal muscle and enhances muscle performance. *Mol Cell Biol* **28**, 3600-3609, doi:10.1128/MCB.00189-08 (2008).

105   Fielitz, J. *et al.* Requirement of protein kinase D1 for pathological cardiac remodeling. *Proc Natl Acad Sci U S A* **105**, 3059-3063, doi:10.1073/pnas.0712265105 (2008).

106   Li, C. *et al.* Protein kinase D3 is a pivotal activator of pathological cardiac hypertrophy by selectively increasing the expression of hypertrophic transcription factors. *J Biol Chem* **286**, 40782-40791, doi:10.1074/jbc.M111.263046 (2011).

107   Steiner, T. S., Ivison, S. M., Yao, Y. & Kifayet, A. Protein kinase D1 and D2 are involved in chemokine release induced by toll-like receptors 2, 4, and 5. *Cell Immunol* **264**, 135-142, doi:10.1016/j.cellimm.2010.05.012 (2010).

108   Konopatskaya, O. *et al.* Protein kinase C mediates platelet secretion and thrombus formation through protein kinase D2. *Blood* **118**, 416-424, doi:10.1182/blood-2010-10-312199 (2011).

109   Sumara, G. *et al.* Regulation of PKD by the MAPK p38delta in insulin secretion and glucose homeostasis. *Cell* **136**, 235-248, doi:10.1016/j.cell.2008.11.018 (2009).

110   Ferdaoussi, M. *et al.* G protein-coupled receptor (GPR)40-dependent potentiation of insulin secretion in mouse islets is mediated by protein kinase D1. *Diabetologia* **55**, 2682-2692, doi:10.1007/s00125-012-2650-x (2012).

111   Bossard, C., Bresson, D., Polishchuk, R. S. & Malhotra, V. Dimeric PKD regulates membrane fission to form transport carriers at the TGN. *J Cell Biol* **179**, 1123-1131, doi:10.1083/jcb.200703166 (2007).

112   Doppler, H. *et al.* Protein kinase d isoforms differentially modulate cofilin-driven directed cell migration. *PLoS One* **9**, e98090, doi:10.1371/journal.pone.0098090 (2014).

113   Aicart-Ramos, C., He, S. D., Land, M. & Rubin, C. S. A Novel Conserved Domain Mediates Dimerization of Protein Kinase D (PKD) Isoforms: DIMERIZATION IS ESSENTIAL FOR PKD-DEPENDENT REGULATION OF SECRETION AND INNATE IMMUNITY. *J Biol Chem* **291**, 23516-23531, doi:10.1074/jbc.M116.735399 (2016).

114   Zhang, Z. *et al.* Protein kinase D at the Golgi controls NLRP3 inflammasome activation. *J Exp Med* **214**, 2671-2693, doi:10.1084/jem.20162040 (2017).

References

115 Cowell, C. F. *et al.* Mitochondrial diacylglycerol initiates protein-kinase D1-mediated ROS signaling. *J Cell Sci* **122**, 919-928, doi:10.1242/jcs.041061 (2009).

116 Storz, P., Doppler, H., Johannes, F. J. & Toker, A. Tyrosine phosphorylation of protein kinase D in the pleckstrin homology domain leads to activation. *J Biol Chem* **278**, 17969-17976, doi:10.1074/jbc.M213224200 (2003).

117 Doppler, H. & Storz, P. A novel tyrosine phosphorylation site in protein kinase D contributes to oxidative stress-mediated activation. *J Biol Chem* **282**, 31873-31881, doi:10.1074/jbc.M703584200 (2007).

118 Cobbaut, M. & Van Lint, J. Function and Regulation of Protein Kinase D in Oxidative Stress: A Tale of Isoforms. *Oxid Med Cell Longev* **2018**, 2138502, doi:10.1155/2018/2138502 (2018).

119 Sinnett-Smith, J., Zhukova, E., Hsieh, N., Jiang, X. & Rozengurt, E. Protein kinase D potentiates DNA synthesis induced by Gq-coupled receptors by increasing the duration of ERK signaling in swiss 3T3 cells. *J Biol Chem* **279**, 16883-16893, doi:10.1074/jbc.M313225200 (2004).

120 Sinnett-Smith, J., Zhukova, E., Rey, O. & Rozengurt, E. Protein kinase D2 potentiates MEK/ERK/RSK signaling, c-Fos accumulation and DNA synthesis induced by bombesin in Swiss 3T3 cells. *J Cell Physiol* **211**, 781-790, doi:10.1002/jcp.20984 (2007).

121 Mottet, D. *et al.* Histone deacetylase 7 silencing alters endothelial cell migration, a key step in angiogenesis. *Circ Res* **101**, 1237-1246, doi:10.1161/CIRCRESAHA.107.149377 (2007).

122 Wang, S. *et al.* Control of endothelial cell proliferation and migration by VEGF signaling to histone deacetylase 7. *Proc Natl Acad Sci U S A* **105**, 7738-7743, doi:10.1073/pnas.0802857105 (2008).

123 Lemonnier, J., Ghayor, C., Guicheux, J. & Caverzasio, J. Protein kinase C-independent activation of protein kinase D is involved in BMP-2-induced activation of stress mitogen-activated protein kinases JNK and p38 and osteoblastic cell differentiation. *J Biol Chem* **279**, 259-264, doi:10.1074/jbc.M308665200 (2004).

124 Jensen, E. D., Gopalakrishnan, R. & Westendorf, J. J. Bone morphogenic protein 2 activates protein kinase D to regulate histone deacetylase 7 localization and repression of Runx2. *J Biol Chem* **284**, 2225-2234, doi:10.1074/jbc.M800586200 (2009).

125 Dequiedt, F. *et al.* Phosphorylation of histone deacetylase 7 by protein kinase D mediates T cell receptor-induced Nur77 expression and apoptosis. *J Exp Med* **201**, 793-804, doi:10.1084/jem.20042034 (2005).

126 Vega, R. B. *et al.* Protein kinases C and D mediate agonist-dependent cardiac hypertrophy through nuclear export of histone deacetylase 5. *Mol Cell Biol* **24**, 8374-8385, doi:10.1128/MCB.24.19.8374-8385.2004 (2004).

127 Johannessen, M. *et al.* Protein kinase D induces transcription through direct phosphorylation of the cAMP-response element-binding protein. *J Biol Chem* **282**, 14777-14787, doi:10.1074/jbc.M610669200 (2007).

128 Ozgen, N. *et al.* Protein kinase D links Gq-coupled receptors to cAMP response element-binding protein (CREB)-Ser133 phosphorylation in the heart. *J Biol Chem* **283**, 17009-17019, doi:10.1074/jbc.M709851200 (2008).

129 Ziegler, S. *et al.* A novel protein kinase D phosphorylation site in the tumor suppressor Rab interactor 1 is critical for coordination of cell migration. *Mol Biol Cell* **22**, 570-580, doi:10.1091/mbc.E10-05-0427 (2011).

References

130   Du, C., Zhang, C., Hassan, S., Biswas, M. H. & Balaji, K. C. Protein kinase D1 suppresses epithelial-to-mesenchymal transition through phosphorylation of snail. *Cancer Res* **70**, 7810-7819, doi:10.1158/0008-5472.CAN-09-4481 (2010).

131   Bastea, L. I., Doppler, H., Balogun, B. & Storz, P. Protein kinase D1 maintains the epithelial phenotype by inducing a DNA-bound, inactive SNAI1 transcriptional repressor complex. *PLoS One* **7**, e30459, doi:10.1371/journal.pone.0030459 (2012).

132   Du, C., Jaggi, M., Zhang, C. & Balaji, K. C. Protein kinase D1-mediated phosphorylation and subcellular localization of beta-catenin. *Cancer Res* **69**, 1117-1124, doi:10.1158/0008-5472.CAN-07-6270 (2009).

133   Durand, N., Borges, S. & Storz, P. Protein Kinase D Enzymes as Regulators of EMT and Cancer Cell Invasion. *J Clin Med* **5**, doi:10.3390/jcm5020020 (2016).

134   Chen, J., Deng, F., Singh, S. V. & Wang, Q. J. Protein kinase D3 (PKD3) contributes to prostate cancer cell growth and survival through a PKCepsilon/PKD3 pathway downstream of Akt and ERK 1/2. *Cancer Res* **68**, 3844-3853, doi:10.1158/0008-5472.CAN-07-5156 (2008).

135   Mak, P. *et al.* Protein kinase D1 (PKD1) influences androgen receptor (AR) function in prostate cancer cells. *Biochem Biophys Res Commun* **373**, 618-623, doi:10.1016/j.bbrc.2008.06.097 (2008).

136   Hassan, S., Biswas, M. H., Zhang, C., Du, C. & Balaji, K. C. Heat shock protein 27 mediates repression of androgen receptor function by protein kinase D1 in prostate cancer cells. *Oncogene* **28**, 4386-4396, doi:10.1038/onc.2009.291 (2009).

137   Jaggi, M. *et al.* E-cadherin phosphorylation by protein kinase D1/protein kinase C{mu} is associated with altered cellular aggregation and motility in prostate cancer. *Cancer Res* **65**, 483-492 (2005).

138   Eiseler, T., Doppler, H., Yan, I. K., Goodison, S. & Storz, P. Protein kinase D1 regulates matrix metalloproteinase expression and inhibits breast cancer cell invasion. *Breast Cancer Res* **11**, R13, doi:10.1186/bcr2232 (2009).

139   Borges, S. *et al.* Pharmacologic reversion of epigenetic silencing of the PRKD1 promoter blocks breast tumor cell invasion and metastasis. *Breast Cancer Res* **15**, R66, doi:10.1186/bcr3460 (2013).

140   Hao, Q., McKenzie, R., Gan, H. & Tang, H. Protein kinases D2 and D3 are novel growth regulators in HCC1806 triple-negative breast cancer cells. *Anticancer Res* **33**, 393-399 (2013).

141   Borges, S. & Storz, P. Protein kinase D isoforms: new targets for therapy in invasive breast cancers? *Expert Rev Anticancer Ther* **13**, 895-898, doi:10.1586/14737140.2013.816460 (2013).

142   Guha, S., Tanasanvimon, S., Sinnett-Smith, J. & Rozengurt, E. Role of protein kinase D signaling in pancreatic cancer. *Biochem Pharmacol* **80**, 1946-1954, doi:10.1016/j.bcp.2010.07.002 (2010).

143   Trauzold, A. *et al.* PKCmu prevents CD95-mediated apoptosis and enhances proliferation in pancreatic tumour cells. *Oncogene* **22**, 8939-8947, doi:10.1038/sj.onc.1207001 (2003).

144   Liou, G. Y. *et al.* Protein kinase D1 drives pancreatic acinar cell reprogramming and progression to intraepithelial neoplasia. *Nat Commun* **6**, 6200, doi:10.1038/ncomms7200 (2015).

145   Guha, S., Rey, O. & Rozengurt, E. Neurotensin induces protein kinase C-dependent protein kinase D activation and DNA synthesis in human pancreatic carcinoma cell line PANC-1. *Cancer Res* **62**, 1632-1640 (2002).

References

146   Yuan, J. & Rozengurt, E. PKD, PKD2, and p38 MAPK mediate Hsp27 serine-82 phosphorylation induced by neurotensin in pancreatic cancer PANC-1 cells. *J Cell Biochem* **103**, 648-662, doi:10.1002/jcb.21439 (2008).

147   Wille, C. *et al.* Protein kinase D2 induces invasion of pancreatic cancer cells by regulating matrix metalloproteinases. *Mol Biol Cell* **25**, 324-336, doi:10.1091/mbc.E13-06-0334 (2014).

148   Rennecke, J. *et al.* Protein-kinase-Cmu expression correlates with enhanced keratinocyte proliferation in normal and neoplastic mouse epidermis and in cell culture. *Int J Cancer* **80**, 98-103 (1999).

149   Arun, S. N., Kaddour-Djebbar, I., Shapiro, B. A. & Bollag, W. B. Ultraviolet B irradiation and activation of protein kinase D in primary mouse epidermal keratinocytes. *Oncogene* **30**, 1586-1596, doi:10.1038/onc.2010.540 (2011).

150   Rashel, M., Alston, N. & Ghazizadeh, S. Protein kinase D1 has a key role in wound healing and skin carcinogenesis. *J Invest Dermatol* **134**, 902-909, doi:10.1038/jid.2013.474 (2014).

151   Kim, M. *et al.* Epigenetic inactivation of protein kinase D1 in gastric cancer and its role in gastric cancer cell migration and invasion. *Carcinogenesis* **29**, 629-637, doi:10.1093/carcin/bgm291 (2008).

152   Shabelnik, M. Y. *et al.* Differential expression of PKD1 and PKD2 in gastric cancer and analysis of PKD1 and PKD2 function in the model system. *Exp Oncol* **33**, 206-211 (2011).

153   Yang, H. *et al.* Higher PKD3 expression in hepatocellular carcinoma (HCC) tissues predicts poorer prognosis for HCC patients. *Clin Res Hepatol Gastroenterol* **41**, 554-563, doi:10.1016/j.clinre.2017.02.005 (2017).

154   Verschueren, K. *et al.* Discovery of a potent protein kinase D inhibitor: insights in the binding mode of pyrazolo[3,4-d]pyrimidine analogues. *Medchemcomm* **8**, 640-646, doi:10.1039/c6md00675b (2017).

155   Zou, Z. *et al.* PKD2 and PKD3 promote prostate cancer cell invasion by modulating NF-kappaB- and HDAC1-mediated expression and activation of uPA. *J Cell Sci* **125**, 4800-4811, doi:10.1242/jcs.106542 (2012).

156   Zhang, L. *et al.* PI4KIIalpha regulates insulin secretion and glucose homeostasis via a PKD-dependent pathway. *Biophys Rep* **4**, 25-38, doi:10.1007/s41048-018-0049-z (2018).

157   Hausser, A. *et al.* Protein kinase D regulates vesicular transport by phosphorylating and activating phosphatidylinositol-4 kinase IIIbeta at the Golgi complex. *Nat Cell Biol* **7**, 880-886, doi:10.1038/ncb1289 (2005).

158   Loffler, M. C. *et al.* Protein kinase D1 deletion in adipocytes enhances energy dissipation and protects against adiposity. *EMBO J* **37**, doi:10.15252/embj.201899182 (2018).

159   Sabatini, D. M. Twenty-five years of mTOR: Uncovering the link from nutrients to growth. *Proc Natl Acad Sci U S A* **114**, 11818-11825, doi:10.1073/pnas.1716173114 (2017).

160   Laplante, M. & Sabatini, D. M. mTOR signaling at a glance. *J Cell Sci* **122**, 3589-3594, doi:10.1242/jcs.051011 (2009).

161   Peterson, T. R. *et al.* DEPTOR is an mTOR inhibitor frequently overexpressed in multiple myeloma cells and required for their survival. *Cell* **137**, 873-886, doi:10.1016/j.cell.2009.03.046 (2009).

162   Wang, L., Harris, T. E., Roth, R. A. & Lawrence, J. C., Jr. PRAS40 regulates mTORC1 kinase activity by functioning as a direct inhibitor of substrate binding. *J Biol Chem* **282**, 20036-20044, doi:10.1074/jbc.M702376200 (2007).

References

163   Oshiro, N. *et al.* The proline-rich Akt substrate of 40 kDa (PRAS40) is a physiological substrate of mammalian target of rapamycin complex 1. *J Biol Chem* **282**, 20329-20339, doi:10.1074/jbc.M702636200 (2007).

164   Yang, H. *et al.* mTOR kinase structure, mechanism and regulation. *Nature* **497**, 217-223, doi:10.1038/nature12122 (2013).

165   Guertin, D. A. *et al.* Ablation in mice of the mTORC components raptor, rictor, or mLST8 reveals that mTORC2 is required for signaling to Akt-FOXO and PKCalpha, but not S6K1. *Dev Cell* **11**, 859-871, doi:10.1016/j.devcel.2006.10.007 (2006).

166   Kim, J. & Guan, K. L. mTOR as a central hub of nutrient signalling and cell growth. *Nat Cell Biol* **21**, 63-71, doi:10.1038/s41556-018-0205-1 (2019).

167   Saxton, R. A. & Sabatini, D. M. mTOR Signaling in Growth, Metabolism, and Disease. *Cell* **168**, 960-976, doi:10.1016/j.cell.2017.02.004 (2017).

168   Holz, M. K., Ballif, B. A., Gygi, S. P. & Blenis, J. mTOR and S6K1 mediate assembly of the translation preinitiation complex through dynamic protein interchange and ordered phosphorylation events. *Cell* **123**, 569-580, doi:10.1016/j.cell.2005.10.024 (2005).

169   Jefferies, H. B. *et al.* Rapamycin suppresses 5'TOP mRNA translation through inhibition of p70s6k. *EMBO J* **16**, 3693-3704, doi:10.1093/emboj/16.12.3693 (1997).

170   Pende, M. *et al.* S6K1(-/-)/S6K2(-/-) mice exhibit perinatal lethality and rapamycin-sensitive 5'-terminal oligopyrimidine mRNA translation and reveal a mitogen-activated protein kinase-dependent S6 kinase pathway. *Mol Cell Biol* **24**, 3112-3124, doi:10.1128/mcb.24.8.3112-3124.2004 (2004).

171   Dorrello, N. V. *et al.* S6K1- and betaTRCP-mediated degradation of PDCD4 promotes protein translation and cell growth. *Science* **314**, 467-471, doi:10.1126/science.1130276 (2006).

172   Pardo, O. E. & Seckl, M. J. S6K2: The Neglected S6 Kinase Family Member. *Front Oncol* **3**, 191, doi:10.3389/fonc.2013.00191 (2013).

173   Brunn, G. J. *et al.* Phosphorylation of the translational repressor PHAS-I by the mammalian target of rapamycin. *Science* **277**, 99-101, doi:10.1126/science.277.5322.99 (1997).

174   Gingras, A. C., Kennedy, S. G., O'Leary, M. A., Sonenberg, N. & Hay, N. 4E-BP1, a repressor of mRNA translation, is phosphorylated and inactivated by the Akt(PKB) signaling pathway. *Genes Dev* **12**, 502-513, doi:10.1101/gad.12.4.502 (1998).

175   Sarbassov, D. D. *et al.* Rictor, a novel binding partner of mTOR, defines a rapamycin-insensitive and raptor-independent pathway that regulates the cytoskeleton. *Curr Biol* **14**, 1296-1302, doi:10.1016/j.cub.2004.06.054 (2004).

176   Gan, X. *et al.* PRR5L degradation promotes mTORC2-mediated PKC-delta phosphorylation and cell migration downstream of Galpha12. *Nat Cell Biol* **14**, 686-696, doi:10.1038/ncb2507 (2012).

177   Li, X. & Gao, T. mTORC2 phosphorylates protein kinase Czeta to regulate its stability and activity. *EMBO Rep* **15**, 191-198, doi:10.1002/embr.201338119 (2014).

178   Thomanetz, V. *et al.* Ablation of the mTORC2 component rictor in brain or Purkinje cells affects size and neuron morphology. *J Cell Biol* **201**, 293-308, doi:10.1083/jcb.201205030 (2013).

179   Garcia-Martinez, J. M. & Alessi, D. R. mTOR complex 2 (mTORC2) controls hydrophobic motif phosphorylation and activation of serum- and glucocorticoid-

induced protein kinase 1 (SGK1). *Biochem J* **416**, 375-385, doi:10.1042/BJ20081668 (2008).

180 Inglis, S. K. *et al.* SGK1 activity in Na+ absorbing airway epithelial cells monitored by assaying NDRG1-Thr346/356/366 phosphorylation. *Pflugers Arch* **457**, 1287-1301, doi:10.1007/s00424-008-0587-1 (2009).

181 Murakami, Y. *et al.* Identification of sites subjected to serine/threonine phosphorylation by SGK1 affecting N-myc downstream-regulated gene 1 (NDRG1)/Cap43-dependent suppression of angiogenic CXC chemokine expression in human pancreatic cancer cells. *Biochem Biophys Res Commun* **396**, 376-381, doi:10.1016/j.bbrc.2010.04.100 (2010).

182 McCaig, C., Potter, L., Abramczyk, O. & Murray, J. T. Phosphorylation of NDRG1 is temporally and spatially controlled during the cell cycle. *Biochem Biophys Res Commun* **411**, 227-234, doi:10.1016/j.bbrc.2011.06.092 (2011).

183 Kalaydjieva, L. *et al.* N-myc downstream-regulated gene 1 is mutated in hereditary motor and sensory neuropathy-Lom. *Am J Hum Genet* **67**, 47-58, doi:10.1086/302978 (2000).

184 Cai, K., El-Merahbi, R., Loeffler, M., Mayer, A. E. & Sumara, G. Ndrg1 promotes adipocyte differentiation and sustains their function. *Sci Rep* **7**, 7191, doi:10.1038/s41598-017-07497-x (2017).

185 Sarbassov, D. D., Guertin, D. A., Ali, S. M. & Sabatini, D. M. Phosphorylation and regulation of Akt/PKB by the rictor-mTOR complex. *Science* **307**, 1098-1101, doi:10.1126/science.1106148 (2005).

186 Manning, B. D., Tee, A. R., Logsdon, M. N., Blenis, J. & Cantley, L. C. Identification of the tuberous sclerosis complex-2 tumor suppressor gene product tuberin as a target of the phosphoinositide 3-kinase/akt pathway. *Mol Cell* **10**, 151-162 (2002).

187 Inoki, K., Li, Y., Zhu, T., Wu, J. & Guan, K. L. TSC2 is phosphorylated and inhibited by Akt and suppresses mTOR signalling. *Nat Cell Biol* **4**, 648-657, doi:10.1038/ncb839 (2002).

188 Potter, C. J., Pedraza, L. G. & Xu, T. Akt regulates growth by directly phosphorylating Tsc2. *Nat Cell Biol* **4**, 658-665, doi:10.1038/ncb840 (2002).

189 Porstmann, T. *et al.* SREBP activity is regulated by mTORC1 and contributes to Akt-dependent cell growth. *Cell Metab* **8**, 224-236, doi:10.1016/j.cmet.2008.07.007 (2008).

190 Duvel, K. *et al.* Activation of a metabolic gene regulatory network downstream of mTOR complex 1. *Mol Cell* **39**, 171-183, doi:10.1016/j.molcel.2010.06.022 (2010).

191 Lee, G. *et al.* Post-transcriptional Regulation of De Novo Lipogenesis by mTORC1-S6K1-SRPK2 Signaling. *Cell* **171**, 1545-1558 e1518, doi:10.1016/j.cell.2017.10.037 (2017).

192 Ben-Sahra, I., Hoxhaj, G., Ricoult, S. J. H., Asara, J. M. & Manning, B. D. mTORC1 induces purine synthesis through control of the mitochondrial tetrahydrofolate cycle. *Science* **351**, 728-733, doi:10.1126/science.aad0489 (2016).

193 Ben-Sahra, I., Howell, J. J., Asara, J. M. & Manning, B. D. Stimulation of de novo pyrimidine synthesis by growth signaling through mTOR and S6K1. *Science* **339**, 1323-1328, doi:10.1126/science.1228792 (2013).

194 Jung, C. H. *et al.* ULK-Atg13-FIP200 complexes mediate mTOR signaling to the autophagy machinery. *Mol Biol Cell* **20**, 1992-2003, doi:10.1091/mbc.E08-12-1249 (2009).

References

195   Hosokawa, N. *et al.* Nutrient-dependent mTORC1 association with the ULK1-Atg13-FIP200 complex required for autophagy. *Mol Biol Cell* **20**, 1981-1991, doi:10.1091/mbc.E08-12-1248 (2009).

196   Kim, J., Kundu, M., Viollet, B. & Guan, K. L. AMPK and mTOR regulate autophagy through direct phosphorylation of Ulk1. *Nat Cell Biol* **13**, 132-141, doi:10.1038/ncb2152 (2011).

197   Yuan, H. X., Russell, R. C. & Guan, K. L. Regulation of PIK3C3/VPS34 complexes by MTOR in nutrient stress-induced autophagy. *Autophagy* **9**, 1983-1995, doi:10.4161/auto.26058 (2013).

198   Pena-Llopis, S. *et al.* Regulation of TFEB and V-ATPases by mTORC1. *EMBO J* **30**, 3242-3258, doi:10.1038/emboj.2011.257 (2011).

199   Settembre, C. *et al.* A lysosome-to-nucleus signalling mechanism senses and regulates the lysosome via mTOR and TFEB. *EMBO J* **31**, 1095-1108, doi:10.1038/emboj.2012.32 (2012).

200   Roczniak-Ferguson, A. *et al.* The transcription factor TFEB links mTORC1 signaling to transcriptional control of lysosome homeostasis. *Sci Signal* **5**, ra42, doi:10.1126/scisignal.2002790 (2012).

201   Martina, J. A., Chen, Y., Gucek, M. & Puertollano, R. MTORC1 functions as a transcriptional regulator of autophagy by preventing nuclear transport of TFEB. *Autophagy* **8**, 903-914, doi:10.4161/auto.19653 (2012).

202   Zhao, J., Zhai, B., Gygi, S. P. & Goldberg, A. L. mTOR inhibition activates overall protein degradation by the ubiquitin proteasome system as well as by autophagy. *Proc Natl Acad Sci U S A* **112**, 15790-15797, doi:10.1073/pnas.1521919112 (2015).

203   Rousseau, A. & Bertolotti, A. An evolutionarily conserved pathway controls proteasome homeostasis. *Nature* **536**, 184-189, doi:10.1038/nature18943 (2016).

204   Zhang, Y. *et al.* Coordinated regulation of protein synthesis and degradation by mTORC1. *Nature* **513**, 440-443, doi:10.1038/nature13492 (2014).

205   Inoki, K., Zhu, T. & Guan, K. L. TSC2 mediates cellular energy response to control cell growth and survival. *Cell* **115**, 577-590, doi:10.1016/s0092-8674(03)00929-2 (2003).

206   Dibble, C. C. *et al.* TBC1D7 is a third subunit of the TSC1-TSC2 complex upstream of mTORC1. *Mol Cell* **47**, 535-546, doi:10.1016/j.molcel.2012.06.009 (2012).

207   Tee, A. R., Manning, B. D., Roux, P. P., Cantley, L. C. & Blenis, J. Tuberous sclerosis complex gene products, Tuberin and Hamartin, control mTOR signaling by acting as a GTPase-activating protein complex toward Rheb. *Curr Biol* **13**, 1259-1268, doi:10.1016/s0960-9822(03)00506-2 (2003).

208   Garami, A. *et al.* Insulin activation of Rheb, a mediator of mTOR/S6K/4E-BP signaling, is inhibited by TSC1 and 2. *Mol Cell* **11**, 1457-1466 (2003).

209   Long, X., Lin, Y., Ortiz-Vega, S., Yonezawa, K. & Avruch, J. Rheb binds and regulates the mTOR kinase. *Curr Biol* **15**, 702-713, doi:10.1016/j.cub.2005.02.053 (2005).

210   Ma, L., Chen, Z., Erdjument-Bromage, H., Tempst, P. & Pandolfi, P. P. Phosphorylation and functional inactivation of TSC2 by Erk implications for tuberous sclerosis and cancer pathogenesis. *Cell* **121**, 179-193, doi:10.1016/j.cell.2005.02.031 (2005).

211   Roux, P. P., Ballif, B. A., Anjum, R., Gygi, S. P. & Blenis, J. Tumor-promoting phorbol esters and activated Ras inactivate the tuberous sclerosis tumor

References

suppressor complex via p90 ribosomal S6 kinase. *Proc Natl Acad Sci U S A* **101**, 13489-13494, doi:10.1073/pnas.0405659101 (2004).

212   Menon, S. *et al.* Spatial control of the TSC complex integrates insulin and nutrient regulation of mTORC1 at the lysosome. *Cell* **156**, 771-785, doi:10.1016/j.cell.2013.11.049 (2014).

213   Vander Haar, E., Lee, S. I., Bandhakavi, S., Griffin, T. J. & Kim, D. H. Insulin signalling to mTOR mediated by the Akt/PKB substrate PRAS40. *Nat Cell Biol* **9**, 316-323, doi:10.1038/ncb1547 (2007).

214   Lee, D. F. *et al.* IKK beta suppression of TSC1 links inflammation and tumor angiogenesis via the mTOR pathway. *Cell* **130**, 440-455, doi:10.1016/j.cell.2007.05.058 (2007).

215   Inoki, K. *et al.* TSC2 integrates Wnt and energy signals via a coordinated phosphorylation by AMPK and GSK3 to regulate cell growth. *Cell* **126**, 955-968, doi:10.1016/j.cell.2006.06.055 (2006).

216   Gwinn, D. M. *et al.* AMPK phosphorylation of raptor mediates a metabolic checkpoint. *Mol Cell* **30**, 214-226, doi:10.1016/j.molcel.2008.03.003 (2008).

217   Shaw, R. J. *et al.* The LKB1 tumor suppressor negatively regulates mTOR signaling. *Cancer Cell* **6**, 91-99, doi:10.1016/j.ccr.2004.06.007 (2004).

218   Kim, E., Goraksha-Hicks, P., Li, L., Neufeld, T. P. & Guan, K. L. Regulation of TORC1 by Rag GTPases in nutrient response. *Nat Cell Biol* **10**, 935-945, doi:10.1038/ncb1753 (2008).

219   Sancak, Y. *et al.* The Rag GTPases bind raptor and mediate amino acid signaling to mTORC1. *Science* **320**, 1496-1501, doi:10.1126/science.1157535 (2008).

220   Sancak, Y. *et al.* Ragulator-Rag complex targets mTORC1 to the lysosomal surface and is necessary for its activation by amino acids. *Cell* **141**, 290-303, doi:10.1016/j.cell.2010.02.024 (2010).

221   Bar-Peled, L., Schweitzer, L. D., Zoncu, R. & Sabatini, D. M. Ragulator is a GEF for the rag GTPases that signal amino acid levels to mTORC1. *Cell* **150**, 1196-1208, doi:10.1016/j.cell.2012.07.032 (2012).

222   Bar-Peled, L. *et al.* A Tumor suppressor complex with GAP activity for the Rag GTPases that signal amino acid sufficiency to mTORC1. *Science* **340**, 1100-1106, doi:10.1126/science.1232044 (2013).

223   Chantranupong, L. *et al.* The Sestrins interact with GATOR2 to negatively regulate the amino-acid-sensing pathway upstream of mTORC1. *Cell Rep* **9**, 1-8, doi:10.1016/j.celrep.2014.09.014 (2014).

224   Parmigiani, A. *et al.* Sestrins inhibit mTORC1 kinase activation through the GATOR complex. *Cell Rep* **9**, 1281-1291, doi:10.1016/j.celrep.2014.10.019 (2014).

225   Saxton, R. A. *et al.* Structural basis for leucine sensing by the Sestrin2-mTORC1 pathway. *Science* **351**, 53-58, doi:10.1126/science.aad2087 (2016).

226   Wolfson, R. L. *et al.* Sestrin2 is a leucine sensor for the mTORC1 pathway. *Science* **351**, 43-48, doi:10.1126/science.aab2674 (2016).

227   Chantranupong, L. *et al.* The CASTOR Proteins Are Arginine Sensors for the mTORC1 Pathway. *Cell* **165**, 153-164, doi:10.1016/j.cell.2016.02.035 (2016).

228   Saxton, R. A., Chantranupong, L., Knockenhauer, K. E., Schwartz, T. U. & Sabatini, D. M. Mechanism of arginine sensing by CASTOR1 upstream of mTORC1. *Nature* **536**, 229-233, doi:10.1038/nature19079 (2016).

229   Gu, X. *et al.* SAMTOR is an S-adenosylmethionine sensor for the mTORC1 pathway. *Science* **358**, 813-818, doi:10.1126/science.aao3265 (2017).

References

230   Zoncu, R. *et al.* mTORC1 senses lysosomal amino acids through an inside-out mechanism that requires the vacuolar H(+)-ATPase. *Science* **334**, 678-683, doi:10.1126/science.1207056 (2011).

231   Jung, J., Genau, H. M. & Behrends, C. Amino Acid-Dependent mTORC1 Regulation by the Lysosomal Membrane Protein SLC38A9. *Mol Cell Biol* **35**, 2479-2494, doi:10.1128/MCB.00125-15 (2015).

232   Wang, S. *et al.* Lysosomal amino acid transporter SLC38A9 signals arginine sufficiency to mTORC1. *Science* **347**, 188-194, doi:10.1126/science.1257132 (2015).

233   Rebsamen, M. *et al.* SLC38A9 is a component of the lysosomal amino acid sensing machinery that controls mTORC1. *Nature* **519**, 477-481, doi:10.1038/nature14107 (2015).

234   Liu, P. *et al.* PtdIns(3,4,5)P3-Dependent Activation of the mTORC2 Kinase Complex. *Cancer Discov* **5**, 1194-1209, doi:10.1158/2159-8290.CD-15-0460 (2015).

235   Yang, G., Murashige, D. S., Humphrey, S. J. & James, D. E. A Positive Feedback Loop between Akt and mTORC2 via SIN1 Phosphorylation. *Cell Rep* **12**, 937-943, doi:10.1016/j.celrep.2015.07.016 (2015).

236   Zinzalla, V., Stracka, D., Oppliger, W. & Hall, M. N. Activation of mTORC2 by association with the ribosome. *Cell* **144**, 757-768, doi:10.1016/j.cell.2011.02.014 (2011).

237   Harrington, L. S. *et al.* The TSC1-2 tumor suppressor controls insulin-PI3K signaling via regulation of IRS proteins. *J Cell Biol* **166**, 213-223, doi:10.1083/jcb.200403069 (2004).

238   Shah, O. J., Wang, Z. & Hunter, T. Inappropriate activation of the TSC/Rheb/mTOR/S6K cassette induces IRS1/2 depletion, insulin resistance, and cell survival deficiencies. *Curr Biol* **14**, 1650-1656, doi:10.1016/j.cub.2004.08.026 (2004).

239   Hsu, P. P. *et al.* The mTOR-regulated phosphoproteome reveals a mechanism of mTORC1-mediated inhibition of growth factor signaling. *Science* **332**, 1317-1322, doi:10.1126/science.1199498 (2011).

240   Yu, Y. *et al.* Phosphoproteomic analysis identifies Grb10 as an mTORC1 substrate that negatively regulates insulin signaling. *Science* **332**, 1322-1326, doi:10.1126/science.1199484 (2011).

241   Mossmann, D., Park, S. & Hall, M. N. mTOR signalling and cellular metabolism are mutual determinants in cancer. *Nat Rev Cancer* **18**, 744-757, doi:10.1038/s41568-018-0074-8 (2018).

242   Sengupta, S., Peterson, T. R., Laplante, M., Oh, S. & Sabatini, D. M. mTORC1 controls fasting-induced ketogenesis and its modulation by ageing. *Nature* **468**, 1100-1104, doi:10.1038/nature09584 (2010).

243   Mao, Z. & Zhang, W. Role of mTOR in Glucose and Lipid Metabolism. *Int J Mol Sci* **19**, doi:10.3390/ijms19072043 (2018).

244   Han, J. *et al.* The CREB coactivator CRTC2 controls hepatic lipid metabolism by regulating SREBP1. *Nature* **524**, 243-246, doi:10.1038/nature14557 (2015).

245   Kim, K. *et al.* mTORC1-independent Raptor prevents hepatic steatosis by stabilizing PHLPP2. *Nat Commun* **7**, 10255, doi:10.1038/ncomms10255 (2016).

246   Cornu, M. *et al.* Hepatic mTORC1 controls locomotor activity, body temperature, and lipid metabolism through FGF21. *Proc Natl Acad Sci U S A* **111**, 11592-11599, doi:10.1073/pnas.1412047111 (2014).

References

247   Xu, J. *et al.* Fibroblast growth factor 21 reverses hepatic steatosis, increases energy expenditure, and improves insulin sensitivity in diet-induced obese mice. *Diabetes* **58**, 250-259, doi:10.2337/db08-0392 (2009).

248   Lee, J. H. *et al.* Maintenance of metabolic homeostasis by Sestrin2 and Sestrin3. *Cell Metab* **16**, 311-321, doi:10.1016/j.cmet.2012.08.004 (2012).

249   Howell, J. J. *et al.* Metformin Inhibits Hepatic mTORC1 Signaling via Dose-Dependent Mechanisms Involving AMPK and the TSC Complex. *Cell Metab* **25**, 463-471, doi:10.1016/j.cmet.2016.12.009 (2017).

250   Hagiwara, A. *et al.* Hepatic mTORC2 activates glycolysis and lipogenesis through Akt, glucokinase, and SREBP1c. *Cell Metab* **15**, 725-738, doi:10.1016/j.cmet.2012.03.015 (2012).

251   Yuan, M., Pino, E., Wu, L., Kacergis, M. & Soukas, A. A. Identification of Akt-independent regulation of hepatic lipogenesis by mammalian target of rapamycin (mTOR) complex 2. *J Biol Chem* **287**, 29579-29588, doi:10.1074/jbc.M112.386854 (2012).

252   Lamming, D. W. *et al.* Rapamycin-induced insulin resistance is mediated by mTORC2 loss and uncoupled from longevity. *Science* **335**, 1638-1643, doi:10.1126/science.1215135 (2012).

253   Holst, J. J., Wewer Albrechtsen, N. J., Pedersen, J. & Knop, F. K. Glucagon and Amino Acids Are Linked in a Mutual Feedback Cycle: The Liver-alpha-Cell Axis. *Diabetes* **66**, 235-240, doi:10.2337/db16-0994 (2017).

254   Kaufman, S. A new cofactor required for the enzymatic conversion of phenylalanine to tyrosine. *J Biol Chem* **230**, 931-939 (1958).

255   Fitzpatrick, P. F. Tetrahydropterin-dependent amino acid hydroxylases. *Annu Rev Biochem* **68**, 355-381, doi:10.1146/annurev.biochem.68.1.355 (1999).

256   Hsieh, M. C. & Berry, H. K. Distribution of phenylalanine hydroxylase (EC 1.14.3.1) in liver and kidney of vertebrates. *J Exp Zool* **208**, 161-167, doi:10.1002/jez.1402080204 (1979).

257   Konecki, D. S. & Lichter-Konecki, U. The phenylketonuria locus: current knowledge about alleles and mutations of the phenylalanine hydroxylase gene in various populations. *Hum Genet* **87**, 377-388, doi:10.1007/bf00197152 (1991).

258   Williams, R. A., Mamotte, C. D. & Burnett, J. R. Phenylketonuria: an inborn error of phenylalanine metabolism. *Clin Biochem Rev* **29**, 31-41 (2008).

259   Fitzpatrick, P. F. Allosteric regulation of phenylalanine hydroxylase. *Arch Biochem Biophys* **519**, 194-201, doi:10.1016/j.abb.2011.09.012 (2012).

260   Shiman, R., Mortimore, G. E., Schworer, C. M. & Gray, D. W. Regulation of phenylalanine hydroxylase activity by phenylalanine in vivo, in vitro, and in perfused rat liver. *J Biol Chem* **257**, 11213-11216 (1982).

261   Donlon, J. & Kaufman, S. Glucagon stimulation of rat hepatic phenylalanine hydroxylase through phosphorylation in vivo. *J Biol Chem* **253**, 6657-6659 (1978).

262   Haley, C. J. & Harper, A. E. Glucagon stimulation of phenylalanine metabolism. The effects of acute and chronic glucagon treatment. *Metabolism* **31**, 524-532 (1982).

263   Abita, J. P., Milstien, S., Chang, N. & Kaufman, S. In vitro activation of rat liver phenylalanine hydroxylase by phosphorylation. *J Biol Chem* **251**, 5310-5314 (1976).

264   Martinez, A. *et al.* Expression of recombinant human phenylalanine hydroxylase as fusion protein in Escherichia coli circumvents proteolytic degradation by host

References

cell proteases. Isolation and characterization of the wild-type enzyme. *Biochem J* **306 (Pt 2)**, 589-597, doi:10.1042/bj3060589 (1995).

265   Wretborn, M., Humble, E., Ragnarsson, U. & Engstrom, L. Amino acid sequence at the phosphorylated site of rat liver phenylalanine hydroxylase and phosphorylation of a corresponding synthetic peptide. *Biochem Biophys Res Commun* **93**, 403-408, doi:10.1016/0006-291x(80)91091-8 (1980).

266   Doskeland, A. P. *et al.* Some aspects of the phosphorylation of phenylalanine 4-monooxygenase by a calcium-dependent and calmodulin-dependent protein kinase. *Eur J Biochem* **145**, 31-37, doi:10.1111/j.1432-1033.1984.tb08518.x (1984).

267   Miranda, F. F. *et al.* Phosphorylation and mutations of Ser(16) in human phenylalanine hydroxylase. Kinetic and structural effects. *J Biol Chem* **277**, 40937-40943, doi:10.1074/jbc.M112197200 (2002).

268   Kowlessur, D., Yang, X. J. & Kaufman, S. Further studies of the role of Ser-16 in the regulation of the activity of phenylalanine hydroxylase. *Proc Natl Acad Sci U S A* **92**, 4743-4747, doi:10.1073/pnas.92.11.4743 (1995).

269   Doskeland, A. P., Martinez, A., Knappskog, P. M. & Flatmark, T. Phosphorylation of recombinant human phenylalanine hydroxylase: effect on catalytic activity, substrate activation and protection against non-specific cleavage of the fusion protein by restriction protease. *Biochem J* **313 (Pt 2)**, 409-414, doi:10.1042/bj3130409 (1996).

270   Zhang, T., Braun, U. & Leitges, M. PKD3 deficiency causes alterations in microtubule dynamics during the cell cycle. *Cell Cycle* **15**, 1844-1854, doi:10.1080/15384101.2016.1188237 (2016).

271   Postic, C. *et al.* Dual roles for glucokinase in glucose homeostasis as determined by liver and pancreatic beta cell-specific gene knock-outs using Cre recombinase. *J Biol Chem* **274**, 305-315, doi:10.1074/jbc.274.1.305 (1999).

272   Bligh, E. G. & Dyer, W. J. A rapid method of total lipid extraction and purification. *Can J Biochem Physiol* **37**, 911-917, doi:10.1139/o59-099 (1959).

273   Cox, J. & Mann, M. MaxQuant enables high peptide identification rates, individualized p.p.b.-range mass accuracies and proteome-wide protein quantification. *Nat Biotechnol* **26**, 1367-1372, doi:10.1038/nbt.1511 (2008).

274   Cox, J. *et al.* Accurate proteome-wide label-free quantification by delayed normalization and maximal peptide ratio extraction, termed MaxLFQ. *Mol Cell Proteomics* **13**, 2513-2526, doi:10.1074/mcp.M113.031591 (2014).

275   Mayer, A. E. *et al.* The kinase PKD3 provides negative feedback on cholesterol and triglyceride synthesis by suppressing insulin signaling. *Sci Signal* **12**, doi:10.1126/scisignal.aav9150 (2019).

276   Puri, P. *et al.* A lipidomic analysis of nonalcoholic fatty liver disease. *Hepatology* **46**, 1081-1090, doi:10.1002/hep.21763 (2007).

277   Kotronen, A. *et al.* Hepatic stearoyl-CoA desaturase (SCD)-1 activity and diacylglycerol but not ceramide concentrations are increased in the nonalcoholic human fatty liver. *Diabetes* **58**, 203-208, doi:10.2337/db08-1074 (2009).

278   Nakamura, A. & Terauchi, Y. Lessons from mouse models of high-fat diet-induced NAFLD. *Int J Mol Sci* **14**, 21240-21257, doi:10.3390/ijms141121240 (2013).

279   Burnstock, G., Vaughn, B. & Robson, S. C. Purinergic signalling in the liver in health and disease. *Purinergic Signal* **10**, 51-70, doi:10.1007/s11302-013-9398-8 (2014).

280   Vaughn, B. P., Robson, S. C. & Longhi, M. S. Purinergic signaling in liver disease. *Dig Dis* **32**, 516-524, doi:10.1159/000360498 (2014).

References

281   Bradford, M. D. & Soltoff, S. P. P2X7 receptors activate protein kinase D and p42/p44 mitogen-activated protein kinase (MAPK) downstream of protein kinase C. *Biochem J* **366**, 745-755, doi:10.1042/BJ20020358 (2002).

282   Carrasquero, L. M., Delicado, E. G., Sanchez-Ruiloba, L., Iglesias, T. & Miras-Portugal, M. T. Mechanisms of protein kinase D activation in response to P2Y(2) and P2X7 receptors in primary astrocytes. *Glia* **58**, 984-995, doi:10.1002/glia.20980 (2010).

283   Han, H. S., Kang, G., Kim, J. S., Choi, B. H. & Koo, S. H. Regulation of glucose metabolism from a liver-centric perspective. *Exp Mol Med* **48**, e218, doi:10.1038/emm.2015.122 (2016).

284   Manning, B. D. & Toker, A. AKT/PKB Signaling: Navigating the Network. *Cell* **169**, 381-405, doi:10.1016/j.cell.2017.04.001 (2017).

285   Ipsen, D. H., Lykkesfeldt, J. & Tveden-Nyborg, P. Molecular mechanisms of hepatic lipid accumulation in non-alcoholic fatty liver disease. *Cell Mol Life Sci* **75**, 3313-3327, doi:10.1007/s00018-018-2860-6 (2018).

286   Gluchowski, N. L., Becuwe, M., Walther, T. C. & Farese, R. V., Jr. Lipid droplets and liver disease: from basic biology to clinical implications. *Nat Rev Gastroenterol Hepatol* **14**, 343-355, doi:10.1038/nrgastro.2017.32 (2017).

287   Nguyen, Q., Anders, R. A., Alpini, G. & Bai, H. Yes-associated protein in the liver: Regulation of hepatic development, repair, cell fate determination and tumorigenesis. *Dig Liver Dis* **47**, 826-835, doi:10.1016/j.dld.2015.05.011 (2015).

288   Wang, X. *et al.* Hepatocyte TAZ/WWTR1 Promotes Inflammation and Fibrosis in Nonalcoholic Steatohepatitis. *Cell Metab* **24**, 848-862, doi:10.1016/j.cmet.2016.09.016 (2016).

289   Angulo, P. *et al.* The NAFLD fibrosis score: a noninvasive system that identifies liver fibrosis in patients with NAFLD. *Hepatology* **45**, 846-854, doi:10.1002/hep.21496 (2007).

290   Espenshade, P. J. SREBPs: sterol-regulated transcription factors. *J Cell Sci* **119**, 973-976, doi:10.1242/jcs02866 (2006).

291   Krycer, J. R., Sharpe, L. J., Luu, W. & Brown, A. J. The Akt-SREBP nexus: cell signaling meets lipid metabolism. *Trends Endocrinol Metab* **21**, 268-276, doi:10.1016/j.tem.2010.01.001 (2010).

292   Ono, H. *et al.* Hepatic Akt activation induces marked hypoglycemia, hepatomegaly, and hypertriglyceridemia with sterol regulatory element binding protein involvement. *Diabetes* **52**, 2905-2913, doi:10.2337/diabetes.52.12.2905 (2003).

293   Fleischmann, M. & Iynedjian, P. B. Regulation of sterol regulatory-element binding protein 1 gene expression in liver: role of insulin and protein kinase B/cAkt. *Biochem J* **349**, 13-17, doi:10.1042/0264-6021:3490013 (2000).

294   Leavens, K. F., Easton, R. M., Shulman, G. I., Previs, S. F. & Birnbaum, M. J. Akt2 is required for hepatic lipid accumulation in models of insulin resistance. *Cell Metab* **10**, 405-418, doi:10.1016/j.cmet.2009.10.004 (2009).

295   Ricoult, S. J. & Manning, B. D. The multifaceted role of mTORC1 in the control of lipid metabolism. *EMBO Rep* **14**, 242-251, doi:10.1038/embor.2013.5 (2013).

296   Yecies, J. L. *et al.* Akt stimulates hepatic SREBP1c and lipogenesis through parallel mTORC1-dependent and independent pathways. *Cell Metab* **14**, 21-32, doi:10.1016/j.cmet.2011.06.002 (2011).

297   Gual, P., Gremeaux, T., Gonzalez, T., Le Marchand-Brustel, Y. & Tanti, J. F. MAP kinases and mTOR mediate insulin-induced phosphorylation of insulin receptor substrate-1 on serine residues 307, 612 and 632. *Diabetologia* **46**, 1532-1542, doi:10.1007/s00125-003-1223-4 (2003).

References

298   Shah, O. J. & Hunter, T. Turnover of the active fraction of IRS1 involves raptor-mTOR- and S6K1-dependent serine phosphorylation in cell culture models of tuberous sclerosis. *Mol Cell Biol* **26**, 6425-6434, doi:10.1128/MCB.01254-05 (2006).

299   Tzatsos, A. & Kandror, K. V. Nutrients suppress phosphatidylinositol 3-kinase/Akt signaling via raptor-dependent mTOR-mediated insulin receptor substrate 1 phosphorylation. *Mol Cell Biol* **26**, 63-76, doi:10.1128/MCB.26.1.63-76.2006 (2006).

300   Mihaylova, M. M. & Shaw, R. J. The AMPK signalling pathway coordinates cell growth, autophagy and metabolism. *Nat Cell Biol* **13**, 1016-1023, doi:10.1038/ncb2329 (2011).

301   Li, S., Brown, M. S. & Goldstein, J. L. Bifurcation of insulin signaling pathway in rat liver: mTORC1 required for stimulation of lipogenesis, but not inhibition of gluconeogenesis. *Proc Natl Acad Sci U S A* **107**, 3441-3446, doi:10.1073/pnas.0914798107 (2010).

302   Matthews, D. R. *et al.* Homeostasis model assessment: insulin resistance and beta-cell function from fasting plasma glucose and insulin concentrations in man. *Diabetologia* **28**, 412-419 (1985).

303   Lachmann, A. *et al.* Massive mining of publicly available RNA-seq data from human and mouse. *Nat Commun* **9**, 1366, doi:10.1038/s41467-018-03751-6 (2018).

304   Huang da, W., Sherman, B. T. & Lempicki, R. A. Systematic and integrative analysis of large gene lists using DAVID bioinformatics resources. *Nat Protoc* **4**, 44-57, doi:10.1038/nprot.2008.211 (2009).

305   Brand, L. M. & Harper, A. E. Effect of glucagon on phenylalanine metabolism and phenylalanine-degrading enzymes in the rat. *Biochem J* **142**, 231-245, doi:10.1042/bj1420231 (1974).

306   Trefts, E., Gannon, M. & Wasserman, D. H. The liver. *Curr Biol* **27**, R1147-R1151, doi:10.1016/j.cub.2017.09.019 (2017).

307   Schmitz-Peiffer, C. & Biden, T. J. Protein kinase C function in muscle, liver, and beta-cells and its therapeutic implications for type 2 diabetes. *Diabetes* **57**, 1774-1783, doi:10.2337/db07-1769 (2008).

308   Samuel, V. T. & Shulman, G. I. The pathogenesis of insulin resistance: integrating signaling pathways and substrate flux. *J Clin Invest* **126**, 12-22, doi:10.1172/JCI77812 (2016).

309   Heydemann, A. An Overview of Murine High Fat Diet as a Model for Type 2 Diabetes Mellitus. *J Diabetes Res* **2016**, 2902351, doi:10.1155/2016/2902351 (2016).

310   Szendroedi, J. *et al.* Role of diacylglycerol activation of PKCtheta in lipid-induced muscle insulin resistance in humans. *Proc Natl Acad Sci U S A* **111**, 9597-9602, doi:10.1073/pnas.1409229111 (2014).

311   Pfeilschifter, J. Extracellular ATP stimulates polyphosphoinositide hydrolysis and prostaglandin synthesis in rat renal mesangial cells. Involvement of a pertussis toxin-sensitive guanine nucleotide binding protein and feedback inhibition by protein kinase C. *Cell Signal* **2**, 129-138 (1990).

312   Heyworth, C. M., Whetton, A. D., Kinsella, A. R. & Houslay, M. D. The phorbol ester, TPA inhibits glucagon-stimulated adenylate cyclase activity. *FEBS Lett* **170**, 38-42, doi:10.1016/0014-5793(84)81364-2 (1984).

313   Heyworth, C. M., Wilson, S. P., Gawler, D. J. & Houslay, M. D. The phorbol ester TPA prevents the expression of both glucagon desensitisation and the glucagon-mediated block of insulin stimulation of the peripheral plasma

References

membrane cyclic AMP phosphodiesterase in rat hepatocytes. *FEBS Lett* **187**, 196-200, doi:10.1016/0014-5793(85)81241-2 (1985).

314　Tobias, E. S., Rozengurt, E., Connell, J. M. & Houslay, M. D. Co-transfection with protein kinase D confers phorbol-ester-mediated inhibition on glucagon-stimulated cAMP accumulation in COS cells transfected to overexpress glucagon receptors. *Biochem J* **326 (Pt 2)**, 545-551, doi:10.1042/bj3260545 (1997).

315　Sun, Z. *et al.* Hepatic Hdac3 promotes gluconeogenesis by repressing lipid synthesis and sequestration. *Nat Med* **18**, 934-942, doi:10.1038/nm.2744 (2012).

316　Bisteau, X., Caldez, M. J. & Kaldis, P. The Complex Relationship between Liver Cancer and the Cell Cycle: A Story of Multiple Regulations. *Cancers (Basel)* **6**, 79-111, doi:10.3390/cancers6010079 (2014).

317　Michelotti, G. A., Machado, M. V. & Diehl, A. M. NAFLD, NASH and liver cancer. *Nat Rev Gastroenterol Hepatol* **10**, 656-665, doi:10.1038/nrgastro.2013.183 (2013).

318　Rosen, E. D. & Spiegelman, B. M. What we talk about when we talk about fat. *Cell* **156**, 20-44, doi:10.1016/j.cell.2013.12.012 (2014).

319　Choi, S. H. & Ginsberg, H. N. Increased very low density lipoprotein (VLDL) secretion, hepatic steatosis, and insulin resistance. *Trends Endocrinol Metab* **22**, 353-363, doi:10.1016/j.tem.2011.04.007 (2011).

320　Gusarova, V. *et al.* Golgi-associated maturation of very low density lipoproteins involves conformational changes in apolipoprotein B, but is not dependent on apolipoprotein E. *J Biol Chem* **282**, 19453-19462, doi:10.1074/jbc.M700475200 (2007).

321　Siddiqi, S. A. VLDL exits from the endoplasmic reticulum in a specialized vesicle, the VLDL transport vesicle, in rat primary hepatocytes. *Biochem J* **413**, 333-342, doi:10.1042/BJ20071469 (2008).

322　Amako, Y., Syed, G. H. & Siddiqui, A. Protein kinase D negatively regulates hepatitis C virus secretion through phosphorylation of oxysterol-binding protein and ceramide transfer protein. *J Biol Chem* **286**, 11265-11274, doi:10.1074/jbc.M110.182097 (2011).

323　Steinbusch, L. K. *et al.* Overexpression of AMP-activated protein kinase or protein kinase D prevents lipid-induced insulin resistance in cardiomyocytes. *J Mol Cell Cardiol* **55**, 165-173, doi:10.1016/j.yjmcc.2012.11.005 (2013).

324　Perry, R. J., Samuel, V. T., Petersen, K. F. & Shulman, G. I. The role of hepatic lipids in hepatic insulin resistance and type 2 diabetes. *Nature* **510**, 84-91, doi:10.1038/nature13478 (2014).

325　Petersen, M. C. *et al.* Insulin receptor Thr1160 phosphorylation mediates lipid-induced hepatic insulin resistance. *J Clin Invest* **126**, 4361-4371, doi:10.1172/JCI86013 (2016).

326　Yoon, M. S. The Role of Mammalian Target of Rapamycin (mTOR) in Insulin Signaling. *Nutrients* **9**, doi:10.3390/nu9111176 (2017).

327　Torres-Ayuso, P., Tello-Lafoz, M., Merida, I. & Avila-Flores, A. Diacylglycerol kinase-zeta regulates mTORC1 and lipogenic metabolism in cancer cells through SREBP-1. *Oncogenesis* **4**, e164, doi:10.1038/oncsis.2015.22 (2015).

328　Owen, J. L. *et al.* Insulin stimulation of SREBP-1c processing in transgenic rat hepatocytes requires p70 S6-kinase. *Proc Natl Acad Sci U S A* **109**, 16184-16189, doi:10.1073/pnas.1213343109 (2012).

References

329   Quinn, W. J., 3rd & Birnbaum, M. J. Distinct mTORC1 pathways for transcription and cleavage of SREBP-1c. *Proc Natl Acad Sci U S A* **109**, 15974-15975, doi:10.1073/pnas.1214113109 (2012).

330   Zhang, P., Verity, M. A. & Reue, K. Lipin-1 regulates autophagy clearance and intersects with statin drug effects in skeletal muscle. *Cell Metab* **20**, 267-279, doi:10.1016/j.cmet.2014.05.003 (2014).

331   Huck, B., Duss, S., Hausser, A. & Olayioye, M. A. Elevated protein kinase D3 (PKD3) expression supports proliferation of triple-negative breast cancer cells and contributes to mTORC1-S6K1 pathway activation. *J Biol Chem* **289**, 3138-3147, doi:10.1074/jbc.M113.502633 (2014).

332   Yamamoto, T. *et al.* Protein kinase Cbeta mediates hepatic induction of sterol-regulatory element binding protein-1c by insulin. *J Lipid Res* **51**, 1859-1870, doi:10.1194/jlr.M004234 (2010).

333   Wang, J., Sinnett-Smith, J., Stevens, J. V., Young, S. H. & Rozengurt, E. Biphasic Regulation of Yes-associated Protein (YAP) Cellular Localization, Phosphorylation, and Activity by G Protein-coupled Receptor Agonists in Intestinal Epithelial Cells: A NOVEL ROLE FOR PROTEIN KINASE D (PKD). *J Biol Chem* **291**, 17988-18005, doi:10.1074/jbc.M115.711275 (2016).

334   Hao, F. *et al.* Insulin Receptor and GPCR Crosstalk Stimulates YAP via PI3K and PKD in Pancreatic Cancer Cells. *Mol Cancer Res* **15**, 929-941, doi:10.1158/1541-7786.MCR-17-0023 (2017).

335   Wu, H. *et al.* Integration of Hippo signalling and the unfolded protein response to restrain liver overgrowth and tumorigenesis. *Nat Commun* **6**, 6239, doi:10.1038/ncomms7239 (2015).

336   Werstuck, G. H. *et al.* Homocysteine-induced endoplasmic reticulum stress causes dysregulation of the cholesterol and triglyceride biosynthetic pathways. *J Clin Invest* **107**, 1263-1273, doi:10.1172/JCI11596 (2001).

337   Eisenberg-Lerner, A. & Kimchi, A. DAP kinase regulates JNK signaling by binding and activating protein kinase D under oxidative stress. *Cell Death Differ* **14**, 1908-1915, doi:10.1038/sj.cdd.4402212 (2007).

338   Sekiya, M., Hiraishi, A., Touyama, M. & Sakamoto, K. Oxidative stress induced lipid accumulation via SREBP1c activation in HepG2 cells. *Biochem Biophys Res Commun* **375**, 602-607, doi:10.1016/j.bbrc.2008.08.068 (2008).

339   Ni, Y., Sinnett-Smith, J., Young, S. H. & Rozengurt, E. PKD1 mediates negative feedback of PI3K/Akt activation in response to G protein-coupled receptors. *PLoS One* **8**, e73149, doi:10.1371/journal.pone.0073149 (2013).

340   Lee, J. Y., Chiu, Y. H., Asara, J. & Cantley, L. C. Inhibition of PI3K binding to activators by serine phosphorylation of PI3K regulatory subunit p85alpha Src homology-2 domains. *Proc Natl Acad Sci U S A* **108**, 14157-14162, doi:10.1073/pnas.1107747108 (2011).

341   Cantley, L. C. The phosphoinositide 3-kinase pathway. *Science* **296**, 1655-1657, doi:10.1126/science.296.5573.1655 (2002).

342   Ittner, A. *et al.* Regulation of PTEN activity by p38delta-PKD1 signaling in neutrophils confers inflammatory responses in the lung. *J Exp Med* **209**, 2229-2246, doi:10.1084/jem.20120677 (2012).

343   Ishikawa, E. *et al.* Protein kinase D regulates positive selection of CD4(+) thymocytes through phosphorylation of SHP-1. *Nat Commun* **7**, 12756, doi:10.1038/ncomms12756 (2016).

344   Cuevas, B. *et al.* SHP-1 regulates Lck-induced phosphatidylinositol 3-kinase phosphorylation and activity. *J Biol Chem* **274**, 27583-27589, doi:10.1074/jbc.274.39.27583 (1999).

References

345 Cuevas, B. D. *et al.* Tyrosine phosphorylation of p85 relieves its inhibitory activity on phosphatidylinositol 3-kinase. *J Biol Chem* **276**, 27455-27461, doi:10.1074/jbc.M100556200 (2001).

346 Xu, E. *et al.* Hepatocyte-specific Ptpn6 deletion protects from obesity-linked hepatic insulin resistance. *Diabetes* **61**, 1949-1958, doi:10.2337/db11-1502 (2012).

347 Izawa, Y. *et al.* ERK1/2 activation by angiotensin II inhibits insulin-induced glucose uptake in vascular smooth muscle cells. *Exp Cell Res* **308**, 291-299, doi:10.1016/j.yexcr.2005.04.028 (2005).

348 Haeusler, R. A. *et al.* Integrated control of hepatic lipogenesis versus glucose production requires FoxO transcription factors. *Nat Commun* **5**, 5190, doi:10.1038/ncomms6190 (2014).

349 Chen, J. *et al.* Protein kinase D1 regulates hypoxic metabolism through HIF-1alpha and glycolytic enzymes incancer cells. *Oncol Rep* **40**, 1073-1082, doi:10.3892/or.2018.6479 (2018).

350 Luiken, J. J. *et al.* Identification of protein kinase D as a novel contraction-activated kinase linked to GLUT4-mediated glucose uptake, independent of AMPK. *Cell Signal* **20**, 543-556, doi:10.1016/j.cellsig.2007.11.007 (2008).

351 Dirkx, E. *et al.* Protein kinase D1 is essential for contraction-induced glucose uptake but is not involved in fatty acid uptake into cardiomyocytes. *J Biol Chem* **287**, 5871-5881, doi:10.1074/jbc.M111.281881 (2012).

352 Chen, J., Lu, G. & Wang, Q. J. Protein kinase C-independent effects of protein kinase D3 in glucose transport in L6 myotubes. *Mol Pharmacol* **67**, 152-162, doi:10.1124/mol.104.004200 (2005).

353 Herzig, S. *et al.* CREB regulates hepatic gluconeogenesis through the coactivator PGC-1. *Nature* **413**, 179-183, doi:10.1038/35093131 (2001).

354 Herzig, S. *et al.* CREB controls hepatic lipid metabolism through nuclear hormone receptor PPAR-gamma. *Nature* **426**, 190-193, doi:10.1038/nature02110 (2003).

355 Jhun, B. S. *et al.* Protein kinase D activation induces mitochondrial fragmentation and dysfunction in cardiomyocytes. *J Physiol* **596**, 827-855, doi:10.1113/JP275418 (2018).

356 Karlsson, L., Peleraux, A., Lindstedt, R., Liljedahl, M. & Peterson, P. A. Reconstitution of an operational MHC class II compartment in nonantigen-presenting cells. *Science* **266**, 1569-1573, doi:10.1126/science.7985028 (1994).

357 Zhang, J. *et al.* A tuberous sclerosis complex signalling node at the peroxisome regulates mTORC1 and autophagy in response to ROS. *Nat Cell Biol* **15**, 1186-1196, doi:10.1038/ncb2822 (2013).

358 Benjamin, D. & Hall, M. N. TSC on the peroxisome controls mTORC1. *Nat Cell Biol* **15**, 1135-1136, doi:10.1038/ncb2849 (2013).

359 Rabanal-Ruiz, Y. & Korolchuk, V. I. mTORC1 and Nutrient Homeostasis: The Central Role of the Lysosome. *Int J Mol Sci* **19**, doi:10.3390/ijms19030818 (2018).

360 Tsukita, S. & Yonemura, S. Cortical actin organization: lessons from ERM (ezrin/radixin/moesin) proteins. *J Biol Chem* **274**, 34507-34510, doi:10.1074/jbc.274.49.34507 (1999).

361 Clucas, J. & Valderrama, F. ERM proteins in cancer progression. *J Cell Sci* **127**, 267-275, doi:10.1242/jcs.133108 (2014).

References

362   Ng, T. *et al.* Ezrin is a downstream effector of trafficking PKC-integrin complexes involved in the control of cell motility. *EMBO J* **20**, 2723-2741, doi:10.1093/emboj/20.11.2723 (2001).

363   Wald, F. A. *et al.* Atypical protein kinase C (iota) activates ezrin in the apical domain of intestinal epithelial cells. *J Cell Sci* **121**, 644-654, doi:10.1242/jcs.016246 (2008).

364   Reczek, D., Berryman, M. & Bretscher, A. Identification of EBP50: A PDZ-containing phosphoprotein that associates with members of the ezrin-radixin-moesin family. *J Cell Biol* **139**, 169-179, doi:10.1083/jcb.139.1.169 (1997).

365   Fouassier, L. *et al.* Protein kinase C regulates the phosphorylation and oligomerization of ERM binding phosphoprotein 50. *Exp Cell Res* **306**, 264-273, doi:10.1016/j.yexcr.2005.02.011 (2005).

366   Kunkel, M. T., Garcia, E. L., Kajimoto, T., Hall, R. A. & Newton, A. C. The protein scaffold NHERF-1 controls the amplitude and duration of localized protein kinase D activity. *J Biol Chem* **284**, 24653-24661, doi:10.1074/jbc.M109.024547 (2009).

367   Chen, X. W. *et al.* A Ral GAP complex links PI 3-kinase/Akt signaling to RalA activation in insulin action. *Mol Biol Cell* **22**, 141-152, doi:10.1091/mbc.E10-08-0665 (2011).

368   Martin, T. D. *et al.* Ral and Rheb GTPase activating proteins integrate mTOR and GTPase signaling in aging, autophagy, and tumor cell invasion. *Mol Cell* **53**, 209-220, doi:10.1016/j.molcel.2013.12.004 (2014).

369   Leto, D., Uhm, M., Williams, A., Chen, X. W. & Saltiel, A. R. Negative regulation of the RalGAP complex by 14-3-3. *J Biol Chem* **288**, 9272-9283, doi:10.1074/jbc.M112.426106 (2013).

370   Dibble, C. C. & Cantley, L. C. Regulation of mTORC1 by PI3K signaling. *Trends Cell Biol* **25**, 545-555, doi:10.1016/j.tcb.2015.06.002 (2015).

371   Lo, S. H. C-terminal tensin-like (CTEN): a promising biomarker and target for cancer. *Int J Biochem Cell Biol* **51**, 150-154, doi:10.1016/j.biocel.2014.04.003 (2014).

372   Lo, S. H. Tensins. *Curr Biol* **27**, R331-R332, doi:10.1016/j.cub.2017.02.041 (2017).

373   Blangy, A. Tensins are versatile regulators of Rho GTPase signalling and cell adhesion. *Biol Cell* **109**, 115-126, doi:10.1111/boc.201600053 (2017).

374   Katz, M. *et al.* A reciprocal tensin-3-cten switch mediates EGF-driven mammary cell migration. *Nat Cell Biol* **9**, 961-969, doi:10.1038/ncb1622 (2007).

375   Pylayeva, Y. & Giancotti, F. G. Tensin relief facilitates migration. *Nat Cell Biol* **9**, 877-879, doi:10.1038/ncb0807-877 (2007).

376   Cui, Y., Liao, Y. C. & Lo, S. H. Epidermal growth factor modulates tyrosine phosphorylation of a novel tensin family member, tensin3. *Mol Cancer Res* **2**, 225-232 (2004).

377   Cao, X. *et al.* A phosphorylation switch controls the spatiotemporal activation of Rho GTPases in directional cell migration. *Nat Commun* **6**, 7721, doi:10.1038/ncomms8721 (2015).

378   Eiseler, T., Schmid, M. A., Topbas, F., Pfizenmaier, K. & Hausser, A. PKD is recruited to sites of actin remodelling at the leading edge and negatively regulates cell migration. *FEBS Lett* **581**, 4279-4287, doi:10.1016/j.febslet.2007.07.079 (2007).

379   Saci, A., Cantley, L. C. & Carpenter, C. L. Rac1 regulates the activity of mTORC1 and mTORC2 and controls cellular size. *Mol Cell* **42**, 50-61, doi:10.1016/j.molcel.2011.03.017 (2011).

References

380   Pinna, L. A. & Ruzzene, M. How do protein kinases recognize their substrates? *Biochim Biophys Acta* **1314**, 191-225, doi:10.1016/s0167-4889(96)00083-3 (1996).

381   Yefimenko, I., Fresquet, V., Marco-Marin, C., Rubio, V. & Cervera, J. Understanding carbamoyl phosphate synthetase deficiency: impact of clinical mutations on enzyme functionality. *J Mol Biol* **349**, 127-141, doi:10.1016/j.jmb.2005.03.078 (2005).

382   Nakagawa, T., Lomb, D. J., Haigis, M. C. & Guarente, L. SIRT5 Deacetylates carbamoyl phosphate synthetase 1 and regulates the urea cycle. *Cell* **137**, 560-570, doi:10.1016/j.cell.2009.02.026 (2009).

383   Coughlan, K. A. *et al.* PKD1 Inhibits AMPKalpha2 through Phosphorylation of Serine 491 and Impairs Insulin Signaling in Skeletal Muscle Cells. *J Biol Chem* **291**, 5664-5675, doi:10.1074/jbc.M115.696849 (2016).

384   Huck, B. *et al.* GIT1 phosphorylation on serine 46 by PKD3 regulates paxillin trafficking and cellular protrusive activity. *J Biol Chem* **287**, 34604-34613, doi:10.1074/jbc.M112.374652 (2012).

385   Franz-Wachtel, M. *et al.* Global detection of protein kinase D-dependent phosphorylation events in nocodazole-treated human cells. *Mol Cell Proteomics* **11**, 160-170, doi:10.1074/mcp.M111.016014 (2012).

6 Appendix

6.1 Full MS data

6.1.1 Proteins identified by MS from IP with LxRxx[S*/T*] antibody

Table 15: List of proteins identified by MS from IP with LxRxx[S*/T*] antibody.

Uniprot entry	Protein names	Gene names	Peptides EGFP	Peptides PKD3ca	norm.log2.Ratio. filt.LFQ.intensity	Sig.	Putative PKD substrate motifs
Q5FWX6	Serine/threonine-protein kinase D3	Prkd3	0	46	9,56	2	IlRvsS470
Q9JKP5	Muscleblind-like protein 1	Mbnl1	1	2	7,73	2	
Q3UIL6	Pleckstrin homology domain-containing family A member 7	Plekha7	1	3	6,79	2	IsRkyS229 VpRsiS562 LcResT766 LpReaT943 IiRhtS949 **LeRlyS1060**
Q8QZS1	3-hydroxyisobutyryl-CoA hydrolase, mitochondrial	Hibch	1	3	6,31	2	LsRvsS15
P97861	Keratin, type II cuticular Hb6	Krt86	2	12	6,29	2	
Q6A0A2	La-related protein 4B	Larp4b	1	13	5,68	2	**IlReiS246** **VdRlpS628**
P62984	Ubiquitin-60S ribosomal protein L40	Uba52	9	6	4,94	2	
A2A7S8	Uncharacterized protein KIAA1522	Kiaa1522	3	20	4,37	2	**IqRrgS136** LtRpmS261 **LgRfsS337** LpRppT477 **LrRalS838** **LeRpvS909** **VaRkpS952** **LpRteS967**
F8VQB6	Unconventional myosin-X	Myo10	2	14	4,13	2	**IeRslS961**
Q8BHL4	Retinoic acid-induced protein 3	Gprc5a	0	2	4,04	2	LpRqrS275
Q8K0Y2	Keratin, type I cuticular Ha3-I	Krt33a	2	6	3,93	2	
P11352	Glutathione peroxidase 1	Gpx1	8	10	3,50	2	
Q5SSZ5	Tensin 3	Tns3	1	12	3,50	2	**LiRwdS332** **LlRkpS571** **VqRgiS648**
Q05915	GTP cyclohydrolase 1	Gch1	2	7	3,45	2	
Q3UJB9	Enhancer of mRNA-decapping protein 4	Edc4	1	13	3,44	2	
P11370	Retrovirus-related Env polyprotein from Fv-4 locus	Fv4	2	3	3,40	2	LeRslT540
P17918	Proliferating cell nuclear antigen	Pcna	0	2	3,27	2	IcRdlS152
Q640L5	Coiled-coil domain-containing protein 18	Ccdc18	1	2	3,26	2	LeRnlS281 LdRllT695 **LrRsiS1355**

149

Appendix

Uniprot entry	Protein names	Gene names	Peptides EGFP	Peptides PKD3ca	norm.log2.Ratio. filt.LFQ.intensity	Sig.	Putative PKD substrate motifs
P70275	Semaphorin-3E	Sema3e	4	11	3,21	2	
Q9JJY4	Probable ATP-dependent RNA helicase DDX20	Ddx20	3	6	3,19	2	IiRnyT618
P13020	Gelsolin	Gsn	9	14	3,07	2	
P28740	Kinesin-like protein KIF2A	Kif2a	1	5	3,03	2	
E9QN70	Laminin subunit beta-1	Lamb1	2	2	3,02	2	LlRppS37
F6ZDS4	Nucleoprotein TPR	Tpr	0	14	2,99	2	LeRseT905 LqRasT1130 VeRpsT1881
Q8BQ30	Phostensin	Ppp1r18	5	15	2,91	2	**LeRrsS126**
O88487	Cytoplasmic dynein 1 intermediate chain 2	Dync1i2	3	4	2,86	2	VeRalS212
Q91YD3	mRNA-decapping enzyme 1A	Dcp1a	0	2	2,84	2	LyrnaS121 LpRnsT359 **LeRkaS542**
P35492	Histidine ammonia-lyase	Hal	21	25	2,81	2	LvRshS195
P28271	Cytoplasmic aconitate hydratase	Aco1	1	4	2,68	2	VmRfdT867
Q9CXI3	DBH-like monooxygenase protein 1	Moxd1	0	4	2,54	2	LtRcsS482 IyRpvT503
Q8QZY1	Eukaryotic translation initiation factor 3 subunit L	Eif3l	2	4	2,50	2	LlRlhS282 IqRtkS348
P35564	Calnexin	Canx	2	4	2,49	2	
Q61699	Heat shock protein 105 kDa	Hsph1	1	6	2,49	2	
Q8K2Q9	Shootin-1	Kiaa1598	4	24	2,46	2	
Q9D975	Sulfiredoxin-1	Srxn1	0	3	2,37	2	
Q91YU6	Leucine zipper putative tumor suppressor 2	Lzts2	1	4	2,36	2	
Q9QXL2	Kinesin-like protein KIF21A	Kif21a	5	26	2,36	2	LqRlqT739 VlRrkT829 **VtRklS855** LeRrvT933 **IsRqsS1231** LkRfqS1482
Q62266	Cornifin-A	Sprr1a	14	10	2,07	2	
Q6PEM6	GRAM domain-containing protein 3	Gramd3	4	2	1,98	2	LsRdsT219
P16331	Phenylalanine-4-hydroxylase	Pah	11	16	1,91	2	**LsRklS16** IpRpfS411
Q9Z1Q9	Valine--tRNA ligase	Vars	4	9	2,29	1	
Q04750	DNA topoisomerase 1	Top1	5	4	2,25	1	
Q9CWY4	Gem-associated protein 7	Gemin7	0	2	2,21	1	
Q8K2D3	Enhancer of mRNA-decapping protein 3	Edc3	0	2	2,09	1	VyRriT262
P46062	Signal-induced proliferation-associated protein 1	Sipa1	0	6	2,04	1	**LlRsgS53** **LpRtlS903**
Q91WK0	Leucine-rich repeat flightless-interacting protein 2	Lrrfip2	22	18	1,99	1	LlRstS151

Appendix

Uniprot entry	Protein names	Gene names	Peptides EGFP	Peptides PKD3ca	norm.log2.Ratio. filt.LFQ.intensity	Sig.	Putative PKD substrate motifs
Q91WT9	Cystathionine beta-synthase	Cbs	2	2	1,99	1	IvRtpT190
P61967	AP-1 complex subunit sigma-1A	Ap1s1	1	2	1,98	1	
O35682	Myeloid-associated differentiation marker	Myadm	2	2	1,96	1	
Q3THS6	S-adenosylmethionine synthase isoform type-2	Mat2a	4	5	1,96	1	LrRngT172
Q8CGK3	Lon protease homolog, mitochondrial	Lonp1	5	4	1,93	1	
P09055	Integrin beta-1	Itgb1	2	3	1,92	1	
Q91VY9	Zinc finger protein 622	Znf622	2	2	1,91	1	LpRavT410 VqRmkS452
Q6IMF0	Keratin, type II cuticular Hb3	Krt83	2	13	1,81	1	
Q60953	Protein PML	Pml	3	7	1,76	1	LdRnhS227 LqRirT332 LaRnmS748
A2AN08	E3 ubiquitin-protein ligase UBR4	Ubr4	8	15	1,70	1	LnRldS950 LtRmtT1472 IvRenS1503 VkRtpS1732 **LvRhaS1760** LtRlaS1945 IeRapS2364 VmRllS3057 LaRhnT4938
Q8VDJ3	Vigilin	Hdlbp	0	5	1,70	1	VaRlqT149 ViRgpS706
P84084	ADP-ribosylation factor 5	Arf5	3	4	1,68	1	
E9Q450	Tropomyosin alpha-1 chain	Tpm1	64	56	1,67	1	
P20918	Plasminogen	Plg	3	14	1,64	1	IpRctT264 LsRpaT678
P42125	Enoyl-CoA delta isomerase 1, mitochondrial	Eci1	4	4	1,61	1	
Q91XV3	Brain acid soluble protein 1	Basp1	1	3	1,59	1	
Q921U8	Smoothelin	Smtn	10	23	1,58	1	**VtRlgS521 VqRstS798**
Q9CQA6	Coiled-coil-helix-coiled-coil-helix domain-containing protein 1	Chchd1	1	2	1,58	1	
Q99NB9	Splicing factor 3B subunit 1	Sf3b1	2	2	1,57	1	
Q9DBJ3	Brain-specific angiogenesis inhibitor 1-associated protein 2-like protein 1	Baiap2l1	4	7	1,54	1	**LqRsvS332**
Q8CC35	Synaptopodin	Synpo	0	4	1,54	1	**LgRstS134 LaRcpS740**
Q91YW3	DnaJ homolog subfamily C member 3	Dnajc3	3	2	1,52	1	
Q0VG62	Uncharacterized protein C8orf59 homolog	1810022 K09Rik	2	2	1,52	1	VpRpeT34

Uniprot entry	Protein names	Gene names	Peptides EGFP	Peptides PKD3ca	norm.log2.Ratio. filt.LFQ.intensity	Sig.	Putative PKD substrate motifs
P10648	N-terminally processed;Glutathione S-transferase A2	Gsta2	3	6	1,51	1	
Q62523	Zyxin	Zyx	0	2	1,50	1	
A0A087W Q89	MCG5930	2210011 C24Rik	4	6	1,49	1	LsRpgS48
Q9D0R2	Threonine--tRNA ligase, cytoplasmic	Tars	0	3	1,44	1	
Q8K2I2	Coiled-coil alpha-helical rod protein 1	Cchcr1	0	4	1,44	1	VeRmsT401 VaRipS459
P35700	Peroxiredoxin-1	Prdx1	7	10	1,41	1	IlRqiT143
P07901	Heat shock protein HSP 90-alpha	Hsp90aa 1	10	17	1,39	1	**LIRyyT468**
Q8VE19	WD repeat-containing protein mio	Mios	6	12	1,38	1	
Q9CQ22	Ragulator complex protein LAMTOR1	Lamtor1	4	4	1,36	1	
Q91YD6	Villin-like protein	Vill	8	12	1,25	1	
P99029	Peroxiredoxin-5, mitochondrial	Prdx5	6	5	1,23	1	VlRasT21
O70325	Phospholipid hydroperoxide glutathione peroxidase, mitochondrial	Gpx4	4	5	1,23	1	
Q91ZU6	Dystonin	Dst	18	40	1,21	1	LhRleS682 **VaRkkS739** **IqRkyS833** VeRwqS1272 LeRqdT1703 VlRpeS2146 **<u>LtRqkS3894</u>** **LtRskS4092** **LIRslS4680** LdRakT5202 **<u>LtRqlS5407</u>** **LIRkqS5488** LeRaqS5759 VeRgrS6520 VpRagS7365
Q9D0I9	Arginine--tRNA ligase, cytoplasmic	Rars	5	7	1,18	1	IeRgeS336
Q91YR1	Twinfilin-1	Twf1	17	13	1,16	1	LfRldS75

6.1.2 Proteins identified by MS from IP with Rxx[S*/T*] antibody

Table 16: List of proteins identified by MS from IP with Rxx[S*/T*] antibody.

Uniprot entry	Protein names	Gene names	Peptides EGFP	Peptides PKD3ca	norm.log2.Ratio. filt.LFQ.intensity	Sig.	Putative PKD substrate motifs
Q8BQZ4	Ral GTPase-activating protein subunit beta	Ralgapb	1	3	10,24	2	LaResS156 **IsRprS357** **InRdnS470** LvRgmS971
P63260	Actin, cytoplasmic 2	Actg1	48	44	8,04	2	
Q9JKP5	Muscleblind-like protein 1	Mbnl1	1	2	7,53	2	
P35700	Peroxiredoxin-1	Prdx1	3	11	7,19	2	IlRqiT143
K9J7B2	UDP-glucuronosyltransferase	Ugt1a6b	1	13	6,35	2	VpRfyT197 LkRdvS242 ImRlsS443
Q62426	Cystatin-B	Cstb	1	6	6,22	2	
P70275	Semaphorin-3E	Sema3e	1	14	5,85	2	
Q62266	Cornifin-A	Sprr1a	2	9	5,45	2	
Q5FWX6	Serine/threonine-protein kinase D3	Prkd3	3	42	5,38	2	IlRvsS470
P54823	Probable ATP-dependent RNA helicase DDX6	Ddx6	2	14	5,33	2	
P63168	Dynein light chain 1, cytoplasmic	Dynll1	0	3	5,26	2	
P01887	Beta-2-microglobulin	B2m	1	2	5,24	2	
Q80TV8	CLIP-associating protein 1	Clasp1	0	30	5,04	2	LeRhiS485 **LnRplS568** **__LqRsrS600__** **LgRirT642** VsRiiT1026 IgRtpS1098 LrRsyS1159 ItRedS1333 **IkRaqT1520**
O54962	Barrier-to-autointegration factor	Banf1	1	3	5,00	2	
Q80U30	Protein CLEC16A	Clec16a	1	2	4,96	2	IlRqkS89
P12787	Cytochrome c oxidase subunit 5A, mitochondrial	Cox5a	0	3	4,95	2	
Q8VCH8	UBX domain-containing protein 4	Ubxn4	0	7	4,95	2	IeRrkT230 VkResT310 IwRliS428 **__IyRlrT487__**
P10810	Monocyte differentiation antigen CD14	Cd14	1	10	4,87	2	LkRvdT71 LdRnpS308
O09106	Histone deacetylase 1	Hdac1	0	8	4,83	2	VaRcwT313
Q9CXF4	TBC1 domain family member 15	Tbc1d15	0	3	4,81	2	
Q9CQQ7	ATP synthase F(0) complex subunit B1, mitochondrial	Atp5f1	2	7	4,80	2	
P27773	Protein disulfide-isomerase A3	Pdia3	1	11	4,58	2	**LqReaT485**

Uniprot entry	Protein names	Gene names	Peptides EGFP	Peptides PKD3ca	norm.log2.Ratio. filt.LFQ.intensity	Sig.	Putative PKD substrate motifs
P62821	Ras-related protein Rab-1A	Rab1A	1	4	4,53	2	**IdRyaS114**
P09528	Ferritin heavy chain	Fth1	1	8	4,49	2	
Q9DBG1	Sterol 26-hydroxylase, mitochondrial	Cyp27a1	1	11	4,47	2	VsRdpS439
Q8K0D0	Cyclin-dependent kinase 17	Cdk17	0	4	4,47	2	**LrRphS75** **IhRriS137** LaRakS339
Q8BHL4	Retinoic acid-induced protein 3	Gprc5a	0	3	4,46	2	LpRqrS275
P20918	Plasminogen	Plg	2	12	4,39	2	IpRctT264 LsRpaT678
Q9R049	E3 ubiquitin-protein ligase AMFR	Amfr	0	12	4,34	2	LqRqrT642
Q05421	Cytochrome P450 2E1	Cyp2e1	1	15	4,27	2	
Q3UJB9	Enhancer of mRNA-decapping protein 4	Edc4	0	12	4,22	2	
Q91WT8	RNA-binding protein 47	Rbm47	2	7	4,13	2	**VqRipT533**
P11352	Glutathione peroxidase 1	Gpx1	4	12	4,13	2	
Q8BQ30	Phostensin	Ppp1r18	4	23	4,09	2	**LeRrsS126**
Q9DCX2	ATP synthase subunit d, mitochondrial	Atp5h	1	3	4,06	2	
Q64282	Interferon-induced protein with tetratricopeptide repeats 1	Ifit1	1	13	4,06	2	
Q8R084	UDP-glucuronosyltransferase	Ugt2b1	2	8	4,05	2	LgRptT246
P03975	IgE-binding protein	Iap	1	9	4,02	2	VsRkrS107
Q8VCW8	Acyl-CoA synthetase family member 2, mitochondrial	Acsf2	1	7	3,93	2	
V9GX76	Unconventional myosin-VI	Myo6	73	93	3,93	2	VlRylT169 LnRgcT279
Q8CHQ9	Probable N-acetyltransferase CML2	Cml2	2	7	3,92	2	
P61222	ATP-binding cassette sub-family E member 1	Abce1	1	5	3,91	2	
Q3TJZ6	Protein FAM98A	Fam98a	0	6	3,90	2	IlRtsS283
P14211	Calreticulin	Calr	1	10	3,88	2	
Q6PDK2	Histone-lysine N-methyltransferase 2D	Kmt2d	2	25	3,82	2	LgRagT424 VlRnlT1560 LdRipT1837 IsRgqT2695 **VsRppS2962**
Q9CY27	Very-long-chain enoyl-CoA reductase	Tecr	1	7	3,75	2	
Q02013	Aquaporin-1	Aqp1	1	3	3,75	2	LeRnqT44 LtnfS207
P62071	Ras-related protein R-Ras2	Rras2	1	7	3,73	2	
F8VQB6	Unconventional myosin-X	Myo10	0	24	3,72	2	**IeRslS961**
P58660	Caspase recruitment domain-containing protein 10	Card10	4	9	3,68	2	**VrRvlS629** VeRgsS1011
O88342	WD repeat-containing protein 1	Wdr1	1	3	3,68	2	**VeRgvS20**

Appendix

Uniprot entry	Protein names	Gene names	Peptides EGFP	Peptides PKD3ca	norm.log2.Ratio. filt.LFQ.intensity	Sig.	Putative PKD substrate motifs
Q91YN9	BAG family molecular chaperone regulator 2	Bag2	2	5	3,66	2	
Q99104	Unconventional myosin-Va	Myo5a	3	17	3,65	2	IrRaaT841
Q91YU6	Leucine zipper putative tumor suppressor 2	Lzts2	0	8	3,64	2	
P63242	Eukaryotic translation initiation factor 5A-1	Eif5a	1	3	3,64	2	
Q9CQW9	Interferon-induced transmembrane protein 3	Ifitm3	1	3	3,64	2	
Q922F4	Tubulin beta-6 chain	Tubb6	6	21	3,63	2	
Q8VCX1	3-oxo-5-beta-steroid 4-dehydrogenase	Akr1d1	1	2	3,61	2	
Q99KK2	N-acylneuraminate cytidylyltransferase	Cmas	0	12	3,61	2	LaRggS53 **VhRrsS111**
Q8BG80	F-box only protein 46	Fbxo46	0	8	3,61	2	**LyRhvS453**
Q61937	Nucleophosmin	Npm1	2	5	3,60	2	
Q9JLJ2	4-trimethylaminobutyraldehyde dehydrogenase	Aldh9a1	3	10	3,58	2	
P56593	Cytochrome P450 2A12	Cyp2a12	0	12	3,55	2	IpRriT373
P58137	Acyl-coenzyme A thioesterase 8	Acot8	1	4	3,52	2	VeRirT104
Q9JHU4	Cytoplasmic dynein 1 heavy chain 1	Dync1h1	4	20	3,52	2	IsRdlS387 IdRveT560 IdRqlT657 LpRiqS999 LeRerS1622 LaRlrS2382 IrRitT2521 VhRkyT2966 LeRmnT3008 **LeRlfT4272** LpRswS4462
Q63886	UDP-glucuronosyltransferase 1-1	Ugt1a1	2	12	3,51	2	VkRdsS123 ImRlsS447
Q99K48	Non-POU domain-containing octamer-binding protein	Nono	3	7	3,50	2	
Q8BHD7	Polypyrimidine tract-binding protein 3	Ptbp3	2	11	3,48	2	
Q922P9	Putative oxidoreductase GLYR1	Glyr1	1	6	3,46	2	
A2AIX1	Protein transport protein sec16	Sec16a	0	17	3,44	2	**<u>LtRapS2101</u>** **<u>LsRcsS2315</u>**
Q8BWS5	G protein-regulated inducer of neurite outgrowth 3	Gprin3	0	7	3,43	2	
Q91VY9	Zinc finger protein 622	Znf622	0	8	3,43	2	LpRavT410 VqRmkS452
Q3UMC0	Spermatogenesis-associated protein 5	Spata5	1	4	3,41	2	VeRgsS739
Q61699	Heat shock protein 105 kDa	Hsph1	0	7	3,35	2	

Uniprot entry	Protein names	Gene names	Peptides EGFP	Peptides PKD3ca	norm.log2.Ratio. filt.LFQ.intensity	Sig.	Putative PKD substrate motifs
Q61495	Desmoglein-1-alpha	Dsg1a	2	2	3,31	2	VdRevT120 VfRpgS389 LqRtcT476
Q9D2G2	Dihydrolipoyllysine-residue succinyltransferase component of 2-OGDC, mitochondrial	Dlst	1	8	3,28	2	VsRafS13
Q5U465	Coiled-coil domain-containing protein 125	Ccdc125	0	8	3,28	2	VpRssS9 **LkRscS492**
P17182	Alpha-enolase	Eno1	1	9	3,28	2	
Q9CQF0	39S ribosomal protein L11, mitochondrial	Mrpl11	1	7	3,27	2	
P13020	Gelsolin	Gsn	6	10	3,27	2	
P26039	Talin-1	Tln1	1	10	3,26	2	**LnRcvS1201**
Q921G7	Electron transfer flavoprotein-ubiquinone oxidoreductase, mitochondrial	Etfdh	1	4	3,25	2	**VnRnlS550**
Q62186	Translocon-associated protein subunit delta	Ssr4	1	4	3,25	2	
O35632	Hyaluronidase-2	Hyal2	1	3	3,20	2	VyRqsS155 VrRnpS382
P09803	Cadherin-1	Cdh1	1	4	3,19	2	
P08226	Apolipoprotein E	Apoe	1	12	3,17	2	
Q91ZU6	Dystonin	Dst	9	65	3,16	2	LhRleS682 **VaRkkS739** **IqRkyS833** VeRwqS1272 LeRqdT1703 VlRpeS2146 **LtRqkS3894** **LtRskS4092** **LlRslS4680** LdRakT5202 **LtRqlS5407** **LlRkqS5488** LeRaqS5759 VeRgrS6520 VpRagS7365
Q6PGG6	Guanine nucleotide-binding protein-like 3-like protein	Gnl3l	0	2	3,16	2	
P35564	Calnexin	Canx	1	7	3,16	2	
O35295	Transcriptional activator protein Pur-beta	Purb	1	8	3,14	2	
P34914	Bifunctional epoxide hydrolase 2	Ephx2	1	4	3,14	2	
Q8BGH2	Sorting and assembly machinery component 50 homolog	Samm50	0	8	3,14	2	**LsRtaS243**
Q64433	10 kDa heat shock protein, mitochondrial	Hspe1	1	2	3,13	2	

Appendix

Uniprot entry	Protein names	Gene names	Peptides EGFP	Peptides PKD3ca	norm.log2.Ratio. filt.LFQ.intensity	Sig.	Putative PKD substrate motifs
Q61753	D-3-phosphoglycerate dehydrogenase	Phgdh	2	14	3,12	2	**IvRsaT57** **VgRagT78** **LlReaS383**
P09055	Integrin beta-1	Itgb1	1	5	3,11	2	
P53996	Cellular nucleic acid-binding protein	Cnbp	0	6	3,10	2	**LaRecT173**
Q9CQE8	UPF0568 protein C14orf166 homolog	RTRAF	0	6	3,09	2	
Q9Z2I8	Succinyl-CoA ligase [GDP-forming] subunit beta, mitochondrial	Suclg2	2	15	3,09	2	
Q9Z2I0	LETM1 and EF-hand domain-containing protein 1, mitochondrial	Letm1	0	5	3,05	2	LsRccT55
Q91VW5	Golgin subfamily A member 4	Golga4	9	48	3,02	2	**LvRtsS119** LeRqrS891 **LqRrlS1761**
Q9JHI7	Exosome complex component RRP45	Exosc9	1	6	3,02	2	
P80316	T-complex protein 1 subunit epsilon	Cct5	4	12	3,01	2	
Q91YH5	Atlastin-3	Atl3	1	6	3,01	2	LiRdwS216
Q8K154	UDP-glucuronosyltransferase	Ugt2b34	1	7	3,01	2	LgRptT248
Q8R081	Heterogeneous nuclear ribonucleoprotein L	Hnrnpl	0	4	3,00	2	**VdRaiT434** **VkRptS528**
A0A087W Q89	MCG5930	2210011 C24Rik	1	9	2,97	2	LsRpgS48
Q61029	Lamina-associated polypeptide 2, isoforms beta/delta/epsilon/gamma	Tmpo	14	24	2,96	2	**VgRkaT95** **LtResT250**
Q8CGC7	Bifunctional glutamate/proline--tRNA ligase;Glutamate--tRNA ligase;Proline--tRNA ligase	Eprs	0	9	2,96	2	LaRiaT63 **LrRgmT467** IlRpwS1053
Q3UEP4	UDP-glucuronosyltransferase	Ugt2b36	1	6	2,96	2	VlRpsT60 LgRptT246
P32067	Lupus La protein homolog	Ssb	4	11	2,95	2	LnRltT63 **IrRspS94**
Q0VG62	Uncharacterized protein C8orf59 homolog	1810022 K09Rik	1	2	2,95	2	VpRpeT34
E9Q5F4	Actin, cytoplasmic 1	Actb	30	31	2,94	2	
Q91ZA3	Propionyl-CoA carboxylase alpha chain, mitochondrial	Pcca	0	9	2,94	2	VsRslS48 ViRgvT475
P10639	Thioredoxin	Txn	1	3	2,92	2	
Q6VGS5	Protein Daple	Ccdc88c	0	19	2,91	2	**LqRelS787** **LiRqhS1184** VdRtdT1493 VsRsaS1792 **LsRafS1798** **LaRerT1848**
P24369	Peptidyl-prolyl cis-trans isomerase B	Ppib	0	5	2,90	2	

Uniprot entry	Protein names	Gene names	Peptides EGFP	Peptides PKD3ca	norm.log2.Ratio. filt.LFQ.intensity	Sig.	Putative PKD substrate motifs
Q6ZWQ0	Nesprin-2	Syne2	12	67	2,90	2	IrRgrT968 LrRlmS1184 LaRlqT3013 IiRklS3097 LqRvrS3527 **LsRtnS4096** VkRlyS4634 LhRlqT4927 IsRlvT5687 LqRwrT5743 IsRlqS5794 **LaRieS6030** **LIRqgT6489**
Q8CGB3	Uveal autoantigen with coiled-coil domains and ankyrin repeats	Uaca	0	13	2,90	2	
Q9QUI0	Transforming protein RhoA	Rhoa	0	2	2,89	2	
P56391	Cytochrome c oxidase subunit 6B1	Cox6b1	1	2	2,88	2	
P14602	Heat shock protein beta-1	Hspb1	2	5	2,87	2	**LIRspS15** **LnRqlS86** IsRcfT143
Q791V5	Mitochondrial carrier homolog 2	Mtch2	1	5	2,86	2	
Q9DBF1	Alpha-aminoadipic semialdehyde dehydrogenase	Aldh7a1	3	9	2,85	2	**LgRlvS133** **VdRlrS352**
Q3U0V1	Far upstream element-binding protein 2	Khsrp	2	7	2,84	2	
P97432	Next to BRCA1 gene 1 protein	Nbr1	0	2	2,82	2	LgRpeS351 **ViRslT659**
P52480	Pyruvate kinase PKM	Pkm	1	2	2,82	2	LvRasS403
A2AI08	Taperin	Tprn	2	8	2,82	2	**VnRslS255**
P68373	Tubulin alpha-1C chain	Tuba1c	7	18	2,80	2	LnRliS232
P10649	Glutathione S-transferase Mu 1	Gstm1	1	7	2,78	2	
Q9WU79	Proline dehydrogenase 1, mitochondrial	Prodh	1	6	2,78	2	
Q99PP6	Tripartite motif-containing protein 34A	Trim34a	2	8	2,77	2	LrRewS243
Q8BX02	KN motif and ankyrin repeat domain-containing protein 2	Kank2	0	4	2,76	2	
P53395	Lipoamide acyltransferase component of branched-chain alpha-keto acid dehydrogenase complex, mitochondrial	Dbt	1	10	2,75	2	VlRtwS11
P62835	Ras-related protein Rap-1A	Rap1a	1	4	2,74	2	
Q8JZN5	Acyl-CoA dehydrogenase family member 9, mitochondrial	Acad9	1	3	2,74	2	LsRgaT12 VlRefT28

Appendix

Uniprot entry	Protein names	Gene names	Peptides EGFP	Peptides PKD3ca	norm.log2.Ratio. filt.LFQ.intensity	Sig.	Putative PKD substrate motifs
Q8C052	Microtubule-associated protein 1S	Map1s	0	6	2,74	2	LrRllS324 **LaRrsT659** **LtRkpS831**
P51658	Estradiol 17-beta-dehydrogenase 2	Hsd17b2	2	7	2,73	2	
P19536	Cytochrome c oxidase subunit 5B, mitochondrial	Cox5b	1	2	2,70	2	
Q9D6Y9	1,4-alpha-glucan-branching enzyme	Gbe1	1	7	2,69	2	
Q99MR8	Methylcrotonoyl-CoA carboxylase subunit alpha, mitochondrial	Mccc1	1	10	2,69	2	
Q61037	Tuberin	Tsc2	5	23	2,68	2	IlRelS49 LlRadS625 IyRcaS802 **LvRrpT1203** **LpRsnT1270** LhRsvS1291 **IeRaiS1365**
Q8QZY3	Developmental pluripotency-associated protein 3	Dppa3	0	8	2,68	2	
Q3TDQ1	Dolichyl-diphosphooligosaccharide--protein glycosyltransferase subunit STT3B	Stt3b	0	4	2,67	2	ViRfeS94
Q9R0Q7	Prostaglandin E synthase 3	Ptges3	0	2	2,64	2	
Q80U72	Protein scribble homolog	Scrib	1	10	2,63	2	**LqRraT475** **LiRkdT606** **IdRelS1218** **LqRgpS1271**
;Q8R3L2	Transcription factor 25	Tcf25	1	6	2,63	2	
Q91WQ3	Tyrosine--tRNA ligase;Tyrosine--tRNA ligase, cytoplasmic;Tyrosine--tRNA ligase, cytoplasmic, N-terminally processed	Yars	1	10	2,62	2	**VyRlsS138**
Q8K2I2	Coiled-coil alpha-helical rod protein 1	Cchcr1	0	5	2,62	2	VeRmsT401 **VaRipS459**
P35456	Urokinase plasminogen activator surface receptor	Plaur	1	4	2,60	2	
Q9QYC0	Alpha-adducin	Add1	1	5	2,59	2	VdRgsT212
P28843	Dipeptidyl peptidase 4	Dpp4	1	5	2,59	2	
Q9R0L6	Pericentriolar material 1 protein	Pcm1	5	30	2,59	2	**VgRrrT77** **LtReiS378** **VsRhiS1432**
Q922B9	Sperm-specific antigen 2 homolog	Ssfa2	1	4	2,59	2	**LqRigS268** **LtRsnT290** **LlRtaS502** **LpReeS640** **VdRsqS728** **LiReqS1075**

Appendix

Uniprot entry	Protein names	Gene names	Peptides EGFP	Peptides PKD3ca	norm.log2.Ratio. filt.LFQ.intensity	Sig.	Putative PKD substrate motifs
G3UWQ7	Protein regulator of cytokinesis 1	Prc1	0	2	2,59	2	LqRelS601
Q8C4X2	Casein kinase I isoform gamma-3	Csnk1g3	0	11	2,58	2	
Q9Z0P5	Twinfilin-2	Twf2	1	4	2,57	2	LfRldS75
P16331	Phenylalanine-4-hydroxylase	Pah	0	9	2,56	2	**LsRklS16** IpRpfS411
Q9WVK4	EH domain-containing protein 1	Ehd1	1	6	2,56	2	
Q9Z1M8	Protein Red	Ik	0	5	2,54	2	
P46978	Dolichyl-diphosphooligosaccharide--protein glycosyltransferase subunit STT3A	Stt3a	1	5	2,54	2	VlRfeS43 VdRegS631
P21278	Guanine nucleotide-binding protein subunit alpha-11	Gna11	1	6	2,53	2	**VdRiaT169**
O70194	Eukaryotic translation initiation factor 3 subunit D	Eif3d	1	5	2,51	2	**VqRvgS274 ViRvyS521**
P47740	Fatty aldehyde dehydrogenase	Aldh3a2	2	11	2,49	2	
O70479	BTB/POZ domain-containing adapter for CUL3-mediated RhoA degradation protein 2	Tnfaip1	1	7	2,49	2	LtRhdT51 VkRysT302
Q8BG05	Heterogeneous nuclear ribonucleoprotein A3	Hnrnpa3	0	5	2,46	2	VsRedS94
Q8BJ64	Choline dehydrogenase, mitochondrial	Chdh	2	3	2,44	2	VsRgkT196
P24456	Cytochrome P450 2D10	Cyp2d10	3	10	2,42	2	LpRitS382
Q9WV55	Vesicle-associated membrane protein-associated protein A	Vapa	1	7	2,41	2	
B7ZMP1	Probable Xaa-Pro aminopeptidase 3	Xpnpep3	1	3	2,41	2	LqRryS32
P28656	Nucleosome assembly protein 1-like 1	Nap1l1	1	6	2,40	2	
Q9QXG4	Acetyl-coenzyme A synthetase, cytoplasmic	Acss2	0	3	2,40	2	
Q91VH2	Sorting nexin-9	Snx9	1	9	2,39	2	IqRgnS194 VkRvgT543
P18406	Protein CYR61	Cyr61	1	10	2,39	2	IcRaqS95
Q9DAW6	U4/U6 small nuclear ribonucleoprotein Prp4	Prpf4	2	6	2,38	2	
Q8BP47	Asparagine--tRNA ligase, cytoplasmic	Nars	2	6	2,38	2	VlRdgT164 LeRflS536
Q9R0H0	Peroxisomal acyl-coenzyme A oxidase 1	Acox1	3	13	2,37	2	
P24549	Retinal dehydrogenase 1	Aldh1a1	3	15	2,35	2	
Q64458	Cytochrome P450 2C29	Cyp2c29	2	9	2,33	2	LwRqsS24 VgRhrS336
P61967	AP-1 complex subunit sigma-1A	Ap1s1	0	3	2,31	2	
P16406	Glutamyl aminopeptidase	Enpep	1	8	2,28	2	ViRyiS849 LgRivT885

Appendix

Uniprot entry	Protein names	Gene names	Peptides EGFP	Peptides PKD3ca	norm.log2.Ratio. filt.LFQ.intensity	Sig.	Putative PKD substrate motifs
Q922M3	BTB/POZ domain-containing adapter for CUL3-mediated RhoA degradation protein 3	Kctd10	2	12	2,27	2	
Q62433	Protein NDRG1	Ndrg1	7	10	2,11	2	**LmRsrT328**
P62960	Nuclease-sensitive element-binding protein 1	Ybx1	7	20	2,00	2	**InRndT78**
Q99JB8	Protein kinase C and casein kinase II substrate protein 3	Pacsin3	4	19	2,61	1	
Q9QXZ0	Microtubule-actin cross-linking factor 1	Macf1	15	56	2,47	1	LeRekS418 **IkRkyT814** VfRskT854 IeRnqT1331 IdRqvT1767 **LkRggS3889** **IsRqkS4129** LeRrwT5394 LsRgdS6362 IeRgrS6501
Q9CY66	H/ACA ribonucleoprotein complex subunit 1	Gar1	2	3	2,26	1	
P60766	Cell division control protein 42 homolog	Cdc42	0	3	2,25	1	
Q9DB77	Cytochrome b-c1 complex subunit 2, mitochondrial	Uqcrc2	4	10	2,18	1	LsRagS9 LlRlaS87
Q03963	Interferon-induced, double-stranded RNA-activated protein kinase	Eif2ak2	0	4	2,11	1	
Q99N93	39S ribosomal protein L16, mitochondrial	Mrpl16	1	3	2,07	1	
QQ80YE7	Death-associated protein kinase 1	Dapk1	1	9	2,04	1	IeRevS66 **LsRkaS289** **VsRrdS1433**
P68368	Tubulin alpha-4A chain	Tuba4a	7	18	2,01	1	**LnRliS232**
P42932	T-complex protein 1 subunit theta	Cct8	5	18	1,97	1	**LvRlnS317** **VlRgsT381**
Q9D0M3	Cytochrome c1, heme protein, mitochondrial	Cyc1	3	4	1,96	1	
P50544	Very long-chain specific acyl-CoA dehydrogenase, mitochondrial	Acadvl	2	17	1,93	1	LpRvaS208
Q9DBG6	Dolichyl-diphosphooligosaccharide--protein glycosyltransferase subunit 2	Rpn2	0	5	1,91	1	**LdRpfT46**
Q8C7U1	NEDD4-binding protein 3	N4bp3	0	6	1,91	1	
O88967	ATP-dependent zinc metalloprotease YME1L1	Yme1l1	0	6	1,91	1	
E9Q555	E3 ubiquitin-protein ligase RNF213	Rnf213	8	24	1,90	1	IhRggS427 LdRifS511 LfRtwT1602 LrRclT1845 IlRleS2501

161

Uniprot entry	Protein names	Gene names	Peptides EGFP	Peptides PKD3ca	norm.log2.Ratio. filt.LFQ.intensity	Sig.	Putative PKD substrate motifs
							VlRnfS2949
							LyRkvS3210
							LsRmgS3384
							LlRdaS4057
							LvRklS4233
							LtRllT4537
							LlRvqS4605
							IqRqiS4908
Q8CD15	Bifunctional lysine-specific demethylase and histidyl-hydroxylase MINA	Mina	2	9	1,90	1	VcRsiS107 **VtRklS309**
Q99L45	Eukaryotic translation initiation factor 2 subunit 2	Eif2s2	4	16	1,89	1	VvRvgT212
Q3TGW2	Endonuclease/exonuclease/phosphatase family domain-containing protein 1	Eepd1	3	8	1,87	1	**IpRdpS16** **VfRlaT265**
Q8R0X7	Sphingosine-1-phosphate lyase 1	Sgpl1	2	14	1,87	1	
P97449	Aminopeptidase N	Anpep	12	28	1,87	1	**ViRmlS487** VnRppT745 LnRylS845 VtRrfS909
P19157	Glutathione S-transferase P 1	Gstp1	2	7	1,86	1	
Q6R0H7	Guanine nucleotide-binding protein G(s) subunit alpha isoforms XLas	Gnas	5	15	1,84	1	LpRshT699
Q640L3	Cell cycle progression protein 1	Ccpg1	2	3	1,82	1	LeRcwT286
P80318	T-complex protein 1 subunit gamma	Cct3	6	25	1,81	1	**IsRwsS170** **LlRgaS380**
P49813	Tropomodulin-1	Tmod1	2	11	1,80	1	
Q8JZQ9	Eukaryotic translation initiation factor 3 subunit B	Eif3b	2	5	1,77	1	**VeRrrT741**
O70589	Peripheral plasma membrane protein CASK	Cask	1	5	1,75	1	LkReaS64 **LkRilT433** IhRqgT539
Q9CPR4	60S ribosomal protein L17	Rpl17	3	15	1,75	1	
P09411	Phosphoglycerate kinase 1	Pgk1	3	10	1,74	1	
O09167	60S ribosomal protein L21	Rpl21	6	7	1,71	1	
Q69ZX8	Actin-binding LIM protein 3	Ablim3	3	11	1,67	1	**LhRtpS598** LeRhlS649
P10126	Elongation factor 1-alpha 1	Eef1a1	6	15	1,67	1	**VgRveT269**
Q80TP3	E3 ubiquitin-protein ligase UBR5	Ubr5	8	29	1,66	1	**LsRlgS293** LyRllT1254 LrRsgT1751 LaRayS1783 ViRqiS1790 LeRkrT1971
P11983	T-complex protein 1 subunit alpha	Tcp1	6	18	1,63	1	

Uniprot entry	Protein names	Gene names	Peptides EGFP	Peptides PKD3ca	norm.log2.Ratio. filt.LFQ.intensity	Sig.	Putative PKD substrate motifs
Q0P678	Zinc finger CCCH domain-containing protein 18	Zc3h18	3	4	1,62	1	
Q9DB20	ATP synthase subunit O, mitochondrial	Atp5o	2	7	1,60	1	
Q3UQ44	Ras GTPase-activating-like protein IQGAP2	Iqgap2	3	14	1,59	1	**LdRkqS554** **LkRknS1458**
P62082	40S ribosomal protein S7	Rps7	4	14	1,53	1	
P63037	DnaJ homolog subfamily A member 1	Dnaja1	3	11	1,52	1	
Q64339	Ubiquitin-like protein ISG15	Isg15	4	6	1,50	1	
Q91YD6	Villin-like protein	Vill	7	14	1,49	1	
Q99K51	Plastin-3	Pls3	8	18	1,48	1	**LkRaeS339** LmRryT506 VnRtlS533
P17225	Polypyrimidine tract-binding protein 1	Ptbp1	5	14	1,48	1	
P06151	L-lactate dehydrogenase A chain	Ldha	4	10	1,48	1	
Q62191	E3 ubiquitin-protein ligase TRIM21	Trim21	6	17	1,46	1	**LeRsgS260**
O08749	Dihydrolipoyl dehydrogenase, mitochondrial	Dld	2	9	1,46	1	
P26041	Moesin	Msn	8	21	1,45	1	
Q8VI94	2-5-oligoadenylate synthase-like protein 1	Oasl1	8	20	1,45	1	VlRstT80
Q4U2R1	E3 ubiquitin-protein ligase HERC2	Herc2	22	54	1,42	1	VyRakS97 LaRvgS198 LqRfqS347 **LdRlaT406** LgRggS643 LlRqvS811 VaRriS1036 LlResT2123 **LkRchS2773** LiRkkT2949 IpRqiT3041 LgRggS3191 VnRkpT3302 VnRivS3668 LrRllT3785 LgRggS4184 **VkRsrS4432**
P62858	40S ribosomal protein S28	Rps28	2	3	1,40	1	**LgRtgS23**
Q99KP6	Pre-mRNA-processing factor 19	Prpf19	2	11	1,36	1	
P46735	Unconventional myosin-Ib	Myo1b	78	83	1,34	1	LeRdfS230 **LeRafS325** LyRdlS539 **LkRppT569**
…							
Q9EP53	Hamartin	Tsc1	6	16	0,71	0	**LfRnkS1094**

6.2   List of Figures

Appendix

6.3 List of Tables

6.4 Abbreviations

2D-DIGE	*two-dimensional difference gel electrophoresis*
36B4	*ribosomal protein lateral stalk subunit P0*
4E-BP	*eIF4E-binding protein*
a.u.	*arbitrary units*
AA	*amino acid*
Acaca	*acetyl-CoA carboxylase alpha*
ACC	*acetyl-CoA carboxylase alpha*
Ad	*adenovirus*
AKT	*protein kinase B*
Akti	*AKT inhibitor*
ALT	*alanine transaminase*
AMPK	*AMP-activated protein kinase*
ANOVA	*analysis of variance*

Appendix

APS	*ammonium peroxidisulphate*
AST	*aspartate transaminase*
ATP	*adenosine triphosphate*
AUC	*area under the curve*
BAT	*brown adipose tissue*
BH_4	*tetrahydrobiopterin*
BMI	*body mass index*
BSA	*bovine serum albumin*
BW	*body weight*
C/EBP	*CCAAT/enhancer-binding protein*
c/nPKC	*conventional/novel protein kinase C*
ca	*constitutive active*
Ca^{2+}	*calcium*
$CaCl_2$	*calcium chloride*
CAD	*carbamoyl-phosphate synthetase 2, aspartate transcarbamoylase, dihydroorotase*
calc.	*calculated*
CAMK	*calcium/calmodulin-dependent protein kinase*
CASTOR	*cellular arginine sensor for mTORC1*
cDNA	*complementary DNA*
CE	*cholesteryl ester*
$CHCl_3$	*chloroform*
ChREBP	*carbohydrate-responsive element-binding protein*
CID755673	*2,3,4,5 tetrahydro-7-hydroxy-1H-benzofuro[2,3-c] azepin-1-one*
CO_2	*carbon dioxide*
cPKC	*conventional PKC*
CPS	*carbamoyl phosphate synthetase*
CPT	*carnitine palmitoyltransferase*
CRD	*cysteine-rich domain*
CREB	*cAMP-response element-binding protein*

Appendix

CRT0066101	*2 [4 [[(2R) 2 aminobutyl]amino] 2 pyrimidinyl] 4 (1 methyl 1H pyrazol 4 yl) phenol dihydrochloride*
CRTC	*CREB regulated transcription coactivator*
CTEN	*C-terminal tensin-like protein*
D	*dimensional*
DAG	*diacylglycerol*
DAPK	*death-associated protein kinase*
Deptor	*DEP domain-containing mTOR-interacting protein*
Dhcr7	*7-dehydrocholesterol reductase*
DLC	*deleted in liver cancer*
DMEM	*Dulbecco's modified eagle media*
DMSO	*dimethyl sulfoxide*
DNA	*deoxyribonucleic acid*
DNA-PK	*DNA-dependent protein kinase*
dNTP	*2'-deoxynucleoside 5'-triphosphate*
DOCK	*dedicator of cytokinesis*
DPBS	*Dulbecco's phosphate-buffered saline*
dpm	*disintegrations per minute*
DST	*dystonin*
dUTP	*deoxyuridine triphosphate*
EBSS	*Earle's balanced salt solution*
ECL	*enhanced chemiluminescence*
EDTA	*ethylenediaminetetraacetic acid*
EGFP	*enhanced green fluorescent protein*
eIF4B	*eukaryotic translation initiation factor 4B*
eIF4E	*eukaryotic translation initiation factor 4E*
ELISA	*enzyme-linked immunosorbent assay*
EMT	*epithelial-mesenchymal transition*
ER	*endoplasmic reticulum*
ERK	*extracellular signal–regulated kinase*
ERM	*ezrin/radixin/moesin*

Appendix

ERp	*ER stress protein*
f/f	*flox/flox*
FAO	*fatty acid oxidation*
Fasn	*fatty acid synthase*
FBS	*foetal bovine serum*
FC	*free cholesterol*
Fdft	*farnesyl-diphosphate farnesyltransferase*
Fdps	*farnesyl diphosphate synthase*
FFA	*free fatty acid*
FGF	*fibroblast growth factor*
FLP	*flippase*
FOXO	*forkhead box protein O*
fwd	*forward*
G	*gauge*
g	*gravitation force*
G6pc	*glucose-6-phosphatase catalytic-subunit*
GAP	*GTPase activating protein*
GAPDH	*glyceraldehyde 3-phosphate dehydrogenase*
GH	*growth hormone*
GI	*gastrointestinal*
GLUT	*glucose transporter*
Gö6976	*5,6,7,13-tetrahydro-13-methyl-5-oxo-12H-indolo[2,3-a]pyrrolo[3,4-c]carbazole-12-propanenitrile*
GPCR	*G-protein-coupled receptor*
GSK	*glycogen synthase kinase*
GTT	*glucose tolerance test*
gWAT	*gonadal white adipose tissue*
h	*hour*
H&E	*hematoxylin and eosin*
H_2O_2	*hydrogen peroxide*
H_2SO_4	*sulfuric acid*

Appendix

HBSS	*Hank's balanced salt solution*
HCC	*hepatocellular carcinoma*
HCl	*hydrochloric acid*
HDAC	*histone deacetylase*
HEK	*human embryonic kidney*
HFD	*high-fat diet*
Hmgcr	*3-hydroxyl-3-methylglutaryl-CoA reductase*
Hmgcs	*3-hydroxyl-3-methylglutaryl-CoA synthase*
HOMA-IR	*homeostasis model assessment of insulin resistance*
HPA	*hyperphenylalaninemia*
Hprt	*hypoxanthine phosphoribosyltransferase*
HR	*homologous recombination*
HRP	*horseradish peroxidase*
Hypoth.	*hypothalamus*
I	*isoleucine*
i.p.	intraperitoneal
i.v.	*intravenous*
IB	*immunoblot*
IEF	*Isoelectric focusing*
IF	*immunofluorescence*
IGF	*insulin-like growth factor*
IgG	*immunoglobulin G*
IHC	*immunohistochemistry*
IKK	*IκB kinase*
Ins	*insulin*
Insig	*insulin induced gene*
IP	*immunoprecipitation*
IP$_3$	*inositol trisphosphate*
IPG	*immobilized pH gradient*
IQR	*interquartile range*
IRS	*insulin receptor substrate*

Appendix

ITT	*insulin tolerance test*
L	*leucine*
LB	*lysogeny broth*
LC	*liquid chromatography*
LC/MS	*liquid chromatography/mass spectrometry*
LD	*lipid droplet*
LDS	*lithium dodecyl sulfate*
LFQ	*label-free quantitation*
LKB	*liver kinase B*
log	*logarithm*
LPL	*lipoprotein lipase*
Lss	*lanosterol synthase*
LXR	*liver X receptor*
m	*mature*
M	*molar*
MAPK	*mitogen-activated protein kinase*
MEF2	*myocyte enhancer factor 2*
MEK	*mitogen-activated protein kinase kinase*
MeOH	*methanol*
$MgCl_2$	*magnesium chloride*
$MgSO_4$	*magnesium sulfate*
mLST8	*mammalian lethal with SEC13 protein 8*
MMP	*matrix metalloproteinase*
MOI	*multiplicity of infection*
MOPS	*3-(N-Morpholino) propansulfonsäure*
mRNA	*messenger ribonucleic acid*
MS	*mass spectrometry*
ms	*milliseconds*
mSIN1	*mammalian stress-activated protein kinase interacting protein*
mTOR	*mechanistic target of rapamycin*
mTORC	*mechanistic target of rapamycin complex*

Appendix

Mvd	*mevalonate diphosphate decarboxylase*
Mvk	*mevalonate kinase*
MW	*molecular weight*
MWCO	*molecular weight cut off*
n	*number*
n.s.	*not significant*
N_2	*nitrogen*
NaCl	*sodium chloride*
NAFLD	*non-alcoholic fatty liver disease*
NaOH	*sodium hydroxide*
NASH	*non-alcoholic steatohepatitis*
NCBInr	*National Center for Biotechnology Information non-redundant*
ND	*normal diet*
NDRG	*N-myc downstream regulated*
NEAA	*nonessential amino acids*
NEO	*neomycin resistance cassette*
NF-κB	*nuclear factor kappa-light-chain-enhancer of activated B cells*
NGS	*normal goat serum*
NH_4Cl	*ammonium chloride*
NH_4HCO_3	*ammonium bicarbonate*
NMR	*nuclear magnetic resonance*
NP-40	*Nonidet P-40*
nPKC	*novel PKC*
NT	*non-targeting*
O_2	*oxygen*
OA	*oleic acid*
OXPHOS	*oxidative phosphorylation*
p	*phospho*
P/S	*Penicillin/Streptomycin*
PA	*phosphatidic acid*
PAH	*phenylalanine hydroxylase*

PAK4	*p21-activated kinase 4*
Panc.	*pancreas*
PAP	*phosphatidic acid phosphohydrolase*
PBS	*phosphate-buffered saline*
PC	*phosphatidylcholine*
PCR	*polymerase chain reaction*
PDCD4	*programmed cell death protein 4*
PDGF	*platelet-derived growth factor*
PDK	*3-phosphoinositide-dependent protein kinase*
PDZ	*postsynaptic density-95/discs large/zonula occludens*
PE	*phosphatidylethanolamine*
Pepck	*phosphoenolpyruvate carboxykinase*
PFA	*paraformaldehyde*
PGC	*PPARγ coactivator*
PH	*pleckstrin homology*
pH	*potentia hydrogenii*
Phe	*phenylalanine*
PHLPP	*PH domain and leucine rich repeat protein phosphatase*
pI	*isoelectric point*
PI3K	*phosphoinositide 3-kinase*
PI4KIIα	*phosphatidylinositol 4-kinase IIα*
PIK3C3	*class III PtdIns 3-kinase*
PIP_2	*phosphatidylinositol 4,5-bisphosphate*
PKA	*cAMP-dependent protein kinase A*
PKC	*protein kinase C*
PKD	*protein kinase D*
PKU	*phenylketonuria*
PL	*phospholipids*
PLC	*phospholipase C*
PLD	*phospholipase D*
PMP	*peroxisomal membrane protein*

Appendix

PPAR	*peroxisome proliferator activated receptor*
PPI	*protease and phosphatase inhibitor*
PRAS	*proline-rich AKT1 substrate*
prot.	*protein*
Protor-1	*protein observed with Rictor-1*
PS	*phosphatidylserine*
PtdIns(4,5)P$_2$	*phosphatidylinositol 4,5-bisphosphate*
PtdIns-PLC	*phosphoinositide specific phospholipase C*
PVDF	*Polyvinylidene fluoride*
QEMS	*Q exactive mass spectrometer*
R	*arginine*
Rag	*Ras-related GTPase*
RalGAPβ	*Ral GTPase activating protein non-catalytic beta subunit*
Raptor	*regulatory associated protein of mTOR*
RasGRP	*RAS guanyl-releasing proteins*
RCAS	*receptor-binding cancer-associated surface antigen*
RER	*respiratory exchange rate*
rev	*reverse*
Rheb	*Ras homolog enriched in brain*
Rictor	*rapamycin-insensitive companion of mTOR*
Rin1	*Rab interactor 1*
RNA	*ribonucleic acid*
ROS	*reactive oxygen species*
Rpl13a	*ribosomal protein L13a*
rPS6	*ribosomal protein S6*
RSK	*p90 ribosomal S6 kinase*
RT	*room temperature*
RTK	*receptor tyrosine kinase*
RT-qPCR	*real-time quantitative PCR*
s	*seconds*
S1P	*Site-1 protease*

Appendix

S2P	*Site-2 protease*
S6K	*p70 ribosomal S6 kinase*
SAM	*S-adenosylmethionine*
SAMTOR	*SAM sensor upstream of mTORC1*
sat.	*saturated*
SCAP	*SREBP cleavage-activating protein*
Scd1	*stearoyl-CoA desaturase*
SDS	*sodium dodecyl sulfate*
SDS-PAGE	*sodium dodecyl sulfate-polyacrylamide gel electrophoresis*
SEM	*standard error of the mean*
Ser	*serine*
SGK	*serum and glucocorticoid-regulated kinase*
SHP-1	*Src homology region 2 domain-containing phosphatase-1*
siRNA	*small interfering RNA*
SKM	*skeletal muscle*
SN	*supernatant*
SP	*sodium pyruvate*
SREBP	*sterol regulatory element-binding protein*
SRPK	*serine/threonine-protein kinase*
SSH1L	*slingshot-1L*
sWAT	*subcutaneous white adipose tissue*
T2D	*type 2 diabetes*
TAE	*TRIS-acetate-EDTA*
TBST	*TRIS buffered saline with tween*
TCA	*tricarboxylic acid*
TdT	*terminal deoxynucleotidyl transferase*
TEMED	*tetramethylethylenediamine*
TFEB	*transcription factor EB*
Tg	*transgenic*
TG	*triglycerides*
TGN	*trans-Golgi network*

Appendix

Thr	*threonine*
TLC	*thin-layer chromatography*
TNF	*tumor necrosis factor*
TNS	*Tensin*
TSC	*tuberous sclerosis complex*
TUNEL	*TdT-mediated dUTP-biotin nick end labeling*
Tyr	*tyrosine*
ULK1	*Unc-51 like autophagy activating kinase 1*
unsat.	*unsaturated*
uPA	*urokinase-type plasminogen activator*
USF	*upstream-stimulatory factor*
UV	*ultra violet*
V	*valine*
v-ATPase	*vacuolar H$^+$-ATPase*
VEGF	*vascular endothelial growth factor*
VLDL	*very low density lipoprotein*
WAT	*white adipose tissue*
WB	*Western blot*
wt	*wild type*

Appendix

6.5 Acknowledgments

Appendix

Katja, Mona, and Deya for carefully proofreading my thesis.

The team of the Graduate School of Life Sciences for the organizing the transferable skills courses and for coordinating of the PhD study program.

Last and most important, my deepest gratitude goes to my girlfriend, my family, and friends who were always there for me and who believed in me.

Appendix

6.6 Publications

6.6.1 Research articles

El-Merahbi R, Trujillo Viera J, Loza Valdes A, Löffler MC, Karwen T, **Mayer AE**, Ade CP, Reuter S, Erk M, Eilers M, and Sumara G. Inhibition of adrenergic-induced ERK3 pathway suppresses lipolysis and protects against obesity. Submitted

Mayer AE, Loeffler MC, Schmitz W, Erk M, El-Merahbi R, Zhang T, Braun U, Heikenwalder M, Leitges M, Schulze A, Sumara G. Protein kinase D3 provides the negative feedback on cholesterol and triglyceride synthesis by suppressing insulin signaling. *Sci Signal 12*, (2019). doi: 10.1126/scisignal.aav9150

Loffler MC, **Mayer AE**, Trujillo Viera J, Loza Valdes A, El-Merahbi R, Ade CP, Karwen T, Schmitz W, Slotta A, Erk M, Janaki Raman S, Matesanz N, Torres JL, Marcos M, Sabio G, Eilers M, Schulze A, Sumara G. Protein kinase D1 deletion in adipocytes enhances energy dissipation and protects against adiposity. *EMBO J* 37, (2018). doi: 10.152527embj.201899182

Cai K, El-Merahbi R, Loeffler M, **Mayer AE**, Sumara G. Ndrg1 promotes adipocyte differentiation and sustains their function. *Sci Rep* 7, 7191, (2017). doi: 10.1038/s41598-017-07497-x

6.6.2 Reviews

El-Merahbi R, Loffler M, **Mayer A**, Sumara G. The roles of serotonin in metabolic homeostasis. *FEBS Lett* 589, 1728-1734, (2015). doi: 10.1016/j.febslet.2015.05.054

6.6.3 Oral presentations

Protein Kinase D3 (Pkd3) suppresses lipid accumulation in liver. 3rd Central European Biomedical Congress (CEBC), Best Presentation Award of Young Scientific Investigator's Session. September 15th-18th, 2018. Krakow, Poland

Protein Kinase D3 (Pkd3) suppresses lipid accumulation in liver. Rudolf-Virchow-Center Retreat. October 9th-10th, 2017. Bad Brückenau, Germany

Appendix

6.6.4 Posters

Hepatic PKD3 provides negative feedback on cholesterol and triglyceride synthesis by suppressing insulin signaling. Organ crosstalk in energy balance and metabolic disease, EMBO Workshop. April 8th-11th, 2019. Cadiz, Spain

Hepatic PKD3 provides the negative feedback on Cholesterol and TAG synthesis by suppressing insulin signaling. 13th International Symposium organized by the Students of the Graduate School of Life Sciences. October 10th-11th, 2018. Würzburg, Germany

Pkd3 suppresses lipid accumulation but promotes insulin resistance by blocking mTORC2 activation. 12th International Symposium organized by the Students of the Graduate School of Life Sciences. October 11th-12th, 2017. Würzburg, Germany

Pkd3 suppresses lipid accumulation but promotes insulin resistance by blocking mTORC2 activation. Diabetes, Keystone Symposia, January 22nd-27th, 2017. Keystone, USA

Pkd3 suppresses lipid accumulation but promotes insulin resistance by blocking mTORC2 activation. 11th International Symposium organized by the Students of the Graduate School of Life Sciences. October 12th-13th, 2016. Würzburg, Germany

Protein Kinase D3 (Pkd3) – a new target for improving insulin sensitivity in liver. 10th International Symposium organized by the Students of the Graduate School of Life Sciences. October 14th-15th, 2015. Würzburg, Germany

6.7 Curriculum vitae

6.8 Affidavit

I hereby declare that my thesis entitled, "Protein kinase D3 signaling in the regulation of liver metabolism" is the result of my own work. I did not receive any help or support from commercial consultants. All sources and/or materials applied are listed and specified in the thesis.

Furthermore, I confirm that this thesis has not yet been submitted as part of another examination process neither in identical nor in similar form.

Würzburg, November 2019 _____

Alexander Mayer

6.9 Eidesstattliche Erklärung

Hiermit erkläre ich an Eides statt, die Dissertation „Proteinkinase D3 Signalwirkung in der Regulation des Leberstoffwechsels" eigenständig, d.h. insbesondere selbstständig und ohne Hilfe eines kommerziellen Promotionsberaters, angefertigt und keine anderen als die von mir angegebenen Quellen und Hilfsmittel verwendet zu haben.

Ich erkläre außerdem, dass die Dissertation weder in gleicher noch in ähnlicher Form bereits in einem anderen Prüfungsverfahren vorgelegen hat.

Würzburg, November 2019 _____

Alexander Mayer